THE UNIVERSITY
of EDINBURGH

Identification of cellular gene targets of anti-viral miR-27

Pairoa Praihirunkit

Doctor of Philosophy The University of Edinburgh 2015

Declaration

I hereby declare that the work present in this thesis is my own unless otherwise acknowledged. This thesis has not been submitted for any other degree or professional qualification except to The University of Edinburgh for the degree of Doctor of Philosophy.

Pairoa Praihirunkit

Date:

Acknowledgements

First and foremost, I would like to express my appreciation and gratitude to my supervisor Dr. Amy Buck. Your advice, support and encouragement have been priceless. Thank you so much for being there whenever I needed them. I also would like to thank my second supervisor Dr. Finn Grey for the advice, especially related to viruses.

I am thankful to members of the Buck lab: Katrina Gordon, Nouf Laqtom, Anna Hoy, Divya Malik, Marissa Lear, Juan Quintana, Fabio Simbari, Diwakar Kumar, Gillian Coakley, Jana McCaskill and Kashyap Chhatbar. It has been wonderful and enjoyable time working with all of you. Special thanks to Katrina and Anna for revising my thesis chapters and giving very helpful comments. I also would like to thank the Zamoyska lab, especially Shatakshi Sood, Kaija Stockner and Celine Gracia for helping with experiments and sharing reagents. Many thanks to Dr. Martin Waterfall for helping me on flow cytometry as well as discussions of the results, and to Dr. Alasdair Ivens for the analysis of microarray data. I am grateful for all the support on materials, chemicals and help from staff in IIIR.

My PhD could not have been accomplished without the financial support from the Royal Thai Government Scholarship. I also would like to thank staff of the office of educational affairs, the Royal Thai Embassy for advice and co-ordinating with the funding body in Thailand.

To mom, dad, brothers and the sister, thank you for love and encouragement. I would not have been through a long journey of my PhD without support from you.

Abstract

Murine cytomegalovirus (MCMV) encodes a non-coding RNA, m169, that inhibits the cellular miRNA, miR-27. Previous studies have shown that the overexpression of miR-27 *in vitro* suppresses replication of MCMV and degradation of miR-27 by m169 is important for the viral replication during the lytic stage of infection *in vivo.* To understand why the virus specifically targets this cellular miRNA for degradation, this thesis focuses on identification of cellular target genes of miR-27 that are involved in viral growth in the lytic infection.

Microarray analysis was conducted to globally examine cellular genes differentially expressed following miR-27 overexpression or repression during MCMV infection. Data obtained from the microarray analysis were analysed in order to select potential targets of miR-27 for functional screening. Functional screening involved siRNA knockdown of individual genes followed by infection with a GFP reporter virus (GFP-MCMV) to assess the effects on viral growth. Knockdown of 5 out of 55 genes (*Rpl18a, Lyar, Itga5, Mapkapk3* and *Pik3r1)* led to a significant reduction in GFP expression. Based on luciferase reporter assays, *Mapkapk3* was validated as a direct target of miR-27 with a seed site interaction in its 3'UTR. Mutation of this site in the mRNA was shown to eliminate miR-27-mediated repression. Analysis of MAPKAPK3 protein levels upon infection demonstrates that the protein levels are higher in cells infected with wild type MCMV versus the m169 deletion virus (MCMV Δm169). This is in line with the difference in miR-27 levels in the two infections showing a decrease of miR-27 in wild type MCMV and unaltered levels in MCMV Δm169 infection.

Mapkapk3 is a direct downstream target of p38 mitogen-activated protein (MAP) kinase within the p38 MAP kinase pathway, which has previously been shown to be an essential pathway for CMV replication. Expression levels of substrates of MAPKAPK3 including HSP27 and ATF1 were examined during infection to evaluate whether they are regulated by miR-27. The level of phosphorylation of HSP27 was shown to correlate with the levels of MAPKAPK3 during infection and was higher in cells infected with wild type MCMV versus MCMV Δm169. This

suggests that MAPKAPK3 and its substrate, HSP27, are regulated by miR-27 during MCMV infection. This work provides an important foundation for further functional studies on the role of *Mapkapk3* and its substrates in MCMV infection and its capacity to be dynamically regulated by miR-27.

Based on the microarray analysis upon miR-27 overexpression, it was shown that miR-27 has an impact on the cell cycle, consistent with previous studies. Functional analysis of miR-27 in the cell cycle using miR-27 mimics and inhibitors demonstrated that the mimics cause an increase of cells in S phase at early time points (12 and 14 h), whereas the inhibition of miR-27 results in a significant reduction in the S phase population and accumulation of cells in G1 phase. Luciferase reporter assays confirmed that two genes known to be associated with the cell cycle are direct targets of miR-27: polycomb ring finger oncogene 1 (*Bmi1*) and caveolin 1 (*Cav1*). Knockdown of *Bmi1* and *Cav1* leads to a significant decrease in the number of cells in S phase and accumulation of cells in the G1 phase; however, this is the opposite result to that observed with the miR-27 mimics. These results suggest that the increase in cells in the S phase induced by miR-27 mimics is unlikely to be associated with targeting of *Bmi1* and *Cav1*. Furthermore, knockdown of *Bmi1* and *Cav1* does not affect viral replication *in vitro*. Since miR-27 induces the transition of cells from the G1 to S phase, further studies are required to identify the miR-27 targets involved in this function.

To identify direct targets of miR-27 through biochemical methods, one chapter of this thesis was devoted to developing CLASH datasets (cross-linking, ligation and sequencing of hybrid). This technique can directly map miRNA-mRNA interactions within the Argonaute protein (AGO). Initially, a NIH 3T3 stable cell line expressing AGO2 with a double affinity tag at the N terminus was generated. Analysis of the stable cell line revealed no significant alteration of miR-27 regulation or change in permissiveness to MCMV compared to wild type cells, making this amenable to further studies. Using the stable cell line, the CLASH protocol was carried out and preliminary data collected.

In summary, this thesis identifies a direct target of miR-27, *Mapkapk3*, that is an important gene in MCMV replication that requires further investigation. *Mapkapk3* is a substrate of p38 in the p38 MAP kinase pathway which is a signal transduction mediating numerous biological processes in response to cellular stresses including CMV infection. Furthermore, miR-27 overexpression was found to stimulate the G1/S transition of the cell cycle, and miR-27 inhibition had the opposite effect. Previous evidence has shown that MCMV and HCMV arrest the cell cycle in the G1 phase and inhibit host DNA synthesis to create an optimal condition for viral gene expression and DNA replication. Given that MCMV arrests host cells in the G1 phase, it is possible that degradation of miR-27 by MCMV contributes to this effect. Since miR-27 regulates both *Mapkapk3* and the cell cycle, it seems likely that a number of targets and pathways underlie the antiviral properties of this miRNA.

Lay summary

Cytomegalovirus (CMV) is a virus infecting a majority of the world's population. The infection usually asymptomatic in healthy individuals; however, it can cause serious diseases in patients who have a defect or suppression of immune system such as patients with HIV and organ transplant recipients who are on immunosuppressive drugs. Furthermore, CMV infection is the most common congenital infection and CMV-infected neonates are at risks of hearing, mental and motor defects. Currently, no anti-viral medication for individuals with normal immunity is recommended. Drugs used for patients with congenital infection or symptoms usually cause side effects. Moreover, no vaccine for the prevention of CMV infection is licensed, although vaccines have been evaluated in clinical trials.

A class of small non-coding RNAs, miRNAs, have been reported to be involved in host defences against viral infection. This thesis focuses on a mouse miRNA, miR-27, which has been shown to suppress the replication of mouse CMV (MCMV) in tissue culture. Importantly, it was shown that the virus mediates the degradation of miR-27 and this is important for viral replication in mice. The broad aim of this thesis is to identify host target genes of miR-27 in order to understand its anti-viral role and why the virus specifically targets miR-27 for degradation. One gene was validated as a direct target of miR-27 and shown to be important for MCMV replication. This gene is involved in a cellular pathway essential for CMV replication. Functional studies of the gene may elucidate the anti-viral mechanism of miR-27 and explain why the virus has evolved the strategy to inhibit miR-27. Moreover, studies of miR-27 in the cell cycle showed that miR-27 induces the progression of the cell cycle at a certain stage, which has shown to be arrested by the virus. Since miR-27 was shown to regulate the gene in the important pathway required for the virus, and the cell cycle, it is possible that a number of genes and pathways contribute to the anti-viral properties of miR-27.

Abbreviation

°C	Degrees Celsius
~	Approximately
AGO	Argonaute
AKT	V-Akt murine thymoma viral oncogene homolog
ANOVA	Analysis of variance
APC	Anaphase-promoting complex
APS	Ammonium persulfate
ATF	Activating transcription factor
ATP	Adenosine triphosphate
BCA	Bicinchoninic acid
BHK-21	Baby hamster kidney fibroblasts
BMI1	Polycomb ring finger oncogene 1
bp	Base pairs
CAF1	Chromatin assembly factor 1
CALM3	Calmodulin 3
CaMK	Ca2+/Calmodulin-dependent kinase
cAMP	Cyclic adenosine monophosphate
CAV1	Caveolin 1
CCND3	Cyclin D3
CCNG1	Cyclin G1
CCR4-NOT	C-C chemokine receptor 4-NOT transcription complex
CD4	Cluster of differentiation 4
CD8	Cluster of differentiation 8
CDK	Cyclin-dependent kinase
cDNA	Complementary deoxyribonucleic acid
CLASH	Cross-linking, ligation and sequencing of hybrids
CLIP	Cross-linking and immunoprecipitation
CMV	Cytomegalovirus
CO2	Carbon dioxide
CREB	cAMP response element-binding protein
cRNA	Complementary ribonucleic acid
CSF1	Colony stimulating factor 1
DC	Dendritic cells
DCP2	Decapping mRNA2
DDX6	DEAD-box protein
DGCR8	DiGeorge syndrome critical region 8 protein
dH2O	Distilled water
DMEM	Dulbecco’s modification of eagle’s medium
DMSO	Dimethyl sulfoxide

DNA	Deoxyribonucleic acid
dNTP	Deoxynucleotide triphosphate
E	Early
EBV	Epstein-Barr virus
ECL	Enhanced chemiluminescence
ECM	Extracellular matrix
EDC4	Enhancer of mRNA decapping 4
EDTA	Ethylenediaminetetraacetic acid
EGFR	Epidermal growth factor receptor
eIF4E	Eukaryotic translation initiation factor 4E
eIF4F	Eukaryotic translation initiation factor 4F
ELISA	Enzyme-linked immunosorbent assay
eNOS	Endothelial nitric oxide synthase
ER	Endoplasmic reticulum
ESC	Embryonic stem cell
FACS	Fluorescence-activated cell sorting
FC	Fold change
FCS	Fetal calf serum
FOXO1	Forkhead box O1
g	Gravitational force or grams
GAPDH	Glyceraldehyde 3-phosphate dehydrogenase
GFP	Green fluorescent protein
GRB2	Growth factor receptor-bound protein 2
GTP	Guanosine-5'-triphosphate
GW182	Glycine-tryptophan protein of 182 kDa
h	hour
HBV	Hepatitis B virus
HCMV	Human cytomegalovirus
HCV	Hepatitis C virus
HEK	Human Embryonic Kidney
HEL	Human embryonic fibroblast
HF	High fidelity
HHV	Human herpesvirus
HI-CS	Heat-inactivated calf serum
HI-FBS	Heat-inactivated fetal bovine serum
HIV	human immunodeficiency virus
hpi	Hours post infection
HPV	Human papilloma virus
HSC	Hepatic stellate cell
HSP27	Heat shock protein 27
HSPG	Heparin sulfate proteoglycan

ICAM-1	Intercellular adhesion molecule-1
ICP	Infected cell protein
IE	Immediate early
IFN	Interferon
IgG	Immunoglobulin G
IL	Interleukin
IMEM	Iscove’s modified eagle medium
IPA	Ingenuity pathway analysis
IRES	Internal ribosome entry site
ISG	Interferon-stimulated gene
ITGA5	Integrin alpha 5
K	103
kb	Kilobase
kDa	Kilodalton
KSHV	Kaposi's sarcoma-associated herpesvirus
LYAR	Ly-1 antibody reactive clone
M	Molar or 106 (depending on the context)
m7G	7-methylguanosine cap
MAP	Mitogen-activated protein
MCM	Mini-chromosome maintenance
MCMV	Murine cytomegalovirus
MCMV Δm169	m169 deletion MCMV
MEF	Mouse embryonic fibroblast
MHC	Major histocompatibility complex
MIE	Major immediate early
min	Minute
miRNA	microRNA
ml	Mililitre
mM	Milimolar
MOI	Multiplicity of infection
mRNA	Messenger RNA
mTOR	Mammalian target of rapamycin
ng	Nanogram
Ni-NTA	Nitrilotriacetic acid
nM	Nanomolar
NO	Nitric oxide
nt	Nucleotide
ORF	Open reading frame
P	Probability value
PABPC	Poly(A) binding protein

PACT	Protein activator of PKR (protein kinase R-activating protein)
PBS	Phosphate buffered saline
PCAF	p300/CBP-associated factor
PCI	Phenol-chloroform-isoamly
PCR	Polymerase chain reaction
PFU	Plaque-forming unit
PFV-1	Primate foamy virus 1
pH	Measure for the hydrogen ion concentration
PHB	Prohibitin
PI3K	Phosphatidylinositol 3-kinase
PIK3R1	Phosphoinositide-3- kinase, regulatory subunit 1
PKR	Protein kinase R
pmol	Picomole
PNK	Polynucleotide Kinase
Pol	Polymerase
PPAR-γ	Peroxisome proliferator-activated receptor gamma
pre-miRNA	Precursor microRNA
preRC	Pre-replication complex
pri-miRNA	Primary microRNA
PTH	Protein A-tobacco etch virus (TEV) cleavage site-6xHistidine)
QC	Quality control
qRT-PCR	Quantitative reverse transcription polymerase chain reaction
Rb	Retinoblastoma
RISC	RNA-induced silencing complex
RNA	Ribonucleic acid
RPF	Ribosome-protected mRNA fragment
RPL18a	Ribosomal protein L18
rpm	Rounds per minute
RSV	Respiratory Syncytial Virus
RUNX1	Runt-related transcription factor 1
SD	Standard deviation
SDS-PAGE	Sodium dodecyl sulfate polyacrylamide
sec	Second
SEMA6A	Semaphorin 6A
shRNA	Small hairpin RNA
siRNA	Small interfering RNA
SOCS1	Suppressor of cytokine signaling1
TBE	Tris-borate-EDTA

TBS-T	Tris-buffered saline-Tween
TCA	Trichloroacetic Acid
TCR	T cell signalling pathway
TEMED	Tetramethylethylenediamine
TRBP	Transactivation-response RNA-binding protein
tRNA	Transfer RNA
TSAP	Thermosensitive alkaline phosphatase
U	Unit
U6	Small nuclear RNA U6
uM	Micromolar
UTR	Untranslated region of mRNA
UV	Ultraviolet
VCAM-1	Vascular cell adhesion molecule-1
VSV	Vesicular stomatitis virus
VZV	Varicella zoster virus
XRN1	Exoribonuclease enzyme 1
µg	microgram
µl	microliter

Table of contents

List of Figures

List of Tables

List of Appendices

Chapter 1: Introduction

1.1 miRNAs

In 1993, the discovery of the first miRNA, lin-4 in *Caenorhabditis elegans (C. elegans)* that regulates gene expression during larval development opened up the field of miRNA research. Ambros V. and Ruvkun G. found that *lin-4* gene encoded two small non-coding RNA transcripts of 61 nt and 22 nt in length that were found to be complementary to the 3'UTR of the *lin-14* gene, which controls the transition from the first to the second larval stage (Lee et al., 1993; Wightman et al., 1993). In 2000, Reinhart *et al*. found a second miRNA, let-7, in *C. elegans* that positively controls the L4-to-adult transition of larval development via the regulation of the *lin-41* gene (Reinhart et al., 2000). The fact that *let-7* gene is conserved across many species from flies to humans (Pasquinelli et al., 2000) then triggered extensive research in the field of miRNAs.

1.1.1 Biogenesis of miRNAs

miRNAs are small non-coding RNAs ~22 nt in length that are encoded by animals, plants and some viruses (Griffiths-Jones et al., 2008). Approximately 50% of mammalian miRNA-coding genes are located within the intergenic space, ~40% of them within introns and ~10% of them within exons of protein-coding genes (reviewed in (O'Carroll and Schaefer, 2013)). The biogenesis pathway of miRNAs is shown in Fig 1.1. miRNA genes are generally transcribed by RNA polymerase II (Pol II) (Cai et al., 2004; Lee et al., 2004), with a minority being transcribed by Pol III (Borchert et al., 2006), giving rise to pri-miRNAs. The pri-miRNAs are usually long transcripts often over several kilobases in length and contain cap structures and poly(A) tails, which are the unique feature of class II gene transcripts (Han et al., 2004). The maturation of miRNAs begins with the cleavage of pri-miRNAs by the nuclear microprocessor complex containing RNAse-III enzyme (Drosha) and its cofactor, DiGeorge syndrome critical region 8 (DGCR8). DGCR8 directly interacts with pri-miRNAs to determine the precise cleavage site (Han et al., 2006) and Drosha cleaves the 5' and 3' of the pri-miRNAs to generate precursor-miRNAs (pre-miRNAs), which are generally ~60-70 nt in length (Han et al., 2004). Besides the

canonical miRNA biogenesis with Drosha/DGCR8, a non-canonical pathway called the "mirtron pathway" has also been described. Initially identified in *D. melanogaster* and *C.elegans* (Okamura et al., 2007; Ruby et al., 2007), this pathway was found to be conserved in mammals (Babiarz et al., 2011; Berezikov et al., 2007). Mirtrons are short intronic hairpins of mRNA-coding genes that are debranched to become pre-miRNAs that are able to enter the miRNA-processing pathway in a Drosha/DGCR8-independent manner (Ruby et al., 2007).

Nascent pre-miRNAs including mirtrons are exported from the nucleus to the cytoplasm via Exportin 5 in a GTP-dependent fashion (Lund et al., 2004; Yi et al., 2003). In the cytoplasm, the pre-miRNA is cleaved by the RNase III endonuclease Dicer, which interacts with transactivation-response RNA-binding protein (TRBP) and protein activator of PKR (PACT) (reviewed in (Ha and Kim, 2014)). It was shown that TRBP and PACT facilitate Dicer-mediated cleavage of the pre-miRNAs (Haase et al., 2005; Lee et al., 2006). Dicer cleaves pre-miRNAs into ~22 nt long miRNA duplexes (miRNA:miRNA* duplexes), which are loaded into the RISC. One strand of the duplex called the "guide strand" remains incorporated in the RISC through specific association with an AGO protein, whereas the other strand (miRNA*) namely the "passenger strand" is usually degraded (Bartel, 2004; Castilla-Llorente et al., 2013). AGO proteins are key components of RISC that mediate gene silencing. Four AGO proteins (AGO1-4) have been reported in mammals and each of them appears to bind to a similar pool of miRNAs and target mRNAs (Burroughs et al., 2011; Czech and Hannon, 2011), though some differences in specificity have been reported (Li et al., 2014). All AGO proteins contain two conserved domains: the N-terminal, PAZ (piwi–argonaute–zwille) domain and the C-terminal lobe containing MID (middle) domain and PIWI (*P*-element–induced wimpy testis) domain. Biochemical and structural studies reveal that the PAZ domain binds to the characteristic 2 nt overhangs at the 3' end of miRNAs, whereas PIWI domain resembles to RNase H and contains an active site that enables cleaving of target mRNAs (reviewed in (Ha and Kim, 2014). Among mammalian AGO proteins, only AGO2 has endonucleolytic activity and can thereby cleave the phosphodiester bond of perfectly matched target mRNAs (Liu et al., 2004; Meister et al., 2004).

The specific function of AGO1, 3 and 4 is still unclear; however, their functions appear to be redundant. A functional study of AGOs in mouse embryonic stem cells lacking AGO1-4 showed that the AGO-deficient cells were unable to perform miRNA silencing and undergo apoptosis (Su et al., 2009). The reintroduction of any individual AGO into the AGO-deficient cells is capable of rescuing miRNA silencing machinery, suggesting that AGO proteins have overlapping functions in this biological event. The role of AGO4 was emphasised by a study showing that AGO4 is required for spermatogenesis and *Ago4*$^{-/-}$ mice had a dramatic loss (>20%) of miRNAs, leading to premature meiotic initiation (Modzelewski et al., 2012). Possibly, the expression pattern of individual AGOs may dictate their importance as well, as it was found that AGO3 and AGO4 are highly expressed in the male mouse germ line (Gonzalez-Gonzalez et al., 2008).

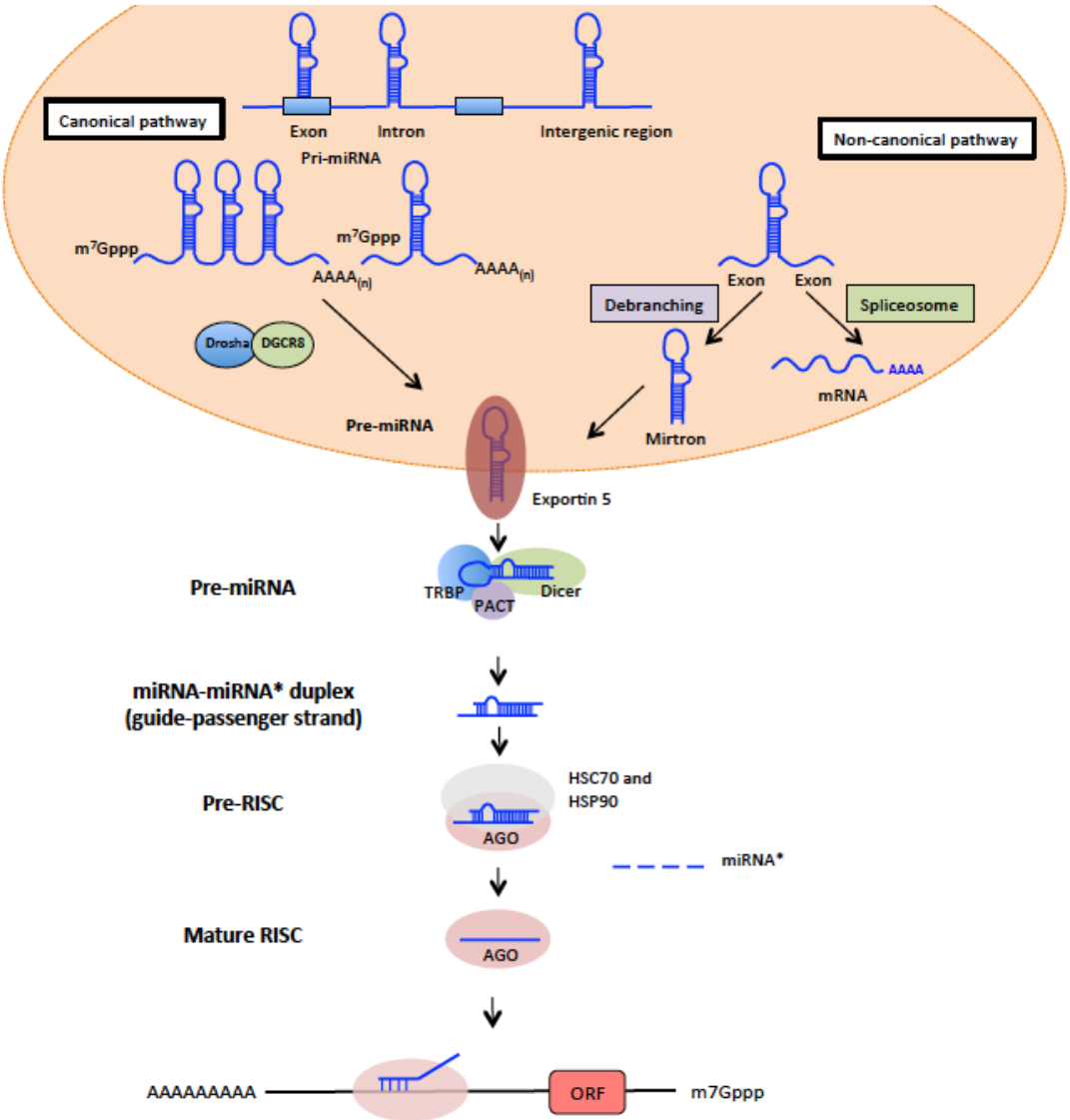

Figure 1.1 Schematic picture of miRNA biogenesis.
In the canonical pathway of miRNA biogenesis **(left)**, pri-miRNAs are transcribed by RNA pol II and contain a 7-methylguanosine cap (m7Gppp) and poly(A) tail at their 3'end. In the nucleus, the stem loop pri-miRNAs are cleaved by the endonuclease Drosha associating with DiGeorge syndrome critical region 8 (DGCR8) to become 60-70 nt pre-miRNAs. The pre-miRNAs are exported via exportin 5 from the nucleus into the cytoplasm where they are further cleaved by the endonuclease Dicer interacting with transactivation-response RNA-binding protein (TRBP) and protein activator of PKR (PACT) to generate a ~22 nt long miRNA:miRNA* duplex. The duplex is incorporated into the RISC with the support of the HSC70-HSP90 chaperone. The guide strand of the duplex remains associated to AGO, whereas the passenger strand (miRNA*) dissociates from the RISC and is subsequently degraded. The guide strand within the RISC binds to a target mRNA through base-pair complementarity. ORF: open reading frame. In the mirtron pathway **(right)**, a debranched intron (mirtron) from a mRNA resembles to the structure of a pre-miRNA and enters the miRNA-processing pathway independent of Drosha-mediated cleavage. This figure is adaped from (Ha and Kim, 2014; O'Carroll and Schaefer, 2013).

1.1.2 Regulatory functions of miRNAs

miRNAs regulate gene expression at the post-transcriptional level by binding to target mRNAs with Watson-Crick base-pair complementarity, usually within the 3'UTR of target mRNAs. Targeting specificity by miRNAs is generally dictated by the "seed sequence" at nucleotides 2 to 8 of the 5' end of miRNAs (Bartel, 2009). The modes of target repression in different organisms depend on the degree of complementarity between the miRNA and the target mRNA. In plants, perfect complementarity between miRNAs and mRNAs triggers mRNA degradation based on the endonuclease activity of AGO2. In animals, miRNAs generally bind with partial complementarity to target sites within the 3'UTR of mRNAs, resulting in mRNA destabilisation and translational suppression (Fabian et al., 2010), whereas the binding of miRNAs and targets at the 5' UTR leads to translation repression (reviewed in (Da Sacco and Masotti, 2012)). Although it is clear that miRNAs regulate gene expression post-transcriptionally, the mechanistic details of gene silencing are still under a debate with several proposed mechanisms involved in mRNA destabilisation/degradation and translational inhibition at initiation or elongation step (reviewed in (Ameres and Zamore, 2013).

1.1.2.1 miRNA-directed degradation of target mRNAs

In plants, miRNAs recognise fully or nearly complementary mRNA targets, and mediate endonucleolytic mRNA cleavage (Llave et al., 2002; Rhoades et al., 2002). In animals, miRNAs are partially complementary to the binding sites within target mRNAs and degradation of the mRNAs occurs via a 5' to 3' mRNA decay pathway whereby mRNAs are initially deadenylated by the CAF1–CCR4–NOT deadenylase complex (Fig 1.2) (reviewed in (Wilczynska and Bushell, 2015)). This process requires AGO and GW182 protein (Behm-Ansmant et al., 2006). GW182 is characterised by the presence of glycine and tryptophan repeats (GW repeats) and is crucially involved in miRNA-induced target mRNA repression. GW182, when associated with AGO, interacts with the poly (A) binding protein (PABPC) bound to poly(A) of a mRNA and recruits the CCR4-NOT deadenylase complex leading to deadenylation of the target mRNA (Behm-Ansmant et al., 2006; Braun et al., 2011; Chekulaeva et al., 2011). Further, the decapping process is mediated by the

decapping enzyme DCP2 enhanced by co-factor DCP1, DDX6 and EDC4. Subsequently, the decapped mRNAs are degraded by 5'-to-3' exonuclease XRN1.

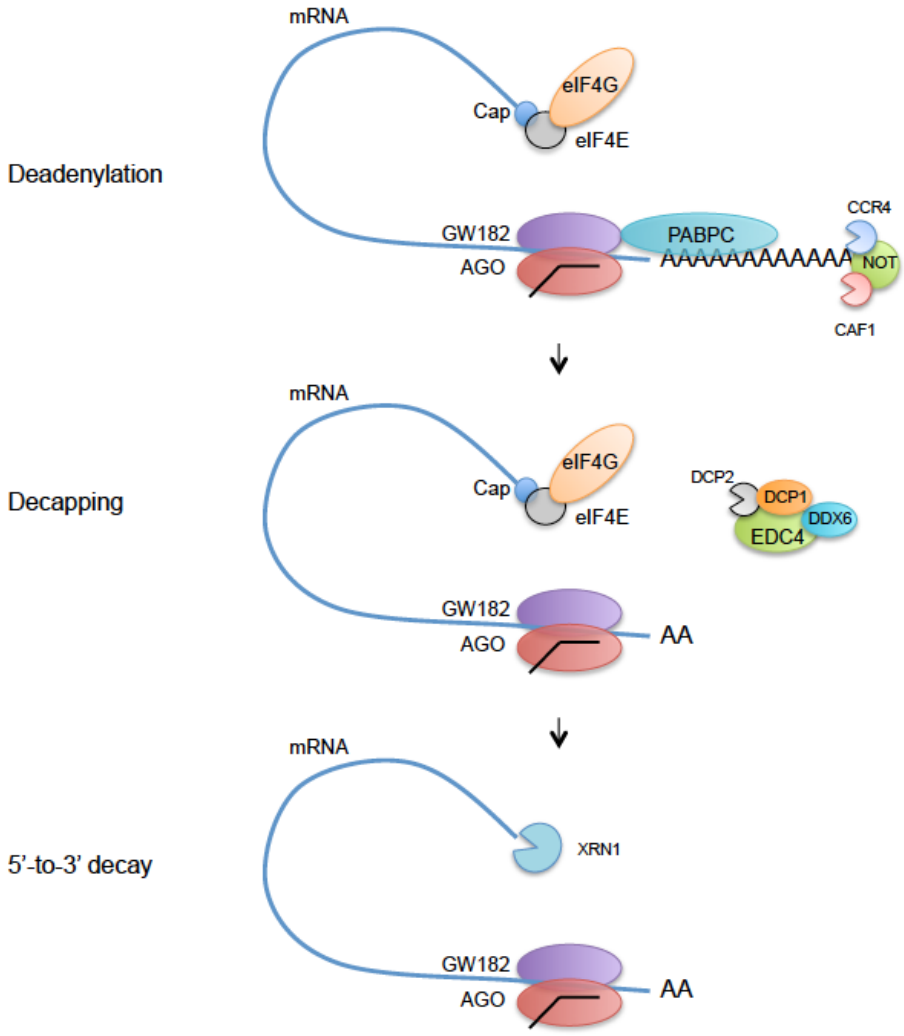

Figure 1.2 miRNAs-mediated mRNA degradation in animals
miRNAs bind to partially complementary sites within the 3'UTR of target mRNAs. GW182 associated with AGO interacts with PABPC bound to the poly(A) tails, leading to mRNA deadenylation. Following deadenylation, the mRNAs undergo decapping through the activity of the decapping enzyme 2 (DCP2) and associated cofactors (DCP1, DDX6 and EDC4). The mRNAs are then further degraded by the 5'-to-3' exonuclease XRN1. The figure is adapted from (Huntzinger and Izaurralde, 2011a).

1.1.2.2 miRNAs mediate translational repression

A number of studies have demonstrated that miRNAs repress translation; however, the mechanism of translation repression has remained unclear and controversial. It is important to note that a majority of studies has focused on miRNA regulating translation through the 3' UTR of target mRNAs and little is known about mechanism of miRNA-regulated translation via the 5'UTR of mRNAs. Several

models suggest that miRNAs repress translation at the initiation and post-initiation steps (reviewed in (Wilczynska and Bushell, 2015). To put in context the mechanism of miRNA-mediated translational repression, the basic mechanism of translation requires description. The predominant mode of translation is cap-dependent. The process is initiated by recognition of the 5' m7G by the cap-binding protein and eIF4E, which is a part of the eIF4F initiation complex. The eIF4F further recruits two complexes: a complex consisting of eIF3, the 40S subunit of the ribosome and the others containing eIF2, GTP and the methionyl-tRNA. The 40S subunit scans the mRNA to identify AUG. When AUG codon is located, the 60S subunit joins the initiation complex to proceed elongation phase of the translation (Kapp and Lorsch, 2004).

Using sucrose gradients to fractionate polysomes, Pillai *et al.* demonstrated that let-7 miRNA inhibited translation initiation through the observation that mRNAs expressed from the reporter vector containing binding sites of let-7 shifted to lighter fractions, which contain less ribosomes, compared to the control vector without the sites of let-7 (Pillai et al., 2005). Moreover, Humphreys *et al.* showed that the miRNA-mediated repression of mRNA translation required the 5' cap and the 3' poly(A) structure as the replacement of the 5'cap with an internal ribosome entry site (IRES) diminished the repression effect (Humphreys et al., 2005). In line with the previous studies, it was later shown that miRNAs interfere with translation initiation, specifically the 5'cap recognition process (Mathonnet et al., 2007). Presumably, miRNAs inhibit translation at the initiation step by interfering with the function of the cap-binding complex eIF4F (Ding and Grosshans, 2009; Zdanowicz et al., 2009).

In other studies however, it has been demonstrated that miRNAs repress translation at the post-initiation step. The first evidence for this was presented in *C.elegans* since no change of the lin-14 polysomal sedimentation profile was observed in response to lin-4 miRNA (Olsen and Ambros, 1999). In HeLa cells, the vast majority of three abundantly expressed miRNAs: miR-21, miR-17 and let-7 associated with mRNAs were found to be co-sedimented with the polysome fractions, suggesting that miRNAs bind to mRNAs that are being translated (Maroney et al., 2006).

As detailed above, it was historically thought that mammalian miRNAs regulate gene expression at the translation level (Olsen and Ambros, 1999). However, Guo *et al*. have shown that the reduction of protein mediated by miRNAs is a result of mRNA degradation. The authors compared data of ribosomal profiling, which involves sequencing ribosome-protected mRNA fragments (RPFs) to evaluate effects of miRNAs on protein production, to simultaneously measured mRNA levels. The effect of a miRNA on the protein production was calculated by dividing changes in RPFs with that of mRNA levels. The authors found that the decrease of mRNA levels accounted for ≥84% of the decrease of protein production, suggesting that destabilisation of mRNAs by miRNAs might explain the protein reduction (Guo et al., 2010).

However, further studies in zebrafish suggested that the translational inhibition could in fact cause mRNA degradation. (Bazzini et al., 2012; Giraldez et al., 2006). Ribosome profiling showed that miR-430 reduced occupancy of ribosomes on target mRNAs and later on caused mRNA decay (Bazzini et al., 2012). In line with this, kinetic studies of miRNA-mediated gene silencing in *D. melanogaster* and mammalian cells demonstrated that miRNAs initially repressed mRNA translation before triggering mRNA deadenylation and decay (Bethune et al., 2012; Djuranovic et al., 2012).

Based on the functions of miRNAs in regulation of gene expression through specific interactions with target mRNAs, cellular miRNAs have been reported to play a role in virus-host interaction by which miRNAs regulate cellular or viral gene expression. This interaction can lead to suppression or promotion of viral replication, depending on functions of cellular and viral genes contributing to the viral life cycle (reviewed in (Ghosh et al., 2009)). This thesis focuses on the miRNAs that have anti-viral activities.

1.1.3 Roles of host miRNAs in viral infection

Host miRNAs have been reported to be a part of host defences against viral infections, either by directly repressing expression of viral genes or by regulating host pathways involved in viral replication (Grassmann and Jeang, 2008; Skalsky

and Cullen, 2010). For example, miR-32 was reported to inhibit viral RNAs in retrovirus primate foamy virus type 1 (PFV-1), resulting in repression of viral growth in HeLa and baby hamster kidney cells (BHK-21). The virus contains several target sites of miR-32 including Gag, Pol, Env and Tas transcript and open reading frame 2 (ORF) shared by Bet and EnvBet protein (Lecellier et al., 2005). It has also been found that host miRNAs suppress viral RNAs in diverse viral infection including HIV-1, HCV, VSV, influenza, HBV and EEEV as summarised in Table 1.1. For example, in HIV-1 infection, resting primary CD4+ T cells a cluster of miRNAs are highly expressed that target the sequence near 3'ends of HIV-1 mRNAs, leading to inhibition of viral production (Huang et al., 2007). It is thought that these miRNAs (miR-28, miR-125b, miR-150, miR-223 and miR-382) are involved in the establishment of viral latency during the resting stage (Huang et al., 2007). Another example of regulation of HIV-1 replication by miRNAs has been published by Ahluwalia and colleagues. They showed that miR-29a targets the viral gene, *Nef* (Ahluwalia et al., 2008), a critical gene for progression of HIV-1 infection (Gorry et al., 2007). ELISA assays revealed that the regulation of *Nef* by miR-29a lead to a reduction in HIV-1 p24 antigen (Ahluwalia et al., 2008). Interestingly, miR-29a was found to enhance the association of HIV-1 mRNAs, RISC and P body protein RCK/p54, which plays a role in miRNA-dependent translational repression (Nathans et al., 2009). Collectively, it is clear that miRNAs can restrict viral gene expression via the direct association with viral RNAs.

Although there is evidence that host miRNAs can directly target viral RNAs leading to suppression of viral replication, it seems unlikely that host miRNAs specifically evolved to target certain viral genes, since due to the high mutation rate of viruses they could readily escape this targeting (Umbach and Cullen, 2009). For example, the stable expression of siRNAs-directed against the viral *Nef* gene of HIV induced a siRNA-resistant virus carrying mutations in or near the target sequences after several weeks in culture. This leads to attenuation of the anti-viral effects of the siRNA (Das et al., 2004; Westerhout et al., 2005). These data demonstrate that viruses could escape from inhibitory effects of RNA interference mediated by siRNAs and possibly miRNAs. Hence, if miRNA-binding sites are presented in viruses it seems

likely that they must confer some advantages to these viruses, as suggested by (Mahajan et al., 2009).

The other mechanism by which miRNAs can operate in host defense is through the regulation of host genes that are required for viral replication. During HIV infection, overexpression of two cellular miRNAs, miR-17-5p and miR-20 were demonstrated to target histone acetyltransferase p300/CBP-associated factor (PCAF), a cofactor of the viral transactivator protein Tat, leading to a dramatic reduction in HIV-1 production (Triboulet et al., 2007). Other evidence comes from Wang *et al*. who demonstrated that miR-100 and miR-101 regulate components of the mammalian target of rapamycin (mTOR) essential during HCMV infection, leading to attenuation of viral progeny production (Wang et al., 2008). More examples of miRNA-regulated cellular genes resulting in the inhibition of viral infection are provided in Table 1.2.

In addition to hosts, viruses, predominantly herpesviruses were also found to encode viral miRNAs using host miRNA biogenesis machinery to modulate expression of viral and host genes (reviewed in (Kincaid and Sullivan, 2012; Skalsky and Cullen, 2010). Studies of herpesvirus-encoded miRNAs have shown that viral miRNAs are involved in inhibition of apoptosis and latency. It was demonstrated that HCMV, KSHV and EBV encode miRNAs targeting pro-apoptotic host genes to prevent cell death. The viral miRNAs have been implicated in maintaining latent infection by which the miRNAs regulate either viral or host gene. For example, KSHV encodes two miRNAs: miR-K12-9-5p and miR-K12-7-5p that can regulate a lytic gene, RTA. KSHV also encodes several miRNAs to target host genes involved in latency. One of which is miR-K12-1-5p regulating IκBα, a critical regulator of NF-κB pathway, leading to attenuation of lytic activation.

Table 1.1 Host miRNAs targeting viral genes

Virus	miRNA	Target of miRNA	Reference
PFV-1 (primate foamy virus type 1)	miR-32	PFV-1 transcript	(Lecellier et al., 2005)
HIV-1 (human immunodeficiency virus type 1)	miR-28, miR-125b, miR-150, miR-223 and miR-382	3'ends of HIV-1 messenger RNAs	(Huang et al., 2007)
	miR-29a	Nef gene of HIV-1	(Ahluwalia et al., 2008)
HCV (hepatitis C virus)	miR-448	Core region in HCV genome	(Pedersen et al., 2007)
	miR-196	NS5A region in HCV genome	
	miR-199a	HCV-1b or -2a	(Murakami et al., 2009)
VSV (vesicular stomatitis virus	miR-24	Viral large protein (L protein)	(Otsuka et al., 2007)
	miR-93	Phosphoprotein (P protein) genes	
Influenza (H1N1)	miR-323, miR-491, miR-654	PB1 gene of H1N1 (encoding the subunit of viral RNA polymerase)	(Song et al., 2010)
HBV (hepatitis B virus)	miR-125a	HBV mRNA	(Potenza et al., 2011)
EEEV (Wild-type North American eastern equine encephalitis virus)	miR-142-3p	The 3'UTR of viral RNA genome	(Trobaugh et al., 2014)

Table 1.2 Indirect inhibition of viral replication by miRNAs targeting host genes

Virus	miRNA	Target of miRNA	Reference
HIV (human immunodeficiency virus type)	miR-17-5p and miR-20	Histone acetyltransferase PCAF, which is a cofactor for the viral transactivator protein Tat	(Triboulet et al., 2007)
HCMV (human cytomegalovirus)	miR100 and 101	The mammalian target of rapamycin (mTOR)	(Wang et al., 2008)
	miR-100	Rapter	
HBV (hepatitis B virus)	miR-155	Suppressor of cytokine signaling 1 (SOCS1)	(Su et al., 2011)
RSV (respiratory syncytial virus)	miR-221	Neurotrophin nerve growth factor (NGF)	(Othumpangat et al., 2012)
HCV (hepatitis C virus)	miR-27a	The lipid synthetic transcription factor RXRα and the lipid transporter ATP-binding cassette subfamily A member 1 (ABCA1)	(Shirasaki et al., 2013)

1.1.4 Host miRNAs influenced by viral infection

Accumulating evidence has shown that host miRNA levels are also regulated during viral infection and some are part of innate immune response. Studies of interferon (IFN)-induced gene expression have demonstrated that interferons can influence the expression of specific miRNAs together with other IFN-stimulated genes (ISGs). Interferons (IFNs) are a family of cytokines that play key roles in anti-viral defence (Randall and Goodbourn, 2008) and are classified into three types: I, II and III. Type I IFNs comprise IFN-α, IFN- β, IFN-ε, IFN-κ and IFN-ω. Among the five of Type I IFNs, IFN-α and IFN- β are directly induced in response to viral infection, whereas IFN-ε, IFN-κ and IFN-ω are not well characterised. IFN-γ is the only member of type

II IFNs and Type III IFNs consist of three members: IFN-λ1, IFN-λ2 and IFN-λ3 (reviewed in (Schneider et al., 2014)). Several studies have exclusively provided evidence that type I IFNs induce the expression of miRNAs upon viral infection, whereas the studies of type II and III IFNs were conducted in absence of viral infection. Pedersen *et al.* demonstrated that in HCV infection, IFN-β modulates the expression of a number of cellular miRNAs and eight IFN-β-induced miRNAs exert anti-viral effects against HCV (Pedersen et al., 2007). Likewise, cellular miR-29a is induced by IFN-α and IFN-β in HIV-infected cells and the expression of miR-29a suppressed HIV replication (Nathans et al., 2009). Another example of IFN-induced miRNAs was shown in cells infected with Sendai virus, a potent activator of IFN responses. In this study, it was demonstrated that miR-203 is dramatically induced (~15 fold) in virus-infected cells compared to mock infection, largely due to IFN-α induction upon infection; however, neither *in vitro* overexpression nor inhibition of miR-203 significantly impacted the viral replication compared to the control miRNAs (Buggele and Horvath, 2013).

Changes of miRNA expression following viral infection can also result from virus mechanisms. For example, miRNA cluster miR-17/92 was shown to be suppressed during HIV-1 infection compared to mock infection and the suppression of pri-miR-17/92 with siRNAs enhanced viral production (Triboulet et al., 2007). In HCMV-infected fibroblasts, miR-100 and miR-101 are downregulated. The authors hypothesised that HCMV selectively reduces miR-100 and miR-101 to help the viral replication since these miRNAs were shown to have anti-viral effects via regulation of mTOR (Wang et al., 2008). In human papillomavirus (HPV)-infected cells, a tumor-suppressive miR-34a was reduced as a result of viral protein E6 destabilising tumor suppressor p53, a known activator of miR-34a (Wang et al., 2009). A global miRNA expression analysis in HCMV and MCMV infection revealed that miR-199a-3p is downregulated upon infection and overexpression of this miRNA leads to a reduction in viral growth (Santhakumar et al., 2010). The anti-viral properties of miR-199a-3p could be relevant to its functions in regulation of genes involved in CMV infection such as viral entry and signaling pathway required for viral replication and survival (Santhakumar et al., 2010). Another anti-viral miRNA, miR-

27, was also found to be downregulated during MCMV infection by which the virus encodes a non-coding RNA, m169, to mediate the degradation of the miRNA; however, it is unclear why the virus specifically targets this miRNA, perhaps to interfere with functions of miR-27 to manipulate cellular processes disadvantageous to viral life cycle (Buck et al., 2010; Libri et al., 2012; Marcinowski et al., 2012). In addition, miR-27 was also inhibited by U-rich non-coding RNAs (HSURs1 and 2) of herpesvirus saimiri (HVS) (Cazalla et al., 2010). As mentioned above, it seems that many host miRNAs are regulated by members of herpesviruses, suggesting a mode of virus-host interaction and it would be interesting to study the significance of miRNA regulation in these viruses.

1.2 Herpesviridae

The herpesvirus family, *Herpesviridae*, is made up of large enveloped viruses (approximately 200 nm of diameter) with double stranded DNA genomes 120 to 240 kb in length. The virions are spherical and consist of four major components: the DNA core, capsid, tegument and lipid bilayer envelope (Fig 1.3). The DNA core contains a single copy of linear double-stranded DNAs. Surrounding the core, the capsid is an icosahedron constructed of 162 capsomeres containing capsid proteins (reviewed in (Arvin et al., 2007)). The tegument surrounding the capsid consists of thirty or more viral proteins that have been shown to play diverse roles in the viral life cycle such as capsid transportation (Pasdeloup et al., 2013), viral DNA packaging (Thurlow et al., 2005) and latency (Penkert and Kalejta, 2011). The envelope is the outer part of viruses and is composed of viral glycoproteins and the host membrane.

The herpesvirus family is divided into three subfamilies based on their biology and genome characteristics: *Alpha*-, *Beta*-, and *Gamma-herpesvirinae* (Table 1.3). The three subfamilies exhibit common viral structures, genome replication processes as well as similar entry and egress mechanisms. Gene products common to all families include envelope glycoprotein B, DNA polymerase, alkaline exonuclease and single stranded DNA-binding proteins. The homology of these common gene products

suggests similarities of the viral life cycle across the diverse viruses involving viral entry, DNA replication and viral assembly (Arvin et al., 2007).

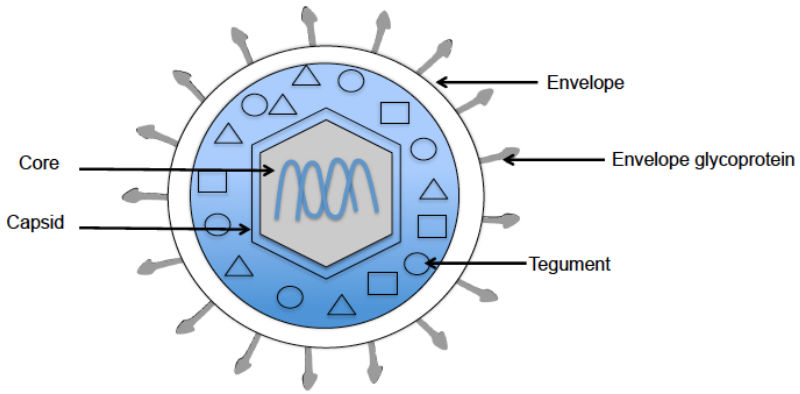

Figure 1.3 Diagram depicting structure of herpesviruses
Herpersvirus particles consist of four distinct structures: the core, capsid, tegument and envelope. This figure is adapted from (Amen and Griffiths, 2011).

Table 1.3 The characteristics of three herpesvirus subfamilies

Characteristic	*Alphaherpesvirinae*	*Betaherpesvirinae*	*Gammaherpesvirinae*
Host range	Variable host	Very restricted host range	Very restricted host range
Replicative cycle	Short replicative cycle (hours)	Long replicative cycle (days)	Short replicative cycle
Latent infection	Sensory ganglia	Endothelial cells and myeloid cells (particularly monocyte and macrophage lineage)	T or B lymphocytes
Viruses infecting human	HSV-1, HSV-2, VZV	HCMV, HHV-6A, HHV-6B, HHV-7	EBV, KSHV

Summarized from (Arvin et al., 2007)

HSV: Herpes simplex virus
VZV: Varicella-zoster virus
HCMV: Human cytomegalovirus
HHV: Human herpes virus
EBV: Epstein-Barr virus
KSHV: Kaposi's sarcoma-associated herpesvirus

1.2.1 Human Cytomegalovirus (HCMV)

Human cytomegalovirus (HCMV) is a member of the *Betaherpesvirinae* subfamily that infects approximately 40-100% of the world's population indicated by the presence of CMV antibody in the blood (Mocarski, 2007). After a primary infection, HCMV establishes lifelong latency that usually causes mild or subclinical diseases in immunocompetent hosts. However, the virus can result in more serious conditions in immunocompromised patients such as patients with HIV and organ transplant recipients who are receiving immunosuppressive therapy (Hodinka, 2007). The clinical manifestation of HCMV infection is found in up to 40% of patients with advanced HIV infection with symptoms including retinitis, colitis, esophagitis, pneumonitis and neurological disorders (Cheung and Teich, 1999). In haematopoietic stem-cell transplantation, pneumonitis caused by HCMV is associated with a high mortality rate (Chaisson et al., 1998).

In developed countries, HCMV is the most common congenital infection with an estimated prevalence between 0.5% and 2% (Demmler, 1996). A literature review of 11 studies conducted in developing countries in Africa, Asia and Latin America revealed that maternal CMV seroprevalence ranged from 84% to 100% and CMV birth prevalence varied from 0.6% to 6.1% (Lanzieri et al., 2014). HCMV can be transmitted from mother to child via three routes 1) intrauterine, 2) intrapartum and 3) post-natal (breast-feeding), leading to birth defects. It was found that CMV-infected neonates with symptomatic diseases show sensorineural hearing loss, microcephaly, motor defects, mental retardation, chorioretinitis and dental defects. Although ~90% of infants born in the USA with congenital CMV infection do not show clinical manifestations, they are at high risk for hearing loss (reviewed in (Nassetta et al., 2009)).

Moreover, studies in human malignancies indicated the presence of HCMV DNA, mRNA and viral proteins in certain tumours including breast cancer (Herbein and Kumar, 2014) and glioblastoma (Cobbs et al., 2002). However, the mechanism by which HCMV might contribute to oncogenesis is still elusive. Based on the fact that HCMV is not an oncogenic virus, it was postulated that the virus might modulate

cellular processes such as cell proliferation, differentiation, migration and angiogenesis, contributing to the progression of tumours (Michaelis et al., 2009).

1.2.2 Mouse cytomegalovirus (MCMV) as a model study for HCMV

Because CMVs are highly host-specific, HCMV cannot be used in any animal model. Thus, MCMV has become an invaluable model for the study of HCMV since it shares many features with HCMV infection of humans. MCMV and HCMV share approximately 78 homologous open reading frames (ORFs), accounting for ~50% of total ORFs encoded by these viruses (Brocchieri et al., 2005; Rawlinson et al., 1996). As both MCMV and HCMV belong to *β-herpesvirinae,* they exhibit the similar features including the viral structure, biology, and the ability to establish persistent and latent infection in their respective host species (reviewed in (Shellam et al., 2007)). More importantly, MCMV develops pathogenesis in mice similar to that of HCMV in humans such as congenital infection, retinitis, hepatitis, myocarditis and atherosclerosis (reviewed in (Shellam et al., 2007)). Thus, this model provides an excellent tool for the study of virus-host interaction.

Below is more detailed introduction to the genomic features of CMV, its life cycle and its impacts on host cell biology. Where possible studies with MCMV are cited however given that there is more information on HCMV.

1.2.3 Biology and life cycle of CMV

1.2.3.1 CMV genome

Genome of HCMV and MCMV is a linear DNA approximately 235 kb. The genome of HCMV encodes an estimated 165-252 open reading frames (ORFs) (Davison et al., 2003; Murphy et al., 2003) and that of MCMV was shown to transcribe 172 ORFs(Tang et al., 2006). The genome of HCMV is organised into two unique regions: long (U_L) and short unique regions (U_S) that both are flanked by direct repeats (TR_L and IR_L; TR_S and IR_S), yielding the overall genome configuration TR_L–U_L-IR_L-IR_S-U_S-TR_S (Davison et al., 2003). Fig 1.4 presents the genome structure of HCMV laboratory stain, AD169 as an example. To date, six strains of HCMV have been sequenced: two laboratory strains (AD169 and Towne) and four clinical

isolated strains (Toledo, FIX, PH, and TR) (Shenk T.E, 2008). The first complete genome sequence of HCMV was obtained from the laboratory-adapted strain AD169 that had been extensively passaged in human fibroblast cell lines (Bankier et al., 1991; Chee et al., 1990). When seronegative individuals were infected with AD169 during the vaccine studies, the virus caused no or very low virulence (Neff et al., 1979). DNA sequencing data of a clinical strain Toledo, which had been passaged significantly less than AD169 revealed that Toledo contains an extra 15 kb at the 3'end of U_L, encoding for additional 19 ORFs (Cha, 1996). This indicates the genetic loss in AD169 is due to the selection that occurs during passaging in human fibroblasts and suggests that this 15 kb long fragment is essential for the virulence *in vivo* (Prichard, 2001). The details of genomic rearrangements and protein-coding ORFs of each strain are further described in (Shenk T.E, 2008). Unlike the HCMV genome, MCMV genome does not have the long unique regions and it consists of a single unique sequence with short terminal direct repeats and several short internal repeats (Shellam et al., 2007).

CMV genomes contain cis-acting elements responsible for DNA replication, packing and transcription. In HCMV genome, the replication origin (ori*Lyt*) is mapped to an approximately 1500 bp domain, situated close to the middle of the U_L domain, whereas a latency origin has not been identified. Due to evolutionary conservation of herpesviruses, the genome of HCMV contains ORFs common to all herpesviruses encoding for core functional proteins involved in viral DNA replication and assembly. The U_L domain contains 40 core HCMV genomes and the U_S domain accommodates CMV-specific genes that are usually nonessential for the viral replication in cell cultures (Shenk T.E, 2008).

Figure 1.4 Conventional ORF map of HCMV AD169 laboratory strain
The genome of AD169 is organised as two regions: unique long (UL) and unique short (US). The UL and US are flanked by two sets of inverted repeats (TRL/IRL) and IRS/TRS, respectively. The UL region contains 132 ORFs and US domain comprises 34 ORFs. This figure is adapted from (Shenk T.E, 2008).

1.2.3.2 CMV life cycle

Like other viruses, CMV is an obligate intracellular pathogen that requires host cells to produce viral progenies. The major steps of the infection involve virus entry, the release of virus content into cells, virus DNA replication, virus assembly and the release of virions from the cells (Fig 1.5). HCMV has been shown to enter the cells through either membrane fusion in fibroblasts or endocytosis of epithelial cells via the interaction of enveloped glycoproteins with receptors of host cells (Bodaghi et al., 1999; Conti et al., 2000). The most abundant and essential glycoproteins of HCMV entry are gB (UL55), gM:gN (UL100:UL73) and gH:gL (UL75:UL115) (Mocarski ES, 2007). At viral entry, HCMV glycoproteins interact with multiple host receptors. The ability of HCMV to infect a wide variety of cells suggests the presence of a number of the cellular receptors. Many studies have identified receptors in permissive cells for HCMV infection. Initially, the virus interacts with heparin sulfate proteoglycans (HSPGs) on the cell surface, mediated by gB and gM (Compton et al., 1993). Following the viral attachment, it is thought that the virus required other cellular receptors for viral entry, including EGFR and integrin heterodimers (Wang and Shenk, 2005). In the case of MCMV, MHC I, beta-2-microglobulin heparan sulfate proteoglycans were shown to facilitate entry of MCMV *in vitro* (reviewed in (Shellam et al., 2007)).

Once the virus enters the host cell, viral teguments are released into the cytoplasm. The teguments associate with the microtubule network and play a role in

transportation of the viral capsid from the cytoplasm to the nucleus where viral DNA replication takes place (Wolfstein et al., 2006). The viral genes are expressed in the following order: immediate-early genes encoding essential regulatory proteins, early genes encoding enzymes for viral DNA replication and late genes encoding viral structural proteins. The first viral genes that are expressed after infection are immediate early genes (IE): IE1 and IE2 in HCMV, or IE1 and IE3 in MCMV, and their expression does not require *de novo* viral protein synthesis. The function of IE genes is to optimise cells for expression of other viral genes and DNA replication. The expression of IE2 mRNA is predominant during the first two hours of the infection and the IE1 expression peaks at later time points between six to eight hours post-infection (hpi) (Stamminger et al., 1991). The IE1 and IE3 protein of MCMV are detected at ~3 hpi and shown to gradually increase over time of infection up to 72 h (Martinez et al., 2010). It appears that IE1 of HCMV is required for infection at low MOI (0.001 to 0.05 PFU/ml), enhancing the potency of IE2 (Greaves and Mocarski, 1998; Mocarski et al., 1996), whereas the absence of IE1 gene is dispensable at high MOI (1 to 5 PFU/cell). The knowledge of IE1 function is not completely understood; however, the possible function of IE1 protein (IE72, 72 kDa) may be involved in anti-apoptosis and promotion of host cell conditions for viral replication (Zhu et al., 1995). It was proposed that the IE1 activates cellular promoters by association with TATA box-associated factors (TAFs) and transcription factors (Sp-1, E2F-1, CTF-1) (Hayhurst et al., 1995; Lukac et al., 1997; Margolis et al., 1995). In addition, IE1 protein was demonstrated to have kinase activities to phosphorylate Rb family (p107 and p130) and the E2F transcription factor, leading to activation of transcription (Pajovic et al., 1997).

HCMV IE2 gene and its functional homologue IE3 in MCMV are absolutely essential for the cascade of viral gene expression and the efficiency of viral replication. The activation of viral early genes along with cellular genes is required in order to prepare the cell for viral DNA synthesis (Shenk T.E, 2008). The DNA synthesis is initiated at the lytic replication origin (oriLyt) (Shenk T.E, 2008). Lastly, the late genes coding structural proteins for virions are expressed.

In the nucleus, the viral DNA is encapsidated into procapsids, giving rise to

nucleocapsids. Once the viral DNA is packed, the nucleocapsid interacts with tegument proteins as well as non-structural proteins. The nucleocapsid passes into the perinuclear space through the inner nuclear membrane, leading to the primary envelopment. The viral particle in the perinuclear space then buds through the outer nuclear membrane and becomes the non-enveloped cytoplasmic particle. Once in the cytoplasm, the nucleocapsid buds into the Golgi apparatus-derived vesicles containing viral glycoproteins, resulting in re-envelopment. The vesicles containing the mature virions are transported to the cell surface to release the virions by fusion of an exocytic vesicle with the plasma membrane (Arvin et al., 2007).

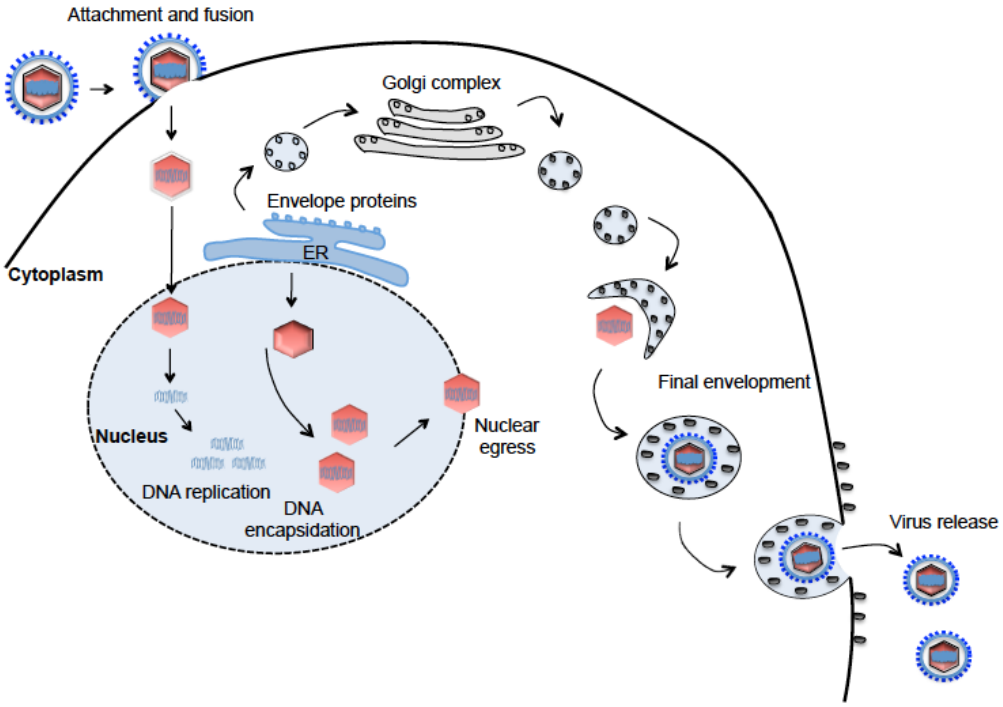

Figure 1.5 CMV life cycle
The virus enters the cell via membrane fusion or using viral glycoproteins to bind to receptors on the cell membrane. This figure shows membrane fusion as an example. The viral envelope fuses with the cell membrane and the nucleocapsid is released into the cytoplasm. The nucleocapsid is translocated into the nucleus where viral DNA is released. In the nucleus, viral and cellular genes are expressed and viral DNA is replicated. The viral DNA is transcribed into the late mRNAs coding for capsids and envelope proteins. The capsid proteins are imported from the ER into the nucleus where the newly synthesised genomes are encapsidated. This capsid egresses from the nucleus into the cytoplasm and buds into the Golgi apparatus-derived vesicle. The vesicle containing virions is transported to and fuses with the plasma membrane to release the infectious virus from the cell. This figure is adapted from (Li and Hayward, 2013).

Both HCMV and MCMV have a number of effects on host cellular pathways by which the viruses manipulate biological processes of host cells to achieve conditions advantageous to infection. This thesis focuses on the cell cycle and the p38 mitogen-activated protein (MAP) kinase signalling pathway that have been reported to be manipulated by the virus and this is important for viral replication.

1.2.4 Manipulation of the cell cycle by CMV

CMV has a complex relationship with the host cell and has evolved numerous strategies that allow it to effectively replicate and disseminate within the host. It is known that HCMV manipulates the host cell cycle from the first stage of the infection, controlling the checkpoints of the cell cycle to create conditions optimal for viral replication. In addition, manipulation of the cell cycle by HCMV may inhibit apoptosis to allow the virus sufficient time for the assembly (Shenk T.E, 2008). Likewise, MCMV was shown to arrest the cell cycle and allowed replication of the virus during the arrest (Wiebusch et al., 2008).

1.2.4.1 The eukaryotic cell cycle

The cell cycle is a vital biological process whereby the cell prepares for division. Cell division is separated into four phases: G1 (Gap1), S (Synthesis), G2 (Gap2) and M (Mitosis) (Fig 1.6). Before G1, G0 is an additional state of temporary or permanent quiescence by which the cell is withdrawn from the cell cycle. The G0 cell can enter the cell cycle when the cell is induced by proliferative signals such as growth factors and serum. The transition of cell cycle phases is tightly regulated by a family of cyclin-dependent kinases (CDKs) whose activity is dependent on their association with a cyclin protein (reviewed in (Lim and Kaldis, 2013; Malumbres and Barbacid, 2009)). Upon the stimulation of G0 cells, CDK4/6 is expressed and forms a complex with cyclin D, inducing cells to enter into G1. The complex of CDK4/6 and cyclin D phosphorylates the tumour suppressor retinoblastoma (Rb), which forms a complex with the E2F family of transcription factors. The phosphorylated Rb liberates E2F, activating transcription of essential genes. The G1 phase is the state when the cell expresses genes that are involved in nucleic acid metabolism and DNA replication. Thus, the cell is metabolically active and grows, but does not synthesise DNA. At the late phase of G1, cyclin E expression is induced

and associates with CDK2 to form the CDK2/cyclin E complex, which promotes the transition into S phase. In S phase, cyclin A is induced and forms a complex with CDK2, promoting DNA replication. The cell with a newly complete set of chromosomes enters G2 phase when the cell accumulates proteins involved in mitosis (M phase). The progression from G2 to M is mediated by CDK1/cyclin B or CDK1/cyclin A which phosphorylate many substrates essential for condensation and segregation of the chromosomes to daughter cells. At late mitosis, CDK1 is inactivated by degradation of cyclin B and cyclin A through the anaphase-promoting complex (APC) E3 ubiquitin ligase and the proteasome (Morgan, 1999).

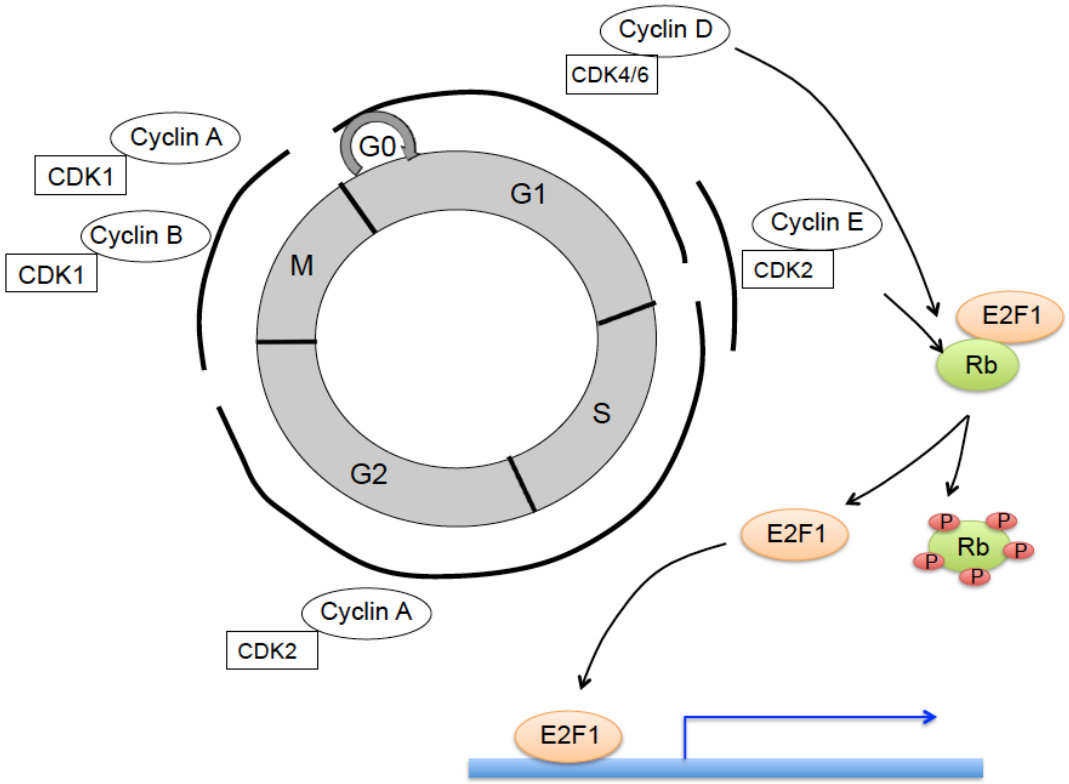

Figure 1.6 The eukaryotic cell cycle
The cell cycle contains four major phases: G1 (Gap1), S (Synthesis), G2 (Gap2) and M (Mitosis). G0 is an additional phase when the cell is in quiescence. The progression through different phases of the cell cycle is strictly regulated by CDK-cyclin complexes. In response to mitogenic signals, cyclin D is synthesised and binds to CDK4/6, directing CDK4/6 to phosphorylate the tumour suppressor Rb. The hyperphosphorylated Rb liberates E2F transcription factor, inducing expression of genes essential for cell cycle progression. CDK2/cyclin E functions at the G1/S transition and triggers the entry into S phase. CDK2/cyclin A collaborates with CDK2/cyclin E to regulate DNA replication. CDK1/cyclin B and CDK1/cyclin A are responsible for mitosis.

1.2.4.2 Effects of CMV on the cell cycle

A number of studies have shown that HCMV has profound effects on the cell cycle although it is still a matter of controversy whether HCMV arrests or promotes the cell cycle since Salvant *et al.* have demonstrated that HCMV affects several points of the cell cycle depending on the cell cycle phase in which the virus infects. The authors showed that infection of cells in G0 and G1 leads to a severe impairment of cellular DNA synthesis, whereas cells infected near or during S phase can proceed through S phase and mitosis prior to cell cycle arrest in G1 at 24 hpi (Salvant et al., 1998). Studies have demonstrated that HCMV causes G1 arrest that is concomitant with the induction of cyclin E and its binding partner CDK2 (Bresnahan et al., 1996; Jault et al., 1995). This evidence is unexpected however because the primary role of cyclin E/CDK2 is to promote the G1/S transition. Importantly, it was shown that cyclin E/CDK2 is required for HCMV DNA replication. The authors showed that transfection of a vector encoding CDK2 mutant followed by HCMV infection leads to suppression of viral replication compared to cells transfected with wild type CDK2 (Bresnahan et al., 1997). The Rb-related protein p107 and Rb are implicated as negative regulators of the cell cycle via interaction with the E2F family of transcription factors. In addition to HCMV-mediated induction of cyclin E/CDK2 levels, it has been reported that viral immediate early protein IE72 and IE86 mediate the G1/S progression by binding to p107 (Poma et al., 1996) and pRB (Hagemeier et al., 1994), respectively. This leads to the release of E2F transcription factors, activating the expression of S-phase genes including cyclin E, thus indicating that IE proteins are also involved in the regulation of cyclin E/CDK2. Taken together, it seems that HCMV specifically induces the certain regulators of the cell cycle (cyclin E and CDK2), presumably to provide a cellular environment at the G1/S boundary that can be exploited by the virus for DNA replication.

In contrast to the ability of IE72 and IE86 to promote the G1/S transition, it was shown that the viral protein IE86 induces G1 arrest in several cell lines (Wiebusch and Hagemeier, 1999). Other groups have shown that IE72 (Muganda et al., 1994) and IE86 (Bonin and McDougall, 1997; Muganda et al., 1994; Speir et al., 1994) increase the level of p53, the tumour suppressor that functions as a transcription

factor inducing expression of genes involved in various cellular processes including the cell cycle arrest, apoptosis and senescence (Giono and Manfredi, 2006). In addition to IE proteins, the viral capsid protein UL69, a homologue of the herpes simplex virus ICP27 protein was shown to induce G1 arrest (Hayashi et al., 2000; Lu and Shenk, 1999). Deletion of UL69 impaired viral DNA replication, suggesting the significance of cell cycle regulation during infection. Similar to G1 arrest in HCMV infection, MCMV was also shown to arrest cells in both G1 and G2 phase and that is dependent on MCMV IE3, the homologue of HCMV IE2 (Wiebusch et al., 2008).

Interestingly, several studies have shown that although HCMV induces S-phase entry, it blocks further progression of the cell cycle and inhibits cellular DNA synthesis (Bresnahan et al., 1996; Dittmer and Mocarski, 1997; Murphy et al., 2000; Wiebusch et al., 2003a). Thus, this strategy probably allows virus to avoid competing with cellular DNA synthesis, providing further resources for viral DNA replication. The ability of HCMV to block cellular DNA synthesis is linked to the assembly of pre-replication complexes (preRCs), critical protein complexes for the initiation of cellular DNA replication. Two independent studies have demonstrated that the virus interferes with the loading of the mini-chromosome maintenance (MCM) complex into preRCs, inhibiting the activation of replication (Biswas et al., 2003; Wiebusch et al., 2003b). Biswas *et al.* observed the reduction of the chromatin licensing and DNA replication factor 1 (Cdt1), which plays a role in the loading of the MCM proteins (Biswas et al., 2003). Moreover, the authors observed the accumulation of a replication inhibitor geminin (Biswas et al., 2003). Collectively, the data suggest that the virus has evolved multiple strategies to dysregulate the host cell cycle.

1.2.5 Manipulation of the p38 mitogen-activated protein (MAP) kinase signalling pathway by CMV

The MAP kinase signalling is a signal transduction pathway that mediates a wide variety of cellular processes in response to extracellular stimuli such as growth factors, mitogens and stresses (reviewed in (Dhillon et al., 2007; Morrison, 2012)). Four distinct cascades within the MAP kinase signalling have been identified: p38, JNKs, ERK1/2 and ERK5. In response to stimuli, the signalling cascade is initiated by activation of a small G protein and/or phosphorylation by kinases downstream

from cell receptors (Fig 1.7). This leads to sequential activation of MAP kinase kinase kinase (MAPKKK), MAP kinase kinase (MAPKK) and MAP kinase (p38, JNKs, ERK1/2 and ERK5). Depending on cell lines and types of stimuli, each cascade can regulate several distinct or overlapping cellular processes. Activation of p38 usually contributes to inflammation, apoptosis, cell differentiation, and cell cycle regulation. Similarly, JNKs plays a role in apoptosis, inflammation, cytokine production and metabolism. The ERK1/2 induces cell growth and differentiation. The ERK5 has been implicated in survival, proliferation and cytoskeleton remodelling (Nithianandarajah-Jones et al., 2012).

In mammals, the family of p38 MAP kinase consists of four members: p38α, p38β, p38γ and p38δ sharing ~60% identity in their amino acid sequence with the conserved Thr-Gly-Tyr (TGY) phosphorylation motif in the activation loop (reviewed in (Cuenda and Rousseau, 2007; Zarubin and Han, 2005)). Among the four isoforms, p38α is the most extensively characterised and ubiquitously expressed in most cell types. The p38 MAP kinase signalling are strongly activated by environmental stresses and inflammatory cytokines. Upon stimulation, the TGY motif of p38 MAP kinase is dually phosphorylated by MKK3 and MKK6. The activated p38 MAP kinase then can phosphorylate a number of target proteins through a specific interaction of the substrate binding motif within p38 MAP kinase and a docking domain present on the substrate. Numerous substrates of p38 MAP kinase have been identified such as transcription factors, other kinases that can phosphorylate transcription factors, cytoskeletal proteins and components of translational machinery (summarised in (Cuenda and Rousseau, 2007), indicating that multiple cellular functions are regulated by p38 MAP kinase signalling.

In the context of HCMV infection, the virus has been shown to activate p38 MAP kinase signalling, which was also shown to be important for viral DNA replication. Johnson *et al.* showed that the virus mediates p38 MAP kinase activation by two distinct mechanisms (Johnson et al., 2000). At an early time point of the infection (8 to 14 hpi) the virus inhibits dephosphorylation of p38 MAP kinase, whereas at the late time point of the infection (48 to 72 hpi) the virus induces activity of MKK3 and MKK6, the upstream regulators of p38 MAP kinase. The authors also showed that

HCMV-activated p38 MAP kinase leads to an increase in phosphorylation of the Rb and heat shock protein 27 (HSP27), and proposed that requirement of p38 MAP kinase by the virus might be related to the cell cycle function of Rb and a role of HSP27 in inhibition of apoptosis (Johnson et al., 2000). Likewise, MCMV was found to increase phosphorylation of p38 MAP kinase (~1.7 fold) in aortas of virus-infected mice compared to uninfected mice at 2.5 months post infection. Inhibition of p38 MAP kinase using the p38 inhibitor SB203580 leads to a reduction of viral load (~12 fold) in aortas of mice treated with the inhibitor compared to untreated mice, suggesting a significance of p38 MAP kinase pathway in MCMV replication. Due to numerous biological processes that p38 MAP kinase signalling involved in, it seems likely that CMV-activated p38 MAP kinase links to multiple cellular processes contributing to infection and replication of the virus. Identification of such cellular processes will provide insight into the complex interaction between CMV and host cells.

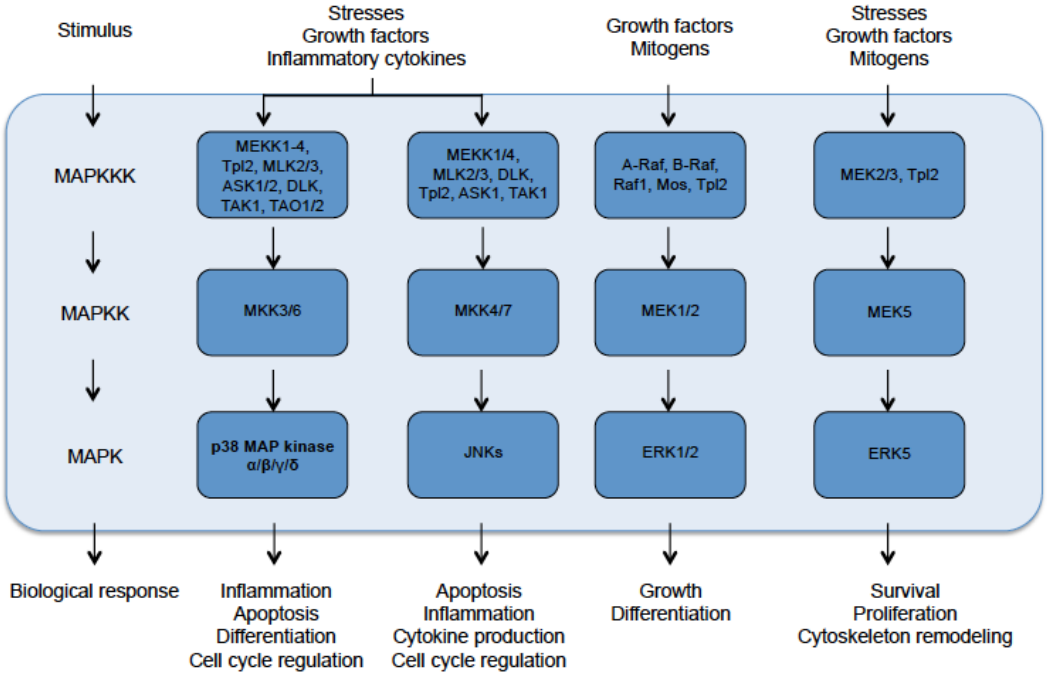

Figure 1.7 MAP kinase pathways
Each of MAP kinases contains three tiers of protein kinases (MAPKKK, MAPKK and MAPK). The signal transduction is mediated by sequential phosphorylation and activation of protein components within the cascades, leading to biological responses towards stimuli. This figure is adapted from (Morrison, 2012).

1.3 miR-27

miR-27 consists of two mature forms: miR-27a and miR-27b. miR-27a is derived from an intergenic miR-23a~27a~24-2 gene cluster on chromosome 8 in mouse or chromosome 19 in human, whereas miR-27b arises from an intronic miR-23b~27b~24-1 cluster on chromosome 13 in mouse or chromosome 9 in human (Fig 1.8A). Alignment of the mature sequences of these miRNAs shows that they are highly conserved in vertebrates (Fig 1.8B). The miR-23a~27a~24-2 cluster encodes pri-miRNA transcript containing 3 miRNAs: miR-23a, miR-27a and miR-24-2. The pri-miRNA of miR-23b~27b~24-1 gives rise to the mature miR-23b, miR-27b and miR-24-1. Based on sequence alignments, mature miR-27a and miR-27b differ by 1 nt at position 3 from the 3' end. Similarly, miR-23a and miR-23b differ by 1 nt, whereas the sequences of miR-24-1 and miR-24-2 are identical (Fig 1.8C) (Zhou et al., 2011). miRNAs are classified into a family based on similarity of the seed sequences and similar biological functions (Kozomara and Griffiths-Jones, 2011). Since the seed sequences of each miRNA in the same families (such as miR-23a/b or miR-27a/b) are identical, the miRNA target prediction database (such as TagetScan) predicts the same targets for both isoforms. Thus, the differential expression of miRNA isoforms in the cell of interest is an important factor that needs to be taken into consideration when determining the effect one miRNA has on potential targets. In case of miR-27, the analysis of expression patterns using public small RNA sequencing databases revealed that miR-27a and miR-27b are equally abundant (Liang et al., 2014), with high expression levels in the lungs, the heart and numerous cell types such as endothelial cells and various cancers (Zhou et al., 2011).

A study of miR-23a~27a~24-2 cluster gene revealed that its promoter contains GC boxes instead of specific DNA elements such as TATA box, the initiator element, the downstream promoter element (DPE), downstream core element (DCE), and the MED-1 (multiple start site element downstream) (reviewed in (Chhabra et al., 2010). This CG region was thought to be a binding site of transcription factors and could be involved in regulation of the cluster. Although a single pri-miRNA cluster gives rise to two or more miRNAs, it was shown in many cases that the expression levels of mature miRNAs derived from the same cluster are not always related to each other

(reviewed in (Bartel, 2004)), suggesting post-transcriptional mechanisms for differential expression. Indeed, Chhabra *et al.* overexpressed the pri-miR-23a~27a~24-2 cluster and observed increased expression of miR-27a and miR-24-2 but not miR-23a (Chhabra et al., 2009).

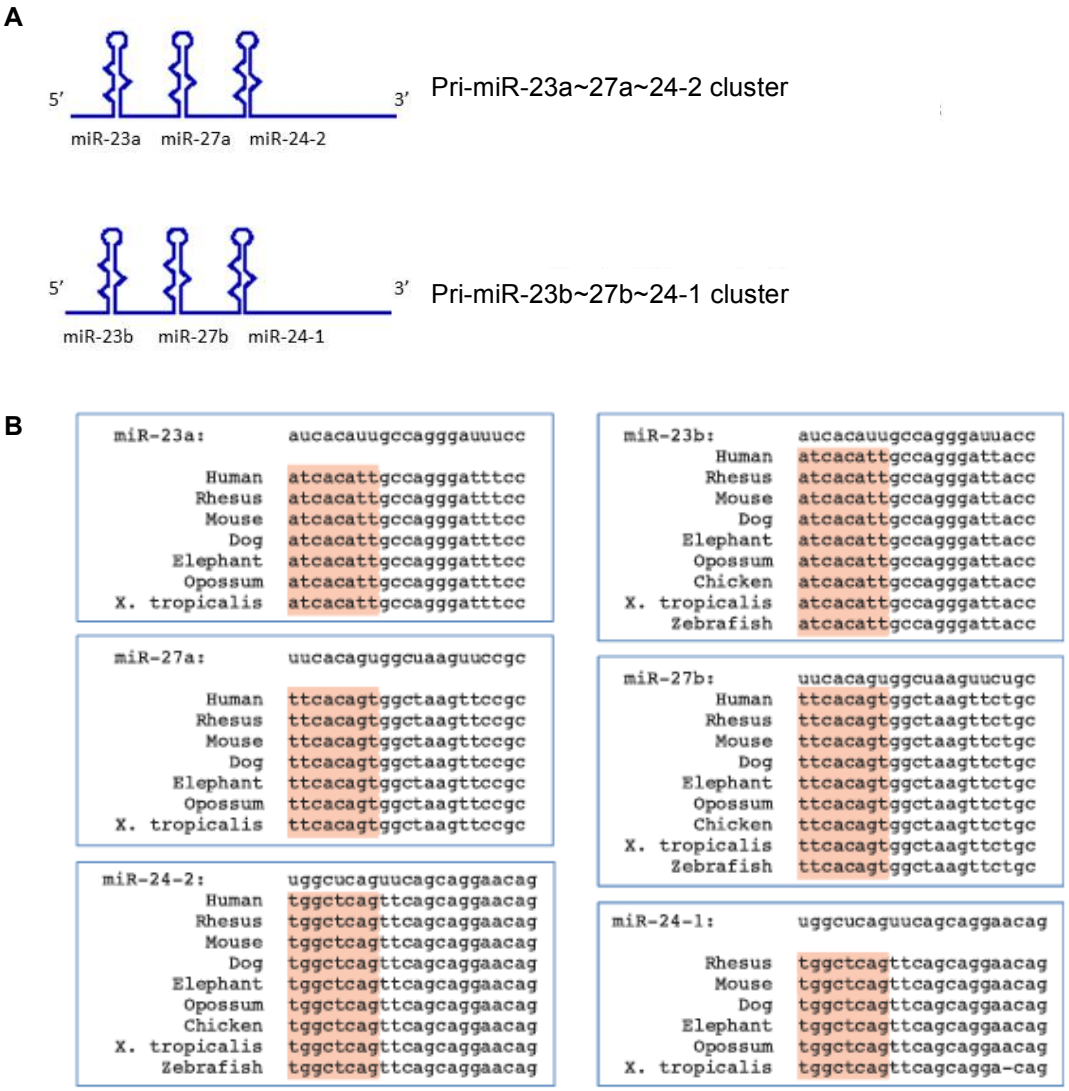

Figure 1.8 Hairpin structures of pri-miR-23a~27a~24-2 and pri-miR-23b~27b~24-1, and nucleotide alignment of mature miR-23, miR-27 and miR-24

(A) Schematic representation of pri-miR-23a~27a~24-2 and pri-miR-23b~27b~24-1. **(B)** The alignment of the mature miRNAs among seven species indicates that they are highly conserved. The seed sequences are highlighted in orange. **(C)** The alignment of mature mouse miR-23a/b and miR-27a/b indicates only one nucleotide difference as shown in red, whereas the sequence of miR-24-1 and miR-24-2 are identical. The figure B and C are taken from (Zhou et al., 2011).

To date, an increasing number of functions of miR-27 has been reported in diverse biological processes ranging from fundamental biological processes such as cell proliferation, metabolism and differentiation, to the involvement in human diseases (Table 1.4).

Two independent studies have shown that miR-27 is a negative regulator of adipogenesis and adipocyte differentiation (Kim et al., 2010; Lin et al., 2009). Both studies demonstrated that miR-27 regulates peroxisome proliferator-activated receptor gamma (PPARγ) and C/EBPα, crucial regulators of adipogenesis. *In viv*o experiments showed that the expression of miR-27 was significantly increased in the epididymal fat tissue of genetically obese mice compared to the genetically matched lean mice with the same gender and age, indicating that obesity induces a negative regulator of adipose tissue miR-27 (Lin et al., 2009). More recently, Kang *et al* demonstrated that miR-27 also inhibited adipocyte differentiation via prohibitin (PHB) in human adipose-derived stem cells (Kang et al., 2013).

miR-27 is highly expressed in endothelial cells and vascularised tissues (Zhou et al., 2011). miR-27 has been demonstrated to promote angiogenesis by targeting the angiogenesis inhibitor semaphorin 6A (SEMA6A) and Sprouty2 (Urbich et al., 2012; Zhou et al., 2011). The inhibition of miR-27 *in vivo* was performed using antagomirs in implanted Matrigel plugs. Matrigel plug assay is an *in vivo* evaluation of pro- and anti-angiogenic molecules that can detect newly formed blood vessels through the immunohistochemistry staining of markers (Malinda, 2009). Human umbilical vein endothelial cells (HUVECs) plated on Matrigel, which is an extract of the Engelbreth-Holm-Swarm tumor composed of basement membrane components, can differentiate into capillary-like tube structures *in vitro.* The Matrigel is then injected into mice to form a Matrigel plug and mouse endothelial cells migrate to the plug to form vessels. Using this assay, it was shown that inhibition of miR-27 decreased the number of vessels invading the implanted Matrigel plug (Urbich et al., 2012).

Functions of miR-27 have also been studied in the myeloid lineage. Feng *et al.* shown that miR-27 regulates the transcription factor Runx1, an important regulator of the growth and differentiation of haematopoietic cells, leading to the

differentiation of myeloblasts into granulocytes (Feng et al., 2009). The introduction of pre-miR-27 into murine myeloid progenitor 32D.cl3 cells resulted in a 3 to 4 fold increase in band-type granulocytes compared to cells transfected with pre-miRNA controls. Furthermore, regulation of Runx1 by miR-27 has been associated with the differentiation of megakaryocytes, which share a common myeloid progenitor with myelocytes (Ben-Ami et al., 2009).

A study of miR-27 in breast cancer cell lines revealed that miR-27a has oncogenic activity by indirectly enhancing the expression of specificity protein (Sp) transcription factors (Mertens-Talcott et al., 2007). The Sp is shown to be overexpressed in tumours and contributes to the cell proliferation and angiogenesis of cancer cells. miR-27 increases the expression of Sp by downregulating zinc finger and BTB domain containing 10 (ZBTB10/RINZF), a putative suppressor of Sp (Scott et al., 2006). In MCF-7 breast cancer cells, miR-27 is highly expressed and has been found to work cooperatively with miR-96 and miR-182 to regulate forkhead box O1 (FOXO1), a transcription factor that regulates genes involved in the apoptotic response, cell cycle checkpoints and cellular metabolism (Guttilla and White, 2009). The inhibition of miR-27 using antisense inhibitors results in a significant increase in FOXO1. Furthermore, the overexpression of FOXO1 leads to a decrease in cell viability due to the inhibition of the cell cycle and the induction of apoptosis (Guttilla and White, 2009). This suggests that the regulation of FOXO1 by miR-27 may contribute to the maintenance of an oncogenic state in breast cancer cells. In addition, the regulation of FOXO1 by miR-27 was also found in endometrial cancer (Myatt et al., 2010). Similar to the overexpression of FOXO1 observed in MCF-7 breast cancer cells (Guttilla and White, 2009), the induction of FOXO1 in endometrial cancer cells leads to G1 arrest and cell death (Myatt et al., 2010).

Beyond the functional data, miR-27 has also been found to be upregulated in other kinds of cancers. For example, miRNA profiling in kidney carcinomas showed that miR-27 is significantly increased in cancer cells compared to normal kidney cells (Gottardo et al., 2007). qRT-PCR data revealed that miR-27 was significantly upregulated in gastric cancer tissues compared to matched normal tissues located 5 cm away from the tumour margin (Zhang et al., 2011). In the context of viral

infection, functions of miR-27 in regulation of cell growth and differentiation might influence viral infection since viruses depend on host cellular machinery for their replication.

Table 1.4 Disease contexts in which miR-27 functions

Associated condition	Target	Putative role of the target	Reference
Adipogenesis and adipocyte differentiation	PPARγ and C/EBPα	Negative regulator of adipogenesis and adipocyte differentiation	(Lin et al., 2009), (Kim et al., 2010)
	PHB	Negative regulator of adipocyte differentiation	(Kang et al., 2013)
Angiogenesis	SEMA6A and Sprouty2	Promotes angiogenesis	(Urbich et al., 2012), (Zhou et al., 2011)
Differentiation of myeloblasts to granulocytes	Runx1	Enhances differentiation of myeloblasts into granulocytes	(Feng et al., 2009)
Megakaryocytic differentiation	Runx1	Induces megakaryocytic differentiation	(Ben-Ami et al., 2009)
Breast cancer	Sp (indirect target of miR-27)	Contributes to cell proliferation and angiogenic phenotype in cancer cells	(Mertens-Talcott et al., 2007)
	FOXO1	Tumour suppressor	(Guttilla and White, 2009)
Endometrial cancer	FOXO1	Arrests cells in G1 and induce cell death	(Myatt et al., 2010)

1.3.1 miR-27 and herpesvirus infection

miR-27 has been shown to be degraded by non-coding RNAs of two different herpesviruses: herpesvirus saimiri (HVS) (Cazalla et al., 2010) and murine cytomegalovirus (MCMV) (Libri et al., 2012; Marcinowski et al., 2012). HVS, a prototype of the rhadinovirus family, is an oncogenic γ-herpesvirus that can transform primate and human T cells (Ensser and Fleckenstein, 2005). In HVS-infected marmoset T cells, the virus makes seven small U-rich non-coding RNAs (HSURs). It has been shown that one of the HSURs, named HSUR1 mediates the degradation of miR-27 through complementarity in the sequences, although the

mechanism of this degradation is still unknown (Cazalla et al., 2010; Guo et al., 2014). Identification of miR-27 targets using high-throughput sequencing of RNA after cross-linking immunoprecipitation (HITS-CLIP) demonstrated that target mRNAs are enriched in the T cell receptor (TCR) signalling pathway (Guo et al., 2014) which is known to contribute to cell proliferation, differentiation, clonal expansion and effector cytokine secretion during T cell activation (Murphy et al., 2008).

Guo *et al.* have shown that miR-27 directly targets the cell surface signalling protein semaphorin (SEMA7A) and the growth factor receptor-bound protein 2 (GRB2), which is an adaptor protein participating in the activation of TCR signalling. In addition, the authors also demonstrated that miR-27 regulates an effector of T cell activation, interferon-γ (IFN-γ) (Guo et al., 2014). Because miR-27 appears to regulate TCR signalling, the degradation of miR-27 is thought to contribute to the activation of HVS-infected T cells. Thus, it is speculated that the induction of IFN-γ resulted from miR-27 decay in HVS-infected cells could be a viral strategy to maintain the viral genome in latency since IFN-γ is a potent inhibitor of lytic reactivation of γ-herpesviruses (Steed et al., 2006)

Other closely related γ-herpesviruses do not encode HSUR1 but have been proposed to employ a related viral strategy to modulate T cell signalling (Guo et al., 2014). For example, AIHV-1 and OvHV-2 do not appear to encode the HSUR1 homolog; however, their genomes contain the sequences homologous to the host miR-27 target genes: SEMA7A, ATF3 and IL-10 (Guo et al., 2014). ATF3 is a transcription factor that enhances IFN-γ expression (Filen et al., 2010). Hence, AIHV-2 and OvHV-2 use different strategies from HVS to exploit T cell activation. However, functions of miR-27 in TCR signalling is unlikely to be related to miR-27 functions in MCMV infection since the virus does not infect T cells.

The analysis of miRNA expression upon MCMV infection has shown that miR-27 levels dropped rapidly (~50-80% by 6 hpi depending on cell types and MOI) in various mouse cell lines including fibroblasts, endothelial cells, epithelial cells and primary bone marrow-derived macrophages (Buck et al., 2010). The degradation of

miR-27 is mediated by a highly abundant viral non-coding RNA, m169, containing the miR-27 binding site at its 3'UTR (Libri et al., 2012; Marcinowski et al., 2012). The mechanism of miR-27 degradation has been proposed to involve 3'tailing and trimming whereby the 3'end of the miRNA is extended with non-template nucleotides (tailing) followed by the shortening of the sequence of its 3' end (trimming) (Marcinowski et al., 2012).

In vivo studies revealed that the interaction of miR-27 and m169 is important for viral replication. Marcinowski *et al*. showed that infection of BALB/c mice with the m169 mutant containing point mutations at the miR-27 binding sites results in ~10 fold attenuation of the virus in lungs and salivary glands compared to infection with the wild type virus at 14 days post infection (dpi), whereas the revertant virus with completely restored sequences of wild type MCMV including miR-27 binding sites, does not show the attenuation (Marcinowski et al., 2012). Marcinowski *et al*. also examined this phenotype at earlier stages of infection (4 dpi) and found a moderate attenuation of the mutant virus in lungs, whereas ~100 fold decrease in mutant titres was observed in the spleen compared to wild type virus.

In addition, *in vitro* studies have shown that miR-27 can exert anti-viral functions against MCMV when overexpressed. Compared to the negative controls, the overexpression of miR-27 led to the attenuation of the virus (~10 fold decrease) when cells were infected with the virus at MOI of 0.01 (Buck et al., 2010). However, the targets of miR-27 responsible for its anti-viral activity have not yet been identified. It is therefore still unclear why MCMV evolves a mechanism to degrade miR-27.

Recently, it was demonstrated that miR-27 directly targets IL-10 in activated macrophages (Xie et al., 2014). IL-10 is an immunomodulatory cytokine produced by a wide variety of cells including immune cells (monocytes, macrophages, dendritic cells (DCs), T cells, B cells, eosinophils and mast cells), and non-immune cells (keratinocytes, epithelial cells and tumour cells) (reviewed in (Mosser and Zhang, 2008)). The major biological function of IL-10 relates to its capacity to exert immunosuppression on DCs and macrophages. IL-10 inhibits the expression of major

histocompatibility complex class II (MHC II) and differentiation from monocytes to DCs and DC maturation. IL-10 also inhibits the production of pro-inflammatory cytokines, IL-1, IL-6, IL-12 and TNF. It has been reported that some viruses upregulate expression of IL-10 to suppress the immune function, leading to enhancement of infection (reviewed in (Slobedman et al., 2009). Based on the function of IL-10, one hypothesis is that MCMV has evolved the degradation of miR-27 to induce the expression of host IL-10 in order to modulate immune response towards immunosuppression allowing the virus to escape from the host immune response and this could enhance its capacity to replicate and persist.

Unlike upon MCMV infection, HCMV does not downregulate levels of miR-27 based on miRNA microarray analysis in HCMV-infected fibroblasts (Santhakumar et al., 2010). Interestingly, HCMV, but not MCMV, expresses a viral IL-10 (vIL-10) homolog to human IL-10 (hIL-10) (reviewed in (Slobedman et al., 2009)). Indeed, many herpesviruses including HCMV and EBV encode vIL-10. Of interest, cmvIL-10 shares only 27% amino acid sequence identity with hIL-10 (Kotenko et al., 2000); however, cmvIL-10 can bind to IL-10 receptors and modulates the host immune system (Jones et al., 2002). cmvIL-10 was shown to inhibit peripheral blood mononuclear cell (PBMC) proliferation and the production of proinflammatory cytokines IL-1α, IL-6, granulocyte-macrophage colony-stimulating factor and TNFα in LPS-treated PBMC and monocytes (Spencer et al., 2002). Moreover, cmvIL-10 was shown to decrease the expression of MHC class I and MHC class II by monocytes, interfering with antigen presentation processes (Spencer et al., 2002). A study in plasmacytoid DCs has demonstrated that cmvIL-10 suppresses the production of type I IFNs (Chang et al., 2009). Since type I IFNs prevents susceptible cells from HCMV infection, the secretion of cmvIL-10 may aid the viral dissemination and attenuation of anti-viral immune responses. Taken together, it is possible that the anti-viral properties of miR-27 could relate to its regulation of IL-10 and HCMV circumvents this by encoding the viral IL-10 instead of targeting miR-27 for degradation, whereas MCMV induces cellular IL-10 via the degradation of miR-27. Based on the fact that one miRNA can target hundreds of mRNAs, it is possible and likely however that the degradation of miR-27 can result in the upregulation of

many other cellular factors in addition to IL-10, leading to alteration of host cell environment conducive to the infection. Further understanding of miR-27 functions in cellular pathways related to MCMV infection will provide insight into the significance of MCMV-mediated degradation of miR-27.

1.3.2 Hypotheses and aims of the thesis

This thesis focuses on understanding the functions of miR-27 during MCMV infection through an analysis of its targets. Based on the findings that the virus specifically inhibits miR-27 and this miRNA shows anti-viral functions, it is hypothesised that miR-27 regulates cellular genes or pathways required during the viral life cycle. Thus, the virus has evolved the strategy of miR-27 degradation to de-repress genes that are targeted by miR-27, leading to upregulation of target genes essential for the viral infection.

To test these hypotheses, this thesis aims to:

1. Identify and evaluate direct cellular targets of miR-27 important for MCMV replication
2. Investigate the role of miR-27 target genes in the context of viral infection

Chapter 2: Materials and methods

2.1 Tissue culture

2.1.1 Cell lines and culture media

NIH 3T3 fibroblasts (ATCC CRL1658) are mouse cells generated from a NIH Swiss mouse embryo. The cells were obtained from American Type Culture Collection (Manassas, VA). The cells were grown in Dulbecco's Modification of Eagle's Medium, DMEM (Sigma) with 10% heat-inactivated calf serum (HI-CS) (Sigma), 0.293 mg/ml (1%) of L-glutamine (L-glu) (Gibco, Life technologies) and 50 U (1%) of Penicillin/Streptomycin (Pen/Strep) (Gibco, Life technologies) per ml.

P53-null mouse embryonic fibroblasts ($p53^{-/-}$ MEFs) (ATCC CRL 2645) are derived from mouse embryos with a p53 null mutation and cells were maintained in the same media as used for NIH 3T3 except HI-CS was substituted with heat-inactivated fetal bovine serum (HI-FBS) (Sigma).

Human embryonic kidney 293T cells, HEK293T (ATCC CRC 3216) were maintained in complete Iscove's Modified Eagle Medium, IMEM (Sigma) containing 10% HI-FBS, 1% L-glu, 1% Pen/Strep and 25 mM (4-(2-hydroxyethyl)-1-piperazineethanesulfonic acid), HEPES (Invitrogen).

All cells were grown at 37°C with 5% CO_2 and 95% humidity.

2.1.2 Isolation of primary mouse embryonic fibroblasts (MEFs)

Pregnant mice at 13-14 days of gestation were sacrificed to obtain embryos. Mice were sprayed with 70% ethanol and dissected to take out uterine horns containing embryos. The horns were placed in ice-cold PBS and individual embryos separated. The head and viscera of each embryo were removed. The remaining embryos were transferred into a petri dish and cut into small pieces. About three or four cut embryos were transferred to a 15 ml falcon tube containing 6 ml of trypsin-EDTA (Gibco, life technologies) and the suspension was pipetted up and down to disperse the tissue. The tube was placed on ice for 2 h and incubated at 37°C for 30 min. 6 ml of complete media (DMEM containing 10% HI-FCS, 1% L-glu and 1% Pen/Strep)

was added into the tube. To allow the remaining tissues to settle, the tube was left at room temperature for 5 min. The supernatant containing cells was collected and transferred into a T150 culture flask with 50 ml complete media. Cells were incubated at 37°C, 5% CO_2, overnight. The next day, the media was replaced with fresh media and cells were continuously incubated until they were confluent.

2.1.3 Freezing and thawing cells

NIH 3T3 cells or $p53^{-/-}$ MEFs were harvested and resuspended in the appropriate freezing media (50% HI-FCS or HI-CS, 40% DMEM and 10% DMSO (Sigma)). Specifically, the freezing media of primary MEFs consists of 90% HI-FCS and 10% DMSO. 1ml of freezing media containing approximately $1x10^6$ cells was added into a cryotube (Sarstedt). The tube was placed in a Mr.Frosty 1°C freezing container (Nalgene, Thermo Scientific) at -80°C, overnight. The next day, the tube was transferred to liquid nitrogen for long-term storage.

To thaw frozen cells from liquid nitrogen, a cryovial was placed in a 37°C water bath until cells were completely thawed. Cells were transferred into a 15 ml falcon tube and 5 ml of pre-warmed media was added to the cells. The tube was spun at 1,000 rpm, room temperature for 5 min. Supernatant was decanted and the cell pellet was resuspended with 10 ml complete media prior to transfer into a 75 cm^2 flask.

2.2 Cell viability test

In order to assess the viability of cells, 20 µl of cell titre blue (Promega) was added to each well of a 96-well plate containing 100 µl media. The plate was incubated at 37°C for 2 h. The assay is based on the ability of live cells to reduce resazurin into resorufin, which is highly fluorescent. The fluorescent signal was measured using Varioskan reader (Thermo Scientific).

2.3 miRNA/siRNA transfection

siRNAs or miRNAs were transfected into cells using DharmaFECT-1 (GE healthcare). The transfection mixture of each plate format was shown in Table 2.1. A 4% lipid mixture was prepared by diluting DharmaFECT-1 with Opti-MEM and incubated at room temperature for 5 min. The lipid mixture was then mixed with the

siRNA/Opti-MEM mixture. The transfection mixture was incubated at room temperature for 20 min and pipetted into a well. The appropriate density of cells in antibiotic-free media was added into each well to mix with the transfection mixture. Cells were incubated at 37°C with 5% CO_2.

Table 2.1 Volumes per well of transfection in different plate formats

Plate format	Volume of 500 nM siRNA or miRNA (µl)	Opti-MEM (µl)	4% DharmaFECT1 in Opti-MEM (µl)	Cell density	Total transfection volume (µl)
96	5	5	10	$1.5x10^4$ in 80 µl	100
24	12.5	12.5	25	$1x10^5$ in 450 µl	500
6	50	50	100	$3x10^5$ in 800 µl	1000

2.4 Methods for virology

2.4.1 Viruses

The Smith strain of murine cytomegalovirus was used for all studies, which contains the complete MCMV genome originally derived from bacterial artificial chromosome clone pSM3fr BAC (Wagner et al., 1999).

MCMV Δm169 lacking m169 and m168 gene was previously generated by Valentina Libri (Buck lab). Briefly, primers containing 60 bp homologous to region flanking m168 and m169 (overlapped genes, Fig 2.1) were used to amplify a kanamycin (Kan) resistance cassette from plasmid pCP015 by PCR. The forward primer is 5'-AAGTGTATAAAAGCTGAGTGTGGAGCGGTCGCAGTCGACACAGGAACAC TTAACGGCTGA-3' and the reverse primer is 5'-AGACGGGAAACCGTCGTCGTTCGACCGTTACTCACGCCAAGAAAAGTGC CACCTGCAGAT-3'. Competent EL250 bacteria containing MCMV BAC (with chloramphenicol resistance, Cm) were electroporated with the PCR fragment for recombination and selected for Kan and Cm resistance. The Kan cassette was excised from Kan-Cm resistant clones, resulting in the BAC carrying only Cm with the deletion of m168 and m169.

The GFP reporter MCMV (GFP-MCMV) contains GFP expression cassette in front of IE2 gene (Angulo et al., 2000). The insertion of GFP at this location was proven that it does not alter the viral growth (Manning and Mocarski, 1988).

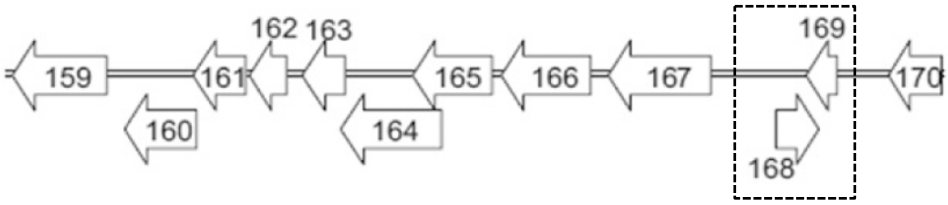

Figure 2.1 Genomic organisation of m168 and m169 (dashed box), this figure is taken from (Marcinowski et al., 2012)

2.4.2 Preparation of viral stock

To produce the viral stock, primary mouse embryonic fibroblasts (MEFs) were seeded at a density of $1x10^6$ cells per 150 cm^2 flask in DMEM supplemented with 10% HI-FBS, 1% L-glu and 1% Pen/Strep. The next day, cells were infected with viruses at MOI of 0.05 in 15 ml DMEM with 5% HI-FBS, 1% L-glu and 1% Pen/Strep. The infected culture was maintained at 37°C for 5-7 days or until a cytopathic effect was observed. The cells and supernatant were collected and centrifuged at 3000 rpm, 4°C for 20 min. The supernatant from multiple flasks was combined and cell debris was discarded. The viral stock was aliquoted and stored at -80°C.

2.4.3 Titration of virus by plaque assays

The plaque assay is a method to quantify virus concentration. To preform the method, $p53^{-/-}$ MEFs were seeded in a 48-well plate at a density of $2x10^4$ cells in 300 µl and incubated overnight at 37°C. On the day of the assay, the viral stock was diluted with DMEM containing 3% HI-FCS, 1% L-glu and 1% Pen/Strep at 10 fold serial dilutions ranging from 10^1 to 10^6. The total volume of 100 µl was prepared in triplicate and added to each well of a 48-well plate. The viral dilution was incubated with cells at 37°C for 2 h. Cells were washed with DMEM without additives and overlaid with 0.25% agarose-media mixture, which was prepared from 0.25% agarose in DMEM containing 3% HI-FCS, 1% L-glu and 1% Pen/Strep. Cells were

incubated at 37°C for 3-4 days until plaques became visible. To determine the viral titre, the numbers of plaques were counted and viral concentration calculated as plaque forming units to ml (PFU/ml) by using the equation below:

PFU/ml = Numbers of plaques in average*individual dilution factor*10

2.4.4 Viral infection

The titre of the viral stock was used to calculate multiplicity of infection (MOI) for performing infection experiments. MOI refers to the number of virus particles that are added per cell during infection. To infect cells, the virus inoculum was prepared according to the desired MOI by mixing virus stock with media containing 10% serum. The total volume of inoculum varies depending on plate formats as described below:

50 µl of virus inoculum per well of 96-well plates

100 µl of virus inoculum per well of 48-well plates

200 µl of virus inoculum per well of 24-well plates

1 ml of virus inoculum per well of 6-well plates

Cells were incubated with the virus inoculum at 37°C for 2 h, after which cells were washed once and replaced with complete media. The time hour post infection was counted at the end of virus incubation period.

2.4.5 Viral growth curves

2.4.5.1 Viral growth by plaque assays

Growth curves were used to determine viral replication. Cells were seeded in a 96-well plate and incubated overnight at 37°C. On the next day, cells were infected with viruses at MOI of 0.01 as described in 2.4.4. The supernatant was collected on day 1 to 5 post infection for measuring viral titre by plaque assay.

2.4.5.2 Growth curves based on GFP-MCMV

MCMV encoding a green fluorescent protein (GFP) under the control of immediate-

early control was used to monitor the viral growth (Angulo et al., 2000). Cells were seeded in a 96-well plate and incubated at 37°C, overnight. Cells were infected with GFP-MCMV at MOI of 0.2 at 37°C for 2 h. Cells were then washed and 150 µl of phenol-red-free DMEM, 10% HI-CS, 1% L-glu and 1% Pen/Strep was added into each well. The GFP signal was measured at excitation wavelength of 493 nm and emission wavelength of 520 nm using Varioskan Flash (Thermo Scientific).

2.5 RNA method

2.5.1 RNA extraction

Total RNA was extracted using TRIzol (Invitrogen). Cells in a 24-well plate were washed with pre-warmed PBS twice and 200 µl TRIzol was added into each well. The plate was incubated at room temperature for 5 min and cells were collected into 1.5 ml tubes. 40 µl of chloroform was added to samples and tubes were mixed by inverting. Samples were centrifuged at 12,000 rpm at 4°C for 20 min. The aqueous phase was transferred into fresh tubes. 300 µl of isopropanol and 1 µl of 15 mg/ml glycogen blue (Ambion, USA) were added into the aqueous phase. The mixture was incubated at room temperature for 5 min following by centrifugation at 12,000 rpm, 4°C for 10 min. The supernatant was discarded and the pellet was washed twice with 70% ethanol. After the final wash, the pellet was dried at room temperature. The pellet was resuspended in 20 µl of RNase/DNase free water (GIBCO, Invitrogen) and incubated at 55°C for 10 min. RNA was immediately placed on ice or kept at -20°C.

2.5.2 Assessment of RNA quantity, purity and integrity

RNA was quantified and the purity was assessed using Nanodrop ND-1000 spectrophotometer (Thermo scientific). The maximal absorbance for nucleic acid and protein is 260 and 280 nm, respectively. A 260/280 ratio of 1.8-2.0 is generally accepted to indicate RNA with minimal protein contamination. In addition, the ratio of 260/230 can indicate phenol contamination and the ideal ratio is above 1.5. In addition, RNA integrity was determined by polyacrylamide gel electrophoresis. A 12% RNA gel was prepared from the UreaGel Concentrate, UreaGel Diluent and UreaGel Buffer (National Diagnostic). To make 2 small gels (0.75 mm thickness), 4.8 ml UreaGel concentrate was mixed with 4.2 ml UreaGel Diluent, 1 ml UreaGel

Buffer, 80 µl APS and 4 µl TEMED. RNA samples were prepared by mixing 1 µg RNA with RNA loading buffer. The samples were heated at 70°C for 2 min and immediately placed on ice. The samples were loaded onto the gel and run at 100-120 Volt for 1-2 h. To visualise RNA bands, the gel was stained with ethidium bromide (Invitrogen) and examined under a UV transilluminator (Syngene). Intact RNA is indicated by clearly separated bands of 5S and tRNA.

2.5.3 Reverse transcription polymerase chain reaction and quantitative real-time polymerase chain reaction (qRT-PCR)

Reverse transcription (RT) was carried out using miScript II RT kit (QIAGEN). The total reaction volume of 5 µl reaction contains 1 µl of 5x miScript HiFlex buffer, 0.5 µl of 10x miScript Nucleics Mix, 0.5 µl of miScript Reverse Transcriptase and 200 ng of RNA in H_2O. The RT reaction was incubated at 37°C for 1 h followed by inactivation of reverse transcriptase at 95°C for 5 min and the complete reaction was held at 4°C to prevent cDNA degradation. Prior to the qPCR reaction, cDNA was diluted 1:10 with RNase-free water.

The qPCR of mature miRNAs was carried out using miScript SYBR Green PCR kit (QIAGEN). Primers used for quantification of miRNAs are miRScript Primer assay (QAIGEN). The reactions were done in 384-well plates. The total reaction volume of 5 µl contains 2 µl of 2x QuantiTect SYBR Green PCR Master mix, 0.5 µl of 10x miScript universal primer, 0.5 µl of 10x miScript specific primer, 0.5 µl of cDNA template (1:10 dilution) and 1.5 µl of RNase-free water. The reactions were performed on a LightCycler 480 Real-time PCR instrument (Roche) with an initial incubation at 95°C for 15 min following by 45 cycles of denaturation at 94°C for 15 sec, annealing at 55°C for 30 sec and extension at 72°C for 30 sec.

For analysis of mRNA levels, qRT-PCR was conducted using the LightCycler 480 SYBR Green I Master Kit (Roche). Primers were designed using the online Roche Universal Probe Library primer design tool and the sequences are shown in Table 2.2 and 2.3. The reactions were carried out in 384-well plates. The total reaction volume of 5 µl contains 2.5 µl of SYBR mix, 0.25 µl of forward primer (10 pmol/µl), 0.25 µl

of reverse primer (10 pmol/µl), 0.5 µl of cDNA template (1:10) and 1.5 µl of RNase-free water. The plate was run on the LightCycler 480 Real-time PCR instrument (Roche). The cycling conditions consist of the initial denaturation at 95°C for 5 min, amplification for 45 cycles comprising 95°C for 10 sec, 60°C for 10 sec and 72°C for 10 sec.

Table 2.2 Primers for qRT-PCR of mouse and MCMV genes

Primer	Sequence (5' to 3')
Mouse gene	
Bmi1_F	CAAAACCAGACCACTCCTGAA
Bmi1_R	TCTTCTTCTCTTCATCTCATTTTTGA
Calm3_F	TGGCCAGAAAGATGAAGGAT
Calm3_R	GGCAGCGCTAATATAGCCATT
Cav1_F	AACGACGACGTGGTCAAGA
Cav1_R	CACAGTGAAGGTGGTGAAGC
Mouse_Ccng1_F	TGGACAGATTCTTGTCTAAAATGAAG
Mouse_Ccng1_R	CAGTGGGACATTCCTTTCCTC
Itga5_F	CACCATTCAATTTGACAGCAA
Itga5_R	TCCTCTCCCTTGGCACTGTA
Lyar_F	GGGGACCATTAAGGCTGTTT
Lyar_R	CATCACCGCATGGTACTGAG
Mapkapk3_F	CTGAATGGTTAGATGTCTCTGAGG
Mapkapk3_R	GCCTCTCTGTGGGATCTGTC
Pik3r1_F	GACGGCACTTTCCTTGTCC
Pik3r1_R	TGACTTCGCCGTCTACCAC
Rpl18a_F	CGCGAAAGACAACACTTCCT
Rpl18a_R	GTGGTGTGTGGCATTTTGG
Gapdh_F	CATGGCCTTCCGTGTTCCTA
Gapdh_R	GCGGCACGTCAGATCCA
MCMV gene	
m169_F	AGACGACGATCTGCGGAATA
m169_R	TTCTCAGGCAGACATCCGAA

Table 2.3 Primers for qRT-PCR of human genes

Primer	Sequence (5' to 3')
Human_Ccng1_F	CTGGACAGATTCCTGTCTAAAATG
Human_Ccng1_R	GTCAGTTGCCAATGGGACAT
Human_Gapdh_F	AGCCACATCGCTCAGACAC
Human_Gapdh_R	GCCCAATACGACCAAATCC

2.5.4 Northern blot analysis

2.5.4.1 Buffers and solutions for Northern blot analysis

2x loading dye: 8M urea (Sigma), 5mM EDTA (Promega), 0.05% bromophenol blue (Sigma), 0.05% xylene cyanol (Sigma)

10x TBE buffer (Tris-borate-EDTA): 109 g Tris base, 55.6 g Boric acid, 50 ml 500 mM EDTA, adjust the volume to 1L with dH_2O

15% TBE-UREA gel: 6 ml concentrate reagent (SequaGel, National digagnostics), 3ml dilute reagent (SequaGel, National digagnostics), 0.5 ml 10x TBE, 0.5 ml dH_2O, 100 µl 10% APS (Sigma) and 4 µl TEMED (Sigma)

Cross-linking solution: 245 µl 12.5 M 1-methylimidazole in 9 ml of dH_2O, adjust pH to 8, and 0.753 g of EDC, adjust the volume to 25 ml using dH_2O

Wash buffer 1 (2x SSC, 0.1% SDS): 100 ml 20x SSC (Biosciences), 10 ml 10% SDS (Sigma), adjust the volume to 1L with dH_2O. SSC-sodium chloride-sodium citrate buffer; SDS-sodium dodecyl sulphate

Wash buffer 2 (1x SSC, 0.1% SDS): 50 ml 20x SSC (Biosciences), 10 ml 10% SDS (Sigma), adjust the volume to 1L with dH_2O

Wash buffer 3 (0.1x SSC, 0.1% SDS): 5 ml 20x SSC (Biosciences), 10 ml 10% SDS (Sigma), adjust the volume to 1L with dH_2O

Stripping buffer (0.1% SDS): 5 ml 10% SDS and 495 ml dH_2O

2.5.4.2 Labelling of probes and RNA marker with γ-^{32}P, and northern blotting

Complementary oligonucleotides (Invitrogen) to target RNAs are shown in Table 2.4. The 5'end labelling was carried out at with 1.0 μM of the oligonucleotide, ^{32}P-γ-ATP (Perkin Elmer), T4 kinase (Invitrogen) and the forward reaction buffer supplied with the kit in a final volume of 20 μl. The reaction was incubated at 37°C for 1h, diluted to 50 μl in 3mM EDTA and unincorporated ATP was then removed using illustra MicroSpin G-25 columns (GE healthcare). The purified probes were stored at -20°C. The ladder was prepared according to manufacturer's instruction for the Decade Marker RNA system (Life technology) in a total volume of 10 μl with 100 ng RNA. 1 μl 10x kinase buffer, 1 μl ^{32}P-γ-ATP and 1 μl T4 kinase. The reaction was incubated at 37°C for 1h. 2 μl of the 10x cleavage reagent and 8 μl of water was added into the mixture and incubated at room temperature for 5 min. The labelled marker was then mixed with 20 μl loading buffer and kept at -20°C. The marker was heated at 95°C for 5 min before use.

5 μg of RNA was separated on 15% or 4% polyacrylamide gels for miRNA and mRNA analysis, respectively, and transferred onto a nylon membrane (Hybond N) (GE Healthcare) in 0.5% TBE at 80 Volt, 4°C for 1 h. The RNA was crossed-linked using EDC at 50°C for 2 h. The membrane was pre-hybridised in the Perfect HybPlus Hybridisation buffer (Sigma) at 42°C for 30 min. 10 μl of the labelled probe was added to the hybridisation buffer and incubated overnight at 42°C. The membrane was sequentially washed with pre-warmed (42°C) wash buffer 1, 2 and 3 for 10 min. The membrane was sealed and exposed in the phosphoimager (Molecular Dynamics, USA) for 24 to 48 h. The screen was then scanned using a Typhoon scanner (GE healthcare). To strip a membrane, stripping buffer was boiled and the membrane was placed in the buffer for up to 2 h. The membrane was re-exposed in a phosphoimager to ensure complete stripping before re-hybridisation with a new probe.

Table 2.4 Probe sequences used in Northern blot analysis

RNA of interest	Probe sequence (5' to 3')
miR-27	GCGGAACTTAGCCACTGTGAA
miR-16	CGCCAATATTTACGTGCTGCTA
m169	TCTCAGGCAGACATCCGAAGGGACTTCTTTTC ACAGCTTATTATTCCGCAGATCGTCGTCTGGG GGAGATCACGGACGGG

2.6 Western blot analysis

2.6.1 Buffers and solutions for Western blot analysis

4x SDS-PAGE loading buffer: 50 mM Tris-Cl (pH 6.8), 12.5mM EDTA, 2% SDS, 10% glycerol, 1% β-mercaptoethanol and 0.02% bromophenol blue.

NP-40 lysis buffer: 50 mM Tris-Cl (pH 7.5), 100 mM NaCl, 1% NP40 (IGEPAL), protease inhibitors and phosphatase inhibitors.

10% Ammonium Persulfate (APS): 1g of APS in 10 ml dH_2O

Laemmli running buffer (10x), pH8.3: 30.3g Tris, 144.2g Glycine, 10g SDS in 1L dH_2O

Transfer buffer (10x): 29g Tris, 144g Glycine, 3.7g SDS in 1L dH_2O. 1L of 1x buffer was prepared with 100 ml of 10x transfer buffer, 200 ml methanol and 700 ml dH_2O

1 M Tris-HCl, pH 6.8: 120g of Tris dissolved in total volume of 1L with dH_2O

1.5 M Tris- HCl, pH 8.8: 181g of Tris dissolved in total volume of 1L with dH_2O

ECL-based detection

Tris-buffered saline-Tween (TBS-T): 10 mM Tris-HCl, 100 mM NaCl, 0.2% Tween-20.

Blocking buffer: 5% skimmed milk powder in TBS-T

Fluorescence-based detection

Blocking buffer: Odyssey Blocking Buffer (LI-COR Biosciences) diluted with PBS in 1:1 ratio

Buffer for primary antibodies: 0.1% Tween-20 in blocking buffer

Buffer for secondary antibodies: 0.1% Tween-20 and 0.01% SDS in blocking buffer

Washing buffer: 0.1% Tween-20 in PBS

2.6.2 Sample preparation and gel electrophoresis

Protein lysate was prepared on ice by washing cells once with cold PBS and cells were lysed using NP-40 lysis buffer containing protease and phosphatase inhibitor (Roche). Cells with lysis buffer were transferred into fresh tubes and placed on ice for 30 min. The supernatant was obtained by centrifugation at 12,000 g, 4°C for 15 min. The protein was quantified by BCA assay (Thermofisher) following the manufacturer's protocol. A standard curve was generated using bovine serum albumin (BSA) at a concentration from 0 to 2,000 ng/µl. The protein concentration of samples was calculated using the standard curve as the reference. The protein lysate (between 20-30 µg) was mixed with 4x SDS loading buffer and heated at 95°C for 5 min and loaded onto a sodium dodecyl sulfate polyacrylamide (SDS-PAGE) gel.

The SDS-PAGE gel consists of 12% resolving gel and 5% stacking gel. To prepare 30 ml of the resolving gel, 9.9 ml of dH_2O was mixed with 12 ml of 30% polyacrylamide, 7.5 ml of 1.5M Tris (pH 8.8), 300 µl of 10% SDS, 300 µl of 10% APS and 12 µl of TEMED. The gel mixture was poured into the glasses and immediately overlaid by isopropanol. Once the gel solidified, isopropanol was removed and the gel was washed with dH_2O. 10 ml of stacking gel was prepared with 6.8 ml of dH_2O, 1.7 ml of 30% polyacrylamide, 1.25 ml of 1.0M Tris (pH 6.8), 100 µl of 10% SDS, 300 µl of 10% APS and 10 µl of TEMED and was poured on top of the resolving gel.

2.6.3 Western blot analysis for enhanced chemiluminescence (ECL)-based detection

Samples were loaded onto the gel along with Fermentas PageRuler Plus Prestained Protein Ladder (Thermo scientific). The gel was run at 100-120 Volt for 2-3 h. The separated protein on the gel was transferred onto a nitrocellulose Hybond EC (BIO-RAD) by wet blot procedure. The transfer was carried out at 35 Volt, 4°C, overnight. After protein transfer, the membrane was incubated with 5% skimmed milk in TBS-T at room temperature for 1 h or 4°C, overnight. The blocking buffer was replaced with primary antibody diluted in 5% skimmed milk in TBS-T and was incubated at 4°C, overnight. The list of antibodies used was provided in Table 2.5. The membrane was washed three times with TBS-T for 10 min and it was incubated with the secondary antibody diluted in blocking buffer at room temperature for 2 h. The unbound antibody was removed by washing the membrane three times with TBS-T for 10 min. The protein was detected using ECL Western blotting detection system (Thermo scientific), X-ray films (Fuji) and the film developer (Konica Minolta).

2.6.4 Western blot analysis for fluorescence-based detection

Samples were loaded onto the gel along with Precision Plus Protein All Blue Standards (BIO-RAD) and the gel was run at 100-120 Volt for 2-3 h. Proteins were transferred onto a PVDF membrane, which was soaked with absolute methanol. The transfer was performed using the wet blotting procedure at 35 Volt, 4°C, overnight. The blotted membrane was incubated with the blocking buffer at room temperature for 1 h and incubated with the primary antibody at 4°C, overnight. The membrane was washed four times with washing buffer (PBS-T) for 10 min and incubated with the secondary antibody diluted in blocking buffer at room temperature for 45 min. The secondary antibody solution was prepared by mixing two antibodies: a secondary antibody specific to the primary antibody and Alexa Fluor 680 Goat Anti-mouse IgG binding to the ladder. The membrane was washed four times with washing buffer for 10 min and analysed using Odyssey Infrared Imaging System (LI-COR Biosciences).

Table 2.5 A list of antibody used in Western blot analysis

Antibody	Dilution	Supplier
Anti-AGO2	1:2000	Cell signaling, 2897
Anti-BMI1	1:1000	Cell signaling, 5855
Anti-CALM3	1:2500	Abcam, ab124742
Anti-CAV1	1:2000	BD, 610059
Anti-CCNG1	1:500	Santa cruz, sc-7865
Anti-ITGA5	1:1000	Cell signaling, 4705
Anti-MAPKAPK3	1:1000	Cell signaling, 7421
Anti-PIK3R1	1:1000	Cell signaling, 13666
Anti-phospho-HSP27 (Ser86)	1:1000	Abcam, ab17938
Anti-phospho-CREB (Ser133) and ATF-1	1:1000	Cell signaling, 9198
Anti-phospho-p38 (Thr180/Tyr182)	1:1000	Cell signaling, 9215
Anti-β-actin	1:3000	Cell signaling, 4967
Anti-GAPDH	1:3000	Cell signaling, 2118
Peroxidase anti-peroxidase soluble complex antibody (PAP)	1:20000	Sigma, P1291
Anti-rabbit IgG, HRP-linked antibody (ECL-based detection)	1:3000	Cell Signaling, 7074
Anti-mouse IgG, HRP-linked antibody (ECL-based detection)	1:3000	Cell Signaling, 7076
Goat anti-rabbit IgG secondary antibody, DyLight800 (Fluorescence-based detection)	1:20000	Thermo Scientific, SA5-35571
Alexa Fluor 680 Goat Anti-mouse IgG (Fluorescence-based detection)	1:20000	Life technologies, A-21058

2.7 Sample preparation for microarray analysis

To examine gene expression using microarray analysis, six treatment groups were carried out in three technical replicates: 1) untreated cells, 2) cells transfected with RISC-free siRNAs, 3) cells transfected with miR-27a mimics, 4) cells infected with wild type MCMV, 5) cells infected with MCMV Δm169 and 6) cells transfected with miR-27a mimics followed by wild type MCMV infection. NIH 3T3 cells were untreated or transfected in a 6-well plate with RISC-free siRNAs or miR-27a mimics for 48 h. For viral infection, NIH 3T3 cells were seeded at a density of $3x10^5$ cells in a 6-well plate for 24 h prior to infection with the wild type MCMV or MCMV Δm169 at MOI of 5 for 24 h. To carry out the combined treatment of transfection and infection, cells were transfected with miR-27a mimics for 24 h prior to infection with the wild type MCMV at MOI of 5 for 24 h. Total RNA was extracted and RNA integrity was qualitatively assessed by polyacrylamind gel electophoresis. The levels of miR-27 and m169 were determined using qRT-PCR. Amplified RNAs for microarray analysis were prepared using Illumina TotalPrep RNA Amplification kit (Ambion, Life technologies) according to the manufacturer's instructions.

The amplified RNAs were subjected to the quality assessement using Bioanalyzer (Agilent Technologies) and microarray analysis using Illumina mouseref-6 array, which were carried out by Wellcome Trust Clinical Research Facility (WTCRF, Western general Hospital, Edinburgh). Analyses of the microarray data including quality control and differential gene expression were carried out by Alasdair Ivens (Centre for Infection Immunity and Evolution, Ashworth Laboratories, University of Edinburgh).

2.8 Functional screening of genes required for MCMV replication

NIH 3T3 cells were transfected with siGENOME SMARTpool siRNAs or individual siGENOME siRNAs that make up the pool (Dharmacon, GE healthcare) in 96-well plates for 48 h as described in section 2.3. Cells were infected with 50 µl of viral mixture of GFP-MCMV (MOI of 0.2) at 37°C for 2 h. The virus was then removed and 150 µl phenol-red-free DMEM containing 10% HI-CS, 1% L-glu and 1%

Pen/Strep was added into each well. Cells were incubated at 37°C for 70 h and the fluorescent signal was measured using Varioskan Flash Reader (Thermofisher).

2.9 Validation of direct targets of miR-27 by a dual luciferase reporter assay

Validation of direct interactions between miRNAs and target mRNAs was carried out using a dual luciferase reporter system (Promega). The reporter vector is psi-CHECK2 encoding *Renilla* and firefly luciferase. The vectors were constructed by cloning the full length of 3'UTRs of target genes downstream of *Renilla* luciferase. The levels of firefly luciferase were used to control for transfection efficiency. The constructed vector was co-transfected into cells along with miRNAs mimics or inhibitors, and expression of *Renilla* and firefly measured.

2.9.1 Cloning of the 3'UTR into psi-CHECK2

The primers used to amplify the 3'UTR of *Bmi1* (~1.5 kb), *Cav1* (1.1 kb), *Ccng1* (1.5 kb) and *Mapkapk3* (~1.2 kb) are shown in Table 2.6. The 50 µl PCR reaction contains 5 µl of 10x buffer, 1 µl of 10 mM dNTPs, 1 µl of 10 µM forward primer, 1 µl of 10 µM reverse primer, 1 µl of *Pfu* DNA polymerase (Promgea) and 20 ng of cDNA in dH_2O. The cycling conditions are listed in Table 2.7.

The PCR products were gel purified using QIAquick Gel Extraction Kit (QIAGEN). Empty psi-CHECK2 and the purified products were digested using NotI-HF (NEB) and XhoI (NEB) according to the manufacturer's protocol. To prevent self-ligation, the 5' phosphates of digested psi-CHECK2 were removed using Antarctic Phosphatase (NEB) following the manufacturer's protocol. Subsequently, digested PCR products and dephosphorylated psi-CHECK2 were gel purified using QIAquick Gel Extraction Kit (QIAGEN).

To ligate the purified PCR product into the vector, the 10 µl ligation reaction contained 1 µl of 10x buffer, 1 µl of T4 DNA ligase (NEB) and the mixture of the PCR insert and the digested vector at a molar ratio of 3:1. The reaction was incubated at 16°C, overnight. 5 µl of the ligation reaction was then transferred into 30 µl of thawed DH5α competent cells (Invitrogen). Cells were placed on ice for 30

min, heat shocked at 42°C for 45 sec and put on ice for 2 min. 150 µl of SOC (Invitrogen) was added to the transformed cells and the cells were incubated at 37°C with shaking for 1 h. The transformed cells were plated onto LB agar plates (Sigma) containing 100 µg/ml of penicillin (Sigma). The plates were incubated at 37°C, overnight. Vectors were extracted using a standard mini-prep, digested using appropriate restriction enzyme to identity positive colonies containing the insert. The positive vectors were sent for sequencing to confirm correct insert sequences.

2.9.2 Mutagenesis of the miR-27 binding site within the 3'UTR of *Mapkapk3*

The mutagenesis of the miR-27 binding site within the 3'UTR of *Mapkapk3* was carried out using QuickChange lightning multisite-directed mutagenesis kit (Agilent Technologies) according to the manufacturer's protocol. psi-CHECK2 containing the 3'UTR of *Mapkapk3* was subjected to mutagenesis using primers with three base substitutions (Table 2.6). Primers were designed using the QuickChange Primer Design Program available online at http://www.genomics.agilent.com.

2.9.3 Luciferase reporter assays

To perform the luciferase reporter assay, NIH 3T3 cells were co-transfected with the reporter vectors and miRNAs in a 96-well plate using Lipofectamine 2000 (Life Technologies) as shown in Table 2.8. At 48 h post transfection, samples were prepared according to the manufacturer's protocol (Promega). Expressions of *Renilla* and firefly luciferase were measured using Varioskan Flash Reader (Thermofisher).

Table 2.6 A list of primers for PCR amplification, DNA sequencing and mutagenesis of *Mapkapk3* 3'UTR

Primer	Sequence (5' to 3')
Amplification of *Bmi1* 3'UTR	
Bmi1_3'UTR_XhoI_F	ATTCTCGAGCATGTGACTGTCGTCCAGTTTGC
Bmi1_3'UTR_NotI_R	ATTGCGGCCGCTGACACACACACAATGGGAC
Amplification of *Cav1* 3'UTR	
Cav1_3'UTR_XhoI_F	ATTCTCGAGTTAAACCCATTCCTGCTCTCTC
Cav1_3'UTR_NotI_R	ATTGCGGCCGCAGTAGGTAGCAGGTTGGTAAAG
Amplification of *Ccng1* 3'UTR	
Ccng1_3'UTR_XhoI_F	ATTCCTCGAGATAAGCCCATGCAGAACAAC
Ccng1_3'UTR_NotI_R	ATTGCGGCCGCTGGAGGTGTCTCCTTACG
Amplification of *Mapkapk3* 3'UTR	
Mapkapk3_3'UTR_XhoI_F	CCAGCTCGAGTGTAATGTCCTGAGGCTCTGG
Mapkapk3_3'UTR_NotI_R	ATTGCGGCCGCGATCTAAGGTTTCCCAGCC
Mutagenesis of *Mapkapk3* 3'UTR	
Mapkapk3_mut_F	CCTTTTTCCAGTTTGGAAACCTCACTCACACAAA AGCCCCCACC
Mapkapk3_mut_R	GGTGGGGGCTTTTGTGTGAGTGAGGTTTCCAAA CTGGAAAAAGG
Sequencing Bmi1_3'UTR	
Bmi1_3'UTR_XhoI_F	ATTCTCGAGCATGTGACTGTCGTCCAGTTTGC
Sequencing Cav1_3'UTR	
Cav1_3'UTR_NotI_R	ATTGCGGCCGCAGTAGGTAGCAGGTTGGTAAAG
Sequencing Ccng1_3'UTR	
2380_CCNG1 mRNA_mmu	CTCACGGTTAGGGGAAACTCCTG
Sequencing Mapkapk3_3'UTR and Mapkapk3 3'UTR mutant	
Mapkapk3_3'UTR_XhoI_F	CCAGCTCGAGTGTAATGTCCTGAGGCTCTGG
Mapkapk3_3'UTR_NotI_R	ATTGCGGCCGCGATCTAAGGTTTCCCAGCC

Table 2.7 PCR conditions to amplify the 3'UTR of *Bmi1, Cav1, Ccng1* and *Mapkapk3*

Step	Temperature	Time	Number of cycles
Initial denaturation	95°C	2 min	1
Denaturation	95°C	30 sec	30
Annealing • Bmi1 3'UTR • Cav1 3'UTR • Ccng1 3'UTR • Mapkapk3 3'UTR	 55°C 55°C 55°C 56°C	 30 sec 30 sec 30 sec 30 sec	
Extension • Bmi1 3'UTR • Cav1 3'UTR • Ccng1 3'UTR • Mapkapk3 3'UTR	 72°C 72°C 72°C 72°C	 2.5 min 2.5 min 2.5 min 2 min	
Final extension	72°C	5 min	1
Hold	4°C	Indefinite	1

Table 2.8 Volumes per well of co-transfection for luciferase reporter assays in 96-well plates

psi-CHECK2 (50 ng/ µl) (µl)	Volume of 500 nM siRNA or miRNA (µl)	Opti-MEM (µl)	2.5% Lipofectamine 2000 in Opti-MEM (µl)	Cell density	Total transfection volume (µl)
1	5	4	10	$1.5x10^4$ in 80 µl	100

2.10 Cell cycle analysis

NIH 3T3 cells were untreated or transfected with RISC-free siRNAs, miR-27a mimics, miR-27a inhibitors or gene-specific siRNAs in a 6-well plate for 24 h prior to serum starvation for further 24 h. To synchronise cells in G0/G1, cells were kept in media containing 0.5% HI-CS (Sigma), 1% L-glu and 1% Pen/Strep for 24 h due to data showing that the majority of cells is in G0/G1 at this time point (Fig. 2.2). To re-stimulate cells, the media was replaced with media containing 10% serum. At the desired time points, cells were washed once with 1 ml warm PBS and trypsinised using 300 µl trypsin (Gibco, Life Technologies). Cells were spun at 1,000 rpm at 4°C for 5 min and resuspended in 1 ml cold FACS-PBS buffer (PBS, 5%BSA and 0.05% sodium azide). Cells were fixed in 70% cold ethanol by slowly adding 1 ml cell suspension dropwise into 9 ml of 70% ethanol. Cells were kept overnight or several weeks at -20°C before staining.

To stain DNA content, the cell suspension in ethanol was centrifuged at 2,000 rpm, 4°C for 10 min. The supernatant was discarded and the cell pellet was resuspended in 2 ml FACS-PBS buffer. Cells were spun at 1,700 rpm, 4°C for 3 min and the buffer was completely discarded by tapping the tube on a tissue paper to remove excess buffer. Cells were stained with 300 µl FACS-PBS containing 50 µg/ml propidium iodide (Sigma) and 100 µg/ml RNase A (Sigma). The cell mixture was incubated in the dark at 37°C for 20 min. Samples can be stored at 4°C for a few days before analysis by flow cytometry (BD FACSCanto, Becton Dickinson). Data obtained from flow cytometry was analysed using FlowJo software.

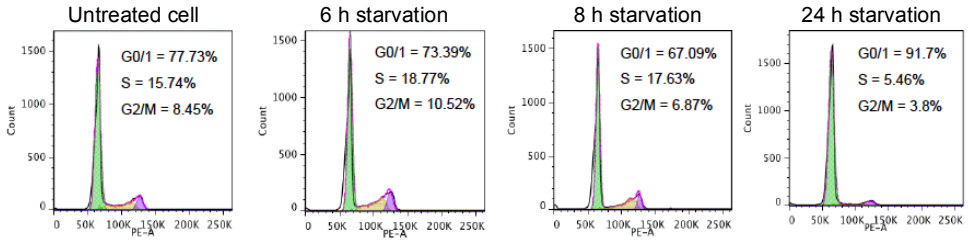

Figure 2.2 DNA histograms of G0/G1 synchronisation by serum starvation
NIH 3T3 cells were seeded in a 6-well plate at a density of $3x10^5$ cells in 1 ml media containing 10% serum for 24 h. The media was replaced with media containing 0.5% serum for 6, 8 and 24 h. Cell cycle was examined using propidium iodide staining followed by flow cytometry. The data present cell cycle profiles consisting of G0/G1 (2N), S and G2/M (4N) phase.

2.11 Generation of the NIH 3T3-PTH-mAGO2 stable cell line expressing PTH-mAGO2 using lentiviral transduction

2.11.1 Generation of the transfer plasmid encoding PTH-mouse AGO2 (pLVX-CAG-PTH-mAGO2)

The PTH-mAGO2 fragment (3 kb) was amplified from pCDNA3-PTH-mAGO2 and cloned into pLVX-CAG (Fig 2.3). To amplify PTH-mAGO2, a 50 µl PCR reaction volume contained 5 µl of 10x buffer, 1 µl of 10 mM dNTPs, 1 µl of 10 µM forward primer, 1 µl of 10 µM reverse primer, 1 µl of *Pfu* DNA polymerase (Promega), 20 ng of pCDNA3-PTH-mAGO2 and dH_2O. The cycling conditions consist of the initial denaturation at 95°C for 2 min, amplification for 30 cycles comprising 95°C for 30 sec, 65°C for 30 sec and 72°C for 3 min, followed by final extension at 72°C for 5 min. The PCR product was held at 4°C. Table 2.9 provides a list of primers using for PCR and sequencing to check the sequences. The amplified products and pLVX-CAG vector were digested with XhoI (NEB) and NotI (NEB) and gel purified using QIAquick Gel Extraction Kit (QIAGEN) according to manufacturers' protocols. The purified fragments were ligated into digested pLVX-CAG at a molar ratio of 3:1 based on the protocol described in section 2.9.1.

2.11.2 Transfection of plasmids

NIH 3T3 cells were transfected with pLVX-CAG-PTH-mAGO2 in a 6-well plate format using lipofectamine 2000 (Invitrogen). The general procedure of the

transfection is described in section 2.3. 200 µl of transfection mixture was prepared from 100 µl Opti-MEM containing 1.5 µg of the plasmid and 100 µl of 3% lipofectamine in Opti-MEM. 200 µl of transfection mixture was mixed with 800 ul of $3x10^5$ cells. Cells were incubated at 37°C for 30 h and the cell lysate was collected for Western blot analysis to examine the expression of PTH-mAGO2.

2.11.3 Lentiviral production

HEK293T cells were seeded in 4 of 10 cm dish at a density of $4.5x10^6$ cells/dish for 24 h prior to transfection with 16 µg of pLVX-CAG-PTH-mAGO2, 4.5 µg of pMD2.G-VSV-G (envelope plasmid) and 11.5 µg of psPAX2 (packaging plasmid) using the calcium chloride method. At 14-16 h post transfection, the media was replaced with 12 ml complete media containing 10 µM sodium butyrate. The supernatant was collected at 30 h after media changing, then filtered through 0.22 µm filters and ultracentrifuged at 19,500 rpm at room temperature for 2 h. Pellets were resuspended with 570 µl of complete IMEM and stored at -80°C.

2.11.4 Lentiviral transduction

NIH 3T3 cells were seeded in a 6-well plate at a density of $1x10^5$ cells in 2 ml complete media and incubated at 37°C for 24 h. Cells were transduced with three different volumes (12, 24 and 48 µl) of the concentrated virus in 1 ml complete media containing 4 µg/ml polybrene. The transduction was enhanced by centrifugation at 500g, room temperature for 1 h. Cells were incubated at 37°C for 18 h and the media was replaced with 2 ml complete media. At 24 h later, the media was once again replaced with 2 ml complete media. Cells were maintained in the complete media with 1 µg/ml puromycin for 7 days with daily media changing to positively select transduced cells.

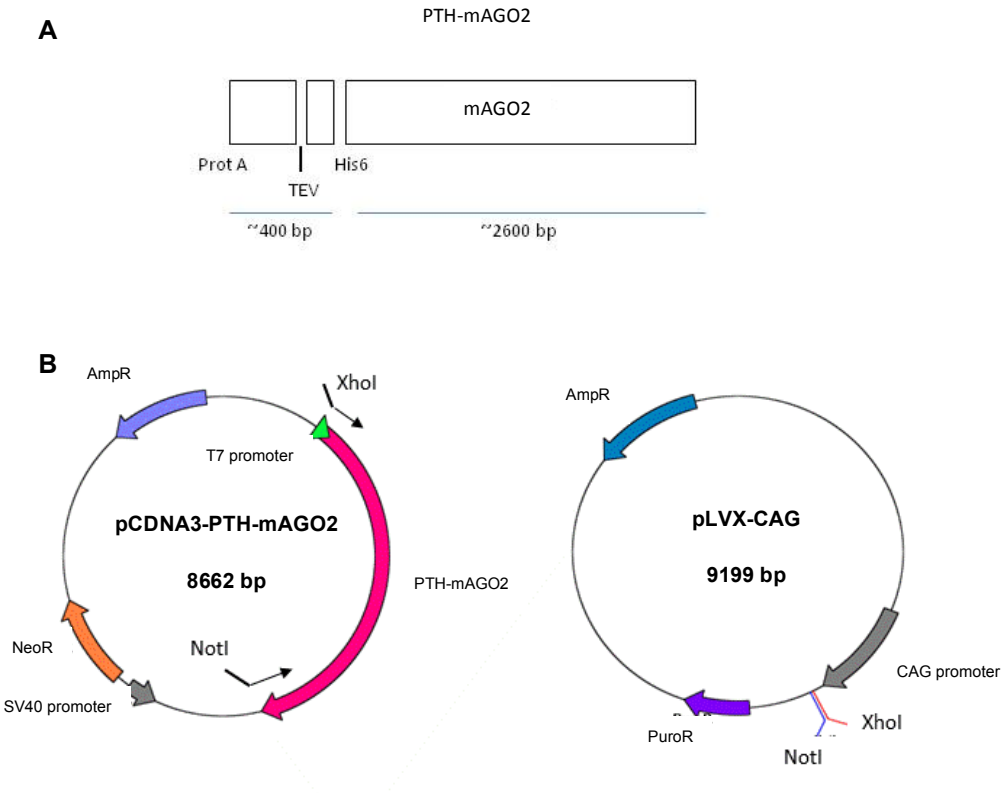

Figure 2.3 Diagram of PTH-mAGO2, pCDNA3-PTH-mAGO2 and pLVX-CAG
(A) A schematic diagram of PTH-mAGO2 consisting of protein A (ProtA), tobacco etch virus (TEV) protease cleavage site, histidine tag (6x His) and mAGO2. **(B, left)** pCDNA3-PTH-mAGO2. The forward primer with XhoI restriction site and the reverse primer containing NotI restriction site were used to amplify PTH-mAGO2. **(B, right)** The amplified fragment was cloned into pLVX-CAG plasmid at XhoI and NotI site.

Table 2.9. A list of primer for amplifying PTH-mAGO2 from pCDNA3-PTH-mAGO2 and sequencing

Primer	Sequence
Primers for amplification	
PTH-mAGO2_XhoI_F	CACCTCGAGGAGACCCAAGCTTGGTAC
PTH-mAGO2_NotI_R	AATGCGGCCGCTCAAGCAAAGTACATGG
Primers for sequencing	
PTH-mAGO2_XhoI_F	CACCTCGAGGAGACCCAAGCTTGGTAC
PTH-mAGO2_NotI_R	AATGCGGCCGCTCAAGCAAAGTACATGG
pLVX CAG_3824	GGCTCTAGAGCCTCTGCTAACC

The restriction sites are underlined.

2.12 Cross-linking, ligation and sequencing of hybrids (CLASH)

To prepare the samples, NIH 3T3-PTH-mAGO2 cells expressing PTH-mAGO2 were seeded in 15 cm plates at a density of $3x10^6$ cells/plate in 20 ml complete media. A total of 8 plates were used per condition. Cells were incubated at 37°C for 24 h. Cells were mock-infected or infected with wild type MCMV or MCMV Δm169 at MOI of 5 for 24 h. The control from HEK293-PTH-hAGO2 cells was prepared by Katrina Gordon (Buck lab). The cells were seeded in 15 cm plates at a density of $1x10^7$ cells/plate in 30 ml complete media (DMEM containing 10% HI-FBS, 1% L-glu and 1% Pen/strep) for eight plates (four plates per sample). After 24 h cells were untreated or induced for hAGO2 production with 0.5μg/ml doxycycline (Sigma) for 36 h. Cells were then washed once with cold-PBS and UV-irradiated at 254 nm, 400 mJ/cm^2 on ice (CL-1000 Ultraviolet crosslinker, UVP). Cells were lysed with 2.5 ml cold lysis buffer per plate. The cell lysate was centrifuged at 3,000 rpm, 4°C for 20 min. The lysate was either immediately used in the next steps or kept at -80°C for later use. Due to complication of CLASH protocol, it is highly recommended to thoroughly study the published protocol for the whole procedure and materials used (Helwak et al., 2013; Helwak and Tollervey, 2014). Here, it is not possible to describe all details of the protocol. Thus, brief information is provided to understand the principle of the approach and interpretation of results (Fig 2.4).

2.12.1 Major steps of the protocol

Immunoprecipitation: The lysate from one sample was incubated at 4°C for 1 h with 25 mg of Dynabeads (Invitrogen) coated with rabbit IgG (I5006, Sigma).

RNase digestion: On dynabeads, the protein-RNA complex was treated with 0.5 unit of RNaseA and T1 mixture (Agilent) at 20°C for 5 min to trim RNAs. The sample was transferred on ice immediately to slow down the reaction. The RNaseA digestion buffer was discarded and beads immediately washed.

Elution of protein-RNA complexes from Dynabeads: The protein-RNA complexes were eluted from Dynabeads with the buffer containing denaturing 6 M guanidine-HCl.

Ni-NTA purification: 80 µl of Ni-NTA suspension was used per sample. The Ni-NTA was washed with buffer and incubated with the eluate from Dynabeads at 4°C for 2 h with rotation. The Ni-NTA was transferred onto a spin column (Thermo Scientific) and washed to remove non-specific binding.

Phosphorylation and inter-molecular ligation: On the column, RNAs were phosphorylated using T4 polynucleotide kinase (T4 PNK) (NEB) at 20°C for 2 h 30 min. The beads were washed several times with buffers as described in the original protocol. Subsequently, RNAs were ligated to one another using T4 RNA ligase (NEB) at 16°C, overnight.

Dephosphorylation and 3'linker ligation: RNA was dephosphorylated with thermosensitive alkaline phosphatase (TSAP) (Promega) at 20°C for 45 min and ligated to the 3'linker (miRCat-33) with T4 RNA ligase 2, truncated (NEB) at 16°C for 10-24 h.

Radioactive labelling and elution from Ni-NTA: RNA was radiolabeled with ^{32}P-γ-ATP using T4 PNK (NEB). The labeled RNA was eluted from Ni-NTA with buffer containing 200 mM imidazole in a total volume of 450 µl.

Acetone precipitation: This step is a modified version of the original protocol. The protein-RNA complexes were precipitated using acetone instead of TCA. 450 µl of eluate was precipitated with 1,125 µl acetone and 1.5 µl glycoblue at -20°C, overnight. The sample was spun at full speed, 4°C for 20 min. The pellets were dried at room temperature and resuspended in 25 µl of water. 10 µl of 2xNuPAGE LDS sample buffer was added into samples. The samples were heated at 65°C for 10 min prior to loading onto a SDS-PAGE gel.

SDS-PAGE gel and the transfer of protein-RNA complexes onto a membrane: Samples were resolved with a Bis-Tris 4–12% NuPAGE gel. The protein-RNA complexes were transferred to a nitrocellulose membrane and the membrane was wrapped with cling film and put in the cassette. An autoradiography film (Hybond-C Extra, GE healthcare) was placed on top of the membrane and developed using the X-ray developer (Konica Minolta).

Proteinase K digestion and RNA purification: The developed autoradiography film was precisely aligned on the nitrocellulose membrane. The bands with expected size around 110-130 kDa were carefully cut out and the protein-RNA complexes in the membrane eluted and treated with proteinase K mixture at 55°C for 2 h. The membrane was discarded and RNA was extracted from the solution using phenol-chloroform-isoamyl (PCI). The RNA pellets were air-dried and can be kept at -80C before proceeding to the next step.

Phosphorylation and 5'adapter ligation: The pellets were resuspended with phosphorylation mixture and incubated at 37°C for 30 min. The mixture of 5' ligation was added and samples were incubated at 16°C, overnight.

RNA purification: RNA from the previous reaction was extracted using PCI extraction.

Reverse transcription (RT) and PCR amplification: RNAs were used as the templates to synthesise cDNAs. PCR amplification to generate the library was conducted using cDNAs as templates.

Gel running and purification of the cDNA library: The PCR products from the previous step were loaded onto a 3% MetaPhor agarose gel (Lonza). The expected bands of DNA between 150-200 bp were excised and purified using MinElute Gel extraction kit (QAIGEN).

Deep sequencing of the cDNA library: The purified PCR products with unique barcode within 5' adapters (Table 2.10) were pooled and sequenced using Illumina HiSeq (GenePool, the University of Edinburgh)

Analysis of deep sequencing data: The analysis was carried out by Kashyap Chhartbar.

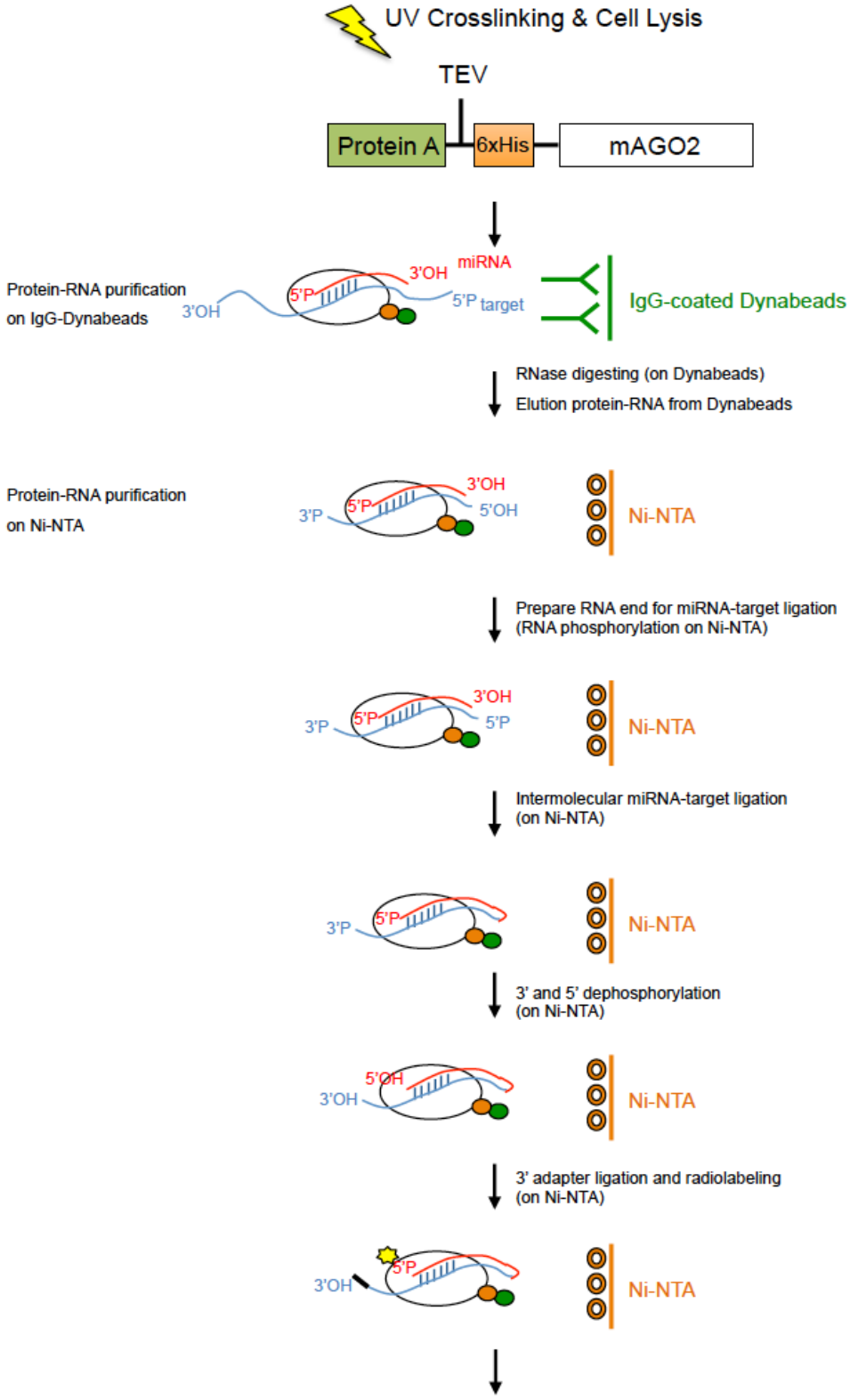
UV Crosslinking & Cell Lysis
TEV
Protein A
6xHis
mAGO2
Protein-RNA purification
on IgG-Dynabeads
3'OH
5'P
miRNA
5'P target
3'OH
IgG-coated Dynabeads
RNase digesting (on Dynabeads)
Elution protein-RNA from Dynabeads
Protein-RNA purification
on Ni-NTA
3'P
5'P
3'OH
5'OH
Ni-NTA
Prepare RNA end for miRNA-target ligation
(RNA phosphorylation on Ni-NTA)
3'P
5'P
3'OH
5'P
Ni-NTA
Intermolecular miRNA-target ligation
(on Ni-NTA)
3'P
5'P
Ni-NTA
3' and 5' dephosphorylation
(on Ni-NTA)
3'OH
5'OH
Ni-NTA
3' adapter ligation and radiolabeling
(on Ni-NTA)
3'OH
5'P
Ni-NTA

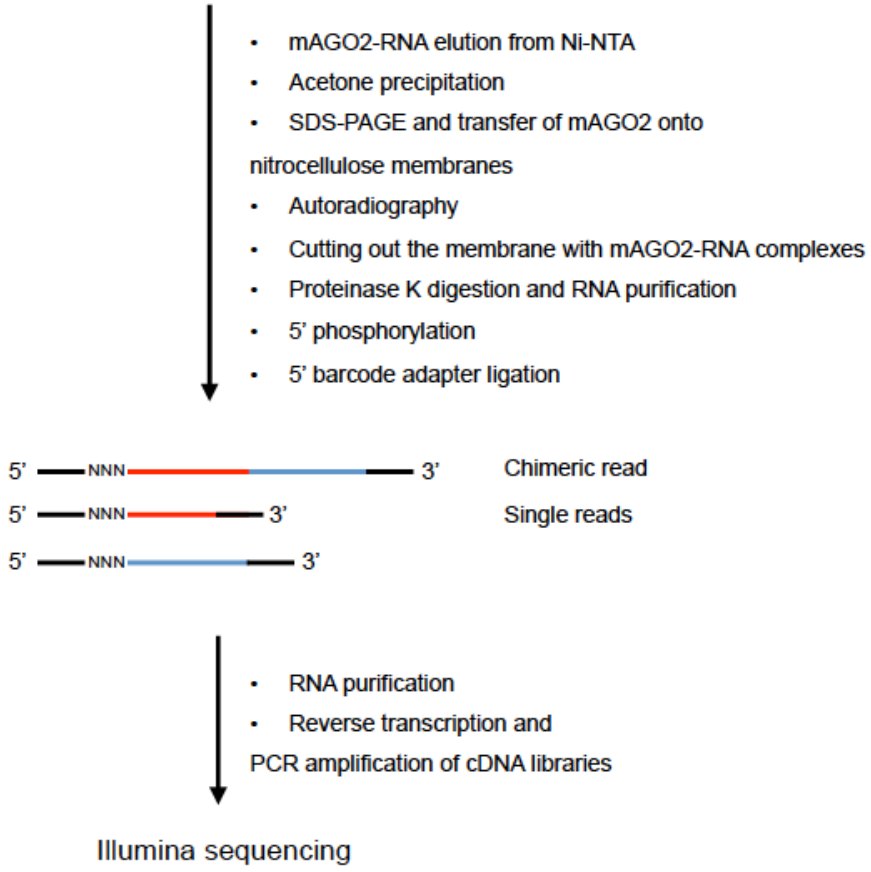

Figure 2.4. Overview of CLASH protocol (adapted from (Helwak and Tollervey, 2014))

Table 2.10 Sequences of barcodes used in CLASH protocol

Sample	Barcode name	Barcode sequence (5' to 3')
Mock infection	L5Ad	CGCUUAGC
Wild type MCMV	L5Aa	UAAGC
MCMV Δm169	L5Ab	AUUAGC
HEK293-PTH-hAGO2	L5Bd	UCUCUAGC

Chapter 3: Identification of miR-27 targets associated with MCMV infection

3.1 Introduction

Mouse cytomegalovirus (MCMV) encodes a non-coding RNA inhibitor, m169, which inhibits cellular miR-27 via a binding site within the 3'UTR of the m169 transcript. Figure 2.1 in materials and methods shows the location of m169 gene in the viral genome. Although it is still unknown why the virus mediates the degradation of host miR-27, it has been shown that the overexpression of miR-27 suppresses the replication of MCMV *in vitro* (Buck et al., 2010). There are two miR-27 family members, both of which are recognised by m169: miR-27a is encoded from an intergenic miR-23a~27a~24-2 cluster on chromosome 8 in mouse or chromosome 19 in human, whereas miR-27b is transcribed from intronic miR-23b~27b~24-1 on chromosome 13 in mouse or chromosome 9 in human. The mature forms of miR-27a and miR-27b have identical seed sequences allowing them to potentially share the same target mRNAs (Zhou et al., 2011). In this thesis, miR-27a and miR-27b are collectively referred to as "miR-27". It has previously been published that *in vitro* overexpression of miR-27 followed by MCMV infection at low MOI (MOI of 0.01) results in more than a log-fold decrease of viral titres, indicating strong anti-viral properties of this miRNA (Buck et al., 2010). In addition, Marcinowski *et al.* have shown that, *in vivo,* the degradation of miR-27 by m169 is important for the viral replication during the lytic stage of infection (Marcinowski et al., 2012). Mice were infected with wild type MCMV or m169 mutant in which the binding site of miR-27 was mutated to prevent the interaction with miR-27. Viral titres obtained from lungs, spleens and salivary glands of mice infected with m169 mutant showed at least 10 fold attenuation compared to wild type infection (Marcinowski et al., 2012). The phenotype observed from the *in vivo* study underscores the biological significance of miR-27 inhibition by m169 and suggests a viral strategy to interfere with functions of miR-27.

To date, little is known about m169. An analysis of MCMV transcriptomes using both classical cDNA cloning followed by sequencing of viral transcripts and next

generation sequencing of transcripts (RNA-Seq) revealed that m169 was the most abundant transcript and encoded for a novel protein (~17 kDa) with uncharacterised functions (Juranic Lisnic et al., 2013). It was proposed that m169 might employ a dual function as a non-coding RNA mediating miR-27 degradation and a protein-coding gene (Juranic Lisnic et al., 2013). The mechanism by which miR-27 is degraded is still not known but is likely to occur in the cytoplasm based on the observed co-localisation of miR-27 and m169 (Libri et al., 2012). Marcinowski *et al.* showed that m169-mediated degradation of miR-27 involved the addition of nucleotides to the 3'end of miR-27 (tailing) followed by the trimming of the sequence from the 3' end (trimming) (Marcinowski et al., 2012). Indeed, the degradation of miRNAs via a tailing and trimming process has been generally found for other cellular miRNAs in flies and mammals in which adenosine or uracil is added to the miRNA and 3'-to-5' exonucleases then digest the 3'end of the miRNA (reviewed in (Ameres and Zamore, 2013)).

The degradation of miR-27 by a viral non-coding RNA has also been observed in an oncogenic γ-herpesvirus, *Herpesvirus saimiri* (HVS). The virus encodes a viral U-rich non-coding RNA 1 (HSUR1), which mediates the degradation of miR-27 by an unknown mechanism (Cazalla et al., 2010). Interestingly, functional studies of miR-27 in human T cells revealed that miR-27 regulated the T cell receptor (TCR) signalling pathway via the adapter protein of TCR signalling, the growth factor receptor-bound protein 2 (GRB2) and two effectors of T cell activation: semaphorin 7A (SEMA7A) and interferon-γ (IFN-γ) (Guo et al., 2014). It was therefore proposed that HVS induced the degradation of miR-27 to ensure the activation of T cells that could sustain the viral genome and enhance viral latency (Guo et al., 2014).

This chapter focuses on an investigation of the targets of miR-27 in the context of MCMV infection in order to better understand why the virus targets this miRNA for degradation. In the final part of the chapter, the mechanism by which miR-27 suppresses MCMV replication and implications of miR-27 degradation upon the infection are discussed.

3.2 Aims

There are four aims of the present chapter:

1. To globally identify genes regulated by miR-27 in uninfected and infected NIH 3T3 cells
2. To identify and validate which of the genes regulated by miR-27 are required for MCMV infection
3. To determine whether these miR-27-regulated genes are direct targets of the miRNA
4. To understand the role of miR-27 target genes in the context of viral infection using wild type MCMV and m169 deletion strains (MCMV Δm169)

3.3 Results

3.3.1 Identification of genes regulated by miR-27 using microarray analysis

3.3.1.1 Overview and experimental design for microarray analysis

Microarray analysis of mRNAs following overexpression or inhibition of miRNAs is a widely used method to examine changes in the abundance of mRNAs, which could be potentially regulated by miRNAs. It is known that miRNAs can destabilise the mRNAs to which they bind. This is thought to occur via miRNA-mediated deadenylation of target mRNAs promoting de-capping and subsequent RNA degradation (Wu et al., 2006). In addition, a study has shown that the effects of miRNAs have on their targets at the mRNA levels are closely related to the effect in the protein levels (Guo et al., 2010). The author employed ribosome profiling which is a method based on deep sequencing of ribosome-protected mRNA fragments (RPFs) to determine the effect of miRNAs on protein production (Guo et al., 2010). Based on the studies reporting that miRNAs can repress translation either through inhibition of translation initiation (Chendrimada et al., 2007; Humphreys et al., 2005; Pillai et al., 2005) or inducing dissociation of ribosomes from mRNAs during translation elongation (Petersen et al., 2006), this would result in fewer ribosomes on target mRNAs leading to fewer RPFs. Guo *et al.* simultaneously compared ribosome profiling to the effect of miRNAs at mRNA level and demonstrated that the decrease of mRNA levels accounted for ~84% of the protein reduction, indicating that the decrease of protein is predominantly derived from mRNA repression (Guo et al., 2010). In the present chapter, microarray analysis was carried out to globally examine mRNA changes to identify genes that are regulated by miR-27 and functional screening was used to then examine those important for MCMV replication.

The outline of the experiment including the experimental design, sample preparation, assessments of sample quality, microarray analysis and analyses of microarray data is summarised in Fig 3.1. The mouse fibroblast cell line NIH 3T3 was used in this experiment for many reasons. First, the cells are permissive for MCMV infection (Smee et al., 1989). Second, miR-27 degradation by the viral transcript m169 has

been reproducibly conducted in NIH 3T3 cells (Libri et al., 2012; Marcinowski et al., 2012). Last, NIH 3T3 cells are available in the Buck lab and protocols related to the cell culture, transfection and infection for these cells are well optimised. To prepare samples for microarray analysis, six treatment groups were included as follows: 1) untreated cells, 2) RISC-free siRNA transfection, 3) miR-27a mimic transfection, 4) wild type MCMV infection, 5) m169 deletion MCMV (MCMV Δm169) infection and 6) miR-27a mimic transfection followed by wild type MCMV infection. Table 3.1 shows anticipated levels of miR-27 and its potential targets in each treatment for each of the samples. For comparison across the groups, the miR-27 and target levels in untreated cells are set as the baseline. The RISC-free siRNA transfection serves as a control for general expression changes associated with transfection. RISC-free siRNAs are chemically modified on both strands so that they cannot be processed and taken up by RISC; it is expected that neither miR-27 or its targets will be altered in this condition. In the miR-27a mimic transfection, it is expected that miR-27 will be highly overexpressed, leading to a reduction in miR-27 target mRNAs. In the context of infection, other viral factors in addition to miR-27 are expected to contribute to changes in host gene expression, complicating the interpretation of data when comparing uninfected and infected cells. To try to address this, the comparison of gene expression changes induced by MCMV and MCMV Δm169 was included. The expectation is that this would permit the identification of miR-27 targets specifically upregulated by m169 during MCMV infection. Taken together, the analysis of gene expression from all six conditions should increase the possibility of identifying miR-27 targets that play a role in MCMV infection.

To conduct the experiments, NIH 3T3 cells were seeded 24 h prior to infection with MCMV or MCMV Δm169 at MOI of 5 for 24 h. The time point of 24 hours post infection (hpi) was selected since previous studies have shown that MCMV (MOI of 5) dramatically degraded miR-27 (~90% degradation) at this time point (Buck et al., 2010; Libri et al., 2012). The combined miR-27a mimic transfection and MCMV infection was performed by transfection of the mimics for 24 h followed by infection with the virus at MOI of 5 for a further 24 h. As outlined in Fig 3.1, total RNA was extracted from samples and RNA integrity was determined by polyacrylamide gel

electophoresis (data not shown). The levels of miR-27 and m169 were quantified using qRT-PCR to evaluate the efficiency of transfection and infection. It was anticipated that miR-27 would be overexpressed in the transfected samples and downregulated in wild type virus-infected samples, due to the presence of m169, whereas infection with MCMV Δm169 should not alter miR-27 expression. After assessing the efficiency of transfections and infections, the corresponding cRNA samples were prepared and sent to the Wellcome Trust Clinical Research Facility (WTCRF, Western General Hospital, Edinburgh) for microarray analysis. The quality of amplified cRNAs was assessed using a Bioanalyzer before hybridisation to Illumina mouseref-6 array. Bioinformatic analysis of the data including quality control and analysis of differentially expressed genes was carried out by Alasdair Ivens (Centre for Infection Immunity and Evolution, Ashworth Laboratories, University of Edinburgh).

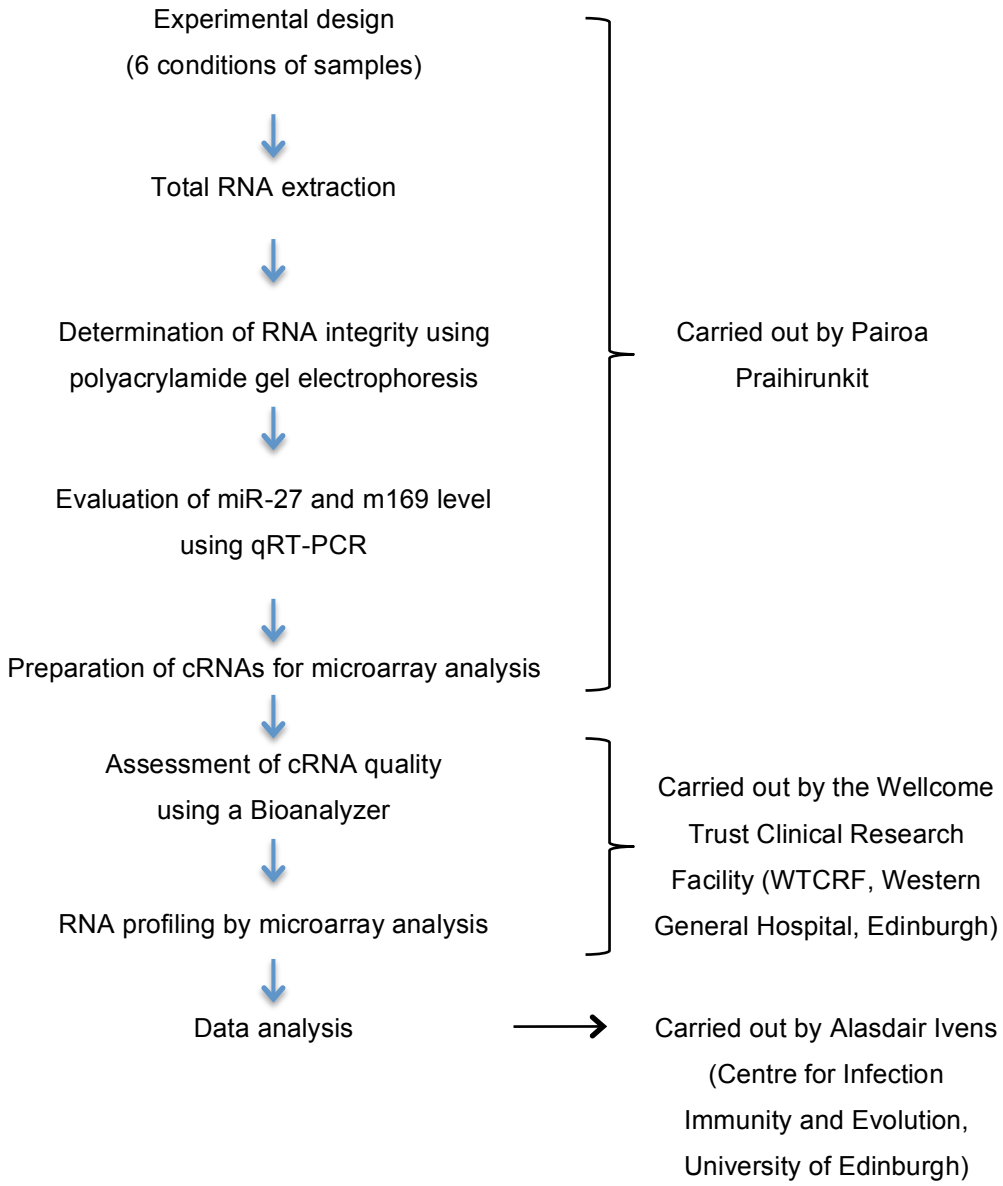

Figure 3.1 Overview of the workflow for microarray analysis
Six treatment conditions of NIH 3T3 cells (n=3) were included in the microarray analysis as described in the text. Total RNA was extracted from cells and RNA integrity was determined using polyacrylamide gel electophoresis. Expression of miR-27 and m169 was determined using qRT-PCR. Samples for microarray analysis were prepared as cRNAs using Illumina TotalPrep RNA Amplification (Ambion). The cRNAs were quantified and qualified using Bioanalyzer prior to microarray analysis. Microarray data quality was checked and quality control-passed samples were further analysed.

Table 3.1 Schematic of the expected levels of miR-27 and its targets across the sample conditions

Condition	miR-27	Target mRNA
1. Untreated cells	Baseline expression	Baseline expression
2. RISC-free siRNA transfection	Baseline expression in response to transfection	Baseline expression in response to transfection
3. miR-27a mimic transfection	Overexpression	Downregulation
4. Infection of wild type MCMV*	Downregulation due to the viral transcript m169	Upregulation as a result of miR-27 degradation
5. Infection of MCMV Δm169*	Comparable to baseline expression observed in untreated cells due to the absence of m169	Comparable to baseline expression observed in untreated cells due to unaltered miR-27
6. miR-27a mimic transfection followed by wild type MCMV infection*	Overexpression	Downregulation

*It is worth noting that altered expression of targets in infected cells (compared to uninfected cells) may also result from other effects of the virus that is difficult to predict.

3.3.1.2 miR-27 and m169 expression levels in the samples prepared for microarray analysis

Using qRT-PCR, the levels of miR-27 and m169 were assessed in cells transfected with miR-27 mimics, or infected with wild type MCMV or MCMV Δm169. As described in 3.3.1.1, eighteen samples were collected, corresponding to the six sample conditions with three technical replicates. As expected, miR-27 was upregulated ~50 fold in cells transfected with miR-27 mimics compared to RISC-free siRNAs (Fig 3.2A). Wild type MCMV significantly downregulated miR-27 (~10 fold reduction) in comparison to untreated cells, whereas MCMV Δm169 did not alter miR-27 levels. The comparison of miR-27 levels upon MCMV and MCMV Δm169 infection revealed that miR-27 was significantly reduced only by wild type MCMV. Similar to miR-27 mimic transfection, the combined miR-27 mimic transfection and wild type MCMV infection showed a significant increase in miR-27

compared to infection alone. However, it is worth noting that the levels of miR-27 were significanlty decreased in cells transfected with miR-27 mimics followed by MCMV infection compared to cells transfected with miR-27 mimics that were uninfected (perhaps due to MCMV-induced miR-27 degradation of the synthetic RNA). In virus-infected samples, m169 was observed only upon infection with MCMV and not in MCMV Δm169, as expected (Fig 3.2B). Collectively, these results confirmed that the transfections and infections of the cells were successful and levels of miR-27 and m169 were consistent with what was expected (Table 3.1).

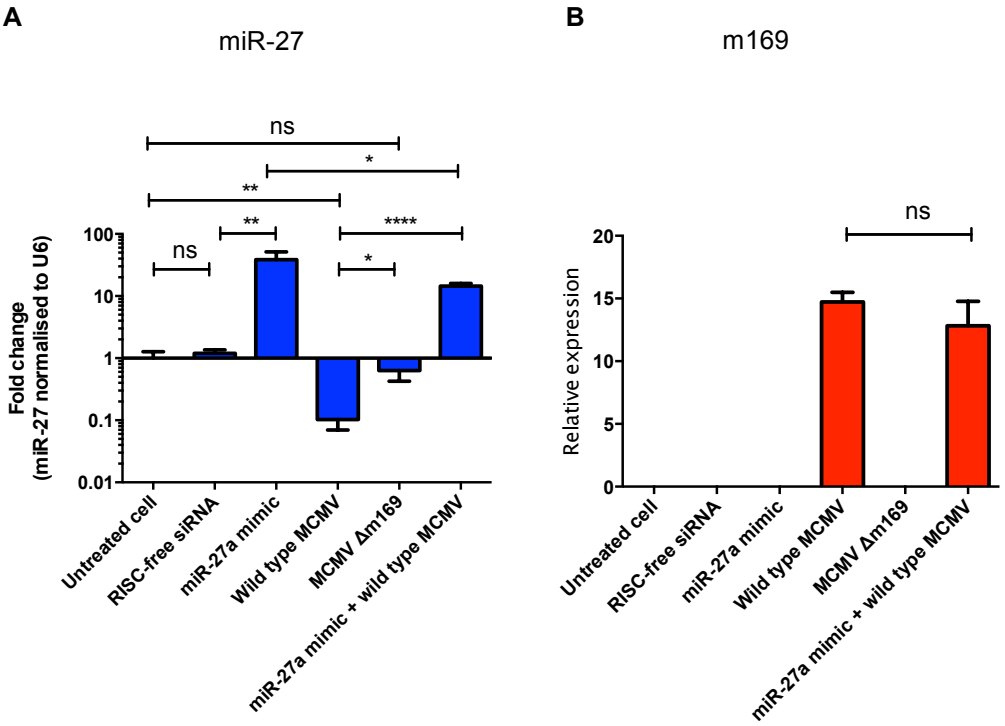

Figure 3.2 Levels of miR-27 and m169 in transfected and/or infected cells
(A) miR-27 and **(B)** m169 levels based on qRT-PCR across six sample conditions. The X-axis notes the samples transfected with RISC-free siRNAs or miR-27a mimics (25 nM, 48 h transfection) and infection status (MOI=5, 24 hpi). **(A)** miR-27 was normalised to U6 and fold changes (±SD) were calculated as compared to untreated cells (three technical replicates). **(B)** m169 was normalised to Gapdh. Data are represented as relative expression. Significant noted is based on an unpaired t test (*p<0.05, **p<0.01 and ****p<0.0001).

3.3.1.3 Comparison of viral growth properties of wild type MCMV and MCMV Δm169

In order to determine miR-27 targets in infected cells that are likely regulated under infection conditions, growth curve analysis of viruses was carried out in cells infected with MCMV or MCMV Δm169. Again, the difference between these two viruses is the lack of m169 gene, which encodes the miR-27 inhibitor and has recently also been shown to encode a small protein ~17 kDa (Juranic Lisnic et al., 2013). Due to the fact that other viral factors in addition to m169-mediated degradation of miR-27 also have an effect on cellular gene expression, it is logical to compare gene expression between cells infected with wild type MCMV and MCMV Δm169 rather than to compare infected cells to uninfected cells. This was expected to identify potential targets of miR-27 in the context of MCMV infection.

For this comparison to be valid, it is important that the viral infectivity of the two viruses is comparable. To address this, the viral growth of both wild type MCMV and MCMV Δm169 was assessed by standard plaque assays. NIH 3T3 cells were seeded in a 96-well plate for 24 h prior to infection with wild type MCMV or MCMV Δm169 at MOI of 0.01. As shown in Fig. 3.3, the growth curves of two viruses were almost identical throughout the time course of the infection and no significant differences in viral titres were observed. These data indicate that the deletion of m169 does not affect the viral infectivity. This implies that the subsequent comparison of differential host gene expression between these two viruses will not be complicated by differences in the amount of replicating virus.

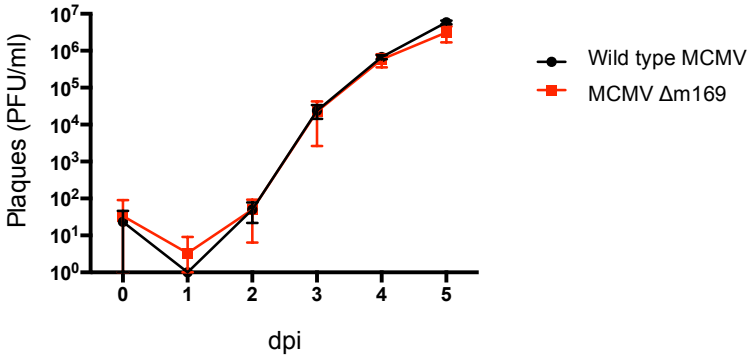

Figure 3.3 Viral growth curve of wild type MCMV and MCMV Δm169
NIH 3T3 cells were infected with wild type MCMV or MCMV Δm169 at MOI of 0.01. Supernatant was collected from day 0 to 5 days post infection (dpi) for standard plaque assays using MEFs P53$^{-/-}$ cells. Data are presented as means (±SD) of plaque forming units per ml of supernatant (PFU/ml) from three technical replicates. The result is a representative of two independent experiments.

3.3.1.4 Analysis of microarray data

3.3.1.4.1 Data processing and gene expression analysis

The analysis of raw data obtained from the microarray analysis was performed by Alasdair Ivens (Centre for Infection Immunity and Evolution, Ashworth Laboratories, University of Edinburgh). In brief, the raw data from Illumina mouseref-6 array BeadChip were QC analysed using the arrayQualityMetrics package in Bioconductor (Kauffmann and Huber, 2010). All arrays were QC-passed (data not shown) and subsequently filtered to include features with p-values of less than 0.01. Of 45,281 probes, 17,876 ($p<0.01$) represent 10,652 out of a possible 21,712 distinct transcripts. Next, normalisation of the 17,876 features across all arrays was performed using the robust spline normalisation (RSN) method. The differential expression was analysed using empirical Bayesian approaches in three comparisons: 1) miR-27a mimic versus RISC-free siRNA transfection, 2) miR-27a mimic transfection followed by MCMV infection versus MCMV infection and 3) MCMV Δm169 versus MCMV infection. The differential expression was presented as fold change (FC) with a positive FC indicating upregulation and a negative FC representing downregulation.

The differential gene expressions of the three comparisons are presented in volcano plots wherein differential expression was plotted in log2 FC against statistical significance (log10 of *p* value) (Fig 3.4). As mentioned earlier, the present chapter focuses on genes downregulated in these comparisons as potential targets of miR-27. The FC cut off of 1.20 and *p* value <0.05 was applied to filter genes for further analyses. The rationale for using this cut off was based on a previous study showing that miRNAs with 7 mer seed sequences typically resulted in subtle downregulation (1.18 fold) of target mRNAs (Nielsen et al., 2007). Thus, the cut off of 1.20 fold was thought to be a threshold to specifically identify potential targets of miR-27.

Based on the cut off of 1.20 ($p< 0.05$), a total of 97 genes were downregulated in cells transfected with miR-27a mimics compared to RISC-free siRNAs (Fig 3.5A, Appendix 1). miR-27a mimic transfection followed by MCMV infection resulted in 84 downregulated genes relative to MCMV infection alone (Fig 3.5B, Appendix 2). Infection with MCMV Δm169 compared to MCMV showed downregulation of 242 genes (Fig 3.5C, Appendix 3). To determine whether the transfection alone alters gene expression, the differential gene expression was analysed in cells transfected with RISC-free siRNAs compared to untreated cells. Transfection of RISC-free siRNAs resulted in downregulation of 22 genes (FC of 1.20 to 1.3, $p<0.05$) (Appendix 4). Only 1 out of 22 genes was found to be common with any of the comparisons described above and this gene (*Pja2*) was not analysed further as its expression differences likely related to transfection rather than miR-27. As shown in Fig 3.5, one gene (*Gaa*) was in common among the three comparisons and 23 genes were significantly downregulated in two or three of the comparisons.

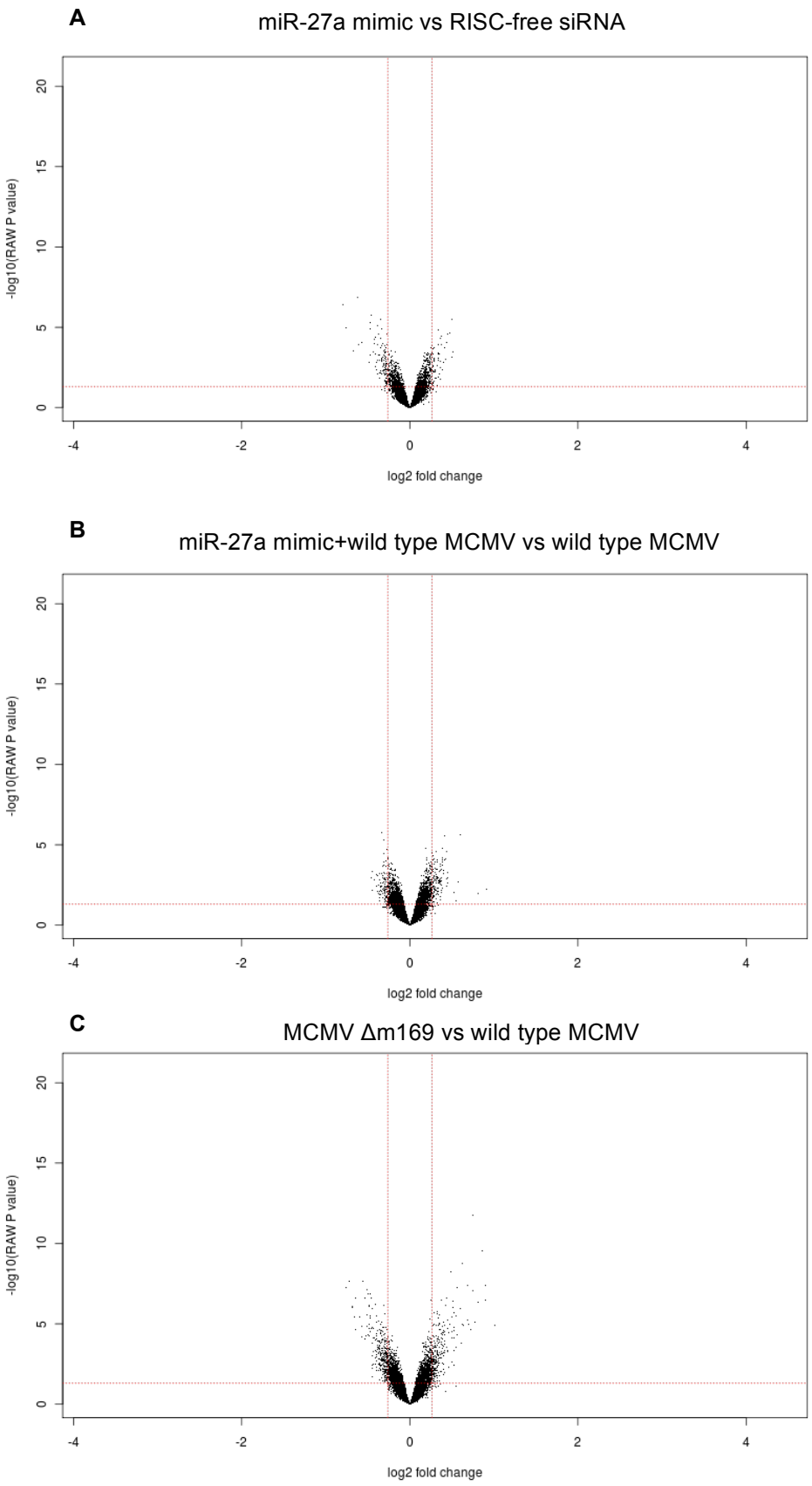
A
miR-27a mimic vs RISC-free siRNA
-log10(RAW P value)
log2 fold change
B
miR-27a mimic+wild type MCMV vs wild type MCMV
-log10(RAW P value)
log2 fold change
C
MCMV Δm169 vs wild type MCMV
-log10(RAW P value)
log2 fold change

Figure 3.4 Volcano plots of fold differences in gene expression obtained from microarray analysis
Differential gene expression of **(A)** miR-27a mimic versus RISC-free siRNA transfection, **(B)** miR-27a mimic transfection followed by wild type MCMV infection versus wild type MCMV infection and **(C)** MCMV Δm169 versus wild type MCMV infection. The plots represent statistical significance, *p* value (unadjusted *p* value) from a t test (log10) against fold change (log 2), from three technical replicates. The horizontal line indicates the *p* value cut off of 0.05 and verticle lines indicates 1.2 fold change.

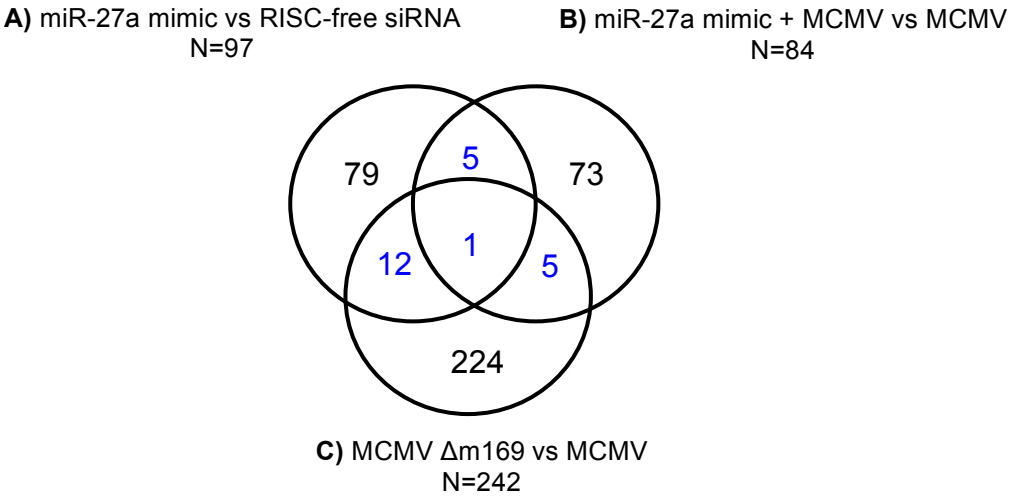

Figure 3.5 Venn diagram depicting the overlap of downregulated genes among the three comparisons
Downregulated genes (cut off ≥1.2, p <0.05) from the three datasets were overlapped. Numbers inside the circles represent numbers of genes.

3.3.1.4.2 Pathway and biological function analysis

The microarray analysis provides a large dataset of differential gene expression that requires the analysis approaches to extract the biological meaning hidden under the changes of gene expression. One of such approaches is pathway analysis, which reduces the complexity of data by grouping genes into small sets of related genes based on the cellular pathways or biological functions. In this chapter, Ingenuity Pathway Analysis (IPA) (http://www.ingenuity.com/), a web-based software application, was used to identify pathways and biological functions that might be regulated by miR-27 with or without MCMV infection.

Two sets of genes were submitted to IPA: 1) the 97 genes downregulated by miR-27a mimics compared to RISC-free siRNA transfection and 2) the 242 genes downregulated by MCMV Δm169 compared to wild type MCMV infection. The first comparison is a more straightforward way to examine the effects of miR-27 in uninfected cells, but holds the caveat that transfection of mimics could induce off-target effects (reviewed in (Thomson et al., 2011)). Table 3.2 shows the top canonical pathways enriched in genes regulated by miR-27 under these conditions. As shown in Table 3.3, the cell cycle was the most enriched biological function regulated by miR-27, suggesting a potential role of miR-27 related to the cell cycle. Based on these results, the functional role of miR-27 in the cell cycle was studied further in the next chapter.

The analysis of MCMV Δm169 compared to wild type MCMV infection should identify pathways regulated by miR-27 but holds the caveat that viral factors in addition to miR-27 could directly or indirectly affect the levels of miR-27 targets. It is worth noting that the effects of miRNAs are often subtle, whereas the change in gene expression induced by infection is often quite large, such that any subtle differences between MCMV and MCMV Δm169 derived from miR-27 could be missed out. Pathway analysis revealed that the top ranked pathways de-regulated in MCMV Δm169 versus wild type MCMV infection appeared to be involved in cholesterol biosynthesis (Table 3.4). As mentioned above, the pathway analysis of cells transfected with miR-27a mimics versus RISC-free siRNAs was expected to identify pathways regulated by miR-27 in the absence of infection, whereas MCMV Δm169 versus wild type MCMV infection would reveal biological pathways regulated by miR-27 in the context of viral infection.

Table 3.2 Top canonical pathways enriched for genes downregulated in miR-27a mimic versus RISC-free siRNA transfection.

Canonical pathway	p-value	Ratio	Gene
eNOS signalling	7.19E-06	6/151 (0.039)	*Aqp1*, *Calm1* (including others), *Cav1*, *Hsp90aa1*, *Kng1*, *Vegfb*
Nitric oxide signalling in the cardiovascular system	6.81E-05	5/99 (0.051)	*Calm1* (including others), *Cav1*, *Hsp90aa1*, *Kng1*, *Vegfb*
Hepatic fibrosis/hepatic stellate cell activation	9.99E-04	5/146 (0.034)	*Il1rl1*, *Vegfb*, *Acta2*, *Pdgfra*, *Ednra*
Aldosterone signalling in epithelial cells	1.49E-03	4/168 (0.023)	*Sgk1*, *Slc12a2*, *Hsp90aa1*, *Hspd1*
Glycogen degeneration III	1.58E-03	2/17 (0.118)	*Gaa*, *Pgm2*

Pathway analysis was performed using Ingenuity Pathway Analysis (IPA). The p-value is calculated using the right-tailed Fisher Exact Test ($p<0.05$). The ratio represents the number of genes in the dataset divided by the total number of genes in a given pathway. Predicted targets of miR-27 obtained from TargetScan (www.targetscan.org) are underlined.

Table 3.3 Biological functions enriched for genes downregulated in miR-27a mimic versus RISC-free siRNA transfection

Function	p-value	Number of genes	Gene
Cell cycle progression	4.24E-04	23	*Adora2b*, *Akr1b1, Btg1, Calm1* (includes others), *Cav1, Ccng1*, *Cenpb, Bmi1, Dph1, Dynlt3, Gas7, Ifi204* (includes others), *Kng1, Map2k4, Marcks, Pdgfra, Prkar1a, Rhou, Sgk1, Spp1, Tcp1, Xrcc6, Zwint*
Proliferation of fibroblasts	1.18E-04	12	*Aqp1, Cav1, Ccng1, Dph1, Ednra, Idh2, Kng1, Pdgfra, Phf14, Plau, Sfrp1, Top1*mt
Degeneration of cells	5.47E-05	11	*Arnt, Cav1, Cd81, Celf1, Bmi1, Cp, Dtna, Plau, Sgcb, Spp1, Vegfb*
Homeostasis of blood	6.34E-06	7	*Acadm, C3, Cav1, Gnas, Gpd2, Top1mt, Vav3*
Permeability of blood vessel	1.55E-06	7	*Acta2, Aqp1, C3, Cav1, Dtna, Kng1, Plau*
Degeneration of muscle cells	9.54E-09	7	*Arnt, Cav1, Cd81, Celf1, Dtna, Plau, Sgcb*

Analysis of biological functions was performed using Ingenuity Pathway Analysis (IPA). The p-value is calculated using the right-tailed Fisher Exact Test ($p<0.05$). The ratio represents the number of genes in the dataset divided by the total number of genes in a given pathway. Predicted targets of miR-27 obtained from TargetScan database are underlined (www.targetscan.org).

Table 3.4 Top canonical pathways enriched for genes downregulated in MCMV Δm169 versus wild type MCMV infection

Canonical pathway	p-value	Ratio	Gene
Superpathway of cholesterol biosynthesis	8.5E-08	7/87 (0.08)	*Acat2/Acat3, Dhcr24, Fdps, Hsd17b17, Mvd, Nsdhl, Sqle*
Cholesterol Biosynthesis I	1.75E-05	4/40 (0.1)	*Dhcr24, Hsd17b17, Nsdhl, Sqle*
Cholesterol Biosynthesis II (via 24,25-dihydrolanosterol)	1.75E-05	4/40 (0.1)	*Dhcr24, Hsd17b17, Nsdhl, Sqle*
Cholesterol Biosynthesis III (via Desmosterol)	1.75E-05	4/40 (0.1)	*Dhcr24, Hsd17b17, Nsdhl, Sqle*
Epithelial Adherens Junction signalling	1.98E-05	9/132 (0.068)	*Actn1, Acvr2b, Ctnnb1, Mras, Tcf7l1, Tgfbr1, Tgfbr2, Tuba1a, Tubb2b*
Telomerase Signalling	4.4E-05	8/105 (0.0755)	*Pik3r3, Ppp2r1a, Hsp90ab1, Pik3r1, Hdac7, Mras, Terf1, Hdac5*
Human Embryonic Stem Cell Pluripotency	5.49E-05	9/161 (0.0559)	*Pik3r3, Tgfbr2, Tgfbr1, Pik3r1, Mras, Pdgfra, Fgfr2, Tcf7l1, Ctnnb1*
Regulation of the Epithelial-Mesenchymal Transition Pathway	1.09E-04	10/196 (0.051)	*Pik3r3, Tgfbr2, Lox, Tgfbr1, Gab1, Pik3r1, Mras, Fgfr2, Mmp2, Tcf7l1*
PTEN Signalling	1.25E-04	8/137 (0.058)	*Pik3r3, Tgfbr2, Tgfbr1, Pik3r1, Mras, Pdgfra, Itga5, Fgfr2*
PI3K/AKT Signalling	1.77E04	8/152 (0.0526)	*Pik3r3, Ppp2r1a, Gab1, Hsp90ab1, Pik3r1, Mras, Itga5, Ctnnb1*
NF-κB Signalling	2.81E-04	9/174 (0.0517)	*Pik3r3, Tgfbr2, Tgfbr1, Pik3r1, Ube2v1, Mras, Pdgfra, Fgfr2, Tbk1*

Pathway analysis was performed using Ingenuity Pathway Analysis (IPA). The p-value is calculated using the right-tailed Fisher Exact Test ($p<0.05$). The ratio represents the number of genes in the dataset divided by the total number of genes in a given pathway. Predicted targets of miR-27 obtained from TargetScan (www.targetscan.org) are underlined.

3.3.1.5 Selected genes from microarray analysis for the functional screening of genes involved in MCMV replication

The microarray data were analysed using various approaches including gene overlapping (Fig 3.5), pathway analysis (Table 3.2 and 3.4) and biological function (Table 3.3). The aim of using several methods of analyses was, ideally, to identify overlap in order to select the most promising targets of miR-27 for further functional screening. In addition to microarray analysis performed in the present study, the Buck lab previously carried out microarray analysis in cells transfected with RISC-free siRNAs, miR-27a mimics or miR-27a inhibitors (unpublished data). These data were previously analysed and Table 3.5 shows 14 genes with the largest downregulation in cells transfected with miR-27a mimics relative to miR-27a inhibitors that could be potential targets of miR-27. All of these 14 genes were included in the functional screening and a total of 3 out of the 14 (*Serpina3n, Mmd* and *Ccng1*) overlaps with genes identified in the present microarray analysis.

In summary, from the microarray data a total of 53 genes were selected for the functional screening (Table 3.6): 23 genes overlapping between comparisons of microarray data, 19 genes from pathway analysis and biological function that are computationally predicted targets based on TargetScan (www.targetscan.org) and 14 genes from the previous microarray analysis (3 out of the 14 overlap with genes obtained from the microarray analysis in the present study).

Table 3.5 Data from a previous microarray analysis showing most downregulated genes in cells transfected with miR-27a mimics versus miR-27a inhibitors

Gene	FC (miR-27a mimic vs miR-27a inhibitor)	FC (miR-27a mimic vs RISC-free siRNA)	FC (miR-27 inhibitor vs RISC-free siRNA)	No. of conserved binding site	No. of poorly conserved binding site
1. *Il1rl1*	-4.0622	-1.8686	2.1739	0	0
2. ***Serpina3n***	-3.7837	-2.1515	1.7586	0	0
3. *Serpine1*	-3.2466	-1.2394	2.6194	0	0
4. ***Mmd***	-2.5660	-1.7323	1.4812	1	0
5.*Ccl2*	-2.3675	-1.3911	1.7018	0	2
6. ***Ccng1***	-2.2226	-1.3521	1.6437	1	0
7. *Mapkapk3*	-2.1494	-1.4635	1.4686	1	0
8. *Gpr176*	-2.0051	-1.3887	1.4438	0	1
9. *Hmga1*	-1.8497	-1.3998	1.3213	0	0
10. *Plekhj1*	-1.7713	-1.3838	1.2799	0	1
11. *Csf1*	-1.7630	-1.2623	1.3966	2	0
12. *Nsg1*	-1.7335	-1.3183	1.3149	0	2
13. *Dusp5*	-1.6304	-1.2509	1.3034	0	0
14. *Lyar*	-1.6153	-1.2239	1.3198	0	0

FC: fold change
Predicted binding sites were obtained from TargetScan database (www.targetscan.org).
Serpina3n, Mmd and ***Ccng1*** overlap with genes obtained from the microarray analysis presented in Table 3.6.

Table 3.6 The 53 genes selected for the functional screening

Analysis of microarray data	Numbers of genes	Gene
1. Overlap of miR-27a mimic vs RISC-free siRNA, miR-27a mimic&WT vs WT and MT vs WT	1	*Gaa*
2. Overlap of miR-27a mimic vs RISC-free siRNA and miR-27a mimic&WT vs WT	5	*C3, Kng1, Spp1, Ugt1a10, Serpina3n*
3. Overlap of miR-27a mimic vs RISC-free siRNA and MT vs WT	12	*0610007P14Rik, B4galt3, Calm3, Cd99l2, Celf1, Mmd, Pdgfra, Pdia5, Pgm2, Sfrp1, Tmsb10, Ubtd2*
4. Overlap of miR-27a mimic &WT vs WT and MT vs WT	5	*Papola, Setd5, Usp1, Nudt18, Rpl18a*
5. Pathway analysis and biological functions of miR-27a mimic vs RISC-free siRNA*	11	*Hsp90AA1, Vegfb, Phf14, Plau, Top1mt, Ednra, Gas7, Ccng1, Map2k4, Marcks, Zwint*
6. Pathway analysis of MT vs WT*	8	*Dhcr24, Gab1, Itga5, Lox, Pik3r1, Pik3r3, Tgfbr1, Ube2v1*
7. Genes with the largest downregulation in miR-27a mimic vs miR-27a inhibitor **(Data from the previous microarray analysis carried out in the Buck lab)**	11	*Il1rl1, Serpine1, Ccl2, Mapkapk3, Gpr176, Hmga1, Plekhj1, Csf1, Nsg1, Dusp5, Lyar*

miR-27a mimic&WT: Cells transfected with miR-27a mimics followed by infection with wild type MCMV
WT: Wild type MCMV infection
MT: MCMV Δm169 infection
*Genes from pathway analysis and biological function that are predicted as targets of miR-27 based on TargetScan (www.targetscan.org)

3.3.2 Functional screening of genes required for MCMV infection

The primary aim of this chapter is to identify cellular targets of miR-27 that might play a role in MCMV infection. In the previous section, 53 genes were chosen from the analysis of microarray data based on their differential expression in at least one of the datasets, as described above. Functional screening was then carried out to determine whether any of the 53 genes impacts MCMV replication *in vitro*. The replication of MCMV was assessed using a virus that contains a green fluorescent protein (GFP-MCMV) upstream of the immediate early gene 2 (*ie2*), where the insertion does not alter the viral growth (Manning and Mocarski, 1988). Genes required for MCMV growth *in vitro* are expected to cause a reduction in the GFP signal following siRNA knockdown. Hence, this approach should identify genes that play an important role in supporting MCMV replication, which are also potentially regulated by miR-27.

To perform the screen, NIH 3T3 cells were untreated or transfected in a 96-well plate with controls or siRNA pools targeting each of the 53 genes. The negative controls include RISC-free siRNAs and negative pools: pool 2 and pool 3 containing four siRNAs with a minimum of 4 mismatches to all human, mouse and rat genes and are confirmed to have minimal gene targeting examined by microarray analysis. The positive control is eGFP siRNAs targeting the expressed GFP. Each siRNA pool consists of a mixture of four siRNAs targeting one gene at multiple locations. There are a few advantages of using pooled siRNAs compared to individual siRNAs. First, the use of pooled siRNAs is expected to reduce off-target effects due to lower concentrations of each siRNAs diluting their off-target effects (Hannus et al., 2014). Second, pooled siRNAs targeting multiple locations of the same gene reduce false negatives caused by mutations and splice variants (claimed by Dharmacon (Smith, 2006)). Last, for an initial large-scale screen, the approach using pooled siRNAs saves reagents and time compared to that using multiple individual siRNAs.

At 48 h post transfection, cells were infected with GFP-MCMV at MOI of 0.2. To quantify viral growth (and by inference, replication capacity), GFP expression was measured at approximately 70 hpi, after multiple rounds of replication have occurred

(Santhakumar et al., 2010). As shown in Fig 3.6A, GFP signals are reported in fold change relative to the RISC-free siRNA transfection samples. Cells transfected with eGFP siRNAs showed a significant reduction (~50%) of GFP expression, whereas negative pool2 and 3 did not affect GFP signals. Knockdown of five genes (*Rpl18a, Lyar, Itga5, Mapkapk3* and *Pik3r1*) led to a significant reduction in GFP expression, whereas knockdown of each of 10 other genes (*Gaa, Nsg1, B4galt3, Gab1, Nudt18, Ugt1a10, Tgfbr1, Serpine1, Phf14* and *Plau*) significantly induced GFP expression. Cell viability assays were performed in parallel at 48 h post-transfection to determine toxicity of the transfection. The cell viability was evaluated through the measurement of a fluorescent product converted from a redox dye in living cells. As shown in Fig. 3.6B, transfection of *Hsp90aa1* siRNAs caused toxicity (~60% cell viability compared to untreated cells). Based on the high level of toxicity of *Hsp90aa1* siRNAs, it was not included in further studies. Knockdown of the five genes that showed anti-viral activity (*Rpl18a, Lyar, Itga5, Mapkapk3* and *Pik3r1*) did not appear to substantially induce cell toxicity as cell viability was in a range of 80-100%.

As mentioned above, knockdown of each of the 10 genes (*Gaa, Nsg1, B4galt3, Gab1, Nudt18, Ugt1a10, Tgfbr1, Serpine1, Phf14* and *Plau*) led to a significant increase of GFP expression. This could be due to a pro-viral effect of the knockdown or off-target effects of siRNAs causing unreliable results. Here, the focus is the effects of genes that caused GFP repression to infer whether they could be directly regulated by miR-27.

Although pool siRNAs have been thought to reduce off-target effects compared to individual siRNAs (as described above), there is still a risk that some of individual siRNAs could still cause off-target effect and could lead to false positive “hits” for the pool. To confirm the positive results obtained from pooled siRNAs, the functional screening was repeated using individual siRNAs that make up the pool. NIH 3T3 cells were untreated or transfected in a 96-well plate with RISC-free siRNAs, eGFP siRNAs, pooled siRNAs or individual siRNAs of the five genes (*Rpl18a, Lyar, Itga5, Mapkapk3* and *Pik3r1*) for 48 h. The cells were infected with GFP-MCMV at MOI of 0.2 and GFP expression was measured at approximately 70

hpi. In agreement with the results observed in cells transfected with pooled siRNAs, knockdown of the five genes using individual siRNAs significantly reduced GFP expression (Fig 3.7A). Knockdown of *Rpl18a* and *Mapkapk3* using three individual siRNAs significantly decreased GFP signals, whereas knockdown of *Lyar*, *Itga5* and *Pik3r1* by two individual siRNAs led to a significant repression of GFP. It is important to note, however, that due to limited amount of purchased siRNAs, the experiment to quantify the mRNA levels following the knockdown was not carried out.

In parallel, the cell viability assay was conducted to examine the toxicity of the transfection and results showed that viability of transfected samples was approximately 80-100% (Fig 3.7B). In conclusion, the significant decrease of GFP expression in knockdown of the five genes (*Rpl18a, Lyar, Itga5, Mapkapk3* and *Pik3r1*) using pooled or individual siRNAs suggests that these genes play a role in MCMV infection.

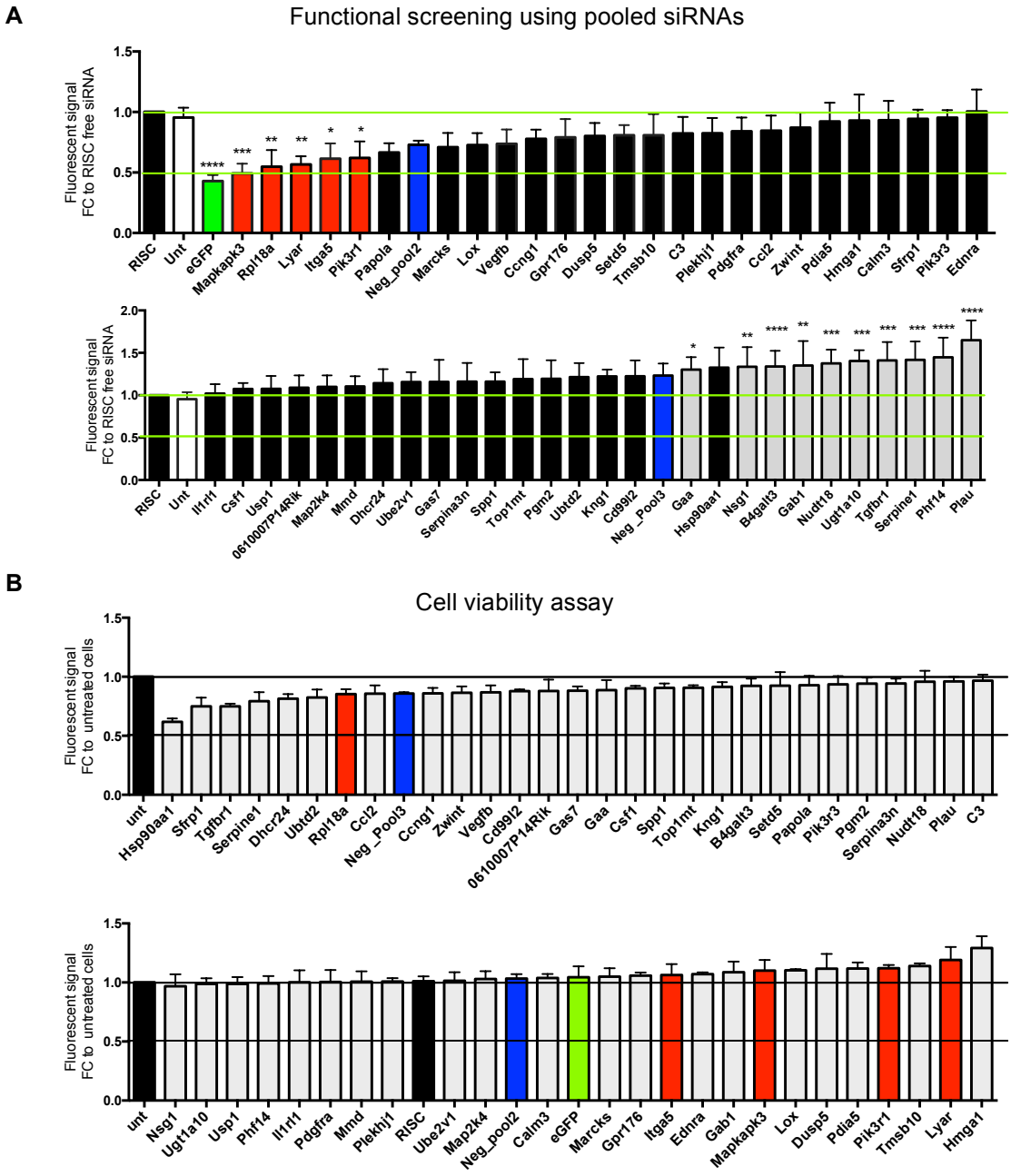

Figure 3.6 Functional screening to identify genes involved in MCMV infection
(A) GFP expression from knockdown cells using pooled siRNAs followed by infection of GFP-MCMV. The GFP signal is presented as means of fold change (±SD) from five technical replicates compared to cells treated with RISC-free siRNAs. Data presented here are representative of independent experiments. The statistics are based on one-way ANOVA, Kruskal-Wallis test (*p<0.05, **p<0.01, ***p<0.001 and ****p<0.0001). **(B)** Cell viability assays. Cells as described above were incubated with cell titer blue at 37°C for 2h. Results are shown as means of fold change (± SD) from three technical replicates compared to untreated cells.

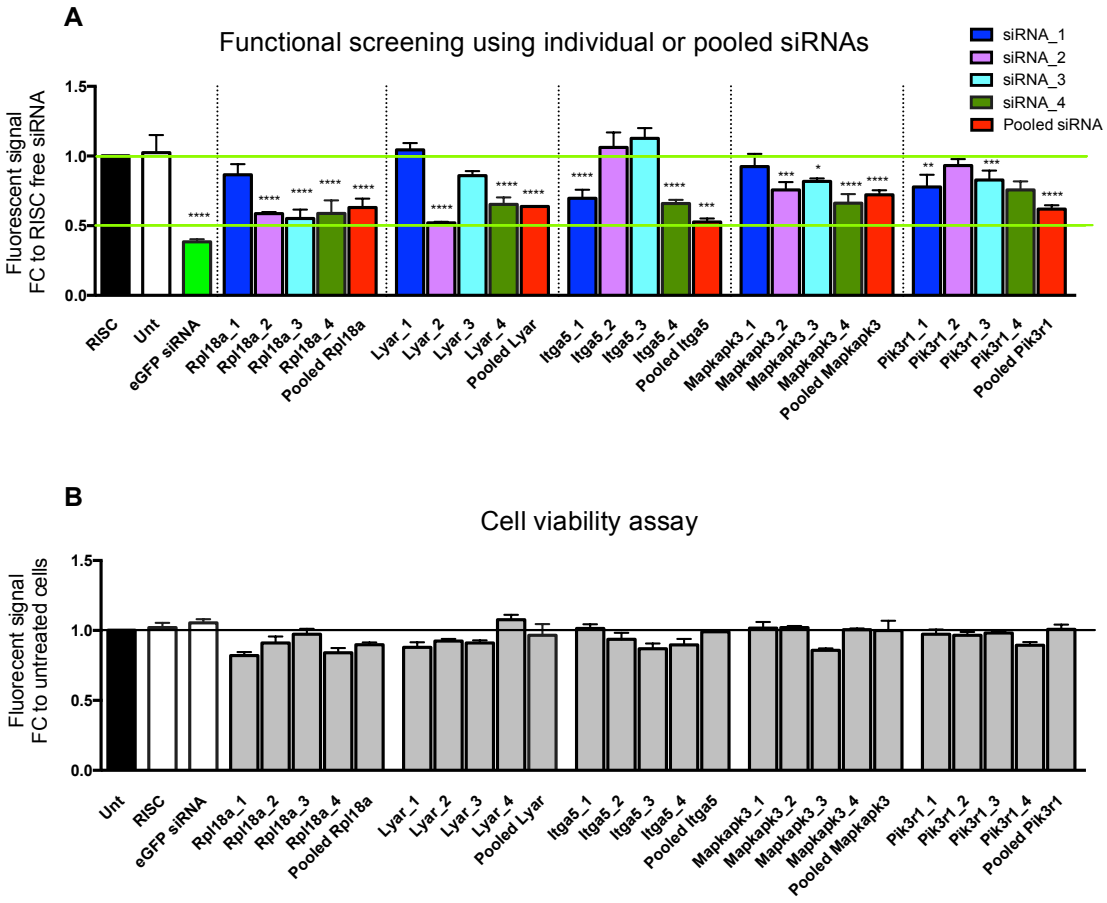

Figure 3.7 Comparison of pooled versus individual siRNAs for the effect of knockdown of *Rpl18a, Lyar, Itga5, Mapkapk3* and *Pik3r1* on MCMV infection
(A) GFP expression from knockdown cells using individual or pooled siRNAs followed by infection of GFP-MCMV. The GFP signal is presented as means of fold change (±SD) from five technical replicates compared to cells treated with RISC-free siRNAs. Data presented here are representative of independent experiments. The statistics are based on one-way ANOVA, Kruskal-Wallis test (*p<0.05, **p<0.01, ***p<0.001 and ****p<0.0001). **(B)** Cell viability assays. Cells as described above were incubated with cell titer blue at 37°C for 2h. Results are shown as means of fold change (± SD) from three technical replicates compared to untreated cells.

3.3.3 miR-27 target validation of *Rpl18a, Lyar, Itga5, Mapkapk3 and Pik3r1*

According to the functional screening, knockdown of 5 (*Rpl18a, Lyar, Itga5, Mapkapk3* and *Pik3r1)* out of 53 genes showed a significant reduction in MCMV growth based on the reporter assay. This observation suggests a supportive role of these genes upon MCMV infection. One hypothesis is therefore that miR-27 normally would suppress MCMV through one of these genes. To examine whether these genes are directly regulated by miR-27, their mRNA and protein levels were examined in cells in which miR-27 was overexpressed or inhibited. Subsequently, luciferase reporter assays were performed to confirm whether effects were based on direct target interactions.

3.3.3.1 Examination of *Rpl18a, Lyar, Itga5, Mapkapk3* and *Pik3r1* at mRNA and protein levels in response to miR-27

miRNAs regulate gene expression via mRNA destabilization/degradation or translation repression (Huntzinger and Izaurralde, 2011b). This allows the evaluation of miRNA targets to be conducted through determination of mRNA and protein levels upon miRNA overexpression or inhibition. NIH 3T3 cells were untreated or transfected with RISC-free siRNAs, miR-27a mimics or miR-27a inhibitors for 48 h. Total RNA and protein were collected to measure gene expression by qRT-PCR and Western blot analysis, respectively. At the mRNA levels, only *Mapkapk3* was significantly downregulated in cells transfected with miR-27a mimics, and the inhibition of endogenous miR-27 using miR-27a inhibitors caused a significant increase of *Mapkapk3* mRNAs (Fig 3.8A). The inhibition of miR-27 using the inhibitors also caused a significant increase of *Lyar*; however, miR-27 overexpression did not alter the levels of *Lyar*.

Further, Western blot analysis was carried out to determine the effect of miR-27 on the protein expression since miRNAs can repress protein translation without causing changes at mRNA levels (reviewed in (Wilczynska and Bushell, 2015)). To prioritise genes for Western blot analysis, data obtained from computational target prediction (TargetScan, www.targetscan.org) providing binding sites of miR-27 within the 3'UTR were taken into consideration. Three (*Itga5, Mapkapk3* and *Pik3r1*) out of the

five genes are predicted to have the target sites conserved in human and mouse, thus these genes were selected for Western blot analysis (Fig 3.8B). To examine the effects of miR-27 on protein expression of ITGA5, MAPKAPK3 and PIK3R1, NIH 3T3 cells were untreated or transfected with RISC-free siRNAs, negative inhibitors (*C. elegans* inhibitors), negative mimics (*C. elegans* mimics), miR-27a mimics or miR-27a inhibitors for 48 h. The negative inhibitors and negative mimics designed from sequences of *C.elegans* miR-67 with minimal sequence identity with miRNAs in human, mouse and rat were used as the control to distinguish the background effects. As shown in Fig 3.8B, no significant alteration of ITGA5 was observed in all transfected conditions compared to RISC-free siRNAs. Consistent with qRT-PCR results, MAPKAPK3 was decreased (~3 fold) upon miR-27 overexpression as compared to RISC-free siRNAs, whereas miR-27a inhibitors caused an increase in the protein expression (approximately 1.9 fold). Unexpectedly, the inhibition of miR-27 led to downregulation of PIK3R1, 0.39 fold compared to cells transfected with RISC-free siRNAs. This is likely to be due to non-specific effect as the negative mimics also decreased PIK3R1 levels, 0.6 fold compared to RISC-free siRNAs. This indicates a broad non-specific effect of transfection on PIK3R1 protein. Collectively, the determination of gene expression at mRNA and protein levels upon miR-27 overexpression and inhibition suggested that *Mapkapk3* is likely to be a direct target of miR-27.

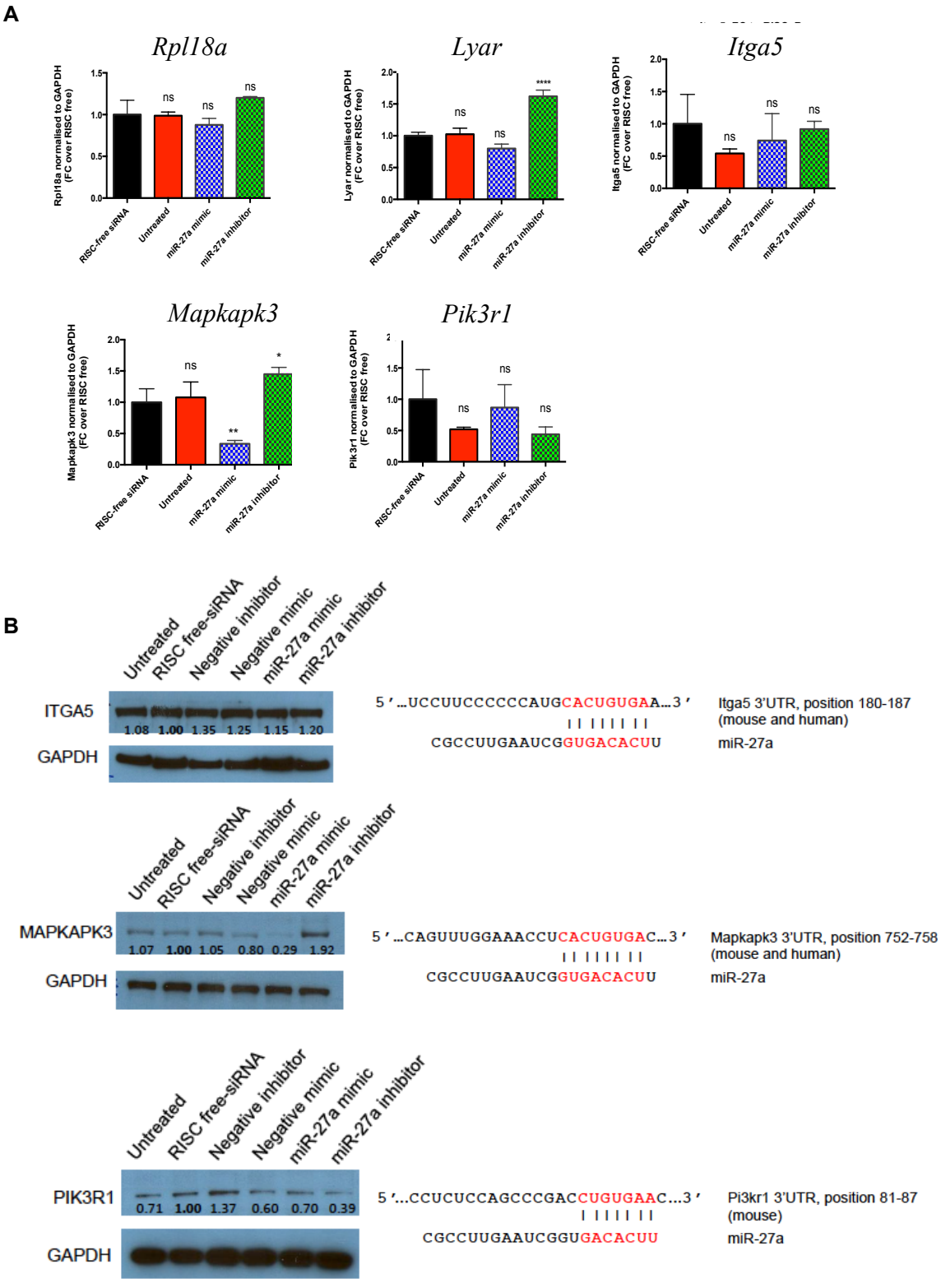
A
Rpl18a
Rpl18a normalised to GAPDH (FC over RISC free)
Lyar
Lyar normalised to GAPDH (FC over RISC free)
Itga5
Itga5 normalised to GAPDH (FC over RISC free)
Mapkapk3
Mapkapk3 normalised to GAPDH (FC over RISC free)
Pik3r1
Pik3r1 normalised to GAPDH (FC over RISC free)
RISC-free siRNA
Untreated
miR-27a mimic
miR-27a inhibitor
ns
B
Untreated
RISC free-siRNA
Negative inhibitor
Negative mimic
miR-27a mimic
miR-27a inhibitor
ITGA5
1.08 1.00 1.35 1.25 1.15 1.20
GAPDH
5′...UCCUUCCCCCCAUGCACUGUGAA...3′
CGCCUUGAAUCGGUGACACUU
Itga5 3'UTR, position 180-187 (mouse and human)
miR-27a
MAPKAPK3
1.07 1.00 1.05 0.80 0.29 1.92
5′...CAGUUUGGAAACCUCACUGUGAC...3′
Mapkapk3 3'UTR, position 752-758 (mouse and human)
PIK3R1
0.71 1.00 1.37 0.60 0.70 0.39
5′...CCUCUCCAGCCCGACCUGUGAAC...3′
CGCCUUGAAUCGGUGACACUU
Pi3kr1 3'UTR, position 81-87 (mouse)

Figure 3.8 Expression of genes at mRNA and protein levels in response to miR-27
NIH 3T3 cells were untreated or transfected with synthetic miRNAs (25 nM) for 48 h. **(A)** Total RNA was extracted from the cells. qRT-PCR was performed to quantify the expression of *Rpl18a, Lyar, Itga5, Mapkapk3* and *Pik3r1*. The expression of each gene was normalised to *Gapdh*. Data are presented as means of fold-change (±SD) of three technical replicates compared to cells transfected with RISC-free siRNAs. One-way ANOVA was used to assess significance (*p<0.05, **p<0.01 and ****p<0.0001). **(B)** Western blot analysis (ECL-based detection) of ITGA5, MAPKAPK3 and PIK3R1 in untreated cells, and cells transfected with RISC-free siRNAs, negative inhibitors (*C. elegans* inhibitors), negative mimics (*C. elegans* mimics), miR-27a mimics or miR-27a inhibitors. The protein levels were quantified using ImageStudioLite software and normalised to GAPDH. Results are shown as fold changes relative to cells transfected with RISC-free siRNAs.

3.3.3.2 Validation of *Mapkapk3* as a direct target of miR-27 using a luciferase reporter assay

The expression analysis studies showed that *Mapkapk3* is downregulated at both mRNA and protein level by miR-27 mimics, whereas the opposite occurs with miR-27 inhibitors. The alteration of *Mapkapk3* expression could result from a direct interaction between miR-27 and *Mapkapk3* or could be an indirect effect of miR-27 targeting upstream regulators of *Mapkapk3*. To specifically test whether *Mapkapk3* is directly targeted by miR-27, a luciferase reporter assay was carried out. This assay evaluates the interaction between the miRNA and its binding sites using a luciferase reporter vector. The predicted miRNA target sequences are cloned downstream of the luciferase gene in the vector. When the vector is co-transfected with miRNA mimics, the miRNAs directly interact with the target sequences, leading to a reduction in luciferase expression. Inhibition of miRNAs using miRNA inhibitors should result in an increase of luciferase levels (Jin et al., 2013).

The present study used the dual-luciferase reporter psi-CHECK2 (Promega) containing two different reporter luciferase genes: *Renilla* and firefly simultaneously expressed under individual promoters. The gene encoding *Renilla* luciferase is fused to target sites of miR-27 and firefly luciferase gene is an internal control to normalise the activity of *Renilla* in order to minimise the experimental variability such as differences in cell viability or transfection efficiency. The activity of the two luciferase enzymes are sequentially measured in the same sample, with the results as the ratio of *Renilla* to firefly luciferase activity. The reporter vector (psi-CHECK2-Mapkapk3 3'UTR) was constructed by cloning the entire 3'UTR of *Mapkapk3* (~1.2 kb) downstream of the *Renilla* luciferase gene. For comparison, a mutant version was constructed (psi-CHECK2-mut-Mapkapk3 3'UTR) that contained 3 nucleotide mutations in the miR-27 binding site within *Mapkapk3* 3'UTR (Fig 3.9A). NIH 3T3 cells were transfected with either psi-CHECK2-Mapkapk3 3'UTR or psi-CHECK2-mut-Mapkapk3 3'UTR in the absence or presence of miR-27 mimics or inhibitors. Both miR-27a and miR-27b mimics were tested which are expected to have the same effects due to their identical seed sites. At 48 h post transfection, luciferase activities were measured.

As controls, NIH 3T3 cells were transfected with empty psi-CHECK2 or a miR-27 sensor generated by Libri *et al*. (Libri et al., 2012), which contains three binding sites of miR-27 behind 3'UTR of *Renilla* luciferase. The three binding sites within the sensor are complementary to miR-27 with an internal loop at nucleotide 9-12 to prevent endonucleolytic cleavage. NIH 3T3 cells were co-transfected with empty psi-CHECK2 or a miR-27 sensor along with RISC-free siRNAs, miR-27a mimics or miR-27a inhibitors for 48 h. As expected, miR-27a mimics significantly downregulated *Renilla* luciferase greater than two fold compared to RISC-free siRNAs, whereas miR-27a inhibitors caused ~1.5 fold increase of *Renilla* luciferase compared to RISC-free siRNAs (Fig 3.9B).

As shown in Fig. 3.9C, co-transfection of miR-27a or miR-27b mimics significantly reduced *Renilla* luciferase of psi-CHECK2-Mapkapk3 3'UTR by ~2 fold as compared to co-transfection with RISC-free siRNAs. The inhibition of miR-27 using the specific inhibitors was expected to upregulate *Renilla* luciferase; however, miR-27a inhibitors did not seem to affect the luciferase expression. This observation is consistent with the study demonstrated that many miRNA inhibitors showed more subtle effects than miRNA mimics (Santhakumar et al., 2010). Several factors could contribute to this observation such as the efficiency of inhibitors and endogenous levels of target miRNAs. The mutant vector containing the mutated nucleotides at positions 2-4 in the seed site showed no alteration of *Renilla* luciferase in all transfection conditions including miR-27a mimics, miR-27b mimics and miR-27a inhibitors. Altogether, the results indicate that *Mapkapk3* is directly regulated by miR-27a and miR-27b.

In parallel, cell viability assays were conducted to ensure that the transfection was not toxic to the cells and the results obtained from luciferase assays were specifically derived from effects of miRNAs. As shown in Fig 3.9D, none of the transfection conditions reduces cell viability compared to untreated cells.

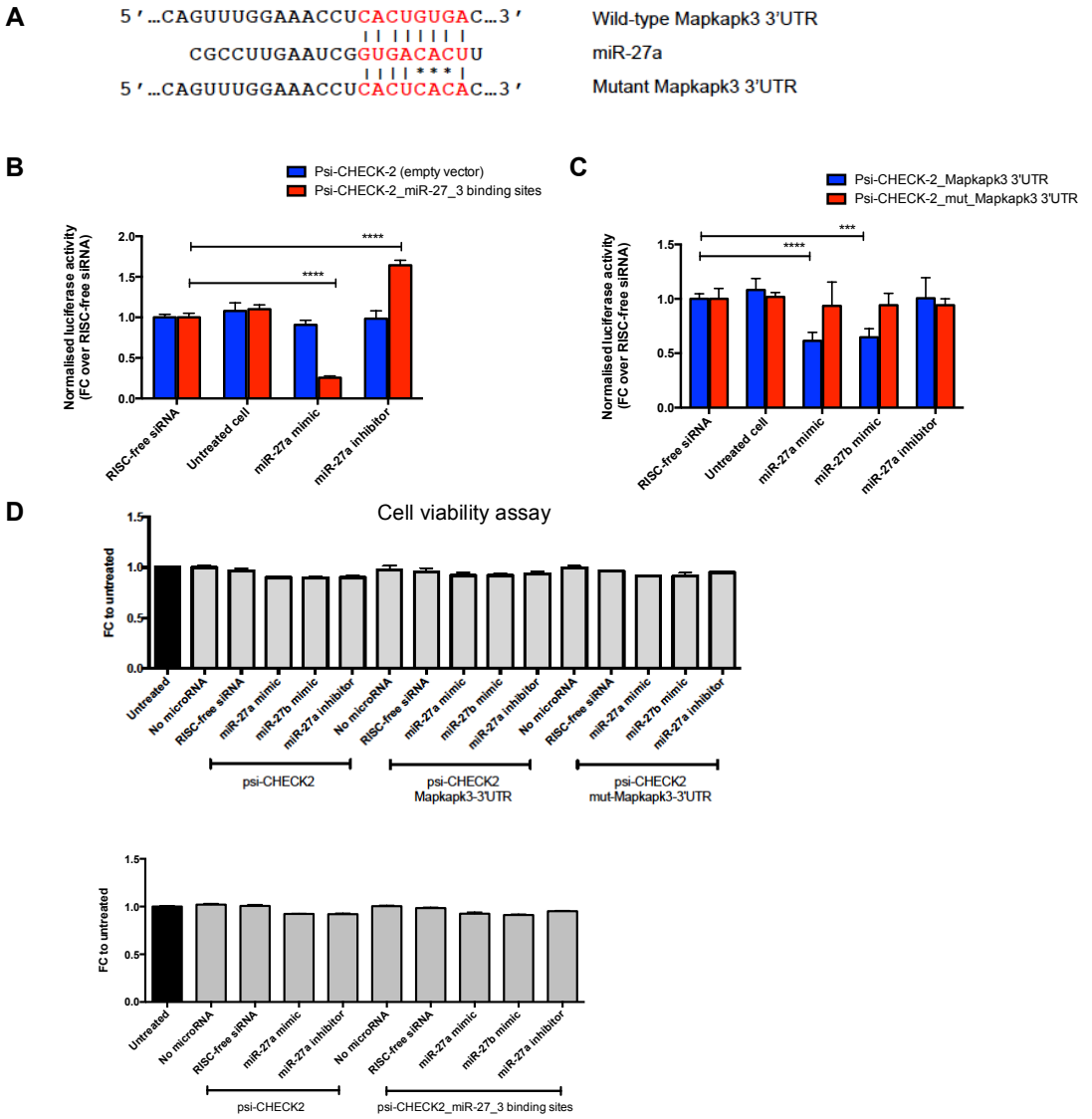

Figure 3.9 *Mapkapk3* is a direct target of miR-27a and miR-27b.
(A) Schematic representation of the miR-27 binding site within *Mapkapk3* 3'UTR. Asterisks indicate mutated nucleotides. **(B)** Luciferase assays with the positive control miR-27 sensors containing three binding sites for miR-27. NIH 3T3 cells were transfected with psi-CHECK2 or miR-27 sensors, or co-transfected with RISC-free siRNAs, miR-27a mimics or miR-27a inhibitors (25 nM) for 48 h. *Renilla* luciferase was normalised to firefly luciferase expression. Data are presented as fold changes (±SD) of five technical replicates compared to RISC-free siRNAs. Significance was assessed by two-way ANOVA, dunnett's multiple comparisons test (****p<0.0001). **(C)** Luciferase assays to determine the regulation of *Mapkapk3* by miR-27. NIH 3T3 cells were transfected with psi-CHECK2 containing wild type *Mapkapk3* 3'UTR (psi-CHECK2 Mapkapk3 3'UTR) or mutant *Mapkapk3* 3'UTR (psi-CHECK2 mut-Mapkapk3 3'UTR), or co-transfected with RISC free siRNAs, miR-27a mimics, miR-27b mimics or miR-27a inhibitors (25 nM, 48 h). Data are presented as fold changes (±SD) of five technical replicates compared to RISC-free siRNAs. Significance was assessed by two-way ANOVA, dunnett's multiple comparisons test (***p<0.001 and ****p<0.0001). **(D)** Cell viability assay performed in the transfected cells. At 48 h post transfection, cells were incubated with cell titer blue at 37°C for 2 h. Fluorescent signals were measured and calculated in fold changes (±SD) compared to untreated cells (three technical replicates).

3.3.4 Analysis of the effect of *Mapkapk3* knockdown on viral growth by plaque assays

In the previous sections, the functional screening showed that knockdown of *Mapkapk3* significantly reduced MCMV growth/replication based on the GFP assay. Although viral replication can be assessed through the determination of GFP levels expressed from GFP reporter virus, plaque assays remain the gold standard for quantifying infectious viral particles that retain the ability to infect and replicate in cells (Cooper, 1961). To examine the effect of *Mapkapk3* on infectious virus, NIH 3T3 cells were untreated or transfected with RISC-free siRNAs, *Mapkapk3* siRNAs or miR-542 mimics for 48 h. As a positive control, the miR-542 mimic was included based on work by others in the lab showing that this is anti-viral against MCMV (Buck lab, unpublished data). Two independent experiments were conducted by infecting cells with GFP-MCMV or wild type MCMV at MOI of 0.01. The reason of including wild type MCMV is to confirm the results obtained from GFP-MCMV. At 3 days post infection (~72 hpi), which is close to the time point post infection used in the functional screening (70 hpi), supernatant was collected to measure infectious virus. As expected, cells transfected with miR-542 mimics dramatically reduced titres of GFP-MCMV (~10^3 fold) compared to RISC-free siRNAs (Fig 3.10A). Consistent with the functional screening, knockdown of *Mapkapk3* significantly attenuated the GFP-MCMV (~10 fold) compared to cells transfected with RISC-free siRNAs. In line with this, cells transfected with miR-542 mimics or *Mapkapk3* siRNAs showed a significant decrease of wild type MCMV titres (~10^4 fold) compared to RISC-free siRNAs (Fig 3.10B). The difference in fold reduction of viral titres between GFP-MCMV and wild type MCMV could be due to variables of viral stocks or other factors happening when experiments are independently conducted such as cell viability, knockdown efficiency and technical variability of pipetting volumes. However, the data obtained from the two experiments were consistent and demonstrated that knockdown of *Mapkapk3* resulted in a significant suppression of MCMV replication, indicating that *Mapkapk3* is important for the viral growth.

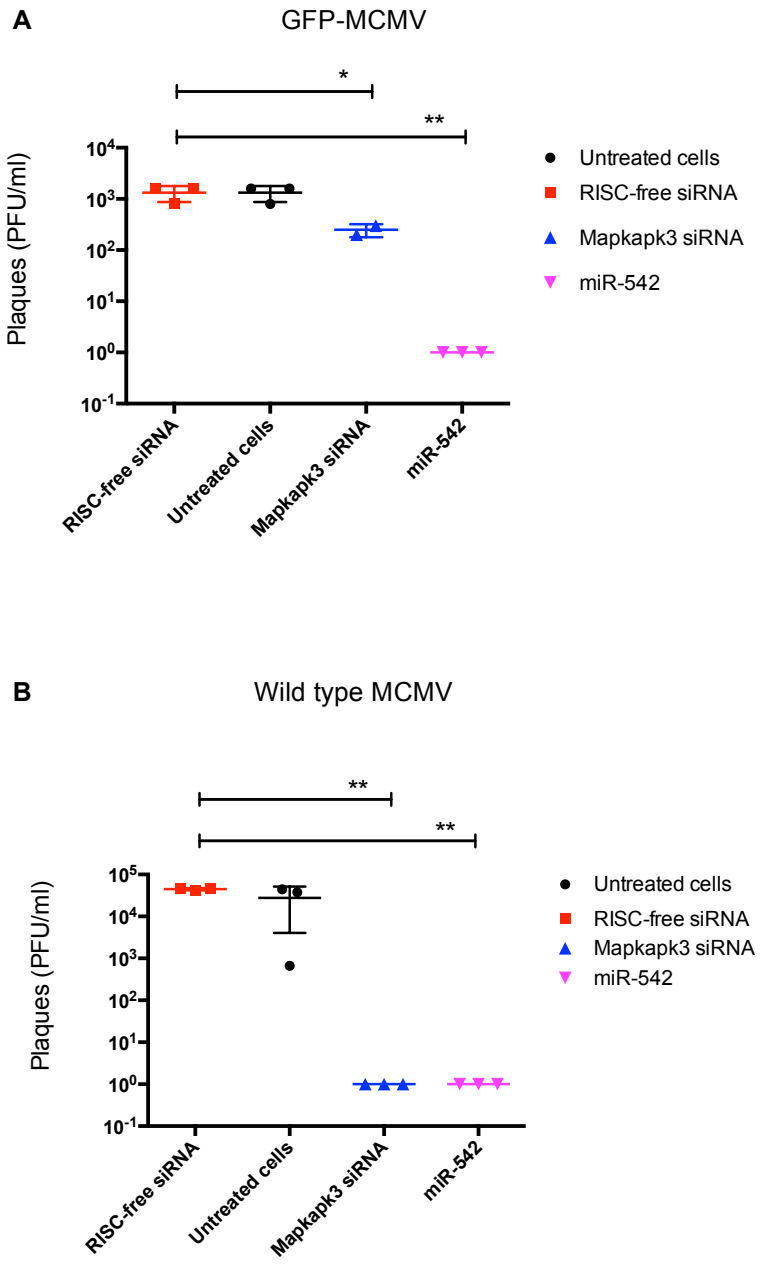

Figure 3.10 Knockdown of *Mapkapk3* reduces viral titres determined by plaque assays
NIH 3T3 cells were untreated or transfected with 25 nM of RISC-free siRNAs, *Mapkapk3* pooled siRNAs or miR-542 mimics for 48 h. **(A)** Cells were infected with a GFP reporter virus (GFP-MCMV) or **(B)** wild type MCMV at MOI of 0.01 for 3 days. Viral titres were determined by standard plaque assays. Data are presented as plaque forming units per ml of supernatant (PFU/ml), showing data for each replicate. Significance was assessed by one-way ANOVA (*$p<0.05$ and **$p<0.01$).

3.3.5 Phosphorylation of HSP27 and ATF1 by MAPKAPK3

The above data suggest that miR-27 directly regulates *Mapkapk3*, which is a downstream kinase of the p38 in the p38 mitogen-activated protein (MAP) kinase pathway. MAPKAPK3 is directly activated by p38 (Ronkina et al., 2008) and it has been found to phosphorylate a number of proteins necessary for diverse cellular processes such as cytokine production, cell migration, actin remodelling, cell cycle and gene expression (reviewed in (Cargnello and Roux, 2011)). In particular, MAPKAPK3 has been shown to activate many substrates including small heat shock protein 27 (HSP27), cAMP response element-binding protein (CREB), transcription factor ATF and lymphocyte-specific protein 1 (LSP1) (reviewed in (Zarubin and Han, 2005)). HSP27 is a multifunctional protein involved in numerous cellular responses including protein folding, inhibition of apoptosis and actin remodelling (reviewed in (Vidyasagar et al., 2012)). In the context of CMV infection, HSP27 and CREB/ATF have been reported to be involved in HCMV infection. HCMV induces phosphorylation of HSP27 (Johnson et al., 2000), whereas CREB activates viral gene expression responsible for reactivation from latency in HCMV (Kew et al., 2014). It was therefore examined here whether the effect of *Mapkapk3* on MCMV infection might occur through these two substrates: HSP27 and CREB/ATF.

Initially, an experiment was conducted to determine whether MAPKAPK3 phosphorylates HSP27 and CREB/ATF in this cell type (NIH 3T3 cell line) before further investigations in the context of MCMV infection in which functions of MAPKAPK3 might be complicated by viral factors. A time course of p38 activation and phosphorylation of HSP27 (pHSP27) and CREB/ATF1 (pCREB/pATF1) was set up using anisomycin, a specific activator of p38. NIH 3T3 cells were untreated or treated with 10 µg/ml of anisomycin at four time points: 30 min, 2 h, 4 h and 24 h (Fig 3.11A). Protein samples were collected at the indicated time points and phosphorylated proteins were analysed by Western blot analysis. As shown in Fig 3.11B, anisomycin induced phosphorylation of all proteins of interest: p38, HSP27 and CREB/ATF1 compared to untreated cells. The phosphorylation of p38 and CREB/ATF1 peaked at 30 min and gradually decreased to the basal level by 24 h. pHSP27 peaked at 30 min to 2 h and it started to decrease at 4 h, returning to the

unstimulated level at 24 h. These data suggest 30 min of anisomycin treatment as the optimal time point to observe the activation of p38 MAP kinase pathway.

To confirm that HSP27, CREB and ATF1 are substrates of MAPKAPK3 in NIH 3T3 cells, the major cell line used in this thesis, a knockdown experiment was performed. NIH 3T3 cells were untreated or transfected with RISC-free siRNAs or *Mapkapk3* siRNAs for 48 h followed by anisomycin treatment for 30 min (Fig 3.12A). Protein samples were collected to determine the expression of MAPKAPK3, p-p38, p-HSP27 and p-CREB/pATF1 using Western blot analysis. As shown in Fig 3.12B, under anisomycin treatment, MAPKAPK3 protein was barely detected in cells transfected with *Mapkapk3* siRNAs as compared to RISC-free siRNAs. Consistent with the previous experiment, the strong expression of p-p38 post anisomycin activation was observed in cells with and without RISC-free siRNAs. As expected, knockdown of *Mapkapk3* resulted in a reduction (~50%) of p-HSP27 and p-ATF1 indicating that the two proteins are substrates of MAPKAPK3. However, in NIH 3T3 cells, MAPKAPK3 did not appear to be required for phosphorylation of CREB, although this has been reported in SK-N-MC neuroblastoma cells (Tan et al., 1996). It is possible that phosphorylation of CREB is a cell-type dependent function of MAPKAPK3. Altogether, the data presented here demonstrate that MAPKAPK3 phosphorylates HSP27 and ATF1 in NIH 3T3 cells.

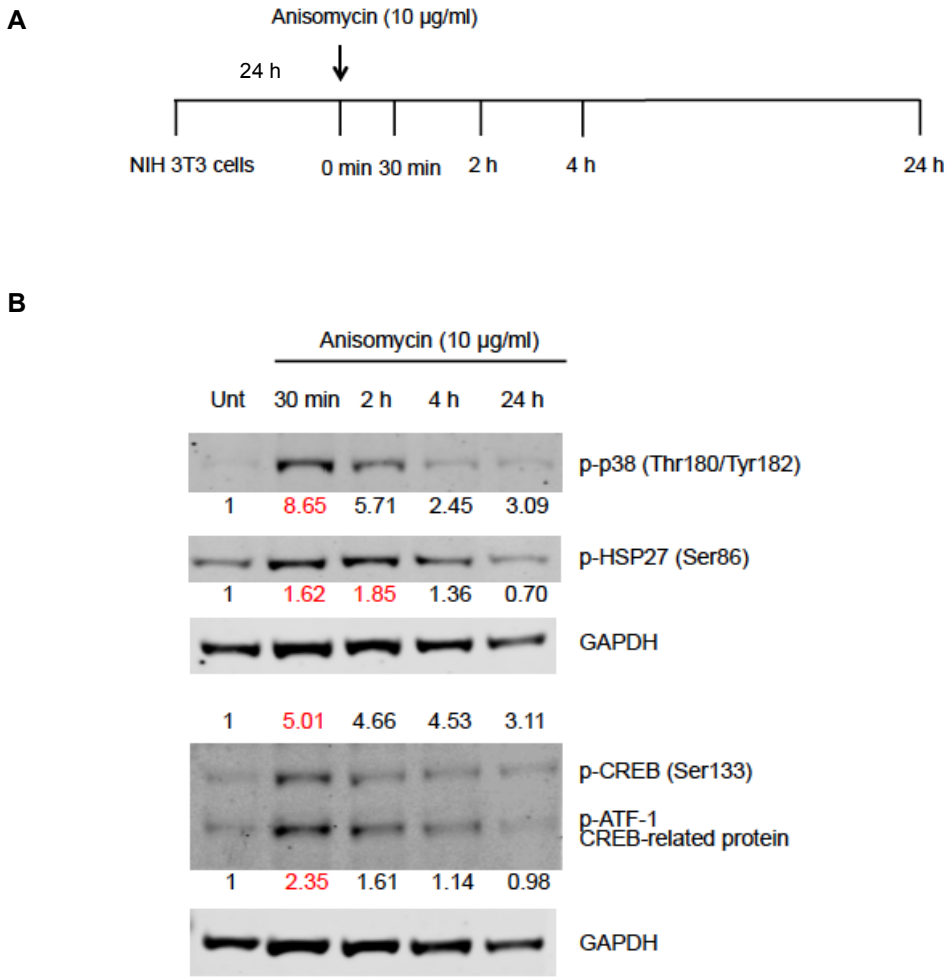

Figure 3.11 Activation of p38 MAP kinase and downstream molecules: p-HSP27, p-CREB and p-ATF1 using anisomycin

(A) Experimental setup to assess the activation of p38 MAP kinase signalling using anisomycin. NIH 3T3 cells were seeded in a 6-well plate for 24 h prior to stimulation with 10 µg/ml anisomycin as indicated. Cell lysate was collected at 30 min, 2 h, 4 h and 24 h post-stimulation for detection of phosphorylated proteins. **(B)** Western blot analysis (fluorescence-based detection) of p-p38, p-HSP27, p-CREB and p-ATF1. Proteins were quantified using ImageStudioLite software and normalised to GAPDH. Results are shown as fold changes relative to unstimulated cells (Unt). Data presented here are representative of repeated experiments.

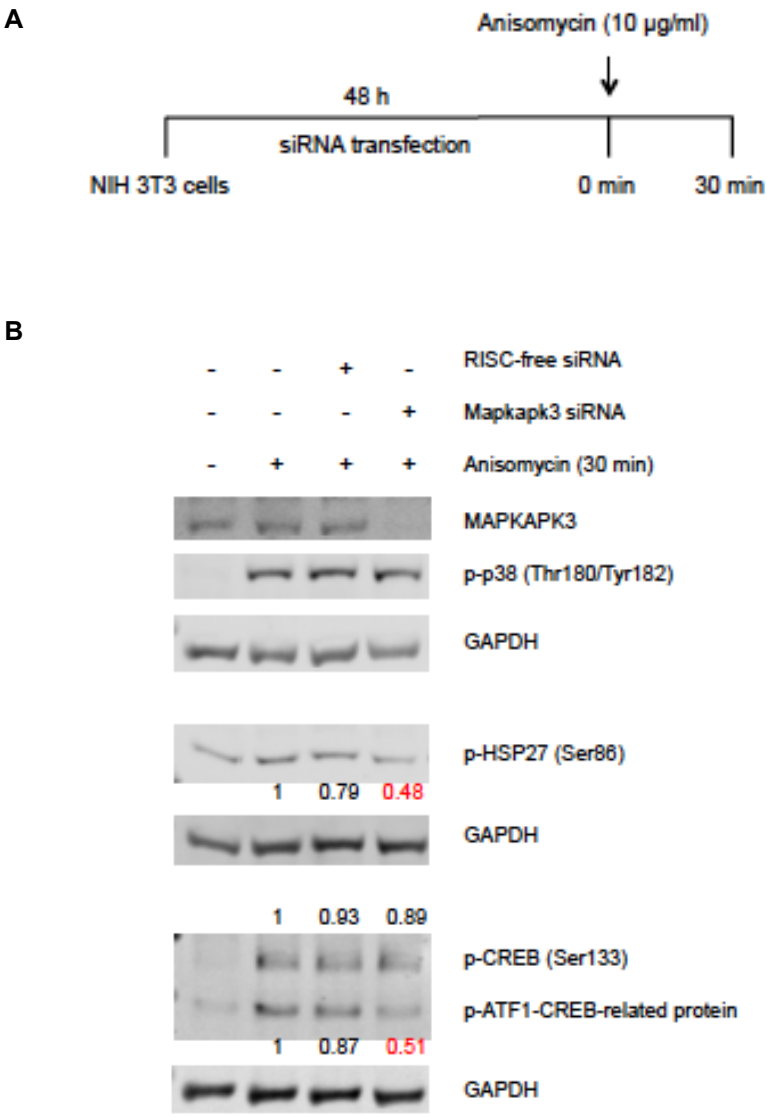

Figure 3.12 MAPKAPK3 phosphorylates HSP27 and ATF1 in a p38-dependent manner
(A) Experimental design to test whether HSP27, CREB and ATF1 are substrates of MAPKAPK3. NIH 3T3 cells were untreated or transfected with RISC-free siRNAs or *Mapkapk3* pooled siRNA (25 nM) for 48 h. Cells were treated with 10 µg/ml anisomycin for 30 min and protein samples were collected for Western blot analysis. **(B)** Western blot analysis (fluorescence-based detection) of MAPKAPK3, p-p38, p-HSP27, p-CREB and p-ATF1 using antibodies specific to phosphorylated proteins. The levels of proteins were quantified using ImageStudioLite software, normalised to GAPDH and fold changes were calculated compared to untransfected cells with anisomycin activation. The results are representative of repeated experiments.

3.3.6 Expression of MAPKAPK3, p-HSP27 and p-ATF1 in wild type MCMV and MCMV Δm169 infection

Here, evidence has been provided that miR-27 directly regulates *Mapkapk3* gene and MAPKAPK3 protein phosphorylates HSP27 and ATF1 in a p38-dependent manner. Given the anti-viral properties of miR-27, it is logical to speculate that miR-27 could act through the regulation of *Mapkapk3* in p38 MAP kinase signalling pathway, a crucial pathway hijacked by HCMV and MCMV to facilitate viral replication (Johnson et al., 1999; Tang-Feldman et al., 2013). To gain further insight into miR-27 regulation of *Mapkapk3* and its two substrates: HSP27 and ATF1, in the context of MCMV infection, expression of MAPKAPK3, p-HSP27 and p-ATF1 was examined in cells infected with wild type MCMV or MCMV Δm169.

NIH 3T3 cells were mock infected or infected with wild type MCMV or MCMV Δm169 in the time series experiment (Fig 3.13A). RNA and protein samples were harvested at the indicated time points to examine levels of miR-27, and MAPKAPK3, p-HSP27 and p-ATF1 protein. As shown in Fig 3.13B, miR-27 was significantly downregulated in the wild type MCMV infection at 8 hpi compared to mock infection and the downregulation continued progressively over the time of infection to 48 hpi. In contrast, MCMV Δm169 did not alter miR-27 levels as expected. Therefore, if miR-27 regulates MAPKAPK3 during infection, it would be expected that phosphorylation of HSP27 and ATF-1 might occur at higher levels in cells infected with wild type MCMV compared to MCMV Δm169. Western blot analyses were used to examine the expression levels of these proteins in three independent experiments. The proteins were quantified and the means of fold changes (±SD) were calculated as compared to mock infection. MAPKAPK3 and p-HSP27 protein levels were relatively higher in the wild type MCMV compared to MCMV Δm169 at 24 to 48 hpi (Fig 3.13C and 3.13D). In contrast, p-ATF1 was comparable in wild type MCMV and MCMV Δm169 infection throughout the time course infection (Fig 3.13E).

Fig 3.13F shows representative data from three independent experiments showing MAPKAPK3 and p-HSP27 protein levels during infection. These data clearly demonstrate difference in these proteins at 36 and 48 hpi. In wild type MCMV

infection, MAPKAPK3 displayed 1.83 fold increase at 36 hpi and 1.46 fold increase at 48 hpi compared to mock infection, whereas MCMV Δm169 showed 0.74 fold at 36 hpi and 0.72 fold at 48 hpi relative to mock infection. At 36 and 48 hpi, the increase of MAPKAPK3 was observed in wild type MCMV but not MCMV Δm169 infection and it correlated to the reduction of miR-27 levels in the wild type MCMV infection. These data demonstrate an inverse correlation between miR-27 and MAPKAPK3 regulation upon MCMV infection. Since it has been shown that HSP27 and ATF1 are substrates of MAPKAPK3, expression levels of phosphorylated forms of HSP27 and ATF1 could be expected to correspond to MAPKAPK3 expression. In contrast to MAPKAPK3 levels at 36 and 48 hpi in wild type MCMV infection, pHSP27 did not appear to increase and showed 0.85 and 0.99 fold compared to mock infection. However, at these time points p-HSP27 was lower in MCMV Δm169 infection as 0.65 fold at 36 hpi and 0.53 fold at 48 hpi compared to mock infection. Hence, the comparison of wild type MCMV and MCMV Δm169 infection at 36 and 48 hpi demonstrates higher levels of p-HSP27 in the wild type MCMV infection. In conclusion, these data imply that in the context of MCMV infection, the regulation of MAPKAPK3 by miR-27 alters the phosphorylation level of HSP27 but not ATF1. Further investigations of the functional properties of HSP27 in MCMV infection would shed light on the importance of MAPKAPK3 and its regulation by miR-27 in infection.

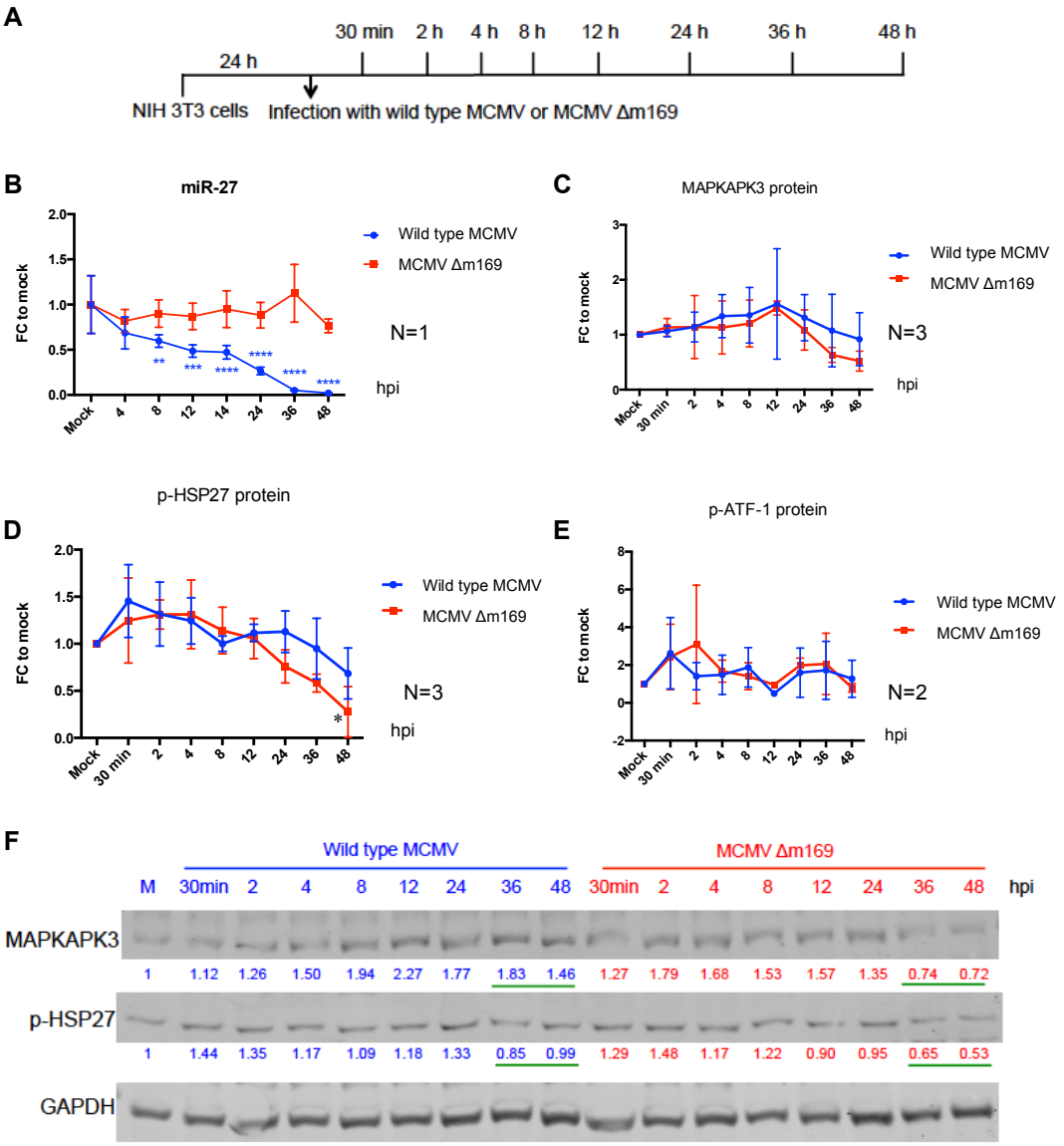

Figure 3.13 miR-27 regulates MAPKAPK3 and phosphorylation of HSP27 upon MCMV infection

(A) Time course infection using wild type MCMV and MCMV Δm169 (MOI of 5) to examine the expression of miR-27 and proteins: MAPKAPK3, p-HSP27 and p-ATF1. At the indicated time points post infection, cells were collected for RNA extraction and protein preparation. **(B)** Expression of miR-27 upon wild type MCMV and MCMV Δm169 infection. miR-27 was quantified using qRT-PCR, normalised to miR-16 and fold changes (FC) were calculated relative to the mock infection. Data represent means of fold change (±SD) of five technical replicates from one experiment. Statistical significance of miR-27 expression compared to mock infection was tested using two-way ANOVA, Dunnett's multiple comparisons test (**p<0.01, ***p<0.001 and ****p<0.0001). **(C, D, E)** Quantification of Western blot analyses (fluorescence-based detection) of MAPKAPK3, p-HSP27 from three experiments and p-ATF1 from two independent experiments. The levels of MAPKAPK3, p-HSP27 and p-ATF1 were quantified using ImageStudioLite software and normalised to GAPDH. Data were plotted as means of fold change (±SD) relative to mock infection. Statistical significance of the protein expression compared to mock infection was tested using two-way ANOVA (*p<0.05). **(F)** Representative of Western blot analysis of MAPKAPK3 and p-HSP27. The protein levels were quantified and normalised to GAPDH. Values represent fold changes relative to mock infection.

3.4 Discussion

The primary aim of this thesis is to identify the cellular targets of miR-27 in order to understand why MCMV has evolved a viral non-coding RNA, m169, to inhibit this miRNA (Buck et al., 2010; Libri et al., 2012; Marcinowski et al., 2012). The significance of miR-27 inhibition has been demonstrated by Marcinowski *et al.* who showed that the degradation of miR-27 by m169 is important for the viral growth *in vivo* (Marcinowski et al., 2012). Importantly, *in vitro* experiments have also demonstrated an anti-viral activity of miR-27 when it is overexpressed in NIH 3T3 cells (Buck et al., 2010). Based on the significance of miR-27 degradation on viral replication *in vivo* and functional implications of miR-27, it was hypothesised that the degradation of miR-27 is a viral strategy to interfere with functions of miR-27 in order to de-repress miR-27 target genes whose expression is advantageous to the virus.

Beyond MCMV, virus-mediated downregulation of miR-27 was found in marmoset T cells infected with *Herpesvirus saimiri* (HVS), a γ-herpesvirus that induces the transformation of T cells (Cazalla et al., 2010). Similar to what was observed in MCMV infection, the degradation of miR-27 in HVS also involves a non-coding RNA, *H. saimiri* U-rich RNA1 (HSUR1), an unrelated RNA to m169 (Cazalla et al., 2010). In attempt to understand the significance of miR-27 degradation in HVS infection, Guo *et al.* demonstrated that miR-27 regulates T cell activation through a direct interaction with an adaptor protein of T cell receptor (TCR) signalling, the growth factor-bound protein 2 (GRB2). miR-27 was also found to directly target semaphorin 7A (SEMA7) and interferon- γ (IFN- γ) which are modulators and effectors of T cell function. The biological significance of miR-27 downregulation in HVS-infected T cells is therefore postulated to relate to constitutive activation of T cells leading to an increase of IFN- γ production (Guo et al., 2014). This could be important for viral latency since IFN- γ strongly inhibits lytic reactivation of γ-herpesviruses (Steed et al., 2006). However, it is not clear how these functions of miR-27 would relate to MCMV infection since the virus does not infect T cells, and the regulation of miR-27 occurs during the lytic phase of infection.

In this chapter, microarray analysis was carried out to identify targets of miR-27 that could play a role in MCMV infection. Genes that were differentially expressed upon miR-27 overexpression (in comparison to cells transfected with RISC-free siRNAs) or during MCMV infection (in comparison to infection with MCMV Δm169 or in comparison to infected cells treated with miR-27 mimics) were overlapped. A total of 23 genes were differentially expressed in at least two of the comparisons and they were included in a functional screening that involves siRNA knockdown of individual genes followed by infection with a MCMV GFP reporter virus to assess the effects on viral growth. In addition to the investigation of overlapped genes, differentially expressed genes in cells infected with MCMV Δm169 compared to wild type MCMV were of interest, even if these did not overlap with other comparisons (a total of 242 genes falls in this category). This comparison is thought to provide the most relevant physiological conditions to identify targets of miR-27 upon viral infection since the only difference between the two viruses is the expression of m169.

In the absence of the miR-27 inhibitor m169 (infection with MCMV Δm169), miR-27 levels were confirmed to be unaltered as compared to untreated cells, whereas wild type MCMV downregulated miR-27 by approximately 10 fold at 24 hpi. Thus, it was expected that genes regulated by miR-27 are downregulated in MCMV Δm169 compared to wild type MCMV infection. The pathway analysis of these 242 downregulated genes (fold change >1.20, $p<0.05$) in cells infected with MCMV Δm169 versus wild type MCMV revealed that the top enriched pathways were involved in cholesterol biosynthesis. This may be relevant to CMV infection as a study showed that disruption of lipid rafts of the cell membrane by depletion of cellular cholesterol inhibited HCMV entry, suggesting the essential of cholesterol for viral entry (Juckem et al., 2008), which might also occur in MCMV. Blanc *et al.* showed that inhibition of cholesterol biosynthesis pathway using pharmacologic compound simvastatin led to the attenuation of virus *in vitro* and *in vivo*, likely due to the reduction of mevalonate, a precursor of cholesterol. The authors conducted the metabolite rescue and found that the addition of mevalonate into cell culture reversely increased the level of infection, whereas the feeding cells with cholesterol

did not affect inhibitory activity of simvastatin, indicating that the anti-viral effect is independent of cholesterol (Blanc et al., 2011). It is therefore expected that the actual cholesterol levels may not be important but aspects of the biosynthesis pathway can influence the ability of MCMV to replicate. One of the genes differentially expressed from the microarray analysis was *Dhcr24,* which encodes the 3β-Hydroxysterol Δ24-reductase that converts desmosterol to cholesterol. Knockdown of this gene in the functional screening did not significantly decrease GFP from the reporter virus. Due to the multiple steps of cholesterol biosynthesis pathway, it seems likely that the intermediate of the pathway could have an effect on the infection rather than the actual level of cholesterol. Several other differentially expressed genes were identified in this pathway (*Acat2/Acat3, Fdps, Hsd17b17, Mvd, Nsdhl* and *Sqle* shown in Table 3.4) that were not examined because they did not have any miR-27 target site. Thus, while these may play a role upon the infection, it is unlikely that they are directly targeted by miR-27.

In addition to carry out pathway analysis on genes in each individual comparison, pathway analysis was also analysed in cells transfected with miR-27 mimics versus RISC-free siRNAs. This comparison is straightforward to identify genes/pathways regulated by miR-27 but a caveat is that transfection with the mimic can lead to supra-physiological increases of the miRNA levels. Measurement of miR-27 following transfection suggested a 50 fold increase in its level. The overexpressed miRNA could potentially generate false positive results since it might saturate the RISC complex and bind to low affinity-binding sites under these conditions that are not targeted under physiological conditions (Khan et al., 2009).

Despite the drawbacks mentioned above, the overexpression of miRNA has been widely used to examine gene regulation in global analyses, providing comprehensive insights into the gene networks regulated by miRNAs (reviewed in (Thomson et al., 2011)). In this chapter, pathway analysis of 97 downregulated genes upon miR-27 overexpression versus RISC-free siRNA showed five top ranked pathways including 1) endothelia nitric oxide synthase (eNOS) signalling, 2) nitric oxide signalling in the cardiovascular system, 3) hepatic fibrosis, 4) aldosterone signalling in epithelial cells and 5) glycogen degeneration III.

eNOS is expressed in endothelial cells, cardiac myocytes and blood platelets (Dudzinski et al., 2006). It is an enzyme that produces nitric oxide (NO), a vasodilator regulating vascular tone by inhibiting the adhesion of leukocytes as well as the adhesion and aggregation of platelets (reviewed in (Dudzinski and Michel, 2007)). Reduction of the NO levels can result in endothelial dysfunction, atherosclerosis and cardiovascular complications. Although there is no evidence directly demonstrating a role of miR-27 in eNOS signalling related to vascular diseases, a number of studies have showed that miR-27 is involved in processes of atherosclerosis such as angiogenesis, adipogenesis, oxidative stress and lipid metabolism (reviewed in (Chen et al., 2012)). Thus, it is possible that miR-27 also regulates eNOS signalling contributing to atherosclerosis but whether and how this relates to its anti-viral properties is not clear.

The pathway analysis also implicated miR-27 in regulation of hepatic fibrosis. Correspondingly, Ji *et al*. demonstrated that downregulation of miR-27 decreased cell proliferation and restored cytoplasmic lipid droplets through the regulation of retinoid X receptor α, leading to the inactivation of hepatic stellate cells (HSCs), suggesting a role of miR-27 in liver fibrosis (Ji et al., 2009). In the context of MCMV infection, retinoic acid (RA) activated the viral major immediate-early enhancer via the binding to multiple RA-responsive elements containing retinoid X receptor (Angulo et al., 1998). Treatment of RA dramatically increased viral growth *in vitro* and oral administration of RA increased the susceptibility of mice to viral infection, suggesting that RA can modulate infection of MCMV (Angulo et al., 1998). Thus, it does not mean there is a link between hepatic fibrosis and MCMV but some of the targets could be associated with both.

Although the pathway analysis of microarray data provided putative pathways regulated by miR-27, the focus of this thesis is to identify the genes regulated by miR-27 that are important for viral infection. With this in mind, the overlapped genes among microarray data and predicted targets of miR-27 in the top ranked pathways (Table 3.6) were selected for the functional screening as described above. The screening revealed that knockdown of five genes (*Rpl18a, Lyar, Itga5, Mapkapk3*

and *Pik3r1*) significantly reduced the GFP expression (approximately 50%), suggesting an important role of these genes for MCMV replication.

Ribosomal protein L18 *(Rpl18a)* encodes a protein component of 60S ribosomal subunit. In addition to roles in translation, ribosomal proteins are implicated as protein chaperones (Kovacs et al., 2009) and regulators of transcription (Lindstrom, 2009). Little is known about the involvement of *Rpl18a* in viral infection. A proteomic study found the presence of RPL18 in ebola virions (Spurgers et al., 2010). The authors demonstrated that the reduction of RPL18 expression using siRNAs effectively inhibited ebola infection in 293T cells assessed by determination of viral genomic RNA using qRT-PCR (Spurgers et al., 2010). RPL18 has been shown to have a function in viral biology of cauliflower mosaic virus. Specifically, RPL18 in *Arabidopsis thaliana* interacts with the viral protein P6 involved in several aspects of the infectious cycle (Leh et al., 2000). In the translation of HCV, it has also been shown that RPL18 interacts with an internal ribosome entry site (IRES) of the viral RNA, leading to the moderate increase of HCV IRES activity by an unknown mechanism (Dhar et al., 2006). In the case of CMV infection, however, no previous literature has implicated a role of *Rpl18a* in the infection. Further studies are required to examine whether the virus uses RPL18 during its life cycle.

Ly-1 antibody reactive clone *(Lyar)* encoding a zinc finger nucleolar protein, has been shown to play a role in cell proliferation and differentiation of embryonic stem cells (ESCs) (Li et al., 2009). This was found to occur via a mechanism whereby LYAR forms a complex with nucleolin, a major nucleolar protein controlling cell growth and apoptosis (Li et al., 2009). Importantly, MEFs isolated from *Lyar*$^{-/-}$ and *Lyar*$^{+/-}$ mice showed cell growth defect with a concomitant increase of p53 and a key effector of growth arrest, p21, as compared to wild type cells (Wang et al., 2012). The present study has shown that the knockdown of *Lyar* significantly reduced GFP expression of GFP-MCMV. It is presumed that this could relate to disruption of *Lyar* functions in cell proliferation required for MCMV replication.

Based on the functional screening, integrin α5 (*Itga5*) was a positive hit, suggesting its importance for some aspect of the MCMV life cycle. The integrin family is the

cell surface glycoprotein comprising an α-subunit and a β-subunit. To date, at least 18 α and 8 β subunits have been identified, giving rise to 24 distinct integrin receptors. The α and β subunits contain large extracellular domains, transmembrane-regions and short cytoplasmic domains (reviewed in (Hynes, 2002)). Integrins play many roles in normal and disease biology. They are receptors of extracellular matrix (ECM) proteins required for cell adhesion and are keys in activating a diverse range of intracellular signalling pathways in response to external stimulation. Integrins are also receptors for many viruses including HCMV and therefore play important roles in entry. Specifically, the glycoprotein gB of HCMV recognises integrins, particularly β1 subtypes to facilitate viral entry (reviewed in (Stewart and Nemerow, 2007)). The β1 subunit forms heterodimer with the α5 subunit to be α5β1 integrins, which are generally known as receptors of fibronectin, the extracellular matrix playing an important role in cell adhesion and migration (Akiyama et al., 1995). Given that HCMV uses the gB glycoprotein binding to β1 subunit of α5β1 to assist the viral entry, although no evidence has been reported in MCMV, the virus may employ the similar mechanism using MCMV gB glycoprotein for the cell entry. Hence, knockdown of the α5 subunit, a component of α5β1 might reduce cell susceptibility to MCMV infection.

The functional screening suggested that mitogen activated protein kinase (MAPK) - activated protein kinase3 *(Mapkapk3)* is required for MCMV growth. *Mapkapk3* is a downstream kinase of p38 MAPK signalling, a critical pathway of signal transduction mediating numerous biological processes in response to extracellular stimuli. p38 MAP kinase is one of four distinct subgroups within MAP kinase family: ERK1/2, ERK5, JNKs and p38. Activation of the p38 MAP kinase is involved in various biological events such as inflammation, apoptosis, cell cycle and cell differentiation (reviewed in (Zarubin and Han, 2005)). Interestingly, it was demonstrated that HCMV activates p38 MAP kinase, which plays an important role in viral DNA replication. Johnson *et al*. showed that at an early time point in the infection (8 to 14 hpi) the virus mediates p38 activation by inhibiting dephosphorylation of p38, whereas at the late time point of the infection (48 to 72 hpi) the virus induces MAPK kinase 3 and 6 (MKK3/6), the upstream regulators of

p38 (Johnson et al., 2000). This evidence suggests the importance of p38 MAP kinase during CMV infection and here it is postulated that this could also involve the downstream *Mapkapk3*.

Phosphoinositide-3-kinase regulatory subunit 1 (*Pik3r1)* encodes p85α, a regulatory subunit of phosphatidylinositol 3-kinase (PI3K). PI3K consists of a regulatory subunit p85 and a catalytic subunit p110 (reviewed in (Katso et al., 2001)). Under resting conditions, p85 stabilises and inactivates the catalytic subunit p110. In activated cells, p85 binds to receptor tyrosine kinases or other tyrosine phosphorylated adaptors such as epidermal growth factor receptor (EGRF) and platelet-derived growth factor receptor (PDGFR), allowing p110 to generate phosphatidylinositol 3,4,5-trisphosphate (PIP_3), a secondary messenger stimulating diverse target proteins. This allows PI3K to control numerous biological processes such as proliferation, differentiation, chemotaxis and survival (reviewed in (Katso et al., 2001)). It has become evident that HCMV requires the upregulation of PI3K signalling, possibly to activate a transcription factor NF-κB to increase cellular gene expression and protein synthesis involved in inhibition of apoptosis (Johnson et al., 2001). The virus activates PI3K via phosphorylation of p85 leading to the activation of Akt, an effector of PI3K/Akt signalling (Johnson et al., 2001). Moreover, the inhibition of PI3K dramatically reduces HCMV titres and decreases protein levels of IE and E genes essential for viral DNA synthesis (Johnson et al., 2001). In addition, it was shown that HCMV induces PI3K activity in monocytes required for monocyte-transendothelial migration that possibly enables virus dissemination (Smith et al., 2004). Similarly, it was also demonstrated that MCMV activates PI3K pathway in fibroblasts leading to phosphorylation of AKT at Ser 473 (Tokuyama et al., 2011). Taken together, these data underscore the significant role of PI3K in support of CMV infection.

Among the five genes identified from the functional screening as positive hits (*Rpl18a, Lyar, Itga5, Mapkapk3* and *Pik3r1*), three out of the five (*Itga5, Mapkapk3* and *Pik3r1)* are predicted as direct targets of miR-27 based on TargetScan (www.targetscan.org). The analyses of gene expression at mRNA and protein level

in response to miR-27 overexpression or inhibition suggested *Mapkapk3* as a potential target, which was further confirmed using luciferase reporter assays.

Mapkapk3 was included in the functional screening because it was previously shown by the Buck lab to be differentially regulated in cells transfected with RISC-free siRNAs, miR-27 mimics or inhibitors (Table3.5). This gene was downregulated ~2.14 fold in cells transfected with miR-27 mimics compared to the inhibitors. Further comparison of the mimic or inhibitor to the transfection control (RISC-free siRNA) demonstrated that *Mapkapk3* is downregulated 1.4635 fold by miR-27 mimics and upregulated 1.4686 fold by inhibitors. In line with this, the microarray analysis performed in the present study showed that *Mapkapk3* expression was decreased by 1.12 fold (p=0.0035), but this was below the cut off used (1.2).

Based on the known links between MCMV infection and MAP kinase signalling, it was hypothesised that miR-27 might exert its anti-viral activity via the regulation of *Mapkapk3*, a component of p38 MAP kinase signalling pathway. Accumulating evidence indicates that the activation of p38 MAP kinase is necessary for CMV replication. Recently, in a study of MCMV induced-atherosclerosis showed that MCMV increased phosphorylated-p38 (p-p38) by ~1.7 fold in aortas of infected mice compared to uninfected mice (Tang-Feldman et al., 2013). The inhibition of p38 using SB203580, a specific inhibitor of p38, reduced MCMV viral load (Tang-Feldman et al., 2013). *In vitro* studies of HCMV infection showed that p38 MAP kinase is strongly activated by ~8 hpi and p38 stimulation is essential for viral DNA replication (Johnson et al., 1999, 2000). Inhibition of p38 MAP kinase by 4-(4-fluorophenyl)-2-(4-hydroxyphenyl)-5-(4-pyridyl)1H-imidazole; (FHPI) resulted in a significant reduction in HCMV DNA replication and viral titres (Johnson et al., 1999).

The biological significances of p38 activation upon CMV infection could relate to the phosphorylation of heat shock protein 27 (HSP27), which has been shown to occur in a p38-dependent manner upon HCMV infection (Johnson et al., 2000). In this chapter, it is demonstrated that HSP27 is a substrate of MAPKAPK3, consistent with the literature (reviewed in (Zarubin and Han, 2005)). The comparison of

MAPKAPK3 and pHSP27 levels between wild type MCMV and MCMV Δm169 in time-course experiments showed that the levels of both proteins are higher in the wild type MCMV compared to MCMV Δm169. These results suggested that MAPKAPK3 and phosphorylation of HSP27 are potentially regulated by miR-27 during MCMV infection.

HSP27 is a multifunctional protein involved in numerous cellular processes such as protein folding, inhibition of apoptosis and actin remodelling. Under stress responses, the protein is phosphorylated by MAPKAPK3 in the p38 MAP kinase pathway (reviewed in (Vidyasagar et al., 2012)). Interesting, a study of HSP27 in HCMV infection demonstrated that the virus induces the phosphorylation of HSP27 in a p38-dependent manner (Johnson et al., 2000). The authors proposed that HSP27 might have two functions required for the virus: anti-apoptotic roles and as a chaperone to correct misfolded proteins necessary for viral permissiveness (Johnson et al., 2000). Moreover, a study in monocytes also showed that HCMV upregulates HSP27 and myeloid cell leukemia 1 (Mcl-1), an anti-apoptotic member of the B-cell lymphoma 2 (Bcl-2) family (Chan et al., 2012). The cooperative functions of HSP27 and Mcl-1 induce the activation of caspase3 allowing monocyte-to-macrophage differentiation to promote viral dissemination and persistence (Chan et al., 2012). Here, it was shown that upon MCMV infection, phosphorylation of HSP27 was mediated by MAPKAPK3, which is a direct target of miR-27. It seems reasonable to speculate that anti-viral effects of miR-27 against MCMV may be in part due to miR-27 regulating *Mapkapk3* and phosphorylation of HSP27. Further studies of HSP27 related to MCMV infection would elucidate anti-viral effects resulting from miR-27-regulated *Mapkapk3*. On this note, functional analysis of HSP27 on MCMV replication can be conducted using siRNA knockdown following by infection of GFP-MCMV to determine whether HSP27 is required for viral growth. It is interesting however that HCMV does not downregulate miR-27. This could be due to redundancy of miR-27 degradation and other factors derived from HCMV can compensate for this effect.

Notably, it was found by others that miR-27 regulates p38 upon the activation of T cells (Guo et al., 2014). Cells transfected with miR-27 followed by the activation of

T cell receptor (TCR) signalling showed the reduction of phosphorylated-p38 (p-p38) levels, indicating that miR-27 regulates TCR-induced activation of p38 (Guo et al., 2014). It is known that TCR stimulation induces p38 phosphorylation (Rincon et al., 2000; Rincon and Pedraza-Alva, 2003). Thus, the authors proposed that the attenuation of p38 activity upon miR-27 overexpression is possibly derived from the regulation of GRB2, SEMA7A or IFN- γ (Guo et al., 2014). In fibroblasts, the present study demonstrated that miR-27 regulates p38 MAP kinase signalling through a direct target *Mapkapk3*, a downstream kinase of p38. Although studies in T cells and fibroblasts showed that miR-27 regulates different genes, it is interesting that genes from both studies are involved in the same pathway (p38 MAP kinase signalling). Due to the function of miR-27 in p38 MAP kinase pathway and the evidence showing that this pathway is essential for HCMV and MCMV, it is reasonable to speculate that the degradation of miR-27 upon MCMV infection is a viral strategy to sustain the activation of p38 MAP kinase signalling.

Interestingly, it appears that the strategy of miR-27 inhibition by MCMV and HVS is not present in other closely related virus. Other herpesviruses including HCMV and *Ovine herpesvirus 2 (*OvHV-2) do not inhibit miR-27 to upregulate expression of cellular genes. Guo *et al.* proposed that these viruses do not inhibit miR-27 because they instead encode homologs of key targets; HCMV encodes viral IL-10 (Slobedman et al., 2009) and OvHV-2 genome contains SEMA7A, ATF-3 and IL-10 gene (Guo et al., 2014). Recently, it was confirmed that IL-10 is a direct target of miR-27 in T cells and macrophages (Guo et al., 2014; Xie et al., 2014). IL-10 expressed from HCMV (cmvIL-10) shares ~27% amino acid identity with human IL-10 (hIL-10) and it can bind to the receptor of hIL-10 exerting immunomodulatory properties similar to hIL-10 (Jones et al., 2002; Kotenko et al., 2000).

IL-10 is an anti-inflammatory cytokine that acts through multiple immunosuppressive modes, mainly affecting the production of pro-inflammatory cytokines, regulating the function of antigen-presenting cells and suppressing effector T cell responses (Couper et al., 2008). Based on studies of herpesvirus infection, and particularly CMV, it was demonstrated that the virus upregulates the expression of IL-10 to enhance the infection and persistence (reviewed in

(Slobedman et al., 2009). Unlike HCMV, MCMV does not encode viral IL-10 but infection is known to modulate cellular IL-10. An analysis of cytokine expression in salivary gland extracts showed a strong expression of IL-10 in MCMV-infected but not naïve mice (Humphreys et al., 2007). Using an antibody (anti-IL-10R) to block IL-10 receptor, at 30 dpi viral titres in salivary glands determined by plaque assays was dramatically inhibited in mice treated with anti-IL-10R compared to mice treated with IgG (Humphreys et al., 2007). In agreement with this, Mandaric *et al.* have shown that IL-10 suppresses the crosstalk of NK/DC cells leading to a reduction in MCMV-specific CD4 T cell responses (Mandaric et al., 2012). In the absence of IL-10, *Il10*$^{-/-}$ mice infected with MCMV showed a decrease of viral loads in lungs and salivary glands during lytic infection due to activation of CD4 T cells (Mandaric et al., 2012). Thus, it is possible that MCMV-mediated downregulation of miR-27 is to induce cellular IL-10 (a target of miR-27), particular in monocytes and macrophages that are major sources of IL-10 and cells permissive to MCMV, in order to modulate cellular immune responses supporting viral persistence.

HSP27 has been demonstrated to induce IL-10 expression in human monocytes (De et al., 2000). ELISA assays revealed that cells treated with recombinant HSP27 shows a significant increase in the amount of IL-10 compared to untreated cells. The authors also showed that the regulation of IL-10 by HSP27 involves activation of p38 and MAPKAPK2 activity (De et al., 2000). MAPKAPK2 is an isoenzyme of MAPKAPK3, sharing 70% amino acid identity, activators and substrates including HSP27 (McLaughlin et al., 1996). As MAPKAPK3 is an activator of HSP27, further investigations to test whether it contributes to IL-10 regulation would be merited, as would analysis of whether IL-10 levels are directly regulated by miR-27 in infected cells. Studies in LPS-treated *Mapkapk3*$^{-/-}$ mice did not show alteration of IL-10 mRNA stability compared to wild type mice (Ronkina et al., 2007). However, it is important to note that expression levels of MAPKAPK3 are less than MAPKAPK2 in most cells and tissue including MEFs, macrophages, heart, livers, kidneys, lungs and spleens (Ronkina et al., 2007). To conduct the functional analysis of MAPKAPK3, it is worth noting that MAPKAPK2 might compensate for MAPKAPK3 deficiency due to its higher expression and activity compared to

MAPKAPK3 (Ronkina et al., 2007). Comparative studies of *Mapkapk2/3* double knockout and single knockout of either *Mapkapk2* or *Mapkapk3* would elucidate biological roles of *Mapkapk3*. Nonetheless, in the present study, a significant reduction in viral replication was observed upon *Mapkapk3* knockdown in NIH 3T3 cells as detailed above, suggesting that in these cells *Mapkapk3* is sufficiently expressed and plays a role in MCMV growth.

In addition to miR-27 inhibition, it is worth noting that m169 might directly mediate other cellular factors to facilitate the infection. An analysis of the MCMV transcriptome during lytic infection revealed that m169 was the most abundant transcript and it also encoded for a small protein (Juranic Lisnic et al., 2013). A specific antibody was successfully generated and interacted with a ~17 kDa protein, which was believed to be encoded from m169 transcript; however, functions of this novel protein are still unknown (Juranic Lisnic et al., 2013). Marcinowski *et al*. have shown that m169 transcript was in turn regulated by miR-27. Using wild type MCMV and the virus containing mutations of miR-27 binding sites, it was found that m169 transcript significantly increased (~2 fold) in the mutant infection compared to wild type MCMV at 24 hpi, raising the possibility that the virus might use highly abundant miR-27 to control the expression of viral genes (Marcinowski et al., 2012). In contrast, Juranic *et al.* did not observe the alteration of m169 at protein levels between wild type MCMV and the mutant infection, suggesting that the non-coding function of m169 transcripts does not affect the protein expression (Juranic Lisnic et al., 2013). Further studies of m169 protein would provide insights into the function of this protein involved in MCMV infection and may clarify the dual function of m169 gene as the miR-27 inhibitor and the protein-coding gene.

In conclusion, the data in this chapter are the first to demonstrate that *Mapkapk3* is a direct target of miR-27 and knockdown of this gene suppresses MCMV replication. Upon MCMV infection, miR-27 appears to directly regulate *Mapkapk3,* a downstream molecule of p38 MAP kinase. MAPKAPK3 protein levels are increased, whereas miR-27 levels are downregulated in the time course infection of wild type MCMV compared to cells infected with MCMV Δm169. In the same time course experiments, the phosphorylation of HSP27, which occurs through MAPKAPK3,

increases in line with the levels of MAPKAPK3, suggesting that both MAPKAPK3 and subsequent phosphorylation of HSP27 are regulated by miR-27 during MCMV infection. This may, at least in part, explain why the virus has evolved the strategy to inhibit miR-27. However, the functional properties of HSP27 in MCMV infection require further investigations and analyses in other cell types including macrophages.

Chapter 4: Analysis of miR-27 functions in cell cycle regulation

4.1 Introduction

The major objective of this thesis is to understand why MCMV specifically encodes a non-coding RNA to degrade the cellular miRNA, miR-27. A central hypothesis is that this is a viral strategy to interfere with functions of miR-27 in regulating cellular pathways involved in the infection process. As described in chapter 3, miR-27 target identification was carried out using microarray analysis where the global changes in gene expression were examined upon miR-27 overexpression. The differentially expressed genes were analysed using pathway analysis software to identify pathways and biological functions regulated by miR-27. Pathway analysis revealed that the cell cycle was one of the six top enriched biological functions regulated by miR-27 (Table 3.3, chapter 3). Thus, this chapter focuses on miR-27 functions in the cell cycle and identification of target genes responsible for these effects.

Previous reports have demonstrated that miR-27 is involved in regulating the cell cycle. Lerner *et al*. demonstrated that miR-27 regulates F-box and WD repeat domain-containing 7 (FBW7), a component of an ubiquitin ligase complex called KSP1, CUL1 and F-box protein (SCF) that mediates degradation of cyclin E, a positive regulatory protein of G1/S transition (Lerner et al., 2011). The overexpression of miR-27 using pre-miR-27 increases the population of cells in S phase compared to cells transfected with pre-miR-control and this was thought to be a result of miR-27-regulated FBW7, leading to an elevation of cyclin E (Lerner et al., 2011). Further, it has been shown that inhibition of miR-27 using antisense oligonucleotides decreases the percentage of cells in S phase by approximately 10% compared to untreated cells (Mertens-Talcott et al., 2007).

In the context of CMV infection, a number of studies have shown that the virus interferes with the host cell cycle to support viral DNA replication (reviewed in (Castillo and Kowalik, 2004)). In particular, several independent lines of evidence have demonstrated that CMV blocks the G1/S phase transition (reviewed in (Flemington, 2001)). For example, HCMV encodes the UL69 protein, which arrests

cells in G1 and viruses lacking UL69 gene showed a growth defect compared to wild type virus (Hayashi et al., 2000; Lu and Shenk, 1999). Besides UL69, the IE86 protein (IE2) and to lesser extent the IE72 protein (IE1) of HCMV have been shown to cause G1 arrest (Noris et al., 2002; Wiebusch and Hagemeier, 1999). Likewise, studies in MCMV revealed that the virus arrests cells in both G1 and G2 and that is dependent on MCMV IE3, the homologue of HCMV IE2 (Wiebusch et al., 2008). Cell cycle arrest is advantageous the CMV since this prevents cells from entering S phase, thereby blocking cellular DNA synthesis that would compete with the virus for the available resources for DNA replication.

Based on the known function of miR-27 in regulating the cell cycle and the fact that CMV is known to induce the cell cycle arrest, it seems logical to speculate that MCMV degrades miR-27 in order to interfere with this function of the miRNA. Through the degradation of miR-27, the virus could manipulate the cell cycle towards the condition that are advantageous to viral replication. In this chapter, the function of miR-27 in the cell cycle regulation was investigated and direct targets of miR-27 that could be involved in this function were examined whether they play a role in MCMV replication.

4.2 Aims

The aims of the present chapter are as follow:

1. Investigate the function of miR-27 in the cell cycle by analysis of cell cycle using propidium iodide followed by flow cytometry
2. Identify and validate miR-27 targets using a target prediction database and experimental approaches
3. Evaluate the role of miR-27 targets in the cell cycle
4. Examine whether miR-27 targets associated with the cell cycle impact MCMV growth *in vitro*

4.3 Results

4.3.1 miR-27-regulated genes are involved in regulation of the cell cycle

As described in chapter 3 (3.3.1.1), the global transcriptomic changes were examined in response to miR-27 overexpression using microarray analysis. NIH 3T3 cells were transfected with miR-27a mimics or RISC-free siRNAs for 48 h. RISC-free siRNAs are synthetic siRNAs that can be transfected into cells but are not loaded into RISC complexes. The RISC-free siRNA transfection therefore serves as a negative control (to account for gene changes associated with transfection rather than miR-27). Thus, it was expected that potential targets of miR-27 are downregulated upon miR-27 overexpression compared to RISC-free siRNAs. At 48 h post transfection, total RNA was extracted and its quality was examined using polyacrylamide gel electophoresis. The levels of miR-27 were quantified using qRT-PCR to confirm the overexpression of miR-27 in cells transfected with the mimics. RNA samples were prepared and sent for microarray analysis.

To select potential targets of miR-27 for further analysis, a fold change cut off of 1.2 ($p<0.05$) was applied. This criterion was used based on the study by Nielsen *et al.* who showed that the magnitude of miRNA-mediated gene repression depending on the number of seed matches. For example, RNAs containing 7-mer seed match show 1.18 fold downregulation (Nielsen et al., 2007). Using the cut off of 1.2 ($p<0.05$), 97 genes showed to be downregulated in cells transfected with miR-27 mimics compared to RISC-free siRNAs (Appendix 1).

To identify cellular pathways and biological functions regulated by miR-27, the 97 genes were analysed using Ingenuity Pathway Analysis (IPA) (http://www.ingenuity.com/) in chapter 3. The analysis revealed that the cell cycle was one of the six top enriched biological functions regulated by miR-27. Thus, the present chapter focuses on examining whether miR-27 regulates the cell cycle in NIH 3T3 cells and determining whether this impacts MCMV infection.

4.3.2 Effect of miR-27 on the cell cycle regulation

To functionally investigate effects of miR-27 on the cell cycle, the cell population of G1, S and G2/M in the cell cycle was analysed in cells in which miR-27 was either overexpressed or inhibited. NIH 3T3 cells were untreated or transfected with RISC-free siRNAs, miR-27a mimics or miR-27a inhibitors for 24 h prior to serum starvation (reducing calf serum concentration from 10% to 0.5%) (Fig 4.1A). Synchronised cells were then stimulated with media containing 10% serum and cells collected after 12, 14, 16, 18, 20, 22 and 24 h. The experiment was performed with three technical replicates by which cells were seeded in individual wells and treated with miRNAs and collected for cell cycle analysis. The result from the three replicates are presented in the bar graphs beside the histograms in Fig 4.1B. The effects of miR-27 are most pronounced at 12 and 14 h. At 12 h, cells transfected with miR-27a mimics displayed 78.95% of cells in S phase compared to 74.91% of untreated cells and 74.2% of RISC-free siRNA transfection, whereas miR-27a inhibitors showed 58.77% of S phase cells. In line with the cell progression to S phase, cells transfected with miR-27a mimics reduced the percentage of cells in G1 as 18.21% compared to untreated cells (21.02%) and cells transfected with RISC-free siRNAs (19.77%), while miR-27a inhibitor showed an accumulation of cells in G1 (40.61%). Consistent with the effects observed at 12 h, at 14 h post serum reactivation, miR-27a mimics induced cells in S phase (77.24%) compared to untreated cells (65.85%) and cells transfected with RISC-free siRNAs (70.27%), while miR-27 inhibitors delayed G1/S progression showing 24.98% of G1 and 63.26% of S phase. Time points from 16 to 24 h showed progression of the cell cycle according to changes at 12 and 14 h. Based on the stimulation of the G1/S transition, at 16, 18 and 20 h, cells transfected with the mimics increased the number of cells in G2/M phase by 30.61%, 39.81% and 32.62% compared to RISC-free siRNA showing 29.98%, 29.29% and 21.74%. At 22 and 24 h, the cell cycle profile of cells transfected with the mimics appeared to be similar to RISC-free siRNAs with the majority of cells in G1 phase. In cells transfected with the inhibitors, the delay of the G1/S transition at 12 and 14 h subsequently caused the delay of cell progression from S to G2/M phase at 16 to 24 h. Taken together, these results indicate that miR-27

induces the G1/S transition and cells in which the miRNA is inhibited show a delay in this progression.

D- and E-type cyclins are key mediators of G1/S progression that activate cyclin dependent kinases (CDKs) to phosphorylate retinoblastoma (Rb) (Masamha and Benbrook, 2009). In quiescent cells, Rb represses transcription of many genes important for cell cycle progression via interaction with transcription factor E2F, blocking ability of E2F to activate transcription. When cells are stimulated to enter the cell cycle by proliferative signals such as growth factors and serum, Rb is phosphorylated by CDKs, which forms a complex with cyclins. The phosphorylated Rb becomes inactive and can no longer repress E2F, thereby inducing the expression of numerous genes required for S phase entry (reviewed in (Henley and Dick, 2012)). While CDKs are generally expressed throughout the cell cycle, cyclins are dynamically expressed in relation to the specific cell cycle phases and can thus serve as markers of the cell cycle (reviewed in (Moore, 2013)). To confirm the observation of miR-27 accelerating the G1/S transition, expression of cyclin D3 (CCND3) proteins was examined. As described for the flow cytometry experiments, NIH 3T3 cells were untreated or transfected with RISC-free siRNAs, negative inhibitors (*C. elegans* inhibitors), negative mimics (*C. elegans* mimics), miR-27a mimics or miR-27a inhibitors for 48 h. In addition to RISC-free siRNA control, additional controls were included: negative inhibitors and negative mimics designed based on *C. elegans* miR-67, which has minimal sequence identity with miRNAs in human, mouse and rat. At 48 h post transfection, CCND3 protein was determined by Western blot analysis. As shown in Fig 4.1C, transfection of cells with miR-27a mimics resulted in a slight increase in the expression of CCND3 (1.20 fold) compared to RISC-free siRNAs, and transfection of the inhibitors caused a small decrease, whereas the other transfection conditions did not significantly alter CCND3 levels. The elevation of CCND3 is consistent with the effect of miR-27 on activating cells from G1 to S phase, supporting the conclusion that miR-27 promotes the G1/S transition and inhibition of miR-27 delays this.

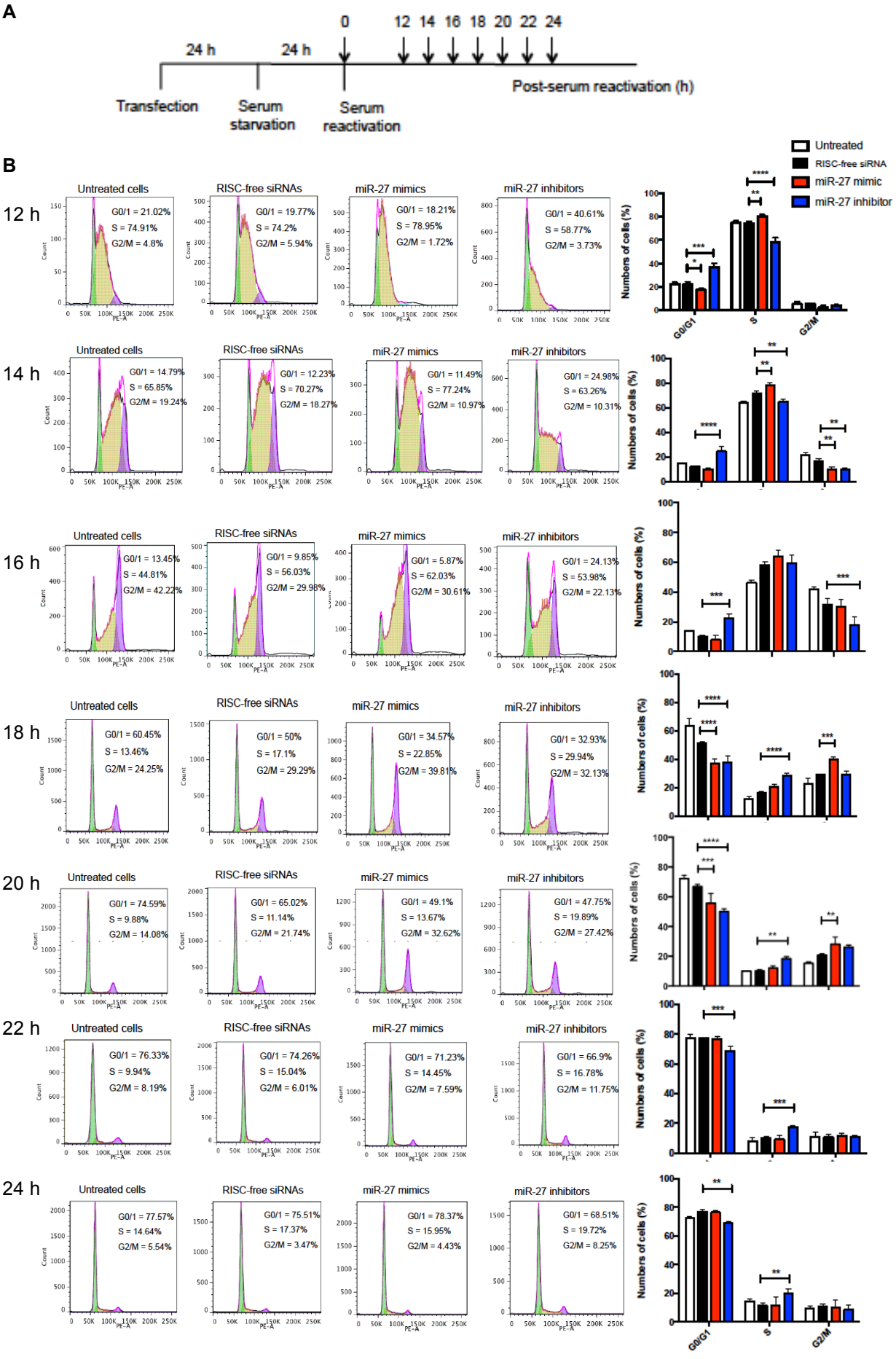
A
0
12 14 16 18 20 22 24
24 h
24 h
Transfection
Serum starvation
Serum reactivation
Post-serum reactivation (h)
B
Untreated
RISC-free siRNA
miR-27 mimic
miR-27 inhibitor
12 h
14 h
16 h
18 h
20 h
22 h
24 h
Untreated cells
RISC-free siRNAs
miR-27 mimics
miR-27 inhibitors
Numbers of cells (%)
G0/G1
S
G2/M

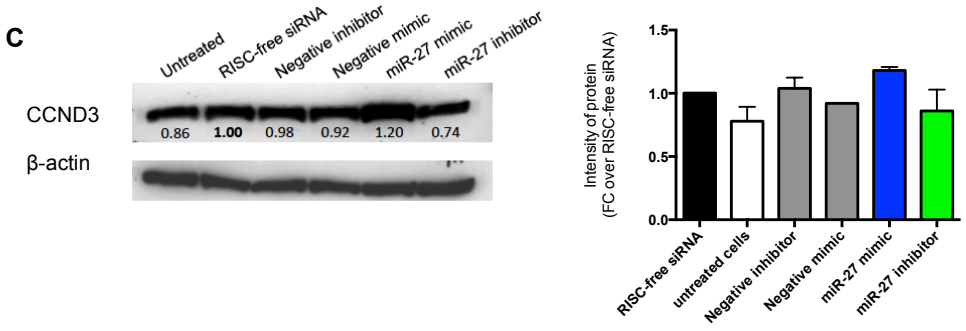

Figure 4.1 miR-27a increases the number of cells in S phase and elevates expression of cyclin D3.

(A) Experimental setup for synchronisation of cells and cell cycle analysis. NIH 3T3 cells were untreated or transfected as described above and collected at the indicated times. DNA was stained with propidium iodide and analysed by flow cytometry. **(B)** Histogram showing cell cycle profiles of one out of three technical replicates. The bar graphs represent percentages of cells as means± SD from three technical replicates. Data were analysed using Flowjo software to determine the percentage of cells in each phase. The statistics is based on turkey's multiple comparisons test, two-way ANOVA (*p<0.05, **p<0.01, ***p<0.001 and ****p<0.0001). **(C)** Western blot analysis (ECL-based detection) of CCND3 in untreated or transfected cells (as described in main text). Protein was quantified using ImageStudioLite software and normalised to beta-actin. Results are shown as fold changes of protein relative to RISC-free siRNA. **(Left)** Images of the immunoblots. **(Right)** Protein quantification of CCND3 from two independent experiments. Data are shown as means ± SD of fold change compared to RISC-free siRNAs

4.3.3 Analysis of mRNA and protein level of *Bmi1, Calm3, Cav1* and *Ccng1* in response to changes in miR-27 expression

As shown in the previous section, the analysis of the cell cycle suggested a role of miR-27 in promoting G1/S transition. To further investigate how miR-27 influences the cell cycle, analysis of potential targets of miR-27 (identified in chapter 3) was carried out. Based on the computational target prediction database TargetScan (www.targetscan.org) and literatures reporting functions of genes in the cell cycle, *Bmi1, Calm3, Cav1* and *Ccng1* were selected to determine their expression when miR-27 was overexpressed or inhibited. These genes are predicted targets of miR-27 but have not been previously validated in the literature. They have been well documented to be involved in cell cycle regulation, as detailed below.

Polycomb ring finger oncogene 1 (BMI1) belongs to the polycomb group proteins and is identified as a positive regulator of G1/S transition by suppressing the transcription of negative regulators: $p16^{Ink4a}$ and $p19^{Arf}$ (Jacobs et al., 1999). *Bmi1*$^{-/-}$ mice and knockdown of *Bmi1* using shRNAs led to G1 arrest in several cell types (Chen et al., 2011; Jacobs et al., 1999; Wu et al., 2011).

Calmodulin genes (*Calm1, Calm2 and Calm3*) encode an identical Ca^{2+}-binding protein that regulates a variety of intracellular enzymes including adenylyl cyclases, phosphodiesterases, protein kinases and the protein phosphatase calcineurin (Chin and Means, 2000). Calmodulins (CaMs) have been implicated in the regulation of the cell cycle due to the observation of the changes of CaM concentration during cell cycle progressions, especially the G1/S transition (Rasmussen and Means, 1989). Interestingly, a CaM binding site was identified near the N terminus of cyclin E, a key regulator of the G1/S transition (Choi and Husain, 2006). The interaction of CaM and cyclin E led to an increase in the activity of cyclin dependent kinase 2 (CDK2), the cyclin E partner responsible for cell progression from G1 to S phase (Choi and Husain, 2006). Moreover, studies in mammalian cells suggested that CaM is also involved in cell cycle regulation via functions of Ca^{2+}/CaM-dependent kinases (CaMKs) (Kahl and Means, 2003; Skelding et al., 2011).

Overexpression of *Cav1* in NIH 3T3 cells and stable expression of *Cav1* in transgenic mice displayed G0/G1 arrest occurring through a p53/p21-dependent pathway (Galbiati et al., 2001). *Cav1*-induced G0/G1 arrest was also reported in human endothelial cells in which *Cav1* prevented downregulation of $p27^{kip1}$ and Rb phosphorylation, causing the accumulation of cells in G0/G1 (Fang et al., 2007).

Cyclin G1 (*Ccng1*) was identified as a transcriptional target of p53 tumor suppressor by which the p53 binds to two binding sites within *Ccng1* gene, leading to an activation of *Ccng1* transcription (Okamoto and Beach, 1994; Zauberman et al., 1995). The precise role of *Ccng1* in regulation of the cell cycle and proliferation is still controversial. After UV irradiation to induce DNA damage, MEFs derived from $Ccng1^{-/-}$ mice showed ~50% reduction of cells in G2/M phase compared to $Ccng1^{+/+}$ MEFs, suggesting that *Ccng1* plays a role in G2/M arrest in response to cellular stress (Kimura et al., 2001). In contrast, evaluations of cell growth and proliferation indicated a positive effect of *Ccng1* in tumour cells (Skotzko et al., 1995; Smith et al., 1997) that is in line with the observations of *Ccng1* overexpression in human cancers (Reimer et al., 1999).

Compelling studies of *Bmi1, Calm3, Cav1* and *Ccng1* in the cell cycle regulation raise the possibility that miR-27-induced G1/S transition might result from miR-27 regulating one of these genes. To examine this, mRNA and protein levels of these genes were examined in NIH 3T3 cells that were either untreated or transfected with RISC-free siRNAs, negative inhibitors (*C. elegans* inhibitors), negative mimics (*C. elegans* mimics), miR-27 mimics or miR-27 inhibitors for 48 h. As shown in Fig 4.2A, miR-27 mimics caused ~2 fold reduction in *Bmi1* mRNAs compared to RISC-free siRNA, although it was not significant suggesting that *Bmi1* might be a target of miR-27. The transfection of negative mimics showed a slight reduction in *Bmi1* mRNA (less than 2 fold) compared to RISC-free siRNA that is potentially due to non-specific effect of the control miRNAs. *Calm3* mRNA was significantly decreased in miR-27 mimic transfection compared to RISC-free siRNAs, whereas inhibition of miR-27 led to an upregulation of *Calm3,* suggesting that *Calm3* is likely to be regulated by miR-27. Although *Cav1* did not significantly alter in cells transfected with miR-27 mimics or the inhibitors, the mimics slightly reduced the

expression of the mRNA compared to RISC-free siRNAs and the inhibitors showed a subtle increase of the mRNA. These small changes suggested that *Cav1* might be regulated by miR-27. Overexpression of miR-27 did not affect levels of *Ccng1* mRNAs; however, inhibition of miR-27 significantly increased *Ccng1* levels. It is worth noting that an increase of *Ccng1* was also seen with the negative mimics and inhibitors, suggesting that the elevation *Ccng1* observed in cells transfected with miR-27 inhibitors could be derived from non-specific effects.

The effect of miR-27 on the expression of the four genes *(Bmi1, Calm3, Cav1 and Ccng1)* was further examined at the protein level. Evaluation of protein expression by Western blot analysis revealed that CALM3 expression was inconsistent with mRNA levels (Fig 4.2B). No significant change in the protein level was observed upon transfection with miR-27 mimics or miR-27 inhibitors compared to RISC-free siRNA. This could be due to the stability and turnover rate of the protein. A mathematical model measuring rates of protein decay showed that fast-decaying proteins were more likely to be detected as miRNA targets than stable proteins (Hausser et al., 2013). This suggests that rates of protein turnover impact the investigation of the effect of miRNAs on protein level. However, the turnover rate of CALM3 has not been reported. Although *Bmi1* and *Cav1* mRNAs were slightly decreased in cells transfected with miR-27 mimics relative to RISC-free siRNAs, at the protein level miR-27 mimics significantly reduced BMI1 and CAV1 protein (~2 fold) compared to RISC-free siRNAs, indicating that miR-27 is likely to regulate these genes. In contrast to overexpression of miR-27, inhibition of this miRNA using the inhibitor did not seem to alter BMI1 and CAV1 protein, in line with an observation that many miRNA inhibitors showed more subtle effects than miRNA mimics (Santhakumar et al., 2010).

In the case of CCNG1, the protein was not detected in NIH 3T3 cells. To overcome this problem, HeLa cells were used since they endogenously express CCNG1 (Min et al., 2009). It is important to note that all of the miR-27 binding sites for these targets shown in Fig 4.2A are conserved in mouse and human. HeLa cells were untreated or transfected with RISC-free siRNAs, miR-27 mimics or miR-27 inhibitors for 48 h. Total RNA was extracted to determine expression of miR-27 and *Ccng1* mRNAs,

and protein samples were collected for Western blot analysis. As shown in Fig 4.3A, miR-27 increased ~100 fold in cells transfected with miR-27 mimics compared to RISC-free siRNAs, whereas miR-27 inhibitors caused a ~10 fold reduction of miR-27. Similar to what was observed in NIH 3T3 cells, a significant decrease of *Ccng1* mRNAs in cells transfected with miR-27 mimics was observed along with an upregulation of *Ccng1* upon miR-27 inhibition (Fig 4.3B). In contrast to the mRNA level, CCNG1 protein was not significantly altered by mimic or inhibitor transfection compared to RISC-free siRNA, indicating that miR-27 does not regulate *Ccng1* (Fig 4.3C) or the regulation is too subtle to readily detect by Western blot analysis. In conclusion, it is likely that *Bmi1* and *Cav1*, but not *Ccng1*, are regulated by miR-27.

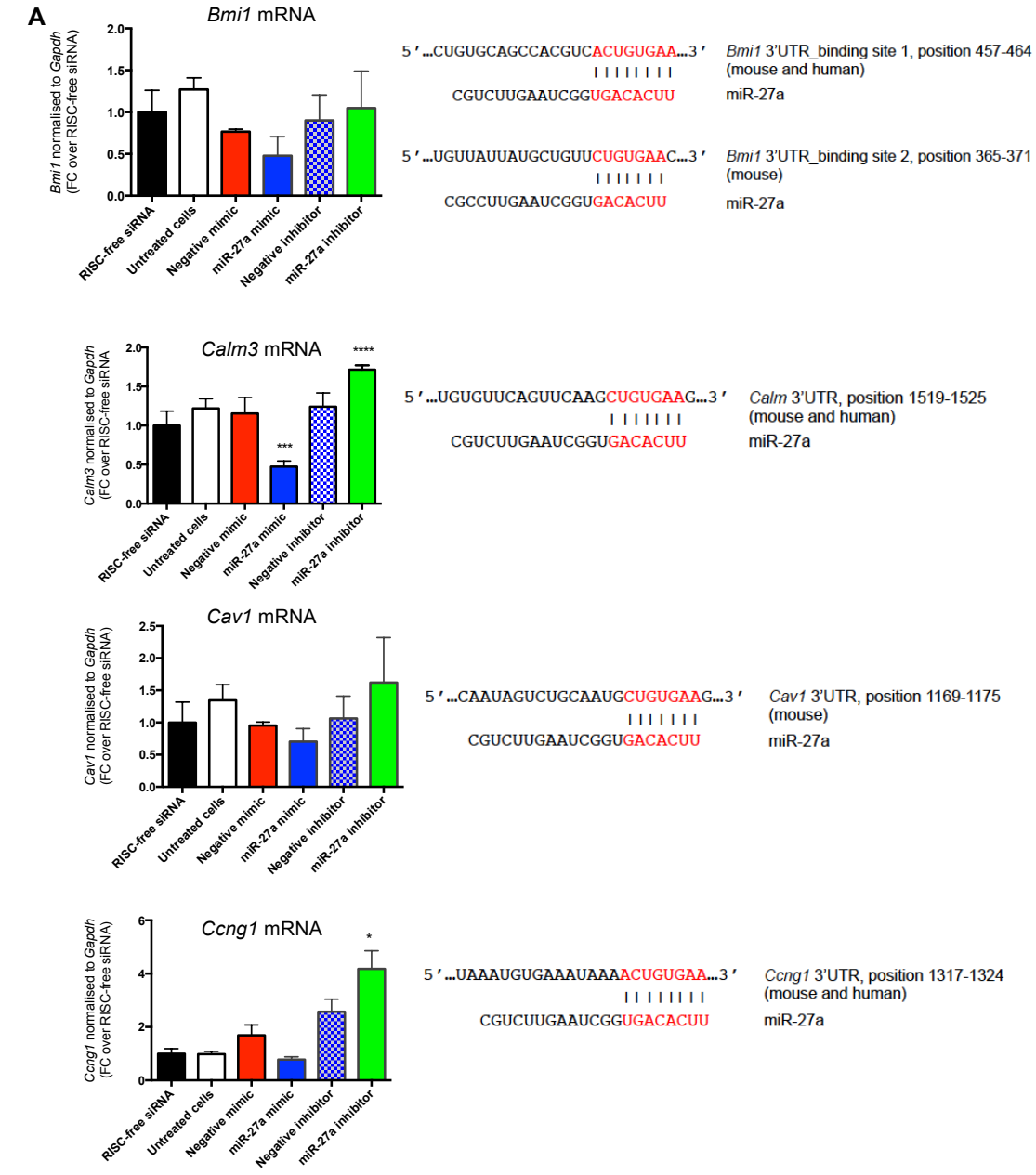
A
Bmi1 mRNA
Bmi1 normalised to Gapdh (FC over RISC-free siRNA)
RISC-free siRNA
Untreated cells
Negative mimic
miR-27a mimic
Negative inhibitor
miR-27a inhibitor
5′...CUGUGCAGCCACGUCACUGUGAA...3′
CGUCUUGAAUCGGUGACACUU
Bmi1 3'UTR_binding site 1, position 457-464 (mouse and human)
miR-27a
5′...UGUUAUUAUGCUGUUCUGUGAAC...3′
CGCCUUGAAUCGGUGACACUU
Bmi1 3'UTR_binding site 2, position 365-371 (mouse)
miR-27a
Calm3 mRNA
Calm3 normalised to Gapdh (FC over RISC-free siRNA
5′...UGUGUUCAGUUCAAGCUGUGAAG...3′
CGUCUUGAAUCGGUGACACUU
Calm 3'UTR, position 1519-1525 (mouse and human)
miR-27a
Cav1 mRNA
Cav1 normalised to Gapdh (FC over RISC-free siRNA)
5′...CAAUAGUCUGCAAUGCUGUGAAG...3′
CGUCUUGAAUCGGUGACACUU
Cav1 3'UTR, position 1169-1175 (mouse)
miR-27a
Ccng1 mRNA
Ccng1 normalised to Gapdh (FC over RISC-free siRNA)
5′...UAAAUGUGAAAUAAAACUGUGAA...3′
CGUCUUGAAUCGGUGACACUU
Ccng1 3'UTR, position 1317-1324 (mouse and human)
miR-27a
B
Untreated
RISC-free siRNA
Negative inhibitor
Negative mimic
miR-27 mimic
miR-27 inhibitor
BMI1
0.97 1.00 1.01 1.09 0.63 0.87
β-actin
CALM3
0.99 1.00 0.96 0.93 0.87 0.82
GAPDH
CAV1
0.92 1.00 0.75 0.75 0.58 1.11
β-actin

Figure 4.2 Expression of *Bmi1, Calm3, Cav1* and *Ccng1* in transfected cells analysed by qRT-PCR and Western blot analysis
NIH 3T3 cells were untreated or transfected with 25 nM RISC-free siRNAs or miRNAs as indicated for 48 h. **(A)** Expression of *Bmi1, Calm3, Cav1* and *Ccng1* in untreated cells and transfected cells determined by qRT-PCR. Data are presented as means of fold-change ±SD from three technical replicates relative to RISC-free siRNA. Significance was assessed by one-way ANOVA (*P<0.05, ***P<0.001 and ****P<0.0001). **(B)** Western blot analysis (ECL-based detection) of BMI1, CALM3 and CAV1. The proteins were quantified using ImageStudioLite software and normalised to β-actin or GAPDH as indicated. Results are shown as fold change of protein compared to RISC-free siRNA transfection.

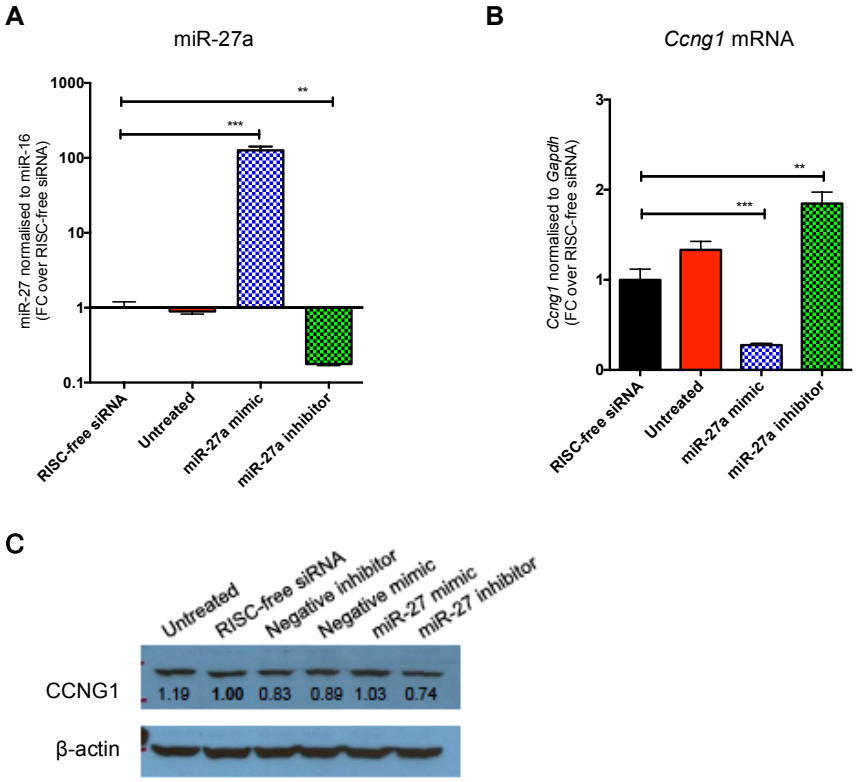

Figure 4.3 Expression of *Ccng1* in transfected cells
HeLa cells were untreated or transfected with 25 nM of RISC-free siRNAs or the indicated mimics or inhibitors for 48 h. Levels of **(A)** miR-27 and **(B)** *Ccng1* mRNA analysed by qRT-PCR. Data are shown as means of fold change ±SD from three technical replicates relative to RISC-free siRNA transfection. Significance was assessed by unpaired t-test (**P<0.01 and ***P<0.001). **(C)** Western blot analysis (ECL-based detection) of CCNG1 protein. CCNG1 and β-actin were quantified using ImageStudioLite software. Values of CCNG1 were normalised to β-actin and fold changes of protein were calculated compared to RISC-free siRNA transfection.

4.3.4 Validation of *Bmi1* and *Cav1* as direct targets of miR-27 using luciferase reporter assays

The studies described above demonstrated that BMI1 and CAV1 protein are downregulated upon miR-27 overexpression, although inhibition of miR-27 does not alter these protein levels. To examine whether this effect is mediated by direct interactions between miR-27 and the 3'UTR of these mRNAs, luciferase reporter assays were carried out. The full length 3'UTR of genes of interest was cloned downstream of *Renilla* luciferase of a reporter vector psi-CHECK2. When this vector is co-transfected with miRNA mimics, luciferase expression should be lower compared to cells transfected with miRNA controls, whereas the co-transfection with miRNA inhibitors results in an increase of luciferase levels. NIH 3T3 cells were transfected with the empty psi-CHECK2 vector or the vector in which the 3'UTR sequences were introduced. To examine the effect of miR-27, cells were co-transfected with miR-27a mimics, miR-27a inhibitors or RISC-free siRNAs for 48 h. Expression of *Renilla* luciferase were measured and normalised to the internal control firefly luciferase in order to minimise variability of experiments due to differences in cell viability or transfection efficiency.

The control experiment was carried out using a miR-27 sensor, which contains three adjacent binding sites for miR-27. Each of the binding sites is complementary to miR-27 with an internal loop to prevent endonucleolytic cleavage and has been previously described in (Libri et al., 2012). As expected, the miR-27 sensor was suppressed by the miR-27 mimics compared to RISC-free siRNAs, while miR-27 inhibitors significantly upregulated expression of *Renilla* luciferase (Fig 4.4A). Consistent with the results obtained from Western blot analysis, miR-27 mimics significantly reduced expression of *Renilla* luciferase (greater than 2 fold) of psi-CHECK2-*Bmi1* 3'UTR containing two binding sites of miR-27 compared to RISC-free siRNA, whereas miR-27 inhibitors increased *Renilla* luciferase expression (Fig 4.4B). Similarly, overexpression of miR-27 significantly decreased *Renilla* luciferase (~2 fold) of psi-CHECK2-*Cav1* 3'UTR compared to RISC-free siRNAs; however, the miR-27 inhibitors did not upregulate the expression of *Renilla* luciferase (Fig 4.4C). Unlike the 3'UTR of *Bmi1* or a miR-27 sensor that contain multiple sites for

miR-27, the 3'UTR of *Cav1* has only one binding site. In the absence of miR-27 inhibitors, endogenous miR-27 binds and represses luciferase expression of psi-CHECK2-*Bmi1* 3'UTR and a miR-27 sensor, giving rise to lower baseline expression of luciferase compare to psi-CHECK2-*Cav1* 3'UTR. Thus, when miR-27 is inhibited, psi-CHECK2-*Bmi1* 3'UTR and a miR-27 sensor should show more pronounced effect on the recovery of luciferase compared to psi-CHECK2-*Cav1* 3'UTR.

Along with luciferase assays, the cell viability test was conducted at 48 h post-transfection to assess toxicity of the transfection. The results revealed that all transfected cells showed more than 95% of cell viability compared to untreated cells, indicating that the transfection was not toxic (Fig 4.4D). In conclusion, the luciferase assays suggest that *Bmi1* and *Cav1* are direct targets of miR-27.

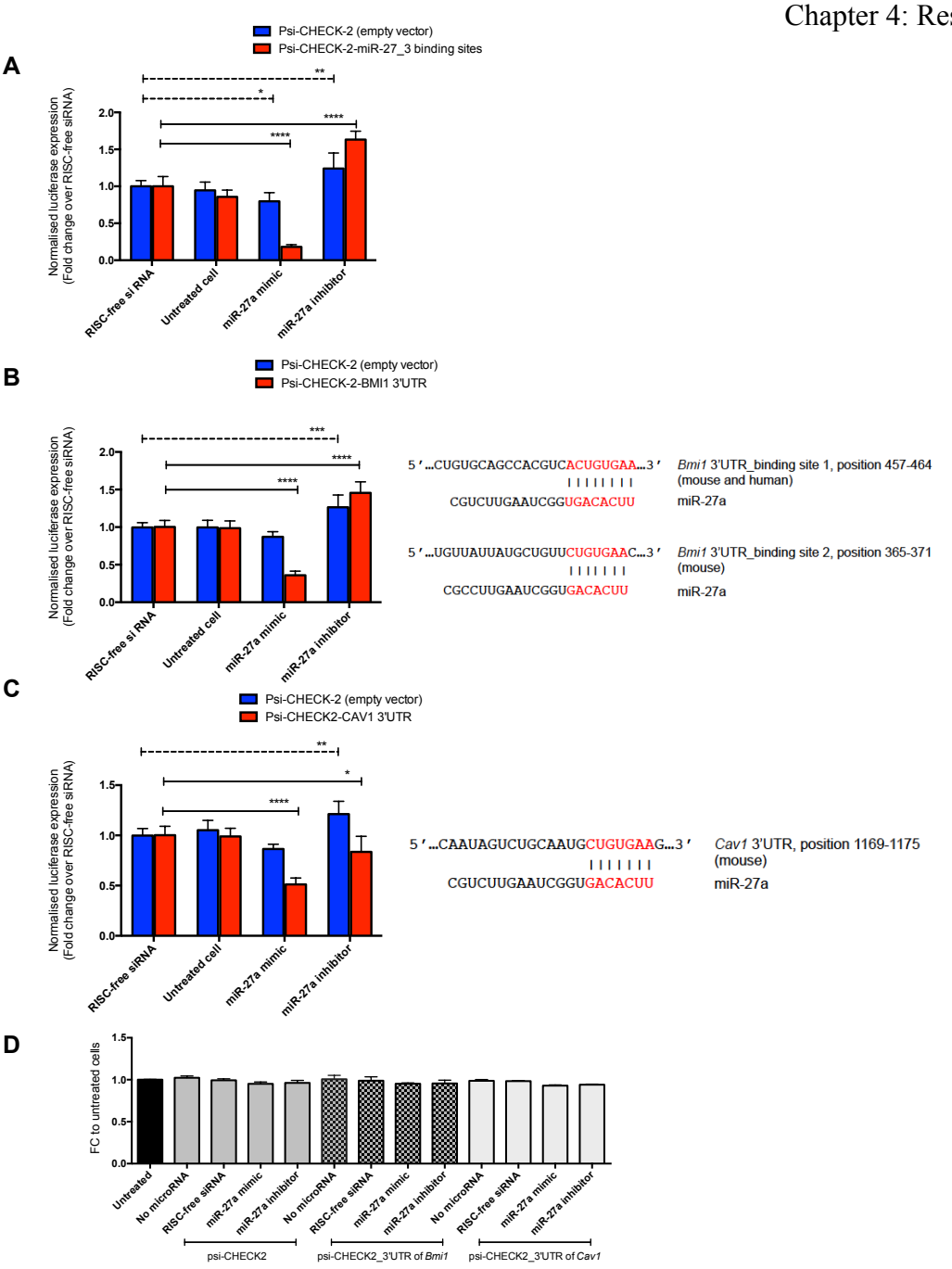

Figure 4.4 *Bmi1* and *Cav1* are direct targets of miR-27.
Luciferase reporter assays using **(A)** a miR-27 sensor containing three binding sites for miR-27 **(B)** psi-CHECK2-*Bmi1* 3'UTR or **(C)** psi-CHECK2 *Cav1* 3'UTR. Schematic illustrations of predicted miR-27 binding sites obtained from TargetScan are shown next to the results (Right). Experiments were carried out in parallel with the empty psi-CHECK2 vector for comparison. NIH 3T3 cells were transfected with indicated vectors with or without miRNA mimics or inhibitors (25nM) for 48 h. *Renilla* luciferase was measured and normalised to firefly luciferase. Data are presented as means of fold change (±SD) of five technical replicates relative to RISC-free siRNA. Significance was assessed by two-way ANOVA, Dunnett's multiple comparisons test (*P<0.05, **P<0.01, ***P<0.001, ****P<0.0001). The experiments were repeated and representative experiments are shown. **(D)** Cell viability test of transfection experiments shown above. Data show means of fold change (±SD) of three technical replicates compared to untreated cells.

4.3.5 Functional analysis of *Bmi1* and *Cav1* on MCMV replication

The work described above shows that miR-27 stimulates the G1/S transition and directly targets two genes, *Bmi1* and *Cav1*, which have been reported to play a role in the cell cycle. The central hypothesis in this chapter is that miR-27 inhibits MCMV replication through the regulation of the cell cycle. To evaluate whether this could be mediated by *Bmi1* or *Cav1,* the effects of these genes on MCMV replication were investigated using siRNAs to knock them down followed by infection with the GFP reporter MCMV (GFP-MCMV). NIH 3T3 cells were untreated or transfected with RISC-free siRNAs, *Bmi1* siRNAs, *Cav1* siRNAs or positive controls eGFP siRNAs and miR-542 mimics for 48 h prior to infection with GFP-MCMV at MOI of 0.2. The positive controls include eGFP siRNAs targeting the expressed green fluorescent protein (eGFP) and miR-542 mimics, which was shown by others in the lab to suppress replication of MCMV (Santhakumar D., unpublished data)

As shown in Fig 4.5A, *Bmi1* and *Cav1* mRNAs were reduced by >95% following knockdown compared to cells transfected with RISC-free siRNAs. The BMI1 protein was undetectable in *Bmi1* knockdown cells, whereas the CAV1 showed ~50% reduction (Fig 4.5B). This could be due to a long half-life of CAV1 (longer than 36 h) reported in monkey kidney cell line and HeLa cells (Hayer et al., 2010). In parallel, cell viability assays were performed at 48 h post-transfection showing no toxicity of transfected cells as compared to untreated cells (Fig 4.5C).

To assess the effect of knockdown (BMI1) or partial knockdown (CAV1) on MCMV replication, the reporter assay was used. At 48 h post-transfection, cells were mock infected or infected with GFP-MCMV at MOI of 0.2. GFP expression was monitored up to 93 hpi. As shown in Fig 4.5D, at 93 hpi, eGFP siRNAs and miR-542 mimics reduced GFP intensity by ~3 and ~5 fold compared to RISC-free siRNAs, respectively. Viral growth in cells in which *Bmi1* or *Cav1* were knocked down had no significant attenuation compared to untreated cells or RISC-free siRNA transfection. Considering the absence of BMI1 protein under these transfection conditions, it was concluded that BMI1 does not impact MCMV replication *in vitro*. However, it is difficult to draw out a definite conclusion regarding the role that *Cav1*

might play in MCMV infection because the protein could not be completely knocked down by siRNAs.

In this regard, *Cav1* knockout mice (*Cav1*$^{-/-}$) were kindly provided by Professor Rose Zamoyska (IIIR, University of Edinburgh). Primary mouse embryonic fibroblasts (MEFs) were isolated from *Cav1*$^{-/-}$ mice for determination of MCMV growth in the absence of *Cav1*. Initially, Western blot analysis was carried out to confirm the elimination of *Cav1* gene. As shown in Fig 4.6A, CAV1 was completely diminished in cells isolated from *Cav1*$^{-/-}$ mice. To carry out the viral growth assay, cells were seeded for 24 h prior to infection with GFP-MCMV at MOI of 0.2. GFP expression was measured at 70 hpi, which is a time point within the exponential expression of GFP observed from previous growth curves (Fig 4.5D). Similar to the results from the *Cav1* knockdown experiments, MCMV growth was not different in MEFs obtained from *Cav1*$^{-/-}$ versus wild type mice (Fig 4.6B). These data suggest that *Cav1* does not influence MCMV replication *in vitro*.

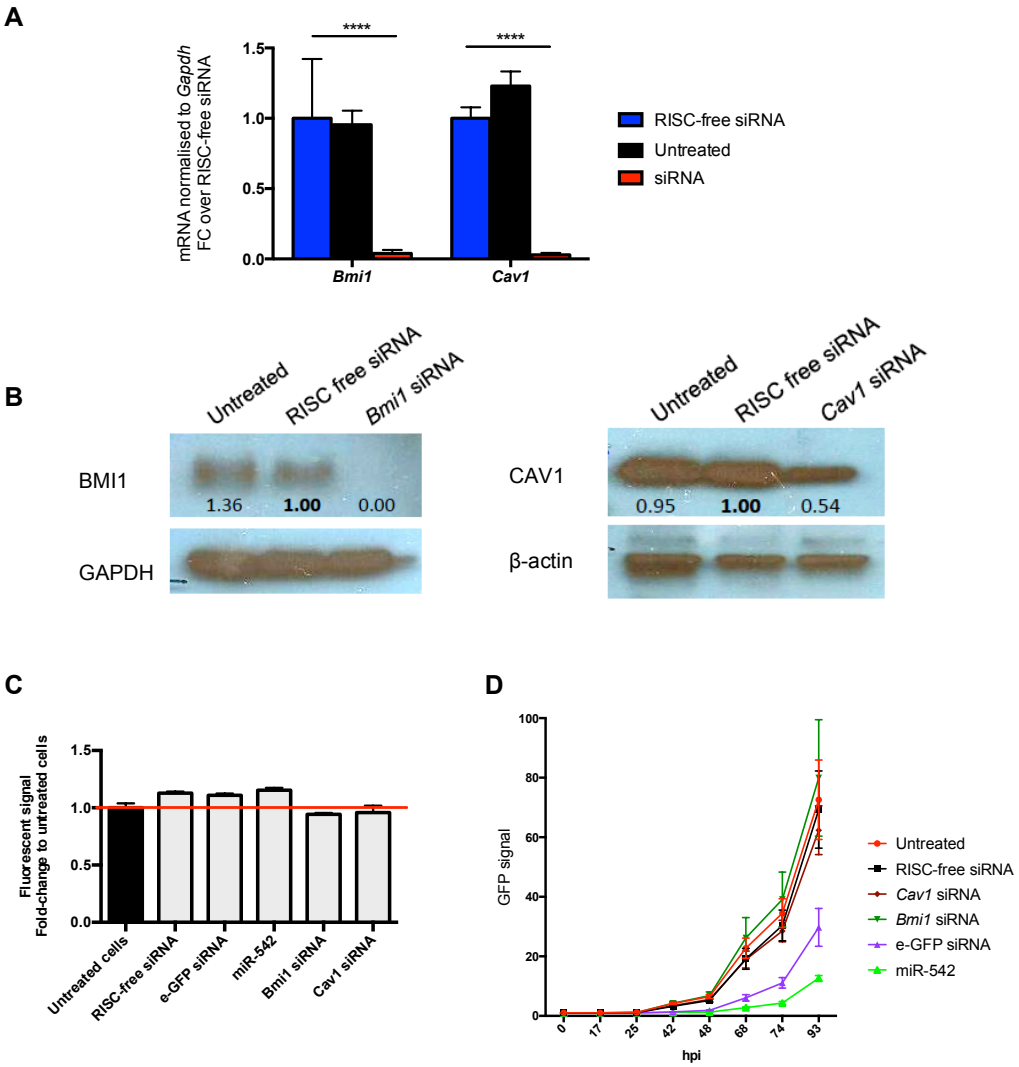

Figure 4.5 Knockdown of *Bmi1* or *Cav1* does not suppress MCMV replication *in vitro*.
(A) The levels of *Bmi1* and *Cav1* mRNAs determined by qRT-PCR and **(B)** the protein expression examined by Western blot analysis. NIH 3T3 cells were untreated or transfected with 25 nM RISC-free siRNAs, *Bmi1* siRNAs or *Cav1* siRNAs for 48 h. **(A)** *Bmi1* and *Cav1* levels were normalised to *Gapdh*. Data are presented as means of fold-change (±SD) from three technical replicates relative to RISC-free siRNA transfection. Significance was assessed by two-way ANOVA (****P<0.0001). **(B)** Western blot analysis (ECL-based detection) of BMI1 and CAV1. Proteins were quantified using ImageStudioLite software and normalised to GAPDH or β-actin as indicated. Results are shown as fold change in protein relative to RISC-free siRNA transfection. **(C)** Cell viability analysis of NIH 3T3 cells transfected with RISC-free siRNAs, eGFP siRNAs, miR-542 mimics, *Bmi1* siRNAs or *Cav1* siRNAs for 48 h. Results are presented as means of fold change (±SD) of three technical replicates relative to untreated cells. **(D)** MCMV viral growth curves. NIH 3T3 cells were untreated or transfected with indicated siRNAs or miRNAs for 48 h prior to infection with GFP-MCMV at MOI of 0.2. The fluorescent signal is presented as means (±SD) of five technical replicates.

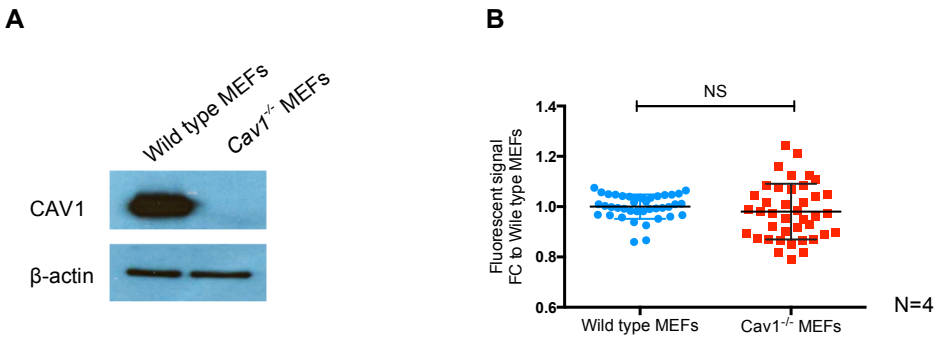

Figure 4.6 MCMV growth in *Cav1*$^{-/-}$ mouse embryonic fibroblasts (MEFs).
(A) Western blot analysis (ECL-based detection) showing the absence of CAV1 protein in *Cav1*$^{-/-}$ MEFs. **(B)** The fluorescent signal of GFP-MCMV in wild type MEFs or *Cav1*$^{-/-}$ MEFs. Cells were seeded at a density of $1.5x10^4$/well in a 96-well plate for 24 h prior to infection with the GFP reporter virus at MOI of 0.2. At 70 hpi, the fluorescent signal was measured. Each dot represents individual replicate from four independent experiments. The fluorescent data in *Cav1*$^{-/-}$ MEFs are presented as fold changes relative to wild type MEFs. Significance was assessed by unpaired t test (*P<0.05).

4.3.6 Analysis of the cell cycle in *Bmi1* or *Cav1* knockdown

The present study has shown that miR-27 overexpression accelerates the G1/S transition, suggesting the role of miR-27 in regulation of the cell cycle. Although, the functional analysis of direct targets of miR-27, *Bmi1* and *Cav1*, on MCMV growth revealed that they do not impact viral replication, it is interesting to determine whether these targets could explain the function of miR-27 in promoting the G1/S transition. From the literature, *Bmi1* has been shown to be involved in progression of G1 to S phase, while *Cav1* is proposed as a negative regulator that arrests cells in G0/G1 when it is overexpressed. *Bmi1* has been identified as an oncogene suppressing the transcription of $p16^{Ink4a}$ and $p19^{Arf}$, negative regulators of the cell cycle. A study of *Bmi1*-deficient mouse embryonic fibroblasts demonstrated that cells failed to progress into S phase of the cell cycle (Jacobs et al., 1999). Moreover, knockdown of *Bmi1* using short hairpin RNAs (shRNAs) in HeLa cells led to G1 arrest and cells in S phase decreased from 27.17% to 19.21% (Chen et al., 2011).

In contrast, *Cav1* arrests the cell cycle at G0/G1 through a p53/p21-dependent pathway (Galbiati et al., 2001). A study revealed that in endothelial cells, overexpression of *Cav1* arrested cells in G0/G1 by preventing downregulation of

cyclin-dependent kinase inhibitor p27 ($p27^{kip1}$) and Rb phosphorylation (Fang et al., 2007). Given that miR-27 is a positive regulator of the cell cycle, particularly at G1/S transition, it was hypothesised that miR-27 stimulates the cell cycle through regulation of *Cav1*, leading to the release of cells from G1 to S phase. To address whether *Bmi1* or *Cav1* affect the cell cycle in NIH 3T3 cells, cell cycle analysis was carried out in cells transfected with *Bmi1* or *Cav1* siRNAs. NIH 3T3 cells were untreated or transfected with RISC-free siRNAs, miR-27 mimics, miR-27 inhibitors, *Bmi1* siRNAs or *Cav1* siRNAs for 24 h. Due to the partial knockdown of CAV1 protein shown above, cells isolated from *Cav1*$^{-/-}$ should be more suitable cells to examine function of CAV1 rather than cells transfected with siRNAs; however such an experiment has not been conducted due to time constrain of the PhD project. Following transfection, cells were serum-starved using media containing 0.5% serum for 24 h prior to reactivation with media containing 10% serum. Cells were collected at indicated time points post serum-reactivation as described above (Fig 4.7A). Consistent with the previous results shown in Fig 4.1B, miR-27 mimics induced the S phase population to 84.22% at 14 h and 58.73% at 16 h, whereas RISC-free siRNAs showed 78.85% of S phase cells at 14 h and 39.98% at 16 h (Fig 4.7B). As expected, miR-27 inhibitors reduced cells in S phase as 70.67% at 14 h.

Similar to miR-27 inhibitor treatment, *Bmi1* knockdown cells showed G1 arrest and the reduction of cell numbers in S phase at 12 and 14 h (Fig 4.7B). Likewise, knockdown of *Cav1* displayed G1 arrest and delayed S phase entry at 12 and 14 h. The knockdown of *Cav1* there did not promote the G1/S transition but rather caused arrest. Altogether, these data indicate that the knockdown of *Bmi1* or *Cav1* did not lead to the stimulation of the G1/S transition and rather resulted in G1 arrest. Thus, *Bmi1* or *Cav1* are unlikely to be involved in miR-27-induced G1/S transition but they do appear to influence the cell cycle in regulating the progression of cells from G1 to S phase.

A

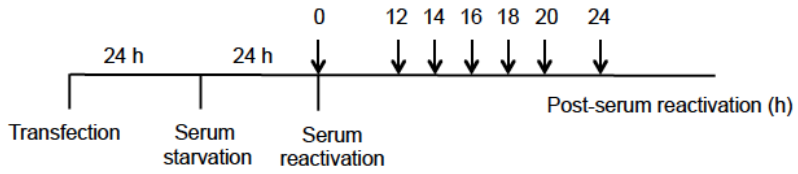

B

12 h post serum reactivation

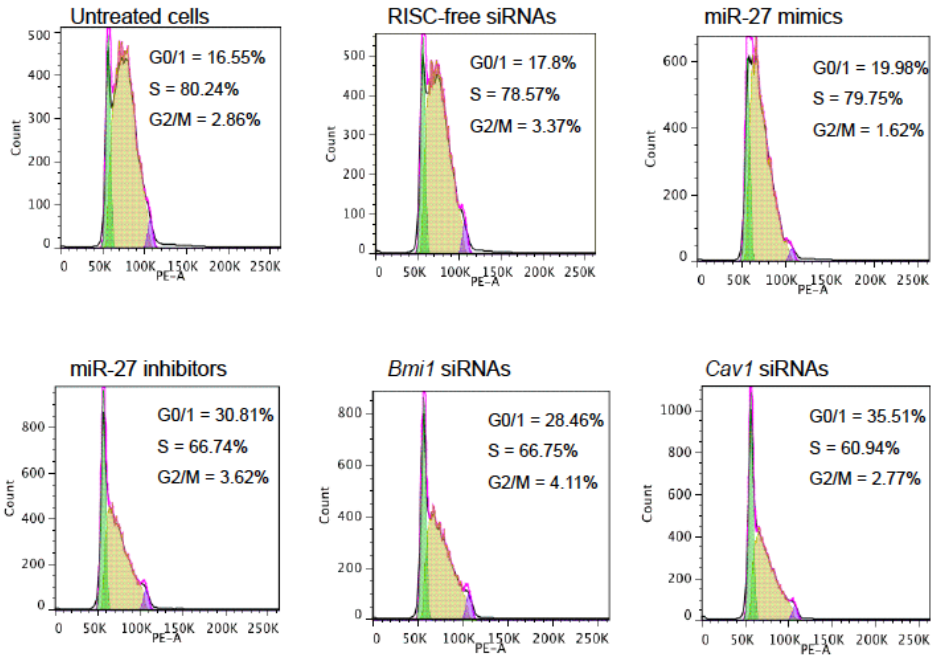

14 h post serum reactivation

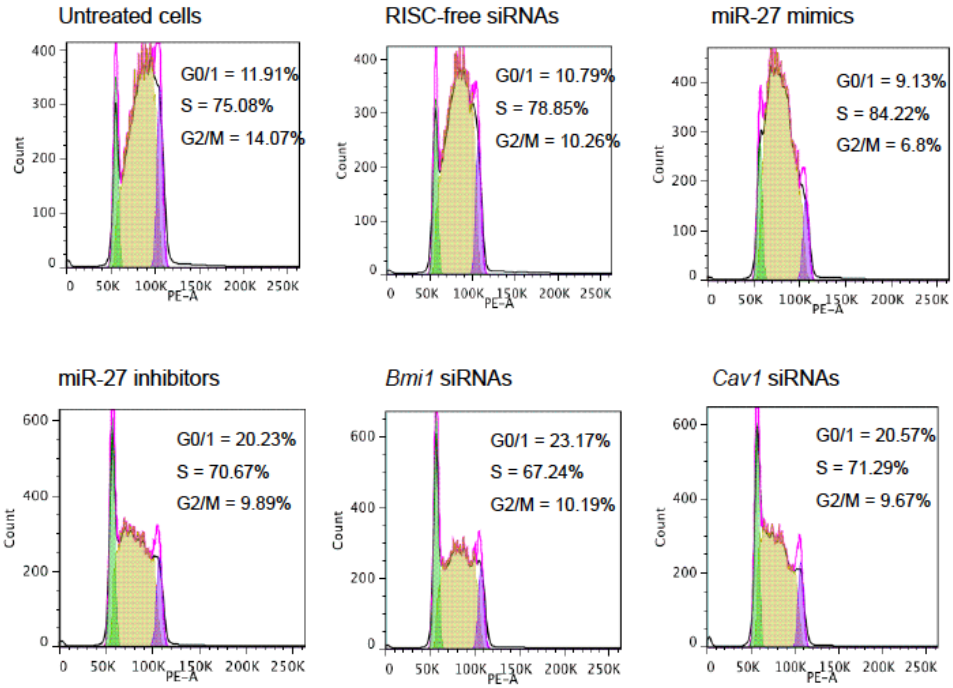

16 h post serum reactivation

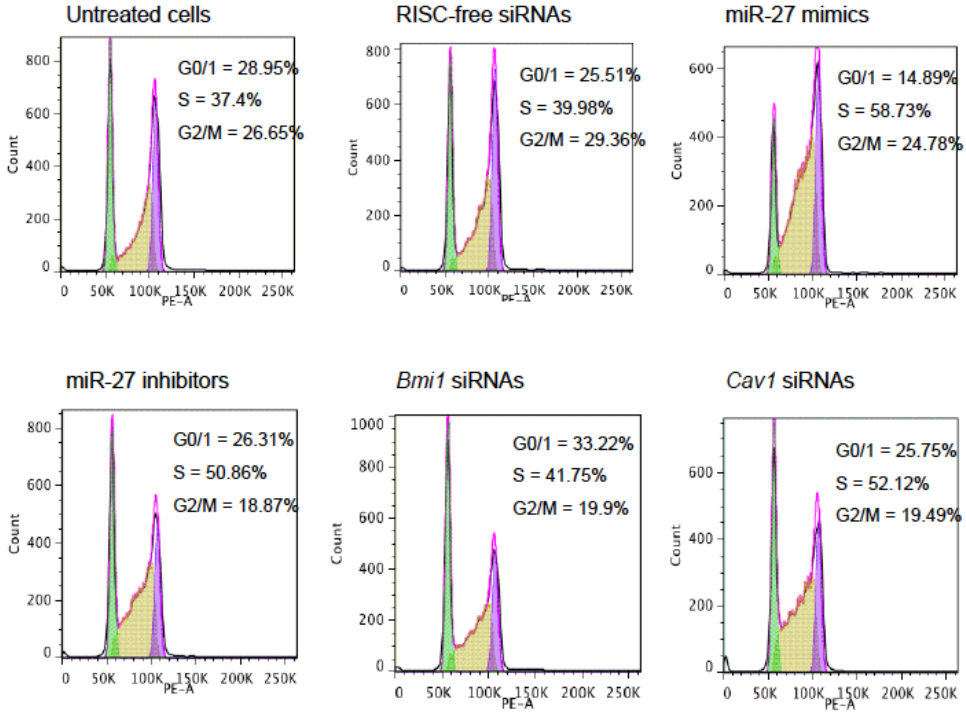

18 h post serum reactivation

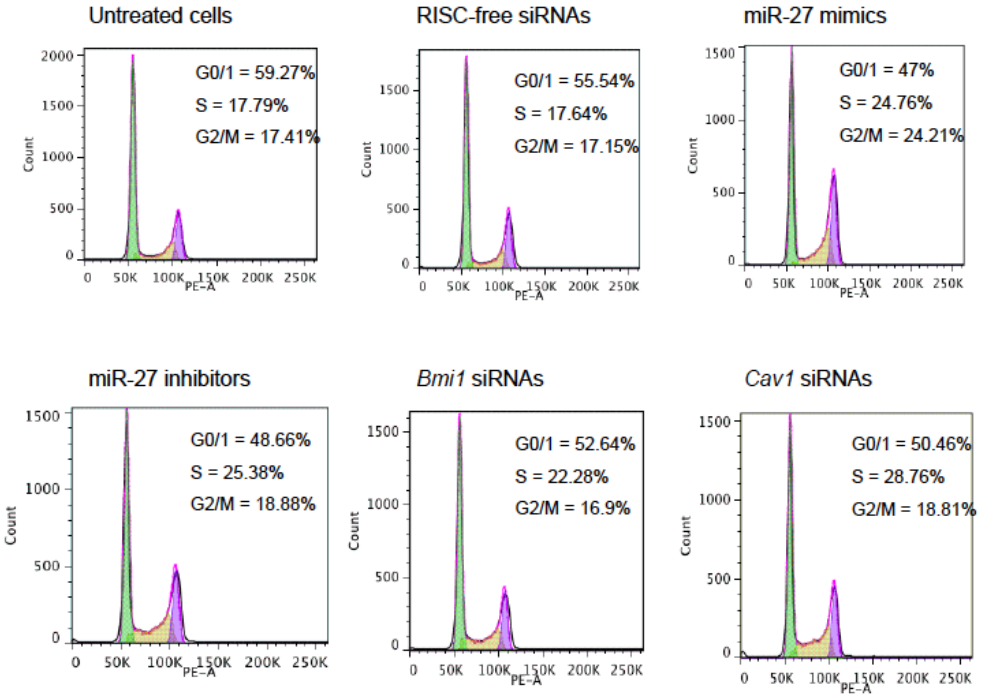

20 h post serum reactivation

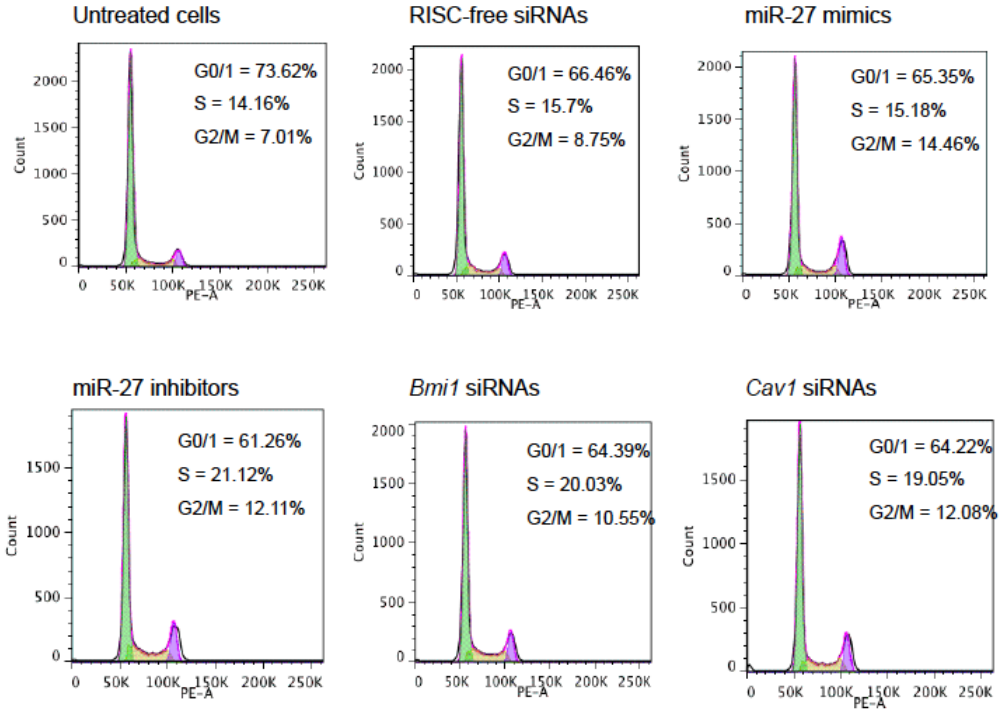

24 h post serum reactivation

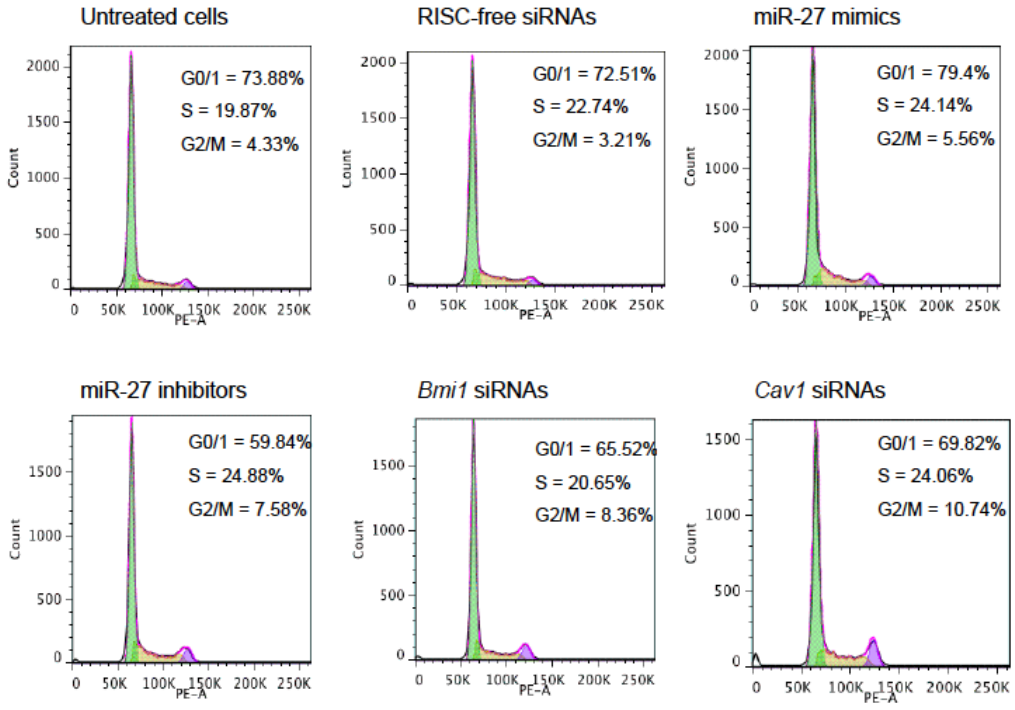

Figure 4.7 *Bmi1* and *Cav1* are not involved in miR-27-induced G1/S transition.
(A) Experimental design for cell cycle analysis of cells transfected with siRNAs as described in Fig 4.1. **(B)** Histograms display the DNA content plotted against cell numbers. The green peak represents G0/G1 cells and the pink peak indicates G2/M cells. Results are representatives of two independent experiments. Data were analysed using FlowJo software.

4.4 Discussion

The present chapter shows that overexpression of miR-27 promotes the G1/S transition of the cell cycle, whereas inhibition of this miRNA leads to a delay of this transition. In agreement with this, overexpression of miR-27 in cells transfected with pre-miR−27 increased the number of cells in S phase to ~55% compared to cells transfected with pre-miR-control (~40%), with a concomitant reduction in G1 population to ~20% compared to the control (~25%) (Lerner et al., 2011). The increase of S phase population upon miR-27 overexpression was a result of elevation of cyclin E, which is a regulatory protein of G1/S transition. miR-27 rescued cyclin E by regulating *Fbw7*, the substrate recognition component of an ubiquitin ligase complex SCF that mediates turnover of cyclin E (Lerner et al., 2011). In line with this, the present chapter showed that the overexpression of miR-27 resulted in an increase of cyclin D3, a key regulator of G1/S progression in addition to cyclin E (Masamha and Benbrook, 2009).

The inhibition of miR-27 using miR-27 inhibitors significantly arrested cells in G0/G1 and led to reduction in the number of cells in S phase. In support of this, others have shown that the inhibition of miR-27 using antisense miR-27 led to a decrease in percentage of cells in S phase, in two different cell types: breast cancer cells and hepatic stellate cells (Ji et al., 2009; Mertens-Talcott et al., 2007). In breast cancer cells, the transfection of antisense miR-27 significantly reduced the percentage of cells in S phase from 30% to 20% as compared to the control (Mertens-Talcott et al., 2007). Ji *et al.* have used BrdU incorporation assays to show relative quantification of cells in S phase. They showed that the inhibition of miR-27 in hepatic stellate cells resulted in a significant reduction of cells in S phase compared to control cells (Ji et al., 2009). Taken together, data presented in this chapter and several independent lines of evidence underscore the role of miR-27 in promoting cell cycle progression from G1 to S phase. Given that miR-27 is involved

in regulation of the cell cycle particularly at the G1/S transition, it is interesting to examine the expression of miR-27 whether it is cell-cycle dependent. Indeed, Lerner *et al*. have determined expression of miR-27 during the cell cycle and mentioned without showing data that changes in miR-27 levels were not significant; however, the authors were able to detect changes of the miR-27 target, *Fbw7* during the cell cycle progression (Lerner et al., 2011), suggesting that the fluctuation of miR-27 expression might be minimal. In addition, miR-27 functions might depend on additional factors, such as RNA-binding proteins, in regulation of *Fbw7* (Lerner et al., 2011).

In addition to its documented functions in regulating the cell cycle, miR-27 has also been identified as an oncogenic miRNA that promotes cell proliferation. Overexpression of miR-27 occurs in various kinds of cancer cells (Guttilla and White, 2009; Liu et al., 2009; Ma et al., 2010; Mertens-Talcott et al., 2007; Prueitt et al., 2008). Since cell proliferation is regulated by the cell cycle (Golias et al., 2004), this may link the positive regulatory function of miR-27 in the cell cycle shown in the present study to its oncogenic property in cell proliferation.

Based on the positive regulatory effect of miR-27 on the G1/S transition, it was further examined whether miR-27 exerts this function through direct regulation of *Bmi1, Calm3, Cav1* or *Ccng1*. These genes have been shown to have a role in the cell cycle (see section 4.3.3) and were identified in chapter 3 as genes regulated by miR-27. Initially, the determination of mRNA and protein expression was carried out in cells transfected with miR-27 mimics or miR-27 inhibitors. Although there was no significant alteration of *Bmi1* and *Cav1* mRNAs under these conditions, BMI1 and CAV1 proteins were downregulated (~2 fold) in cells transfected with miR-27 mimics compared to RISC-free siRNAs. This demonstrates that monitoring mRNA abundance might miss out some of the effects of miR-27 on its target genes. Further, the luciferase reporter assays confirmed that *Bmi1* and *Cav1* are direct targets of miR-27.

Polycomb ring finger oncogene 1 (BMI1) belongs to the polycomb group proteins comprising a set of proteins that form into chromatin-associated complexes that

suppress gene transcription (reviewed in (Sauvageau and Sauvageau, 2010). *Bmi1* has been identified as an oncogene regulating the G1/S transition by suppressing the transcription of negative regulators: $p16^{Ink4a}$ and $p19^{Arf}$ (Jacobs et al., 1999). The deficiency of *Bmi1* in knockout mice and the knockdown of *Bmi1* using shRNAs caused G1 arrest in several cell types (Chen et al., 2011; Jacobs et al., 1999; Wu et al., 2011). In line with previous findings, the present study shows that knockdown of *Bmi1* using siRNAs resulted in G1 arrest and the reduction of cells in S phase at 12 and 14 h post serum reactivation. Based on the observation that the knockdown of *Bmi1* resulted in G1 arrest, it is unlikely that the miR-27-promoted G1/S transition is mediated through regulation of *Bmi1* by miR-27.

Caveolin-1 (CAV1) is a component of the caveolae plasma membrane protein. In mammals, three caveolins (CAV1-3) have been identified (Okamoto et al., 1998). CAV1 and CAV2 express as hetero-oligomers in many cell types (Scherer et al., 1997), while CAV3 is muscle-specific (Song et al., 1996). Interestingly, CAV1 has previously been shown to be involved in the G0/G1 arrest. Specifically, the overexpression of *Cav1* in NIH 3T3 cells caused cell cycle arrest in the G0/G1 phase via a p53/p21-dependent pathway (Galbiati et al., 2001). The authors used MEFs derived from *Cav1* transgenic mice overexpressing *Cav1* to confirm the effect. As expected, they found that MEFs derived from the transgenic mice showed an increase in the G0/G1 population and a significant reduction in the number of cells in S phase compared to wild type MEFs (Galbiati et al., 2001). In line with this, the other study in human endothelial cells showed that overexpression of *Cav1* induces G0/G1 arrest whereby it prevents the downregulation of the cyclin-dependent kinase inhibitor $p27^{kip1}$ and Rb phosphorylation, resulting in the accumulation of cells in G0/G1 (Fang et al., 2007). The previous data therefore would suggest that *Cav1* negatively modulates the cell cycle by arresting cells in G0/G1; thus, knockdown of *Cav1* in this study was expected to attenuate the arrest and induce cells from G0/G1 to S phase. However the work presented here demonstrates that knockdown of *Cav1* using siRNAs results in G0/G1 arrest. It is important to note, however, that the knockdown of *Cav1* using siRNAs resulted in only ~50% reduction of the protein. It is expected that the incomplete knockdown of the protein could relate to a long half-

life of the protein (Hayer et al., 2010). In addition, it was reported that CAV1 protein was upregulated after 24 h serum starvation and remained at a high level at 8 h post serum reactivation, resulting in G1 arrest (Galbiati et al., 2001). In the present study, cells in which *Cav1* was knocked down were serum-starved for 24 h. It is therefore possible that CAV1 protein is induced under these conditions and the elevation of CAV1 may interfere with the knockdown attempts using siRNAs. Thus, it is difficult to draw a conclusion of *Cav1* functions in the cell cycle due to partial knockdown of the protein. Future studies using cells isolated from *Cav1*$^{-/-}$ mice would provide a better model to investigate the function of *Cav1* in the cell cycle.

In the context of MCMV infection, the present study showed that *Bmi1* and *Cav1* do not affect viral replication based on the reporter assay. Indeed, no evidence has been reported whether *Bmi1* or *Cav1* are involved in CMV-modulated cell cycle, although it has been shown that the virus modulates a number of genes in this pathway (Hertel and Mocarski, 2004). To date, studies have shown controversial effects of HCMV on the cell cycle, with some studies suggesting the virus causes arrest and others suggesting the virus causes progression of G1 to S phase. In case of the cell cycle arrest, several studies have shown that HCMV blocked the G1/S phase transition (reviewed in (Flemington, 2001)). The tegument protein UL69 of HCMV was found to be responsible for G1 arrest and the virus lacking UL69 gene displayed a growth defect relative to wild type virus, suggesting the significance of HCMV-induced cell cycle arrest to the viral infection (Hayashi et al., 2000; Lu and Shenk, 1999). In addition, independent studies have shown that IE86 protein of HCMV induced the cell cycle arrest in G1 coincided with a decrease in cell proliferation (Noris et al., 2002; Wiebusch and Hagemeier, 1999). CMV is a large DNA virus that encodes the viral DNA polymerase and other essential viral factors allowing the virus to synthesise viral DNA independently from S phase of host cells (reviewed in (Flemington, 2001)). Therefore, it was proposed that the virus arrests cells to avoid competing with cellular DNA synthesis during S phase in order to use cellular products for its replication.

On the other hand, it has also been reported that HCMV elicits the cell cycle progression in certain systems. Using adenovirus expressing IE86 protein, Murphy *et*

al. found a significant increase in the number of cells in S phase which is contradictory to the previous evidence showing the cell cycle arrest activity of IE86 (Murphy et al., 2000). The authors conducted cell cycle analysis at 48 h after serum stimulation, whereas the previous study by (Wiebusch and Hagemeier, 1999) was carried out at 24 h. Murphy *et al*. then speculated that the different time point after serum stimulation is an issue that gives rise to the opposite data as 48 h serum stimulation allows cells more time to recover from starvation and progress through the cell cycle including the progression from G1 to S phase (Murphy et al., 2000). The inconsistent data could be due to differences of cellular genetic background that should be taken into consideration. For example, in terminally differentiated cells (where cells are irreversibly withdrawn from the cell cycle and are arrested in G0), HCMV appeared to induce cell cycle progression through G1 to early S phase, possibly via the interaction between IE86 and the cyclin-dependent kinase inhibitor $p21^{Cip1}$ (Sinclair et al., 2000).

The effects of HCMV on the cell cycle are still a matter of debate. In the case of MCMV, it was demonstrated that the virus blocks cell cycle progression from G1 to S phase based on the cell cycle arrest ability of IE3, the homologue of HCMV IE2 (Wiebusch et al., 2008). The authors showed that the transient expression of IE3 resulted in 67% of cells in G1 phase compared to 48% of cells in G1 of the negative control (Wiebusch et al., 2008). This indicates that the virus may actively seek to keep cells in the G1 phase. Thus, it is logical to speculate that miR-27 might be targeted by the virus to inhibit the G1/S transition, consistent with the data shown here using miR-27-inhibitors.

Although the present study could not identify cellular targets of miR-27 responsible for its regulating of the G1/S transition, these results provide a starting point for further investigations of miR-27 functions in the cell cycle, specifically in the context of MCMV infection. Based on the effect of miR-27 that was particularly observed at the G1/S transition, identification of miR-27 targets at this certain point would provide a list of regulated genes contributing to this effect. To specifically explore those genes important for the G1/S transition, future work may involve

transcriptomic or proteomic analysis of miR-27 overexpression following by inducing the progression of cells from G1 to S phase.

In conclusion, the results from this chapter support a role of miR-27 in promoting the G1/S transition, in line with the literature. However, this effect did not appear to involve *Bmi1* or *Cav1*, which were validated as direct targets of miR-27 using luciferase reporter assays. Further work to identify miR-27 targets underpinning its impact on the cell cycle would provide a better understanding of miR-27-induced G1/S transition. In the context of MCMV infection, it appeared that *Bmi1* and *Cav1* do not play a role in the replication of MCMV *in vitro*.

Chapter 5: Identification of miR-27 targets using cross-linking, ligation and sequencing of hybrids (CLASH)

5.1 Introduction

The primary aim of this thesis is to identify cellular targets of miR-27 that play a role in MCMV replication. In chapter 3, microarray analysis was conducted to determine mRNA expression changes upon miR-27 overexpression or MCMV infection. However, this technique is unable to distinguish between direct and indirect effects of miR-27. To address this point, the objective of this chapter is to utilise a biochemical technique called "cross-linking, ligation and sequencing of hybrids (CLASH)" to experimentally identify a comprehensive profile of direct targets of miR-27.

miRNAs have been found to function as key regulators of gene expression in a diverse range of species from nematodes, flies, plants and vertebrates to humans (reviewed in (Bartel, 2004; He and Hannon, 2004)). In humans, ~60% of protein-coding genes are predicted to contain at least one conserved miRNA-binding site in vertebrates (Friedman et al., 2009). The miRNA binding sites are generally found in the 3'UTRs of mRNAs and the recognition is largely thought to be mediated by perfect complementarity to the seed sequence of miRNAs, which is the position 2 to 8 from the 5'end (reviewed in (Hausser and Zavolan, 2014)). Binding sites in mRNAs that are based on complementarity to the seed sequences are called "canonical sites". Beyond canonical seed matches, bioinformatic analysis of high-throughput data revealed that there are non-canonical binding sites containing G-U pairs, bulged or mismatched nucleotides. The regulation of transcripts via non-canonical sites was demonstrated to cause average or more modest effects compared to canonical sites; however, it is still unclear whether non-canonical sites have functions other than mRNA repression. (reviewed in (Hausser and Zavolan, 2014)).

Identifying miRNA targets and their biological functions is an area of intense investigation involving both computational predictions and experimental methods

(reviewed in (Hausser and Zavolan, 2014; Thomson et al., 2011)). Although many computational approaches for target prediction are available, the false positive rate remains very high (24-70%) (reviewed in (Thomson et al., 2011). Other factors that contribute to false positives relate to parameters such as RNA structures and RNA-binding proteins that might affect accessibility of binding sites (Ameres et al., 2007; Kedde and Agami, 2008). Since target prediction algorithms are generally based on rules for canonical sites within mRNAs, these often also miss non-canonical sites (Min and Yoon, 2010). This highlights the requirement of experimental approaches to identify and validate direct target sites, including novel non-canonical binding sites. Ideally, this experimental data would then be used to improve prediction programs.

Different experimental approach can be used to identify targets of miRNAs, including analysis of the effect of miRNAs levels on global mRNA or protein expression following overexpression or inhibition of the miRNAs (reviewed in (Hausser and Zavolan, 2014)). Changes in mRNA levels can be measured using microarray analysis or RNA sequencing. The effect of miRNAs on protein levels can be determined using mass spectrometry-based experimental techniques such as SILAC (stable isotope labelling by amino acids in cell culture). In this technique, cells are grown in a media containing labelled amino acids that will be incorporated into newly synthesised proteins and the proteins containing labelled amino acids are then quantified through the isotope signal. Combined methods of ribosomal profiling and measurements of mRNA expression have also provided deeper insights into the effects of miRNAs on rates of translation (Guo et al., 2010). Ribosomal profiling involves deep sequencing of ribosome protected mRNA fragments, allowing determination of which mRNAs are being actively translated into proteins. Thus, comparison of ribosomal profiling to mRNA levels can be used to correlate the effect of miRNAs on transcription versus translation. However, these methods do not globally distinguish direct from indirect effects of the miRNA since they do not provide information on the miRNA-target interaction site.

A common method to identify direct targets of miRNAs is immunoprecipitation of the AGO protein followed by microarray analysis or deep sequencing to identify

AGO-bound RNAs (reviewed in (Hausser and Zavolan, 2014)). Further, a crosslinking step has been introduced to crosslink RNAs to the AGO protein prior to immunoprecipitation, termed "AGO-cross linking and immunoprecipitation (CLIP)" (Ule et al., 2003). Data obtained from sequencing are mapped back to the genome or transciptome to identify the specific miRNA binding sites on mRNAs. Several modifications of the CLIP method have been developed such as high-throughput sequencing of RNA isolated by CLIP (HITS-CLIP), photoactivatable-ribonucleoside-enhanced CLIP (PAR-CLIP) in which cells are fed with a photo-activatable 4-thiouridine (4-TU) before cross-linking, and individual-nucleotide resolution CLIP (iCLIP) (reviewed in (Hausser and Zavolan, 2014)). Although CLIP techniques identify the small RNAs associated with AGOs and the location of binding sites in mRNAs, computational analyses have still been required to predict the exact interactions that occur. To overcome this issue, a modification of this type of immunoprecipitation protocol was developed. The CLASH technique uses an additional step of RNA-RNA ligation to join miRNAs and target mRNAs prior to sequencing thereby defining the both binding partners and the location of interaction (Helwak et al., 2013; Helwak and Tollervey, 2014). This technique also varies from CLIP in that it is carried out with a double affinity tagged version of AGO (Fig 5.1), allowing stringent purification of protein-RNA complexes under denaturing condition in order to reduce background (Helwak and Tollervey, 2014). The development of CLASH opens up an exciting avenue to explore direct targets of miRNAs in a high-throughput manner.

In the original CLASH paper, it was done with AGO1. This thesis however focuses on AGO2 based on its slicer activity and biological significance in mouse development as described below. AGO1-4 are found in human and mouse. These four AGOs are thought to share redundant function in the miRNA pathway (Su et al., 2009); however, only AGO2 has been shown to have slicer activity responsible for cleavage of target mRNAs that have near perfect complementarity to miRNAs, although it occurs much less frequently in mammals than in plants (Bracken et al., 2011; Karginov et al., 2010; Shin et al., 2010). In addition, a study in *Ago2*$^{-/-}$ mice demonstrated that the ablation of *Ago2* leads to embryonic lethality, while other

AGO proteins are dispensable, suggesting a role of AGO2 in mammalian development (Liu et al., 2004).

In the present chapter, a NIH 3T3-PTH-mAGO2 stable cell line expressing tagged-mAGO2 was generated. The expression levels of miR-27 and the growth of MCMV were both examined in NIH 3T3-PTH-mAGO2 cells compared to NIH 3T3 cells to ensure that overexpression of this protein did not impact viral growth or virus-mediated miR-27 degradation. Finally, the CLASH protocol was carried out to generate initial datasets for the direct interactions of miR-27 targets.

5.2 Aims

The aims of the present chapter are to:

1. Establish the NIH 3T3-PTH-mAGO2 stable cell line to allow CLASH in cells permissive to MCMV
2. Evaluate whether the stable cell line is suitable for identification of miR-27 targets during infection
3. Generate datasets of direct targets of miR-27 in the context of MCMV infection using CLASH technique

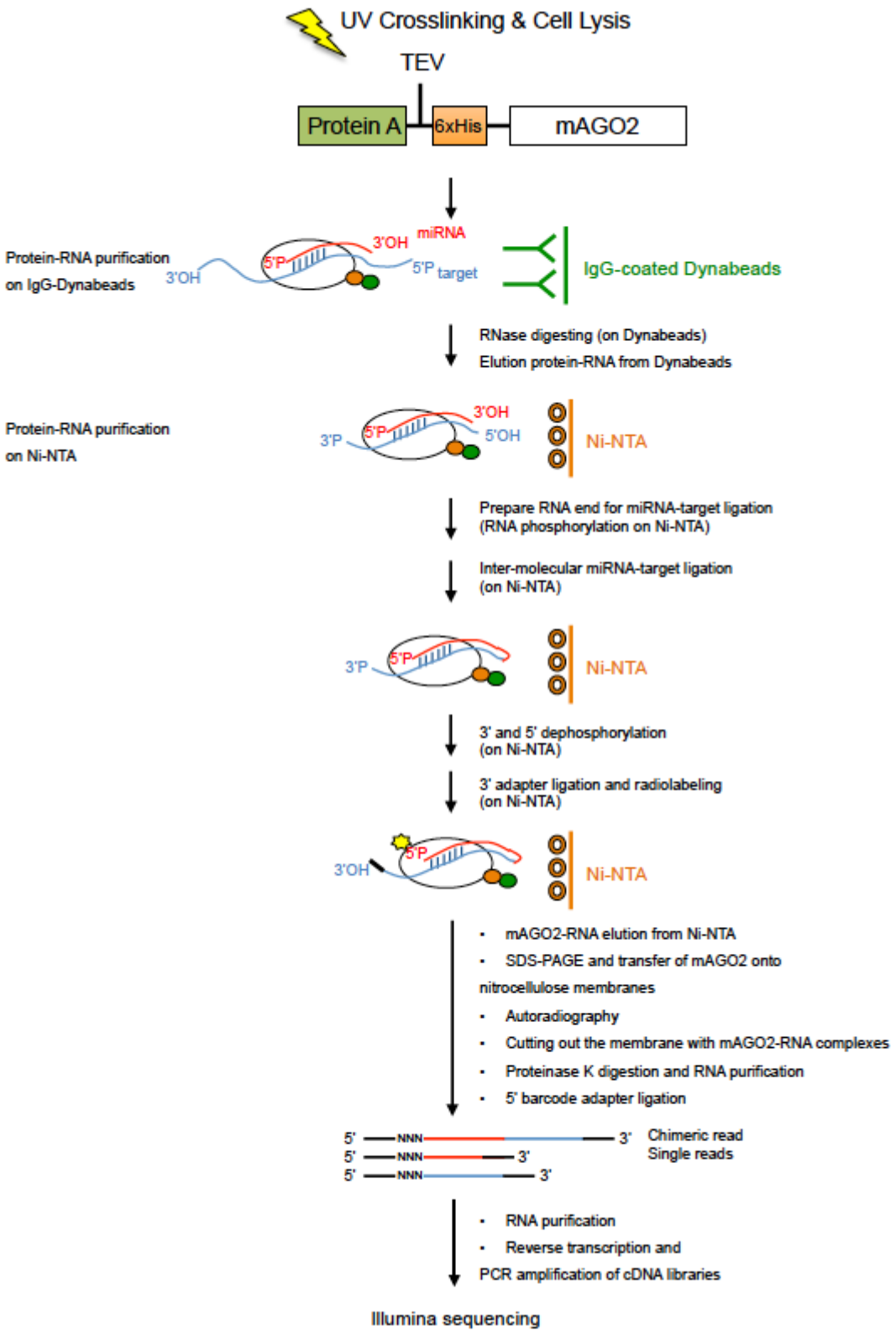

Figure 5.1 Overview of CLASH protocol (adapted from (Helwak and Tollervey, 2014)).

5.3 Results

5.3.1 Generation of the NIH 3T3-PTH-mAGO2 stable cell line expressing PTH-mAGO2 by lentiviral transduction

To generate lentiviruses expressing PTH-mAGO2, the transfer vector pLVX-CAG-PTH-mAGO2 containing PTH-mAGO2 was generated. The vector containing CAG promoter was chosen based on the ability of the promoter to highly drive expression of genes (Alexopoulou et al., 2008). The PTH-mAGO2 insert was amplified from pCDNA3-PTH-mAGO2 using primers containing XhoI and NotI restriction sites. The PCR product was then digested using XhoI and NotI restriction enzyme, gel purified and cloned into pLVX-CAG. The expression of the tagged-protein was examined. NIH 3T3 cells were untreated or transfected with pLVX-CAG-PTH-mAGO2 for 48 h. Protein samples were collected and analysed by Western blot using the antibody specific to the protein A. As shown in Fig 5.2A, cells transfected with pLVX-CAG-PTH-mAGO2 highly expressed PTH-mAGO2, whereas the tagged-protein was absent in untreated cells. The positive control is the protein lysate obtained from Flp-In T-REx 293 cells (HEK293-PTH-hAGO2 cells) expressing PTH-human AGO2.

Next, the verified pLVX-CAG-PTH-mAGO2 was used to produce lentiviruses. This vector expressing the tagged-mAGO2 was co-transfected into HEK293T cells with pMD2.G-VSV-G (envelope plasmid) and psPAX2 (packaging plasmid) to generate lentiviral particles. The viral supernatant was concentrated approximately 100 fold by ultracentrifugation (see section 2.11.3 of materials and methods). To generate the stable cell line, NIH 3T3 cells were untreated or transduced with various volumes of the concentrated viral supernatant (12 µl, 24 µl or 48 µl) to determine the optimum amount of virus for the transduction. Cells were maintained in the media containing puromycin for 7 days to positively select transduced cells. Protein samples were collected to evaluate the expression of PTH-mAGO2 by Western blot analysis using the antibody specific to the protein A tag. As shown in Fig 5.2B, cells treated with all three volumes of lentiviral supernatant expressed PTH-mAGO2 at comparable levels, whereas no tagged-AGO was observed in untreated cells. HEK293-PTH-hAGO2 cells expressing PTH-humanAGO2 were used as the positive control. These

results indicate that the NIH 3T3-PTH-mAGO2 cell line expressing tagged-mAGO2 was successfully generated.

To compare the protein expression levels of the tagged-mAGO2 relative to the endogenous AGO2, cell lysates were prepared from NIH 3T3-PTH-mAGO2 and the parental NIH 3T3 cells. Western blot analysis using an antibody specific to mAGO2 was carried out. As expected, total mAGO2 (tagged-mAGO2 and endogenous mAGO2) from NIH 3T3-PTH-mAGO2 cells was dramatically higher than endogenous protein expressed in wild type NIH 3T3 cells (Fig 5.2C).

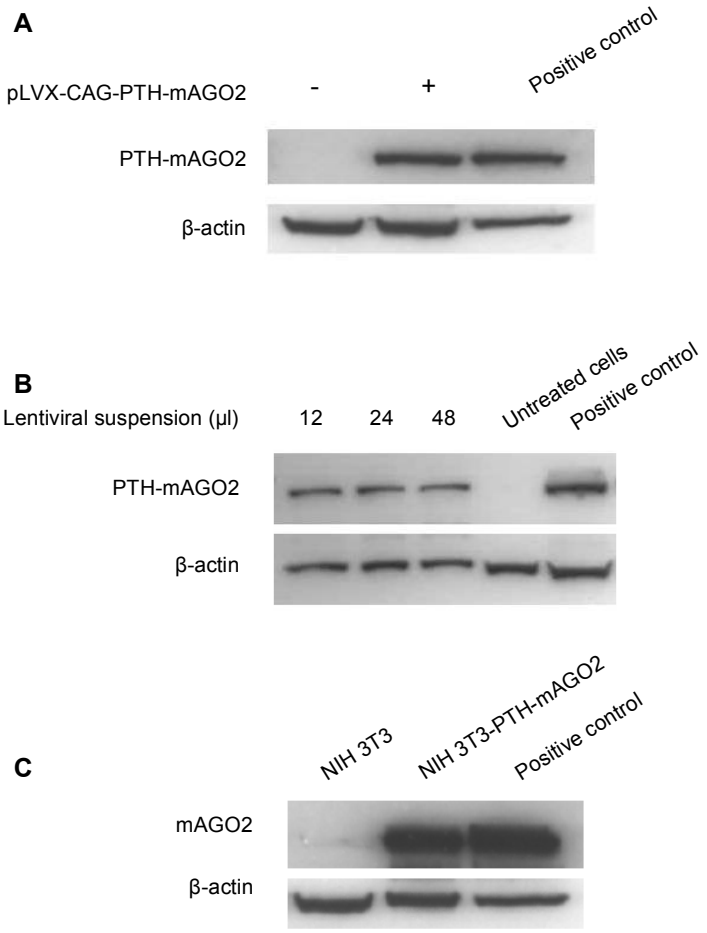

Figure 5.2 Expression of PTH-mAGO2 in cells transfected with pLVX-CAG-PTH-mAGO2 and the NIH 3T3-PTH-mAGO2 stable cell line, and comparison of total mAGO2 between NIH 3T3-PTH-mAGO2 and NIH 3T3 cells
(A) NIH 3T3 cells were untreated or transfected with 1.5 µg pLVX-CAG-PTH-mAGO2 for 48 h. 50 µg of total protein was loaded onto 12% SDS-PAGE gels from untreated cells (-), transfected cells (+) and the positive control, which is extract from HEK293-PTH-hAGO2 cells expressing PTH-human AGO2 protein. Western blot analysis (ECL-based detection) was carried out using peroxidase anti-peroxidase soluble complex antibody (PAP) (Sigma, P1291) specific to protein A within PTH tag with β-actin as the loading control. **(B)** Expression of PTH-mAGO2 protein obtained from cells treated with lentiviruses after 18 h. NIH 3T3 cells were untreated or transduced with various volumes of lentiviruses (12, 24 or 48 µl). Cells were collected and the expression of PTH-mAGO2 was determined by Western blot analysis (ECL-based detection) using the PAP antibody specific to protein A. The positive control is protein lysate from HEK293-PTH-hAGO2 cells. **(C)** Comparison of total mAGO2 (tagged-mAGO2 and endogenous mAGO2) from NIH 3T3-PTH-mAGO2 cells and endogenous mAGO2 from wild type NIH 3T3 cells. Western blot analysis (ECL-based detection) was performed using the antibody specific to both mAGO2 and hAGO2 (Cell signalling, 2897). The positive control is protein lysate from HEK293-PTH-hAGO2 cells.

5.3.2 Expression levels of miR-27 and m169 in NIH 3T3-PTH-mAGO2 cells and wild type NIH 3T3 cells

The purpose of generating the NIH 3T3-PTH-mAGO2 cells overexpressing PTH-mAGO2 was to generate a CLASH dataset utilising the double affinity purification procedure to ultimately directly identify targets of miR-27. One consideration in this experimental design is whether overexpression of AGO2 will have other effects on the cell or infection that would complicate results. For example, in addition to its fundamental role in gene silencing within RISC, AGO2 can also play a role in RISC maturation since it cleaves the passenger strand of perfect or nearly perfect miRNA duplexes (reviewed in (Czech and Hannon, 2011)). The cleaved strand then dissociates from the RISC, yielding the mature AGO2-RISC. Moreover, AGO2 was shown to impact the stability of miRNAs as *Ago2* knockout MEFs showed >80% reduction in levels of multiple endogenous guide strands compared to wild type cells (Winter and Diederichs, 2011). Since AGO2 is involved in miRNA biogenesis and stability, the impact of overexpression of PTH-mAGO2 on miR-27 levels in the NIH 3T3-PTH-mAGO2 cell line was examined. As introduced previously, MCMV encodes a non-coding RNA, m169, that mediates miR-27 degradation (Libri et al., 2012; Marcinowski et al., 2012). It was also therefore examined if overexpression of AGO2 affects miR-27 levels in the context of infection, to determine whether regulation of miR-27 by m169 might be altered in NIH 3T3-PTH-mAGO2 cells compared to NIH 3T3 cells.

Expression of miR-27 in NIH 3T3-PTH-mAGO2 cells was compared to NIH 3T3 cells in the presence or absence of infection. Cells were mock infected or infected with MCMV for 8 and 24 h. Total RNA was collected to determine levels of miR-27 and m169 using Northern blot analysis. In the absence of infection, miR-27 levels in NIH 3T3-PTH-mAGO2 cells were comparable to that of NIH 3T3 cells (Fig 5.3). At 8 and 24 hpi, the levels of m169 were equivalent in NIH 3T3- PTH-mAGO2 cells and NIH 3T3 cells. In addition, miR-27 was reduced upon infection to comparable levels in both cell lines. The comparable expression of miR-27 and m169 observed in the two cell lines suggested that overexpression of the tagged-AGO2 does not affect levels of miR-27 in uninfected cells or m169-mediated degradation of miR-27 during infection.

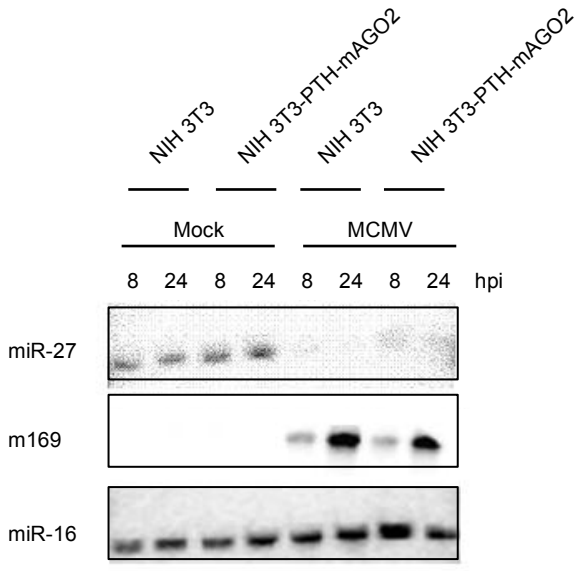

Figure 5.3 Expression levels of miR-27 and m 169 in NIH 3T3-PTH-mAGO2 cells compared to NIH 3T3 cells
Northern blot analysis of miR-27 and m169. Cells were mock infected or infected with MCMV at MOI of 5 for 8 or 24 h. 5 μg of total RNA was loaded per well and probed using oligos perfectly complementary to miR-27, m169 or miR-16 (which served as a loading control).

5.3.3 Comparison of MCMV growth in NIH-3T3-PTH-mAGO2 cells and NIH 3T3 cells

Having determined that overexpression of mAGO2 did not affect the regulation of miR-27 or the degradation of miR-27 by m169, it was further evaluated whether viral growth was the same in both cell types. NIH 3T3-PTH-mAGO2 cells or NIH 3T3 cells were infected with MCMV at MOI of 0.01 and the supernatant containing virus was collected on a daily basis for 5 days post infection. As shown in Fig 5.4, viral growth curves in NIH 3T3-PTH-mAGO2 cells and NIH 3T3 cells were similar in most of time course of infection, based on standard plaque assays. The only exception was on Day 2 where the viral growth was slightly lower (~10 fold decrease) in NIH 3T3-PTH-mAGO2 cells compared to NIH 3T3 cells. The above validation showed that overexpression of mAGO2 in NIH 3T3-PTH-mAGO2 cells does not affect viral growth, apart from a difference at 2 days post infection. It was therefore decided that the cell line was appropriate for further studies.

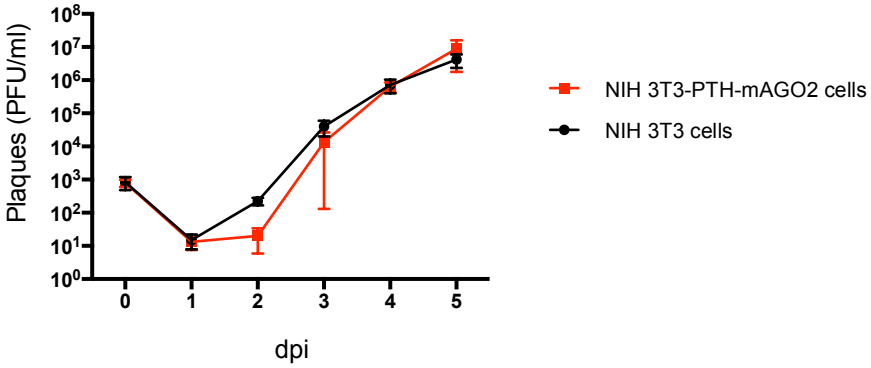

Figure 5.4 MCMV growth curves in NIH 3T3-PTH-mAGO2 cells or NIH 3T3 cells
Cells were infected with MCMV at MOI of 0.01. Supernatant was collected at indicated time points (days post infection, dpi) and viral titres determined by standard plaque assays. Results are shown as means with SD of plaque forming units (PFU)/ml from three technical replicates.

5.3.4 Identification of miRNA targets using cross-linking, ligation and sequencing of hybrids (CLASH)

In order to generate CLASH datasets, NIH 3T3-PTH-mAGO2 cells were mock infected or infected with wild type MCMV or MCMV Δm169 lacking m169 (MOI of 5) in 15 cm plates (eight plates per sample) for 24 h. A control sample from HEK293-PTH-hAGO2 cells was prepared by Katrina Gordon (Buck lab). HEK293-PTH-hAGO2 cells were used as the control based on preliminary work in the lab showing a good recovery (~30%) of protein purification using IgG-conjugated Dynabeads and ~1,500 chimeras of miRNA-mRNA sites (termed "chimeras") were obtained from libraries using this cell line (Gordon K., unpublished data).

As shown in the schematic in Fig 5.1, cells were UV-irradiated at 254 nm to stabilise protein-RNA interactions and protein lysate was collected. Unlike other CLIP-based techniques that immunoprecipitate endogenous protein, CLASH is carried out in cells expressing tagged-protein, allowing two protein purification steps under high stringency conditions. The first involves purification of PTH-mAGO2 using IgG-coated Dynabeads, which bind with high affinity to the protein A of PTH-mAGO2 followed by purification with Ni-NTA, which binds to the His tag. On the Dynabeads, the RNAs and RNA-RNA duplexes protected by AGO2 are trimmed using RNases. The protein-RNA complexes are then eluted from the Dynabeads and further purified using Ni-NTA. It should be noted that in the original design, a TEV cleavage site was introduced to allow for protease cleavage at this step; however, this was not efficient and the protocol was modified as shown in Fig 5.1 (Helwak and Tollervey, 2014).

The first checkpoint for this technique is the evaluation of the protein recovery from Dynabeads and Ni-NTA. To assess this a Western blot analysis was carried out with the input material, flow-through from the Dynabeads, material remaining on Dynabeads after protein elution (boiled Dynabeads), the elution from the Dynabeads and flow-through from Ni-NTA. As shown in Fig 5.5A, the control from HEK293-PTH-hAGO2 cells showed ~20-30% reduction in the tagged-AGO2 in the flow-through compared to the input. Following protein elution from Dynabeads, no protein was detected in the boiled Dynabeads, whereas the tagged-AGO2 protein was

present in two dilutions of the material eluted from Dynabeads: undiluted protein (Elution 1) and a 2 fold dilution of the protein (Elution 2). This suggests a moderately efficient purification with the control sample. However, tagged-AGO2 levels of the input from mock, wild type MCMV and MCMV Δm169 infection were comparable to the flow-through from Dynabeads, indicating that this initial immunoprecipitation was less efficient compared to the control. Consistent with unchanged levels of the protein between the input and the flow-through, all samples showed very low amounts of protein purified from Dynabeads ("Elution Dynabeads" in Fig 5.5A). Despite the low amount of purified protein obtained from Dynabeads in NIH 3T3-PTH-mAGO2 cells, it was decided to carry on the experiment as it is unclear the minimum amount of protein required for the success of the protocol. The protein was further captured using Ni-NTA followed by the inter-molecular ligation step, 3'adapter ligation and radioactive labelling (Fig 5.1).

The protein-RNA complexes containing radiolabelled RNAs were eluted from Ni-NTA, resolved using SDS-PAGE and transferred onto a nitrocellulose membrane. The second checkpoint of the CLASH protocol is the visualization of radiolabelled RNAs. Fig 5.5B shows an autoradiography of radiolabelled protein-RNA complexes from the control HEK 293-PTH-hAGO2 cells and the three samples from the NIH 3T3-PTH-mAGO2 cells (mock infection, cells infected with wild type MCMV or MCMV Δm169). In line with the yields of purified protein from Dynabeads, the strong signal was observed in the control showing expected size between ~110-130 kDa corresponding to AGO-miRNA or AGO-miRNA-mRNA complexes, whereas mock infection and cells infected with wild type MCMV or MCMV Δm169 showed considerably weak signal, particularly in cells infected with MCMV Δm169. The weaker radioactive signal in NIH 3T3-PTH-mAGO2 samples could be due to a number of factors, for example, less protein-RNA complexes purified or inefficient labelling of the RNA. The nitrocellulose membranes containing the protein-RNA complexes were excised, proteinase K digested and RNA extraction was carried out. After band cutting, the membrane was re-exposed using an autoradiography film to ensure that the correct bands were cut out (Fig 5.5C).

RNA extracted from each sample was then ligated with unique 5' barcoded sequencing adapters that allow for pooling of multiple samples for sequencing (Fig 5.5D). RNAs containing 5' and 3' adapters were reverse transcribed into cDNAs for generating DNA libraries by PCR amplification. Fig 5.5E illustrates the anticipated size of fragments observed in an agarose gel. The fragment of ~120 bp represents PCR primer dimers. Based on the length of miRNAs (~21-22 nt), the fragment of ~150 bp is expected to enrich for miRNAs and the PCR product in the range of ~150-200 bp is the expected size for recovery of miRNA-mRNA chimeras and mRNAs. As shown in Fig 5.5F, the predominant bands across all samples were the bands corresponding to PCR primer dimers (~120bp), whereas larger smeared bands (~150-200) were considerably weak. Based on the intensities of signals observed from the autoradiography, it was expected to obtain larger products from the control sample (HEK293-PTH-humanAGO2 cells) compared to the three samples of NIH 3T3-PTH-mAGO2 cells (mock, wild type MCMV and MCMV Δm169 infection). However, the amplified PCR products (smeared bands) of the control appeared to be very low (Fig 5.5F). In contrast, the sample obtained from cells infected with MCMV Δm169, which showed remarkably weak radioactive signals compared to the others gave the stronger smear of the PCR products.

It is clear that PCR products obtained from the present study are low in intensity compared to those described in the original protocol (Helwak and Tollervey, 2014). Despite of low yield of PCR products, the smeared bands enriched for chimeras and targets were observed across all samples. The PCR products between 150-200 bp were gel purified and submitted to HiSeq Illumina sequencing.

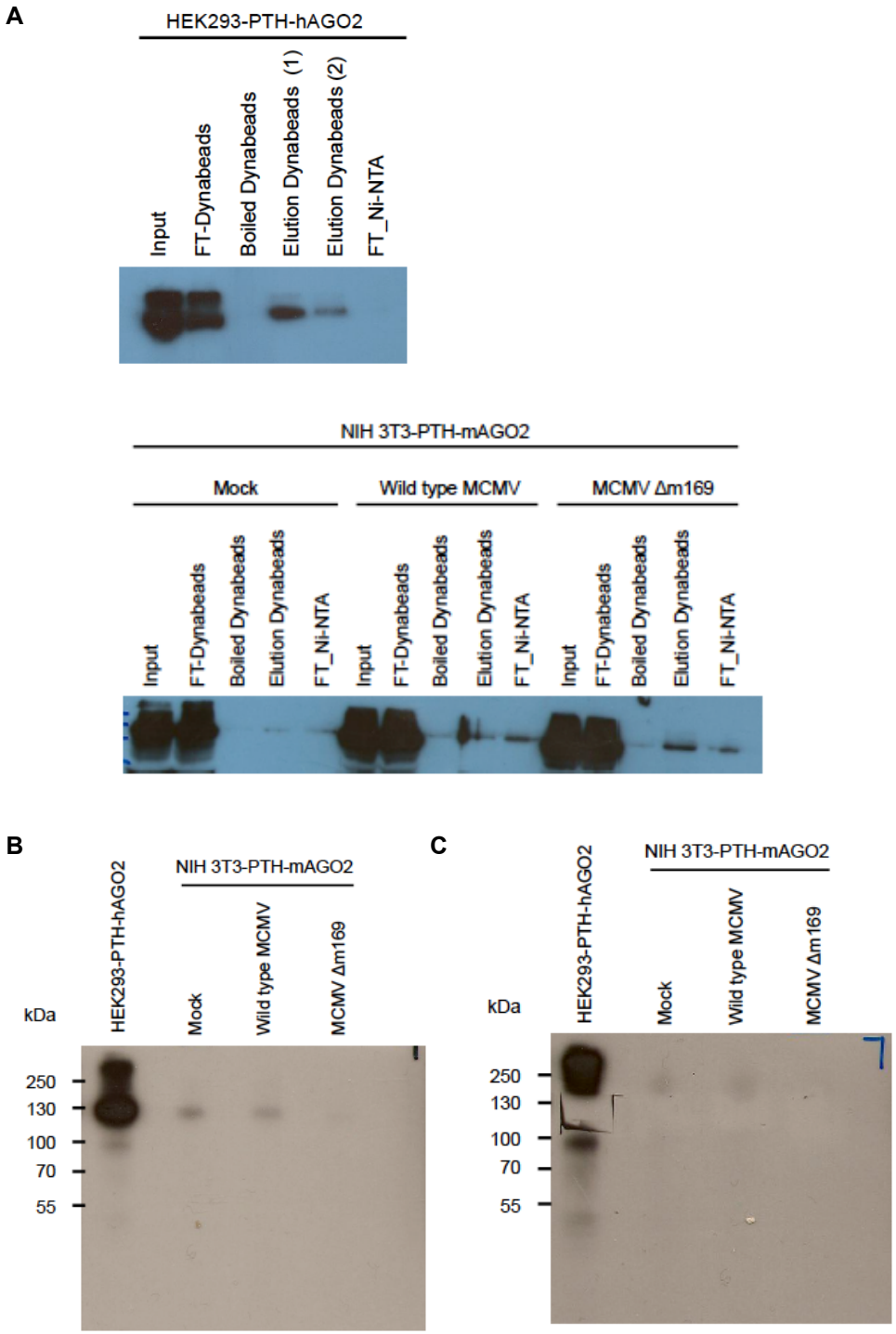
A
HEK293-PTH-hAGO2
Input
FT-Dynabeads
Boiled Dynabeads
Elution Dynabeads (1)
Elution Dynabeads (2)
FT_Ni-NTA
NIH 3T3-PTH-mAGO2
Mock
Wild type MCMV
MCMV Δm169
Input
FT-Dynabeads
Boiled Dynabeads
Elution Dynabeads
FT_Ni-NTA
B
HEK293-PTH-hAGO2
NIH 3T3-PTH-mAGO2
Mock
Wild type MCMV
MCMV Δm169
kDa
250
130
100
70
55
C
HEK293-PTH-hAGO2
NIH 3T3-PTH-mAGO2
Mock
Wild type MCMV
MCMV Δm169
kDa
250
130
100
70
55

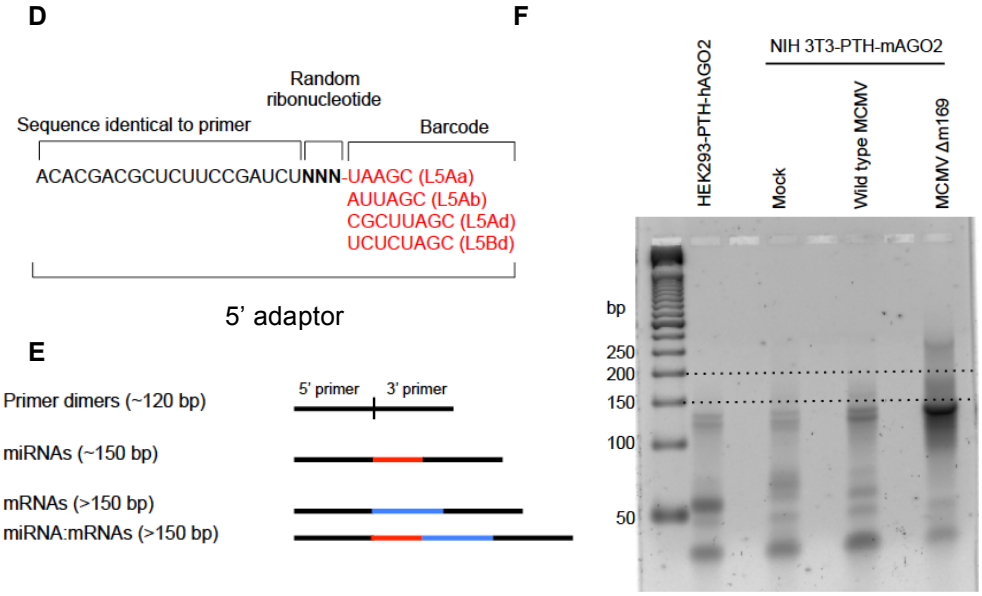

Figure 5.5 Evaluation of the CLASH protocol including purified fractions, radiolabelling of RNAs and amplified cDNA libraries
(A) Western blot analysis (ECL-based detection) of tagged-AGO2. The same volume of the input and flow-through from Dynabeads (FT-Dynabeads) was used to evaluate the recovery of protein on IgG-conjugated Dynabeads. To determine the protein recovery on Ni-NTA, an equal volume of protein (50 µl from a total of 1 ml) from the first purification (Elution Dynabeads) and the flow-through from Ni-NTA (FT-Ni-NTA) was loaded onto the gel. Western blot analysis was carried out using PAP complex antibody specific to protein A of PTH tag. **(B)** Autoradiography of purified protein-RNA complexes resolved by SDS-PAGE. The membranes were exposed to autoradiography films at -80°C, overnight. The expected size is ~110-130 kDa. **(C)** The autoradiography of the same membrane after cutting out the bands for extracting AGO-RNA complexes. **(D)** Sequences of 5'adapters containing sequences identical to PCR primers, three random ribonucleotides to identify PCR duplicates and ribonucleotide barcodes to allow multiple samples to be sequenced in one reaction. **(E)** Schematic diagram of anticipated size of PCR fragments in an agarose gel. **(F)** High resolution agarose (MetaPhor) gel electrophoresis of cDNA libraries. Smears between 150-200 bp were anticipated to enrich for chimeras (miRNAs+targets) and mRNA fragments. The gel between 150-200 bp (dashed lines) was excised and purified for Illumina sequencing.

5.3.5 Analysis of sequencing results

Following the preparation of cDNA libraries, the PCR products were subjected to Illumina sequencing to identify RNAs and potential chimeras associated with AGO2. Four samples (the control HEK 293-PTH-hAGO2 cells and NIH 3T3-PTH-mAGO2 cells (mock, wild type MCMV and MCMV Δm169 infection) were sequenced which contain 5'adapters with unique barcodes for sample identification. This allows for pooling all samples for a single sequencing lane. The total number of raw reads was obtained and bioinformatic analysis was carried out by Kashyap Chhartbar (IIIR, University of Edinburgh). As outlined in Fig 5.6, the 5' and 3' adapters of all reads were identified and trimmed. An insert length of >16 nt is recommended for reliable alignment (Travis et al., 2014). Thus, reads containing >16 nt between the two adapter sequences were included for further analyses. The reads were mapped to genome databases to identify single and chimeric reads.

As shown in Fig 5.7A, after trimming of the adapters, the total number of reads obtained from MCMV Δm169 infection was distinctly high (67M) compared to the control HEK293-PTH-hAGO2 (22M), mock (7.7M) and wild type MCMV infection (13M), in line with the intensity of PCR products observed from the agarose gel shown in Fig 5.5F. Disappointingly, the majority of reads from all samples contained inserts shorter than 16 nt: 42.78% of reads from the control, 54.09% of reads from mock infection, 64.31% of reads obtained from wild type MCMV and 97.09% of reads from MCMV Δm169 infection and these short reads had to be excluded from further analysis (Fig 5.7B). The number of short reads could be due to overdigestion of RNA with RNase following protein purification, particularly in MCMV Δm169 infection that might require optimization to obtain optimal size of RNA fragments (Moore et al., 2014). It could also just represent background signal since the overall amount of material pulled down may have been too low.

After excluding the short reads, the human genome database (Human Ensembl release 78) was used to map reads of the control. For the samples from NIH 3T3-PTH-mAGO2 cells, the reads were mapped to the mouse genome (Ensembl, GRCm37). In the case of virus-infected samples, the reads were mapped to the

MCMV genome (NC_004065) in addition to the mouse genome. The control showed 17.53% (3.9M reads) of reads mapped to the human genome. The sequence alignment showed that 16.93% of reads (1.3M reads) from mock infection mapped to the mouse genome. 27.34% of reads (3.6M reads) from wild type MCMV infection mapped to the mouse or MCMV genome and only 0.13% of reads (90.4K reads) from MCMV Δm169 infection mapped to these databases. The mapped reads were analysed to identify RNA biotypes, single reads and chimeric reads.

As shown in Fig 5.8A to C, identification of RNA biotypes revealed that the control, mock and wild type MCMV infection showed the read length distribution with the peak at 22 nt corresponding to mature miRNAs, whereas MCMV Δm169 (Fig 5.8D) showed the highest peak at 16 nt mapped with protein-coding genes followed by the peak of 22 nt. However, due to the different scales of Y-axis, a number of reads mapped to protein-coding genes from MCMV Δm169 (11.6K reads) were less than mock (16.1K) and wild type MCMV infection (19K). The identification of chimeric reads of miRNAs and protein coding genes showed 7 unique reads from the control, 52 reads from mock, 95 reads from wild type MCMV and 7 reads from MCMV Δm169 infection (Appendix 5). Among 52 unique reads in mock infection, 10 reads represented chimeras of miR-27 and *Zfp560* and 1 chimeric read of miR-27 and *Ppm1f*, whereas wild type MCMV and MCMV Δm169 infection did not show miR-27 chimeras. A reduction in the number of chimeras containing miR-27 in wild type MCMV infection might be expected since this miRNA is degraded by the virus. However, it is difficult to speculate on any differences between the samples since the overall coverage was so low. In conclusion, the present study provided a small coverage of single and chimeric reads, suggesting that optimisations are required in future experiments to increase the number of reads.

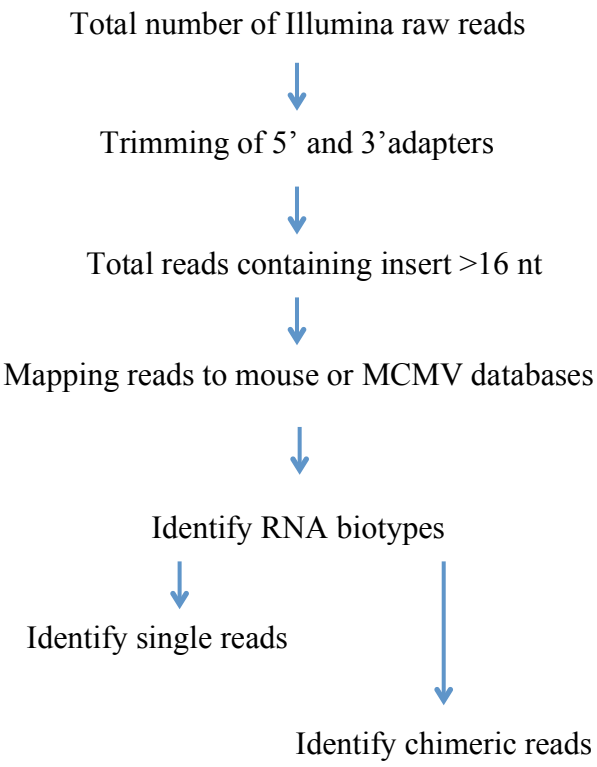

Figure 5.6 Flow diagram of bioinformatic analysis of CLASH

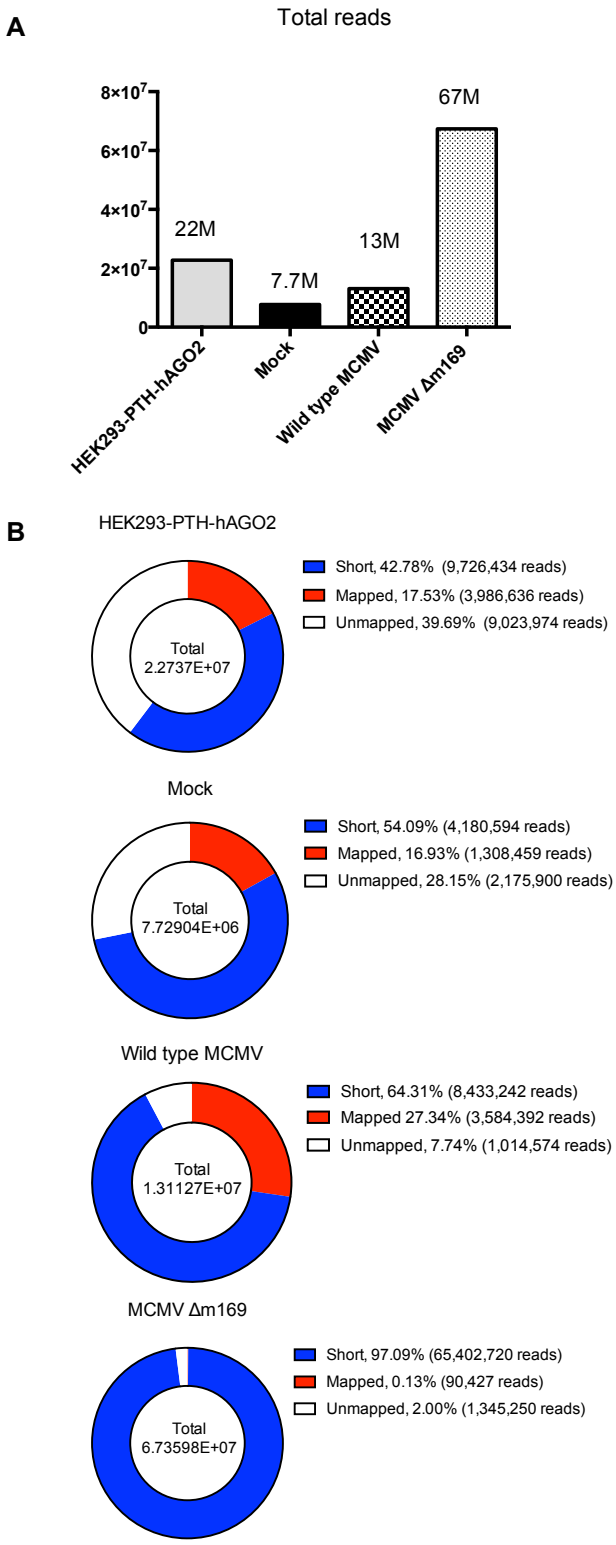

Figure 5.7 Analysis of reads obtained from sequencing
(A) The total numbers of raw reads containing 5' and 3' adapters. **(B)** Graphs representing the number of reads that contain short inserts <16 nt, and inserts that mapped or did not map to the genome databases.

A

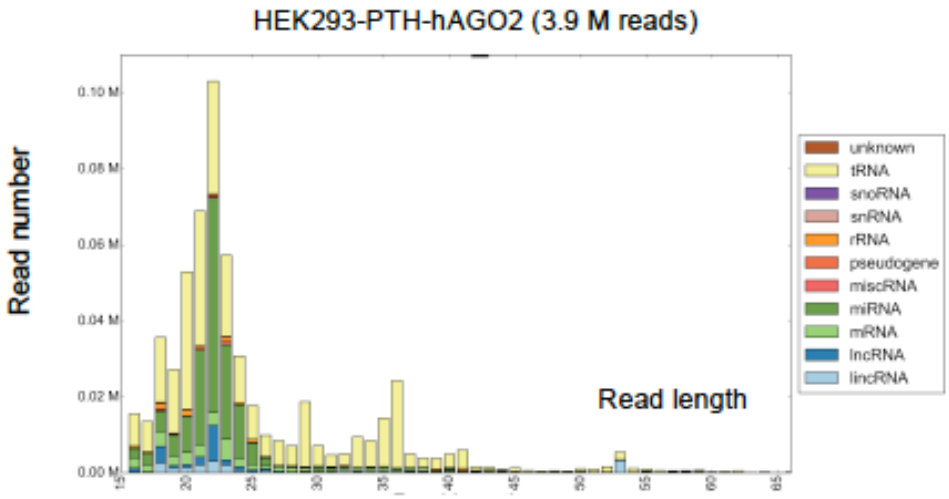
HEK293-PTH-hAGO2 (3.9 M reads)
Read number
Read length
unknown
tRNA
snoRNA
snRNA
rRNA
pseudogene
miscRNA
miRNA
mRNA
lncRNA
lincRNA

B

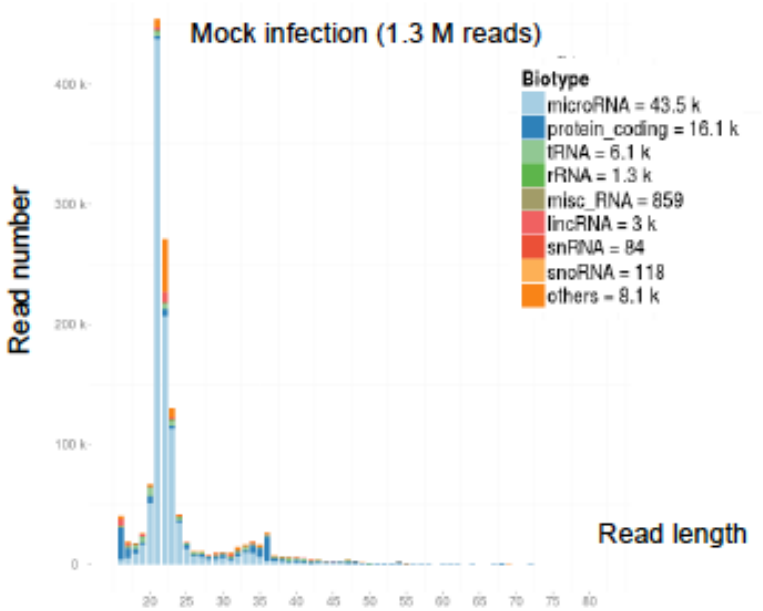
Mock infection (1.3 M reads)
Read number
Read length
Biotype
microRNA = 43.5 k
protein_coding = 16.1 k
tRNA = 6.1 k
rRNA = 1.3 k
misc_RNA = 859
lincRNA = 3 k
snRNA = 84
snoRNA = 118
others = 8.1 k

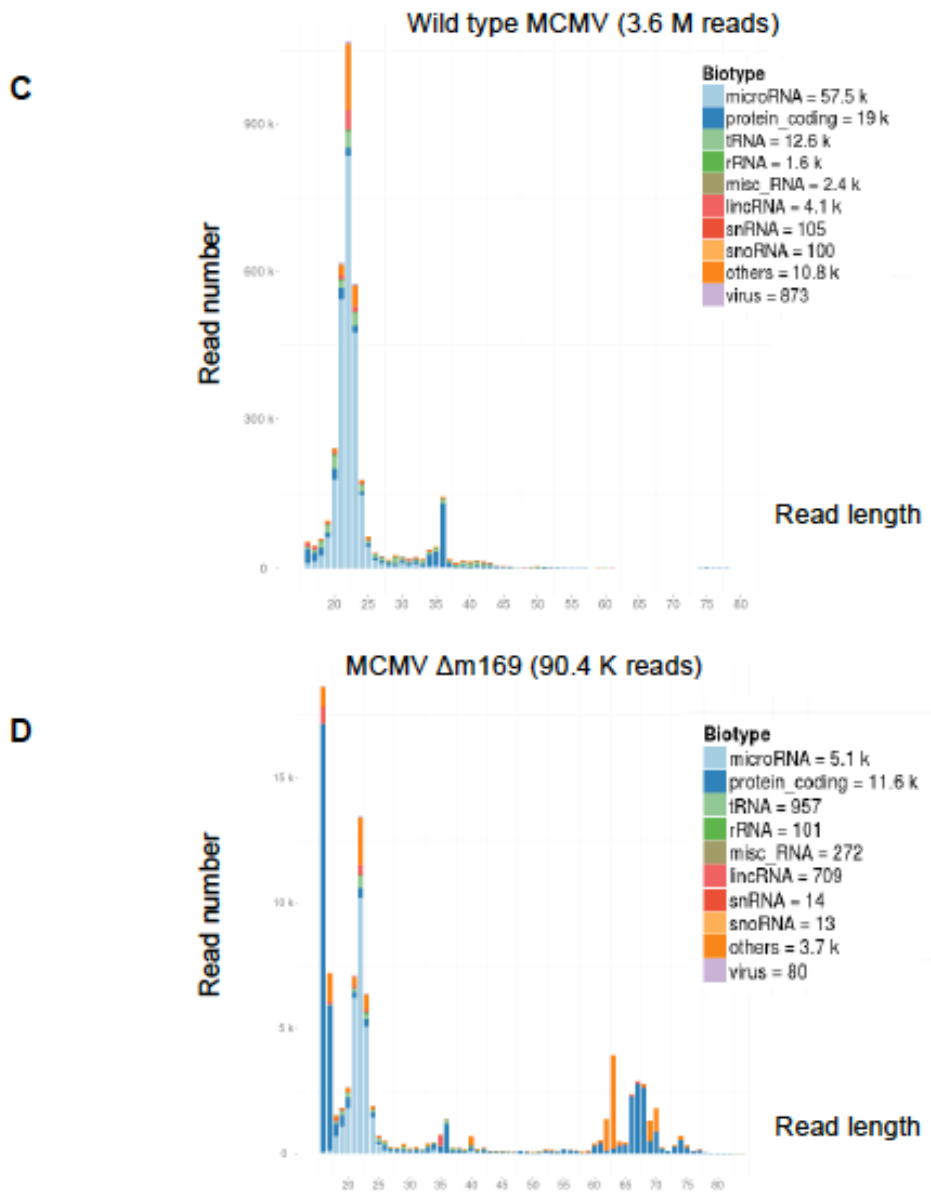

Figure 5.8 Biotypes of the mapped reads
Total reads containing inserts >16 nt with 5' and 3'adapters were analysed to classify the reads into biotypes and lengths. **(A)** The colour coding of the control (HEK293-PTH-hAGO2) is different from **(B-D)** samples of NIH 3T3-PTH-mAGO2. Data are presented as read length versus read numbers.

5.4 Discussion

A common genome-wide approach to map the binding sites of miRNAs on their targets is crosslinking of RNA-protein complexes followed by immunoprecipitation of the AGO protein and sequencing of associated RNAs, widely known as CLIP (reviewed in (Hausser and Zavolan, 2014)). Several modifications of this method

have been proposed and the most recent method, CLASH, has been shown to successfully identify direct targets of miRNAs in a high-throughput manner (Helwak et al., 2013; Helwak and Tollervey, 2014). This technique involves RNA-RNA ligation to join miRNAs with their mRNA targets in order to directly map the miRNA-target interaction. In addition, the technique utilises a double affinity tagged-protein that allows the purification to be carried out under stringent conditions, reducing background that could arise from RNA-RNA interactions formed after cell lysis. In this chapter, CLASH was carried out to explore whether this technique could be used to identify direct targets of miR-27 in the context of MCMV infection. It was envisaged that this would identify direct target genes of miR-27, complementing the other studies in this chapter to understand why the virus has evolved to inhibit this miRNA.

The NIH 3T3-PTH-mAGO2 cell line stably expressing tagged-mAGO2 (PTH-mAGO2) was generated and overexpression of the tagged-mAGO2 was confirmed. It has previously been reported that overexpression of AGO2 in HEK293T cells and human lung adenocarcinoma cells (H1299) causes changes in the levels of certain miRNAs (Zhang et al., 2013). Therefore to determine if this was an issue in terms of regulation of miR-27 in the presence and absence of MCMV, levels of miR-27 and m169 were compared in NIH 3T3-PTH-mAGO2 and NIH 3T3 cells. No significant differences in the levels of RNA expression were observed between the two cell lines, as determined by Northern blot analysis.

The CLASH technique is a challenging molecular protocol with many steps spread over several days and few points at which the efficiency can be monitored. Helwak *et al*. have previously described a number of factors influencing the success of the technique. One of these is the efficiency of tagged-AGO purification using IgG-conjugated Dynabeads. Comparing the amount of tagged-AGO in the input and the remaining protein in the flow-through, the authors usually observed a ~30% reduction in AGO in the flow-through (Helwak and Tollervey, 2014). Similarly, the control (HEK293-PTH-hAGO2 cells) used in the present study showed ~20-30% reduction in the protein from the flow-through compared to the input. However, the same level of reduction of AGO2 was not observed in the flow-through compared to

the input of the three samples from NIH 3T3-PTH-mAGO2 cells: mock, wild type MCMV and MCMV Δm169 infection. It is difficult to find a definite explanation for why the purification efficiency was different between PTH-hAGO2 and PTH-mAGO2 since both tagged-proteins contain the same protein tag (PTH) and AGO2 is highly conserved with amino acid identity ~99.1% between human and mouse (Li et al., 2014). It is still unclear from the protocol what is the minimum amount of material required for the technique to work. Nonetheless improvement of this purification step is likely to be a crucial optimisation of CLASH. Recently, Strauch *et al*. have demonstrated that the binding of IgG and protein A is pH dependent. Using biolayer interferometry, the biosensor system that determines protein-protein interaction in real-time, the authors showed a high efficiency of IgG-protein A binding at pH 8.2 but a dramatic decrease (~500 fold reduction) at pH 5.5 (Strauch et al., 2014). In the CLASH protocol, the purification was performed in protein lysate at pH~7.2 and it is therefore possible this is suboptimal. Alternatively, Helwak *et al*. have suggested the possibility of replacing protein A with FLAG tag that can be purified using an efficient antibody (Helwak and Tollervey, 2014). Furthermore, Domanski *et al.* have demonstrated that 3xFLAG-tagged proteins provide a higher yield in purifications compared to traditional 1xFLAG tagged proteins (Domanski et al., 2012). Thus, the use of a 3xFLAG-tagged protein could increase the yield of protein isolation in the CLASH protocol. Indeed, the Buck lab has recently generated knock-in mice that express a N-terminal 3xFLAG-6xHis tag-mAGO2. These mice are fertile and viable and preliminary data of protein purification using anti-FLAG-coated Dynabeads showed a high yield of purified proteins compared to PTH-mAGO2 (unpublished data), with very little protein in the flow-through.

After radiolabelling the RNAs within the AGO2-RNA complexes, the success of this step of the experiment was evaluated by determining the radioactive signal to estimate the recovery of RNAs. The radioactive signal obtained from NIH 3T3-PTH-mAGO2 cells was considerably weak for all three conditions compared to the signal obtained from the control HEK293-PTH-hAGO2 cells. This is likely due to the low amount of materials obtained following purification with the IgG-coated Dynabeads, emphasizing that the first purification of tagged-AGO is a critical determinant to

obtain the sufficient materials for downstream reactions. One thing that could affect the visualization of radioactively labelled RNAs is the inefficient labelling of miRNAs due to their 5'ends, which may be buried in AGO, leading to less accessibility for the kinase (Parker, 2010). In HITS-CLIP, radiolabelling of 3'adapters before ligation to RNAs was proposed as an alternative strategy that would also allow evaluation of the 3'adapter ligation efficiency (Moore et al., 2014). In CLASH, it is worth noting that the radioactive signal does not truly reflect the amount of purified protein-RNA complexes since a weak signal could be due to inefficient labelling reaction.

According to the PCR products visualized on the agarose gel, the control showed only a very weak smear in the size range thought to be enriched for chimeras (miRNA:mRNA) and mRNAs (~150-200 bp), even though a high radioactive signal was observed from the autoradiography compared to the others from NIH 3T3-PTH-mAGO2 cells. This could be due to low efficiency of 5' and 3' adapter ligations. It was observed in HITS-CLIP that the ligation efficiency is ~50% that is presumably evaluated through using radioactively labelled adapters (Moore et al., 2014) and it is difficult to monitor this. To address the issue of ligation efficiency, Moore M *et al*. suggest the possibility of using ligation-independent cloning to avoid the requirement of adapter ligation (Moore et al., 2014). This technique uses the 3'➔5' exonuclease activity of T4 DNA Polymerase to generate overhangs complementarity between inserts and linear vectors which are then ligated in *E.coli* during transformation (Stevenson et al., 2013). However, further optimisation would be required to adapt this technique for the current CLASH protocol.

The analysis of cDNA libraries using sequencing revealed that the recovery of RNA was very low in all samples. The control from HEK293-PTH-hAGO2 cells showed 3.9M reads mapped to the human genome. The mock infection of NIH 3T3-PTH-mAGO2 cells showed 1.3M reads mapped to the mouse genome. NIH 3T3-PTH-mAGO2 cells infected with wild type MCMV showed 3.6M reads and the cells infected with MCMV Δm169 showed 90.4K reads mapped to the mouse or MCMV databases. As mentioned above, the problem of samples from NIH-3T3-PTH-mAGO2 cells is likely due to insufficient amount of purified protein from the first

purification using IgG-coated Dynabeads. Although the control (HEK293-PTH-hAGO2 cells) showed more yield of purified protein and strong radioactive signal compared to the three samples from NIH-3T3-mAGO2 cells, the number of mapped reads was not significantly larger compared to the others, indicating that troubleshooting has to be carried out also at steps following the protein purification. As mentioned, adapter ligation might be an issue. In addition, a range of technical issues could reduce efficiency as addressed in (Helwak and Tollervey, 2014).

Based on the initial attempt at carrying out the CLASH technique outlined in this chapter, it is clear that further optimisation and modification of the technique are required prior to repeating with the NIH3T3-PTH-mAGO2 cell line. It is important to note to date this technique has only been carried out with overexpressed tagged-protein. It will be interesting to determine the percentage of chimeras obtained with physiological levels of tagged-AGO protein using CLASH. In this regard, the studies with the tagged-AGO2 mouse will be useful.

At this stage, it is not possible to draw conclusions from the sequencing results obtained in the present chapter due to the lack of coverage. Based on the sequencing data, the numbers of reads that mapped to mouse or human genome obtained from the four samples were in the range of 90K to 3.9M reads, considerably less than 23M reads reported in (Helwak et al., 2013). In addition, the number of unique chimeric reads containing miRNAs and mRNAs was 7 in the control, 52 in mock, 95 in wild type MCMV and 7 in MCMV Δm169 infection. This again is substantially lower than the 15,000 unique miRNA-mRNA interactions expected from a good library (Helwak et al., 2013; Helwak and Tollervey, 2014).

In summary, the present work shows that the NIH 3T3-PTH-mAGO2 cell line was successfully generated, evaluated and utilised for the CLASH protocol. Based on the sequencing data, the low number of chimeras was consistent with the low amount of protein purified at the first purification that relied on conjugation between the protein A tag and IgG-coated Dynabeads. Thus, as a starting point optimisation of this step should be carried out to increase the recovery of RNAs associated with PTH-mAGO2 and ideally identify the miRNA-mRNA chimeras.

Chapter 6: Conclusion and future directions

6.1 Rationale and objectives of the thesis

This thesis focuses on understanding the cellular pathways required for MCMV infection, focusing on understanding the targets of miR-27, a miRNA inhibited by the virus. The central hypothesis is that miR-27 degradation by the virus boosts the levels of miR-27 targets during infection and this is advantageous to the virus. While HCMV has not been shown to degrade miR-27, a hypothesis is that similar cellular pathways will also be required by HCMV and this work will therefore also shed light on cellular pathways exploited by this human pathogen.

HCMV affects approximately 40-100% of the world's population (Mocarski, 2007). The virus usually causes little or no symptom in immunocompetent hosts; however, it associates with the significant morbidity and mortality in immunocompromised patients such as patients with HIV and organ transplant recipients who are on immunosuppressive therapies (Hodinka, 2007). In HIV-1-infected individuals with advanced immunosuppression, the most common manifestation is retinitis, followed by gastrointestinal disease and encephalitis (Boeckh and Geballe, 2011). In the case of hematopoietic stem cell recipients, pneumonia and gastrointestinal disease are common manifestations of CMV disease, whereas retinitis, hepatitis and encephalitis are less frequently found (Ljungman et al., 2010).

HCMV is also the most common congenital infection in developed countries with estimated 40,000 cases in the United States each year. The compelling studies conducted in developing countries in Africa, Asia and Latin America revealed that maternal CMV seroprevalence ranged from 84% to 100% and CMV birth prevalence varied from 0.6% to 6.1% (from the number of newborns tested ranged from 317 to 12,195) (Lanzieri et al., 2014). Although ~90% of infants born in the United States with congenital CMV infection do not show clinical manifestations, they are at high risk for hearing loss (reviewed in (Nassetta et al., 2009)). The CMV-infected neonates with symptomatic diseases show sensorineural hearing loss, microcephaly, motor defects, mental retardation, chorioretinitis and dental defects (reviewed in (Nassetta et al., 2009)).

Based on the vast impact of HCMV on the global health, the Institute of Medicine (IOM) has considered HCMV vaccine development as the highest priority with the major focus on reducing congenital CMV infection (Arvin et al., 2004). A number of HCMV vaccines have been evaluated in clinical trials and a Phase 2 clinical trial of HCMV gB vaccine plus F59 adjuvant that was administered to seronegative women of childbearing age showed 50% of vaccine efficacy (reviewed in (Sung and Schleiss, 2010). However, it is still under the debate whether the vaccine is sufficient to prevent HCMV infection and transmission within a community. Although enormous progress has been gained from vaccine clinical trials, no licensed HCMV vaccine is currently available. This triggers research to seek alternatives of HCMV therapeutics or prevention strategies that could alleviate this disease burden. As part of this, it is necessary to better understand how the virus interacts with host cells, and what factors it has evolved to exploit or inhibit.

Cellular miRNAs have been reported to be involved in viral infection, either by interacting with viral genes or regulation of cellular pathways affecting viral replication (Skalsky and Cullen, 2010). Depending on the target genes or cellular pathways regulated by miRNAs, the effects of miRNAs can be a suppression or promotion of viral infection (Grassmann and Jeang, 2008; Skalsky and Cullen, 2010). The effects of miRNAs on viral infection observed in pre-clinical settings opened up the possibility to use synthetic miRNAs (miRNA mimics or inhibitors) for the treatment of viral infection. The substantial progress of development of miRNA therapeutics has been demonstrated by the anti-viral potential of miR-122 inhibitors against HCV. The inhibitor of miR-122 is the first miRNA-targeted drug that has been in Phase 2a clinical trials and showed anti-viral activity (Janssen et al., 2013). This demonstrates the therapeutic potential of miRNAs for the treatment of viral infection.

Previously, research in the Buck lab demonstrated that MCMV encodes a non-coding RNA, m169, to degrade cellular miR-27 (Libri et al., 2012). It was shown that the inhibition of miR-27 by m169 is important for viral replication *in vivo* (Marcinowski et al., 2012) and overexpression of miR-27 suppresses the replication of virus *in vitro* (Buck et al., 2010). Thus, the central hypothesis of this thesis is that the degradation

of miR-27 is a viral strategy to interfere with functions of miR-27 on cellular processes contributing to viral replication. This thesis focuses on identification of cellular targets of miR-27 and functional studies of target genes. Here, it was hypothesised that understanding the cellular pathways regulated by MCMV will be of relevance to HCMV, even though miR-27 itself does not appear to be targeted by HCMV. Such significant genes could be used as targets for drug development in treatment of CMV.

The aims of the study in this thesis are to:

1. Identify and validate cellular targets of miR-27 that are required for MCMV replication
2. Examine cellular pathways regulated by miR-27 in the context of MCMV infection
3. Generate datasets of direct targets of miR-27 using cross-linking, ligation and sequencing of hybrids (CLASH) technique

6.2 Conclusions

The primary aim of this thesis is to identify cellular targets of miR-27 involved in MCMV replication. Microarray analysis was used to globally examine changes in mRNA levels upon miR-27 overexpression or inhibition during MCMV infection in order to identify targets of miR-27 that could play a role in MCMV infection. A number of potential targets of miR-27 were analysed using the functional screening to determine their effects on MCMV replication *in vitro*. The screening involved siRNA knockdown followed by infection of GFP-MCMV and the effect on viral growth was assessed through GFP intensities. The functional screening revealed that *Mapkapk3* is required for viral replication and this gene was validated as a direct target of miR-27 based on luciferase assays. Consistent with the functional screening, knockdown of *Mapkapk3* showed ~10 fold reduction in viral titres compared to cells transfected with RISC-free siRNAs at 3 days post infection. MAPKAPK3 protein is a downstream kinase of p38 in the p38 MAP kinase pathway, which has previously been shown to be an essential pathway for CMV replication. MAPKAPK3 has been found to phosphorylate a number of proteins including heat shock protein 27

(HSP27), a multifunctional protein involved in cellular responses to stresses such as protein folding, inhibition of apoptosis and actin remodelling (reviewed in (Vidyasagar et al., 2012)). Johnson *et al*. showed that HCMV induces phosphorylation of HSP27 in a p38-dependent manner. The authors proposed that the two functions of HSP27 might be required for the virus: an anti-apoptotic role and as a chaperone to correct misfolded proteins necessary for viral permissiveness (Johnson et al., 2000). Importantly, analysis of levels of MAPKAPK3 and pHSP27 protein during MCMV infection revealed that the levels of MAPKAPK3 correlate to the levels of pHSP27 and are higher in cells infected with wild type MCMV versus MCMV Δm169, suggesting that miR-27 regulates MAPKAPK3 and phosphorylation of HSP27 during infection. This could in part explain anti-viral mechanism of miR-27 by which miR-27 acts through MAPKAPK3 and HSP27, inducing apoptosis and accumulation of misfolded protein that cannot be used by the virus. It will be of interest to understand how these proteins are regulated in HCMV, since miR-27 is not known to be targeted by that virus.

It is important to note that MAPKAPK3 and its isoenzyme, MAPKAPK2, share ~70% amino acid identity, activators and substrates (McLaughlin et al., 1996). The expression levels of MAPKAPK3 are lower than MAPKAPK2 in most cells and tissues including MEFs, macrophages, heart, liver, kidneys, lungs and spleens (Ronkina et al., 2007). Thus, to avoid data misinterpretation, it should be taken into account that MAPKAPK2 could compensate for MAPKAPK3 (Ronkina et al., 2007). Comparative studies of *Mapkapk2/3* double knockout and single knockout of either *Mapkapk2* or *Mapkapk3* would be ideal to distinguish biological roles of *Mapkapk3*. Since HSP27 was shown to be phosphorylated by MAPKAPK3 upon infection, it is interesting to examine whether HSP27 is involved in MCMV replication. This could be carried out by determining viral growth in knockdown of HSP27.

miRNAs can regulate a large number of genes involved in diverse cellular pathways and it is possible that miR-27 regulates genes other than *Mapkapk3* that could explain why this miRNA is targeted by the virus. The second aim of this thesis is to identify such genes or cellular pathways regulated by miR-27. The data presented in this thesis demonstrated that miR-27 stimulates the G1/S transition in the cell cycle.

miR-27 has been identified as an oncogenic miRNA in promoting cell proliferation. Overexpression of miR-27 has been observed in various kinds of cancer cells including breast cancer (Guttilla and White, 2009; Mertens-Talcott et al., 2007), gastric adenocarcinoma (Liu et al., 2009), pancreatic cancer (Ma et al., 2010) and prostate cancer (Prueitt et al., 2008). Since the cell cycle regulates cell proliferation (Golias et al., 2004), it is possible that miR-27 exerts the oncogenic activity via the regulation of the cell cycle. Two genes, *Bmi1* and *Cav1* whose functions have been reported in the cell cycle were validated as direct targets of miR-27 using luciferase reporter assays. However, knockdown of *Bmi1* or *Cav1* led to the delay of cell cycle transition from G1 to S phase, opposite to the effect of miR-27 overexpression. This suggests that the two genes are unlikely to be involved in the induction of the G1/S transition by miR-27. It is possible that miR-27 regulates cellular genes other than *Bmi1* and *Cav1,* giving rise to the progression of cells from G1 to S phase. Identification of such genes would shed light on the mechanism by which miR-27 regulates this cell cycle transition. Analysis of transcriptome or proteome in cells transfected with miR-27 mimics or miR-27 inhibitors followed by inducing the transition of cells from G1 to S phase may specifically identify target genes responsible for stimulating the G1/S transition. In the context of MCMV infection, knockdown of *Bmi1* and *Cav1* does not affect viral replication *in vitro*, suggesting that these genes are unlikely to play a role in viral replication or contribute to anti-viral activity of miR-27. Studies have shown that MCMV and HCMV arrest cells in the G1 phase and inhibit host DNA synthesis, allowing expression of viral genes (reviewed in (Spector, 2015)). Several viral proteins have been demonstrated to induce the G1 arrest including tegument UL69 and IE86 of HCMV, and IE3 of MCMV. Since viral gene expression and replication are dependent on the host cell cycle, it is logical to speculate that the MCMV may evolve multiple strategies to modulate the cell cycle in addition to viral factors. Based on the effect of miR-27 on stimulation of the G1/S transition, it is possible that the virus inhibits this miRNA in attempt to maintain the cell in the G1 phase. Identification of miR-27 targets involved in the G1/S transition could elucidate the significance of miR-27 degradation upon MCMV infection associated with the cell cycle.

The p38 MAP kinase signalling has shown to modulate the cell cycle, particularly at the G1/S transition. A study has shown that p38 kinase can either induce progression or inhibition of the cell cycle depending on types of stimuli (Faust et al., 2012). Activation of p38 using serum led to an increase in phosphorylation of Rb and cyclin D1, proteins required for S phase entry, compared to serum-starved cells, whereas cells treated with cellular stress, anisomycin, showed a complete loss of cyclin D1 expression compared to untreated cells (Faust et al., 2012). The authors further demonstrated that only anisomycin-activated p38 but not serum stimulation leads to phosphorylation of MAPKAPK2 (an isoenzyme of MAPKAPK3) and its substrate, transcription factor CREB (Faust et al., 2012). It was found that activation of CREB by bacterial toxins leads to the G1 arrest in mouse macrophages due to induction of p27 (an inhibitor of the G1/S transition) and downregulation of cyclin D1 (Gray and Hewlett, 2011). However, the present study showed that MAPKAPK3 does not phosphorylate CREB under anisomycin treatment. Thus, it is unlikely that MAPKAPK3 is involved in cell cycle arrest through the regulation of CREB.

One caveat of miRNA target identification using microarray analysis is that this method cannot distinguish direct targets from secondary effects (reviewed in (Hausser and Zavolan, 2014)). Thus, the last aim of this thesis is to generate datasets of direct targets of miR-27 using cross-linking, ligation and sequencing of hybrids (CLASH). To carry out the CLASH protocol, the NIH 3T3-PTH mAGO2 stable cell line expressing AGO2 with a double affinity tag (ProteinA-TEV-6xHis, PTH) at the N terminus was generated. It was shown that overexpression of tagged-AGO2 in NIH 3T3-PTH mAGO2 cells does not significantly alter levels of miR-27 or lead to changes in permissiveness to MCMV compared to NIH 3T3 cells, suggesting that this cell line is suitable for identification of miR-27 targets upon infection. Following protein purification using IgG-conjugated Dynabeads, Western blot analysis was carried out to evaluate the efficiency of the purification. The data of three samples (mock-infected cells and cells infected with wild type MCMV or MCMV Δm169) showed no reduction in the levels of tagged-protein in the flow-through compared to the input material, suggesting that the purification is inefficient and requires optimisation. Indeed, the Buck lab has recently generated knock-in mice that express

a N-terminal 3xFLAG-6xHis tag-mAGO2 where the protein A tag is replaced with 3xFLAG tag. The preliminary data of protein purification using anti-FLAG-coated Dynabeads showed a high yield of purified proteins compared to PTH-mAGO2 (unpublished data), with very little protein in the flow-through. In line with the low amount of tagged-protein purified using Dynabeads, sequencing data of the three samples showed the low number of reads (in the range of ~90K to 3.6M) that mapped to the genome databases, remarkably lower than 23M reads reported in (Helwak et al., 2013). Thus, the purification of tagged-AGO seems to be a crucial step and is required optimisation to obtain the sufficient material for the subsequent steps of the CLASH protocol.

6.3 Future directions

The data presented in this thesis provide an interesting base for studying functions of miR-27 and involvement of *Mapkapk3* in MCMV infection. Analysis of miR-27 in regulation of the cell cycle revealed that miR-27 accelerates cells from G1 to S phase. This could in part explain the significance of miR-27 degradation by MCMV as one viral strategy to induce the G1 arrest. Using the NIH 3T3-PTH-mAGO2 cell line in the CLASH protocol, the data suggest that the protein purification step needs optimisation to improve the recovery of RNA associated with the tagged-protein. A number of questions based on the data obtained from this thesis merit further investigation.

Chapter 3:

1. What is the function of *Mapkapk3* involved in MCMV replication?
2. Does HSP27, a substrate of MAPKAPK3, contribute to functions of MAPKAPK3 in the context of MCMV infection? What is the cellular process in which HSP27 affects the MCMV life cycle?
3. Given that MCMV requires the function of *Mapkapk3*, does *Mapkapk2* compensate for, or cooperate with *Mapkapk3* to support MCMV replication? Perhaps, *Mapkapk2* also plays a role in MCMV infection and this point has not been addressed in this thesis. If *Mapkapk2* is significant to the viral

infection, knockdown of *Mapkapk2/3* should show stronger effects compared to knockdown of *Mapkapk3* alone.

4. Beyond MCMV infection, does *Mapkapk3* influence HCMV replication?

Chapter 4:

1. What are the cellular targets of miR-27 contributing to miR-27-induced G1/S transition?
2. Does miR27-stimulated G1/S transition affect MCMV replication?

Chapter 5:

1. Does protein purification using Dynabeads yield sufficient material for subsequence steps of CLASH protocol? How can the purification be improved?
2. Is the ligation of adapters to RNA efficient?

Chapter 7: Appendices

Appendix 1

Appendix 1 A total of 97 genes downregulated in cells transfected with miR-27a mimics versus RISC-free siRNAs (the fold change cut off ≥1.2, p<0.05).

	Symbol	EntrezID	Downregulated fold change	P Value
1	Prl2c4	26421	1.741101127	4.00E-07
2	Prl2c2	18811	1.693490625	1.10E-05
	Prl2c2	18811	1.515716567	0.00012
3	Il1rl1	17082	1.591072968	0.00027
4	Ppif	105675	1.526259209	1.40E-07
5	Prl2c3	18812	1.484523571	9.00E-05
6	Spp1	20750	1.394743666	0.0016
7	Calm3	12315	1.385109468	0.00054
8	Tmbim6	110213	1.385109468	5.00E-06
9	Serpina3g	20715	1.375541818	1.70E-06
10	Cp	12870	1.356604327	0.00032
11	Gbp2	14469	1.337927555	9.50E-05
12	Pdia5	72599	1.337927555	5.70E-05
	Pdia5	72599	1.257013375	0.00089
13	Aox3	71724	1.328685814	0.00047
14	LOC100044968	100044968	1.328685814	4.20E-05
15	Nid1	18073	1.328685814	0.0029
16	Arl6ip1	54208	1.310393404	7.60E-06
17	Ccl7	20306	1.310393404	0.0015
	Ccl7	20306	1.214194884	0.023
18	Marcks	17118	1.310393404	0.0047
19	9930013L23Rik	80982	1.301341855	0.00012
20	Akirin1	68050	1.301341855	5.00E-04
21	Bcap29	12033	1.301341855	0.0079
	Bcap29	12033	1.205807828	0.0041
22	Gaa	14387	1.301341855	0.0012
23	Tmem55b	219024	1.301341855	0.0011
24	2700094K13Rik	72657	1.292352831	2.50E-05
25	2310039H08Rik	67101	1.283425898	5.00E-04
26	Cav1	12389	1.283425898	0.015
27	Serpina3n	20716	1.283425898	0.0073
28	Hsp90aa1	15519	1.274560627	0.0073
29	Acadvl	11370	1.265756594	0.0013
30	AI607873	226691	1.265756594	0.0083

31	B4galt3	57370	1.265756594	3.20E-06
32	Sepp1	20363	1.265756594	2.00E-04
33	Ubtd2	327900	1.265756594	0.0052
34	Zwint	52696	1.265756594	0.001
35	Glipr2	384009	1.257013375	1.30E-05
36	Pgm2	72157	1.257013375	0.0011
	Pgm2	72157	1.205807828	0.032
37	0610007P14Rik	58520	1.257013375	0.00013
	0610007P14Rik	58520	1.283425898	0.0011
	0610007P14Rik	58520	1.265756594	5.00E-05
38	Ak2	11637	1.248330549	0.0028
	Ak2	11637	1.2397077	0.0052
39	Dram2	67171	1.248330549	0.0048
40	Lamp2	16784	1.248330549	0.0068
41	Lbh	77889	1.248330549	1.00E-04
42	Mmd	67468	1.248330549	0.0011
43	Adora2b	11541	1.2397077	0.00057
44	Ccng1	12450	1.2397077	0.0018
45	Gas7	14457	1.2397077	0.0051
46	Ktelc1	224143	1.2397077	0.0052
47	Nagk	56174	1.2397077	0.00029
48	Slc25a17	20524	1.2397077	0.0047
49	Tpm4	326618	1.2397077	0.0024
50	Bmi1	12151	1.231144413	0.00032
51	Celf1	13046	1.231144413	0.00066
52	Ech1	51798	1.231144413	0.0021
53	Gm16385	677448	1.231144413	0.00026
54	Gosr2	56494	1.231144413	0.0012
	Gosr2	56494	1.231144413	0.00041
55	Hat1	107435	1.231144413	0.0094
56	Pdgfra	18595	1.231144413	0.047
57	Slc12a2	20496	1.231144413	0.0043
58	Zfp281	226442	1.231144413	0.0077
59	6330578E17Rik	76178	1.222640278	0.002
60	9430016H08Rik	68115	1.222640278	0.0033
61	Aqp1	11826	1.222640278	0.024
62	Cct6a	12466	1.222640278	0.0045
63	Cnot7	18983	1.222640278	0.00075
64	Cytip	227929	1.222640278	0.00014
65	Ednra	13617	1.222640278	0.0028
66	Gpd2	14571	1.222640278	0.00082
67	Hsd17b11	114664	1.222640278	0.0034

68	Hspd1	15510	1.222640278	0.021
69	Kng1	16644	1.222640278	0.00035
70	LOC100046883	100046883	1.222640278	0.0018
71	Pigp	56176	1.222640278	0.0084
72	Scd2	20250	1.222640278	0.0036
73	Ssr3	67437	1.222640278	0.0031
74	Tcp1	21454	1.222640278	0.00067
75	Vegfb	22340	1.222640278	0.03
76	Acta2	11475	1.214194884	0.044
77	Akap2	11641	1.214194884	0.0081
78	C3	12266	1.214194884	0.026
79	Cd99l2	171486	1.214194884	0.0055
80	Cenpb	12616	1.214194884	0.015
81	Cuedc2	67116	1.214194884	0.025
82	Gnas	14683	1.214194884	0.0044
83	Nudt4	71207	1.214194884	0.023
84	Tmed4	103694	1.214194884	0.00092
85	Top1mt	72960	1.214194884	0.00018
86	Ugt1a10	394430	1.214194884	0.001
87	Acadm	11364	1.205807828	0.0083
88	Efemp2	58859	1.205807828	0.0041
89	Elp2	58523	1.205807828	0.014
90	LOC100044692	100044692	1.205807828	0.048
91	Mrps12	24030	1.205807828	0.011
92	Plau	18792	1.205807828	2.60E-05
93	Psat1	107272	1.205807828	0.0018
94	Sfrp1	20377	1.205807828	0.00012
95	Slc39a11	69806	1.205807828	0.014
96	Tmsb10	19240	1.205807828	0.029
	Tmsb10	19240	1.205807828	0.025
97	Wls	68151	1.205807828	0.037

Appendix 2

Appendix 2 A total of 85 genes downregulated in cells transfected with miR-27a mimics followed by wild type MCMV infection versus cells infected with wild type MCMV (the fold change cut off ≥1.2, p<0.05).

Pja2 was excluded from further analysis since it was downregulated in cells transfected with RISC-free siRNAs versus untreated cells (as shown in Appendix 4).

	Symbol	EntrezID	Downregulated fold change	P Value
1	C3	12266	1.366040257	0.001
2	Rpl18a	76808	1.356604327	0.00048
3	H60a	15101	1.356604327	0.0071
4	Ndrg1	17988	1.337927555	0.0016
5	Csnk2a1	12995	1.310393404	0.0037
6	4933427G23Rik	330053	1.310393404	0.00069
7	Srsf15	224432	1.301341855	0.0078
8	Ccnd2	12444	1.301341855	0.00087
	Ccnd2	12444	1.257013375	0.0038
9	Spp1	20750	1.292352831	0.01
10	Dstn	56431	1.292352831	0.0033
11	Usp1	230484	1.283425898	0.00061
12	Gm4671	100043821	1.283425898	0.0016
13	Eif4ebp1	13685	1.283425898	0.029
14	D15Ertd621e	210998	1.283425898	0.02
15	Ankrd11	77087	1.283425898	0.012
16	Serpina3n	20716	1.274560627	0.0083
17	Nipbl	71175	1.274560627	0.012
	Nipbl	71175	1.214194884	0.02
18	Mettl9	59052	1.274560627	0.0064
19	Btaf1	107182	1.274560627	0.0045
20	2610101N10Rik	67958	1.274560627	0.0026
21	Tspo	12257	1.265756594	0.0081
22	Lars	107045	1.265756594	0.00066
23	2410006H16Rik	69221	1.265756594	0.0038
24	Ptx3	19288	1.257013375	0.02
25	Ndor1	78797	1.257013375	1.70E-06
26	Coq2	71883	1.257013375	0.00081
27	Rrp1b	72462	1.248330549	0.00022
28	Krit1	79264	1.248330549	0.0024
29	Cxcl9	17329	1.248330549	0.01
30	Tollip	54473	1.2397077	0.00011
31	Papola	18789	1.2397077	5.10E-06

32	Nudt18	213484	1.2397077	3.50E-05
33	Kng1	16644	1.2397077	0.00017
34	Iars	105148	1.2397077	0.0054
35	Hif1a	15251	1.2397077	0.0069
36	Casp4	12363	1.2397077	0.0054
37	1110002B05Rik	104725	1.2397077	0.0019
38	Ugt1a6b	394435	1.231144413	0.011
39	Ugt1a10	394430	1.231144413	0.00063
40	Sypl	19027	1.231144413	0.003
41	Stard5	170460	1.231144413	0.0058
42	Slc25a3	18674	1.231144413	0.037
43	Rras	20130	1.231144413	0.0012
44	Ogt	108155	1.231144413	0.009
45	LOC638301	638301	1.231144413	0.0067
46	Leprotl1	68192	1.231144413	0.015
47	Igf2bp3	140488	1.231144413	0.0083
48	Gon4l	76022	1.231144413	0.0013
49	Gaa	14387	1.231144413	0.0074
50	Fas	14102	1.231144413	0.0016
51	Dazap2	23994	1.231144413	0.036
52	Ccl5	20304	1.231144413	0.0013
53	Atg5	11793	1.231144413	0.0038
54	Zfp330	30932	1.222640278	0.00022
55	Zfp326	54367	1.222640278	0.016
56	Wdr45	54636	1.222640278	0.0086
57	Setd5	72895	1.222640278	0.0042
58	Saa3	20210	1.222640278	0.026
59	Parl	381038	1.222640278	0.002
60	Gm7603	665369	1.222640278	0.049
61	Cept1	99712	1.222640278	0.0047
62	Bat5	193742	1.222640278	0.0046
63	Asns	27053	1.222640278	0.021
64	Arrdc4	66412	1.222640278	0.0015
65	1500012F01Rik	68949	1.222640278	0.033
66	Tbl1x	21372	1.214194884	0.021
67	Smcr7l	239555	1.214194884	0.002
68	Rars2	109093	1.214194884	2.00E-04
69	Metapl1	66559	1.214194884	9.60E-05
70	Jak2	16452	1.214194884	0.034
71	H3f3b	15081	1.214194884	0.0058
72	Eif3k	73830	1.214194884	0.0062
73	Zfp639	67778	1.205807828	0.0038

74	Vldlr	22359	1.205807828	0.017
75	Usp7	252870	1.205807828	0.0087
76	Srprb	20818	1.205807828	0.0038
77	**Pja2**	**224938**	**1.205807828**	**0.0047**
78	Irf2	16363	1.205807828	0.0012
79	Golim4	73124	1.205807828	0.008
80	Fam45a	67894	1.205807828	0.0097
81	Emg1	14791	1.205807828	0.0077
82	Dennd4a	102442	1.205807828	0.027
83	Chd1	12648	1.205807828	0.0087
84	Btg1	12226	1.205807828	0.015
85	Btbd1	83962	1.205807828	0.018

Appendix 3

Appendix 3 A total of 242 genes downregulated in cells infected with Δm169 mutant versus wild type MCMV (the fold change cut off ≥1.2, p<0.05).

	Symbol	EntrezID	Downregulated fold change	P Value
1	Dnmt3b	13436	1.693490625	5.50E-08
2	Ifi30	65972	1.658639092	2.20E-08
	Ifi30	65972	1.602139755	9.30E-07
3	Rgs4	19736	1.602139755	8.80E-07
4	LOC100040592	100040592	1.580082624	3.90E-06
5	D0H4S114	27528	1.558329159	2.60E-07
6	Cxcl12	20315	1.558329159	2.40E-05
7	Snn	20621	1.515716567	3.80E-06
8	Calm3	12315	1.494849249	6.70E-05
9	Dhcr24	74754	1.484523571	1.40E-05
	Dhcr24	74754	1.375541818	1.90E-05
	Dhcr24	74754	1.222640278	3.90E-05
10	Mvd	192156	1.464085696	2.40E-08
11	Tubb2b	73710	1.453972517	9.20E-05
	Tubb2b	73710	1.257013375	0.023
12	0610007P14Rik	58520	1.453972517	2.30E-07
	0610007P14Rik	58520	1.414213562	4.90E-05
	0610007P14Rik	58520	1.385109468	3.20E-06
13	Adam23	23792	1.433955248	5.30E-05
14	Sparc	20692	1.424050196	2.90E-06
	Sparc	20692	1.385109468	1.40E-07
15	Ptn	19242	1.424050196	7.90E-08
16	Mknk2	17347	1.424050196	1.40E-05
17	Tnrc6a	233833	1.404444876	1.40E-07
	Tnrc6a	233833	1.385109468	4.20E-06
18	Nasp	50927	1.404444876	8.40E-07
19	Dbp	13170	1.404444876	7.30E-07
20	Stx3	20908	1.394743666	5.40E-05
21	Igf2bp1	140486	1.394743666	1.00E-05
	Igf2bp1	140486	1.2397077	0.0027
22	Gstm1	14862	1.394743666	2.10E-05
23	Vps13a	271564	1.375541818	2.00E-05
24	Sfrp1	20377	1.375541818	2.30E-07
	Sfrp1	20377	1.310393404	0.00022
25	Tuba1a	22142	1.366040257	0.00094
26	Slc40a1	53945	1.366040257	0.0061

27	Rsad2	58185	1.366040257	0.02
28	Nsdhl	18194	1.366040257	0.0037
	Nsdhl	18194	1.265756594	0.0041
	Nsdhl	18194	1.248330549	0.0073
29	Arhgap12	75415	1.366040257	1.10E-06
30	Wfdc3	71856	1.356604327	0.00017
31	Lmnb1	16906	1.356604327	0.001
32	Celf1	13046	1.356604327	1.70E-05
	Celf1	13046	1.214194884	0.0013
	Celf1	13046	1.205807828	0.0052
33	Ang4	219033	1.356604327	0.00055
34	Snx30	209131	1.347233577	7.50E-05
35	Hsd17b7	15490	1.347233577	7.40E-05
36	Gm13212	433801	1.347233577	0.0031
37	Aacs	78894	1.347233577	1.90E-05
38	Ubtd2	327900	1.328685814	0.0014
39	Gm22	195209	1.328685814	9.80E-05
40	Col5a1	12831	1.328685814	6.00E-07
41	Bcl7a	77045	1.328685814	0.00045
42	5430435G22Rik	226421	1.328685814	0.0035
43	Setd1b	208043	1.319507911	0.0021
44	Itgbl1	223272	1.319507911	0.0053
45	Hsp90ab1	15516	1.319507911	0.0079
46	Hbp1	73389	1.319507911	0.0011
	Hbp1	73389	1.257013375	0.00043
	Hbp1	73389	1.248330549	0.0032
47	Zdhhc7	102193	1.310393404	4.10E-05
48	Usp1	230484	1.310393404	3.00E-04
49	Tgfbr2	21813	1.310393404	0.00052
50	Tcf7l1	21415	1.310393404	7.60E-06
51	Sh3bp5l	79566	1.310393404	3.30E-06
52	Sel1l	20338	1.310393404	0.00037
53	Mmp2	17390	1.310393404	2.50E-05
54	LOC100044124	100044124	1.310393404	0.00022
55	Gadd45g	23882	1.310393404	9.40E-05
56	Col4a1	12826	1.310393404	0.00031
57	Pik3r1	18708	1.301341855	3.00E-04
58	Nav1	215690	1.301341855	6.60E-06
	Nav1	215690	1.248330549	0.0032
59	Frrs1	20321	1.301341855	0.00071
60	Epb4.1l3	13823	1.301341855	0.00011
61	Ak3	56248	1.301341855	0.00041

62	Add3	27360	1.301341855	0.00022
63	Tgfbr1	21812	1.292352831	0.00036
64	Rictor	78757	1.292352831	0.0015
65	Pygb	110078	1.292352831	0.00059
66	Nipbl	71175	1.292352831	0.0035
67	Hsph1	15505	1.292352831	0.0077
68	Gab1	14388	1.292352831	0.00028
69	Sumo2	170930	1.283425898	0.028
70	Sqle	20775	1.283425898	0.0014
	Sqle	20775	1.231144413	0.044
71	Sort1	20661	1.283425898	0.00025
72	Slc24a6	170756	1.283425898	0.00031
73	Rpl18a	76808	1.283425898	0.0027
74	Lrp8	16975	1.283425898	0.00056
75	Lpl	16956	1.283425898	0.00041
76	Loxl1	16949	1.283425898	0.00014
77	LOC100046883	100046883	1.283425898	0.00022
78	Kif1b	16561	1.283425898	0.00055
79	Insig1	231070	1.283425898	0.0032
80	Hsd3b2	15493	1.283425898	0.0036
81	Arl2bp	107566	1.283425898	0.00012
82	2810046L04Rik	212127	1.283425898	2.20E-05
83	Tshz3	243931	1.274560627	3.80E-05
84	Timp2	21858	1.274560627	0.0038
85	Sgcb	24051	1.274560627	0.0042
86	Setd5	72895	1.274560627	0.00081
87	Osr2	107587	1.274560627	0.001
88	L3mbtl3	237339	1.274560627	1.00E-05
89	Gga2	74105	1.274560627	3.80E-05
	Gga2	74105	1.214194884	0.00058
90	Cdk8	264064	1.274560627	0.0036
91	Agfg2	231801	1.274560627	0.00016
92	Zmym2	76007	1.265756594	0.0018
93	Vcp	269523	1.265756594	0.0015
94	Tmsb10	19240	1.265756594	0.0063
	Tmsb10	19240	1.214194884	0.021
95	Stard7	99138	1.265756594	0.00075
96	Scd1	20249	1.265756594	0.0042
97	Plxnd1	67784	1.265756594	2.50E-05
	Plxnd1	67784	1.248330549	1.00E-04
98	Nid2	18074	1.265756594	0.00036
99	Lox	16948	1.265756594	0.00044

100	LOC637711	637711	1.265756594	0.0078
101	LOC100048076	100048076	1.265756594	0.00015
102	Lasp1	16796	1.265756594	0.00064
103	Itga5	16402	1.265756594	1.00E-04
104	Gm10125	791318	1.265756594	0.0018
105	Celf2	14007	1.265756594	0.0068
106	Tmem41a	66664	1.257013375	0.0013
107	Terf1	21749	1.257013375	2.50E-05
108	Tbk1	56480	1.257013375	0.0033
109	Rin2	74030	1.257013375	0.00044
110	Nuak1	77976	1.257013375	5.50E-05
111	Nfat5	54446	1.257013375	6.00E-05
112	Mtf2	17765	1.257013375	0.002
113	Dcaf7	71833	1.257013375	7.80E-06
114	Col1a1	12842	1.257013375	0.022
115	Acot1	26897	1.257013375	0.0037
116	Zfp238	30928	1.248330549	0.0011
117	Tubb2c	227613	1.248330549	0.0098
118	Tmem201	230917	1.248330549	0.00065
119	Suv420h2	232811	1.248330549	0.0011
120	Sesn1	140742	1.248330549	0.0015
121	Sertad4	214791	1.248330549	0.00035
122	Rnase4	58809	1.248330549	0.002
123	Pik3r3	18710	1.248330549	0.0016
124	Pdgfra	18595	1.248330549	0.035
125	Nudt18	213484	1.248330549	3.10E-05
126	Nipal1	70701	1.248330549	1.80E-05
127	Mll3	231051	1.248330549	0.0017
128	Maged1	94275	1.248330549	0.0066
129	Gli3	14634	1.248330549	0.0016
130	E330009J07Rik	243780	1.248330549	7.50E-07
131	Acvr2b	11481	1.248330549	8.30E-05
132	Acat2	110460	1.248330549	0.0062
133	Pdia5	72599	1.2397077	0.0012
134	Lmna	16905	1.2397077	0.0044
	Lmna	16905	1.205807828	0.035
135	Ipo5	70572	1.2397077	0.0016
136	Fdps	110196	1.2397077	1.70E-05
137	Edem2	108687	1.2397077	0.0011
138	Dolk	227697	1.2397077	0.0065
139	Csrp2	13008	1.2397077	0.00023
140	Cramp1l	57354	1.2397077	4.80E-05

141	6330406I15Rik	70717	1.2397077	0.0096
	6330406I15Rik	70717	1.205807828	0.012
142	Zfhx3	11906	1.231144413	0.0036
143	Ube2v1	66589	1.231144413	0.0046
144	Tspo	12257	1.231144413	0.017
145	Tmem65	74868	1.231144413	0.024
146	Tmem2	83921	1.231144413	0.00033
147	Stt3b	68292	1.231144413	0.0083
148	Stard4	170459	1.231144413	0.0073
149	Snx24	69226	1.231144413	0.00076
150	Rpap3	71919	1.231144413	0.00012
151	Rnf145	74315	1.231144413	0.011
152	Rbm12	75710	1.231144413	0.013
153	Psme4	103554	1.231144413	0.0088
154	Ppargc1b	170826	1.231144413	2.30E-06
155	Pmp22	18858	1.231144413	0.0054
	Pmp22	18858	1.222640278	0.031
156	Pgm2	72157	1.231144413	0.019
157	Nfix	18032	1.231144413	9.70E-05
158	Mras	17532	1.231144413	0.00066
159	Mpv17	17527	1.231144413	0.001
160	LOC100048645	100048645	1.231144413	0.0019
161	Hist1h1c	50708	1.231144413	0.00035
162	H3f3a	15078	1.231144413	7.40E-05
163	Gm3308	100041388	1.231144413	0.0073
164	Fgfr2	14183	1.231144413	0.00074
165	Erp29	67397	1.231144413	0.0019
166	Ear4	53877	1.231144413	0.0017
167	Ear3	53876	1.231144413	0.018
168	D19Wsu162e	226178	1.231144413	0.00084
169	Ctnnb1	12387	1.231144413	0.035
170	Ccpg1	72278	1.231144413	0.0042
171	Cav1	12389	1.231144413	0.041
172	Blmh	104184	1.231144413	0.00043
173	Bach1	12013	1.231144413	0.012
174	Acss2	60525	1.231144413	0.00061
175	Acsl3	74205	1.231144413	0.009
176	Znf512b	269401	1.222640278	0.00036
177	St3gal5	20454	1.222640278	0.00088
178	Smg1	233789	1.222640278	0.00034
179	Slc12a6	107723	1.222640278	0.00019
180	Mta3	116871	1.222640278	0.00063

181	Mgst1	56615	1.222640278	0.0029
182	Lrpprc	72416	1.222640278	0.0018
183	Fbxo21	231670	1.222640278	0.0025
184	Endod1	71946	1.222640278	0.011
185	Cd99l2	171486	1.222640278	0.0044
186	Ccdc61	232933	1.222640278	1.80E-05
187	Cars	27267	1.222640278	0.00029
188	Caprin1	53872	1.222640278	0.0078
189	Atp6v0d1	11972	1.222640278	7.00E-04
	Atp6v0d1	11972	1.222640278	0.0029
190	Actn1	109711	1.222640278	0.0013
191	Abca3	27410	1.222640278	0.0018
192	Txndc15	69672	1.214194884	0.0078
193	Tubb5	22154	1.214194884	0.0023
194	Tspan14	52588	1.214194884	0.0046
195	Qdpr	110391	1.214194884	0.017
196	Ptpla	30963	1.214194884	0.01
197	Mpp1	17524	1.214194884	0.029
198	Mfap3	216760	1.214194884	0.00027
199	Mat2b	108645	1.214194884	0.001
200	Kdm6a	22289	1.214194884	0.0043
	Kdm6a	22289	1.214194884	0.0044
201	Glg1	20340	1.214194884	0.0087
202	Fam117b	72750	1.214194884	0.0017
203	Ctdsp2	52468	1.214194884	0.0065
204	Bahcc1	268515	1.214194884	0.00011
205	Adnp	11538	1.214194884	0.0086
206	Zkscan17	268417	1.205807828	0.0079
207	Wipi1	52639	1.205807828	0.01
208	Vdr	22337	1.205807828	0.023
209	Tead2	21677	1.205807828	0.0048
210	Slc1a3	20512	1.205807828	0.0024
211	Sgol2	68549	1.205807828	0.0029
212	Ryk	20187	1.205807828	0.00061
213	Rreb1	68750	1.205807828	0.0053
214	R3hdm1	226412	1.205807828	0.005
215	Prickle3	54630	1.205807828	0.036
216	Prelp	116847	1.205807828	0.0025
217	Plat	18791	1.205807828	0.00086
218	Pex19	19298	1.205807828	0.028
219	Pcdh7	54216	1.205807828	0.00034
220	Papola	18789	1.205807828	2.30E-05

221	Pank2	74450	1.205807828	8.70E-05
222	Ncoa6	56406	1.205807828	0.00012
223	Mysm1	320713	1.205807828	0.0071
224	Mmd	67468	1.205807828	0.0035
225	Mapk11	19094	1.205807828	0.00096
226	LOC100046953	100046953	1.205807828	0.00068
227	LOC100046401	100046401	1.205807828	0.029
228	Kif21a	16564	1.205807828	0.005
229	Ikbkap	230233	1.205807828	0.0034
230	Gsta4	14860	1.205807828	0.0045
231	Grb10	14783	1.205807828	0.0081
232	Gaa	14387	1.205807828	0.013
233	Fam57a	116972	1.205807828	0.00015
234	Fam195b	192173	1.205807828	0.015
235	Eif4enif1	74203	1.205807828	0.0073
236	Dpp3	75221	1.205807828	0.0016
237	Ctdspl	69274	1.205807828	0.00064
238	Bicc1	83675	1.205807828	9.00E-04
239	B4galt3	57370	1.205807828	0.018
240	Arnt	11863	1.205807828	0.0021
241	Ak4	11639	1.205807828	0.00039
242	6430527G18Rik	238330	1.205807828	0.0072

Appendix 4

Appendix 4 A total of 22 genes downregulated in cells transfected with RISC-free siRNAs versus untreated cells. Pja2 is common in the dataset of appendix 2.

	Symbol	EntrezID	Downregulated fold change	P Value
1	Hyi	68180	1.328685814	0.00088
2	Igfbp5	16011	1.274560627	0.032
3	Ptrh1	329384	1.248330549	0.00017
6	Hist1h2bk	319184	1.2397077	0.00012
4	Myg1	60315	1.2397077	0.013
5	Col3a1	12825	1.2397077	0.00059
7	Zfp36l1	12192	1.222640278	0.033
8	Gm2174	100039346	1.214194884	0.04
10	Hist1h2bf	319180	1.214194884	0.021
14	Iglon5	210094	1.214194884	0.00092
13	Ndufaf4	68493	1.214194884	0.00099
9	N6amt2	68043	1.214194884	0.024
12	Rsrc1	66880	1.214194884	0.0056
15	Fth1	14319	1.214194884	0.00092
11	Eef1a1	13627	1.214194884	0.0059
20	LOC100048046	100048046	1.205807828	0.0024
19	Gpr176	381413	1.205807828	0.004
16	Pja2	224938	1.205807828	0.033
17	Kdm6b	216850	1.205807828	0.02
21	Nme7	171567	1.205807828	0.0017
18	Mllt4	17356	1.205807828	0.0067
22	Dyrk1b	13549	1.205807828	0.00054

Appendix 5

Appendix 5 Chimeric reads presenting cellular miRNA-RNA interaction identified by CLASH

Chimeric reads identified in the control (HEK293-PTH-hAGO2 cells)

miRNA	Gene	Unique read
hsa-mir-320a	ENST00000490090.5|BTBD11	2
hsa-mir-766	ENST00000401089.3|SZRD1	1
hsa-mir-766	ENST00000566228.4|SNX29	1
hsa-mir-320a	ENST00000490090.5|BTBD11	3

Chimeric reads identified in mock infection (NIH 3T3-PTH-mAGO2 cells)

miRNA	Gene	Unique reads
MIMAT0000127|miR-29b-3p|microRNA	ENSMUST00000107886|Rgp1-001|protein_coding	1
MIMAT0000127|miR-29b-3p|microRNA	ENSMUST00000121646|Plagl1-001|protein_coding	1
MIMAT0000139|miR-127-3p|microRNA	ENSMUST00000075637|Ptpn3-001|protein_coding	1
MIMAT0000148|miR-136-5p|microRNA	ENSMUST00000027373|Ppm1f-001|protein_coding	1
MIMAT0000157|miR-145a-5p|microRNA	ENSMUST00000177458|Pid1-002|protein_coding	1
MIMAT0000157|miR-145a-5p|microRNA	ENSMUST00000182613|Ano4-009|protein_coding	1
MIMAT0000162|miR-152-3p|microRNA	ENSMUST00000020706|Adcy1-001|protein_coding	1
MIMAT0000533|miR-26a-5p|microRNA	ENSMUST00000047037|Thoc2-001|protein_coding	1
MIMAT0000535|miR-29a-3p|microRNA	ENSMUST00000052332|Abi2-201|protein_coding	1
MIMAT0000537|miR-27a-3p|microRNA	**ENSMUST00000068079|Zfp560-001|protein_coding**	**10**
MIMAT0000537|miR-27a-3p|microRNA	**ENSMUST00000027373|Ppm1f-001|protein_coding**	**1**
MIMAT0000538|miR-31-5p|microRNA	ENSMUST00000027373|Ppm1f-001|protein_coding	2
MIMAT0000538|miR-31-5p|microRNA	ENSMUST00000077689|Ssh1-003|protein_coding	1
MIMAT0000538|miR-31-5p|microRNA	ENSMUST00000025402|Gnal-201|protein_coding	1
MIMAT0000538|miR-31-5p|microRNA	ENSMUST00000034811|Cyp19a1-201|protein_coding	1
MIMAT0000538|miR-31-5p|microRNA	ENSMUST00000027373|Ppm1f-001|protein_coding	1
MIMAT0000545|miR-98-5p|microRNA	ENSMUST00000096433|Deptor-001|protein_coding	1
MIMAT0000546|miR-103-3p|microRNA	ENSMUST00000102759|Stam2-001|protein_coding	4
MIMAT0000647|miR-107-3p|microRNA	ENSMUST00000102759|Stam2-001|protein_coding	1
MIMAT0000651|miR-19a-3p|microRNA	ENSMUST00000035444|Chrm1-001|protein_coding	1
MIMAT0000661|miR-214-3p|microRNA	ENSMUST00000105290|Nr2c1-001|protein_coding	1
MIMAT0000661|miR-214-3p|microRNA	ENSMUST00000056014|Ifne-001|protein_coding	1
MIMAT0000661|miR-214-3p|microRNA	ENSMUST00000035931|Pcdh18-201|protein_coding	1
MIMAT0000661|miR-214-3p|microRNA	ENSMUST00000177451|Foxn3-005|protein_coding	1
MIMAT0000661|miR-214-3p|microRNA	ENSMUST00000092213|Nr2c1-002|protein_coding	3

MIMAT0000666|miR-320-3p|microRNA	ENSMUST00000111702|Sspn-002|protein_coding	1
MIMAT0000670|miR-222-3p|microRNA	ENSMUST00000098473|Cnot1-202|protein_coding	1
MIMAT0000740|miR-376a-3p|microRNA	ENSMUST00000072061|Entpd5-202|protein_coding	1
MIMAT0000740|miR-376a-3p|microRNA	ENSMUST00000182613|Ano4-009|protein_coding	1
MIMAT0003732|miR-668-3p|microRNA	ENSMUST00000037099|Clic4-001|protein_coding	1
MIMAT0004522|miR-27b-5p|microRNA	ENSMUST00000182625|Sox12-002|protein_coding	1
MIMAT0004582|miR-106b-3p|microRNA	ENSMUST00000181320|NLRP12-201|protein_coding	1
MIMAT0004667|miR-199b-3p|microRNA	ENSMUST00000064444|Maneal-001|protein_coding	1
MIMAT0017243|miR-669a-3p|microRNA	ENSMUST00000103145|E2f1-001|protein_coding	1
MIMAT0017347|miR-669o-3p|microRNA	ENSMUST00000091458|Nr2f1-001|protein_coding	1
MIMAT0031418|miR-8112|microRNA	ENSMUST00000035037|Pik3cb-001|protein_coding	1

Chimeric reads identified in cells infected with wild type MCMV (NIH 3T3-PTH-mAGO2 cells)

miRNA	Gene	Unique reads
MIMAT0000125|miR-23b-3p|microRNA	ENSMUST00000031227|Zfp326-001|protein_coding	1
MIMAT0000125|miR-23b-3p|microRNA	ENSMUST00000119824|1700016H13Rik-002|protein_coding	2
MIMAT0000126|miR-27b-3p|microRNA	ENSMUST00000085108|Foxn3-201|protein_coding	1
MIMAT0000127|miR-29b-3p|microRNA	ENSMUST00000121646|Plagl1-001|protein_coding	1
MIMAT0000132|miR-99b-5p|microRNA	ENSMUST00000025595|Fam111a-201|protein_coding	1
MIMAT0000132|miR-99b-5p|microRNA	ENSMUST00000096363|Tmem28-001|protein_coding	1
MIMAT0000133|miR-101a-3p|microRNA	ENSMUST00000182613|Ano4-009|protein_coding	1
MIMAT0000135|miR-125a-5p|microRNA	ENSMUST00000038863|Lars2-201|protein_coding	2
MIMAT0000135|miR-125a-5p|microRNA	ENSMUST00000042852|Fam210a-001|protein_coding	1
MIMAT0000136|miR-125b-5p|microRNA	ENSMUST00000020706|Adcy1-001|protein_coding	1
MIMAT0000136|miR-125b-5p|microRNA	ENSMUST00000163300|Arf1-201|protein_coding	1
MIMAT0000136|miR-125b-5p|microRNA	ENSMUST00000075637|Ptpn3-001|protein_coding	1
MIMAT0000136|miR-125b-5p|microRNA	ENSMUST00000141468|Atp11b-005|protein_coding	1
MIMAT0000152|miR-140-3p|microRNA	ENSMUST00000020699|Gatsl3-001|protein_coding	2
MIMAT0000152|miR-140-3p|microRNA	ENSMUST00000015234|Ptgds-004|protein_coding	1
MIMAT0000157|miR-145a-5p|microRNA	ENSMUST00000033088|Rnf40-201|protein_coding	1
MIMAT0000159|miR-149-5p|microRNA	ENSMUST00000033088|Rnf40-201|protein_coding	1
MIMAT0000165|miR-155-5p|microRNA	ENSMUST00000093271|Gpr56-201|protein_coding	1
MIMAT0000211|miR-182-5p|microRNA	ENSMUST00000033088|Rnf40-201|protein_coding	1
MIMAT0000219|miR-24-3p|microRNA	ENSMUST00000027373|Ppm1f-001|protein_coding	1
MIMAT0000229|miR-199a-5p|microRNA	ENSMUST00000022148|Mccc2-201|protein_coding	1
MIMAT0000376|miR-298-5p|microRNA	ENSMUST00000098110|AA474408-201|protein_coding	3
MIMAT0000381|miR-34c-5p|microRNA	ENSMUST00000098473|Cnot1-202|protein_coding	1
MIMAT0000514|miR-30c-5p|microRNA	ENSMUST00000038381|Lats2-005|protein_coding	1

MIMAT0000515|miR-30d-5p|microRNA	ENSMUST00000095141|Prdm13-201|protein_coding	1
MIMAT0000532|miR-23a-3p|microRNA	ENSMUST00000033088|Rnf40-201|protein_coding	1
MIMAT0000532|miR-23a-3p|microRNA	ENSMUST00000022304|Thrb-001|protein_coding	1
MIMAT0000533|miR-26a-5p|microRNA	ENSMUST00000119665|Ccdc33-007|protein_coding	1
MIMAT0000535|miR-29a-3p|microRNA	ENSMUST00000182341|Ano4-001|protein_coding	1
MIMAT0000538|miR-31-5p|microRNA	ENSMUST00000111920|Plekha3-001|protein_coding	2
MIMAT0000545|miR-98-5p|microRNA	ENSMUST00000182047|Rnf4-006|protein_coding	3
MIMAT0000545|miR-98-5p|microRNA	ENSMUST00000113614|Gpr111-001|protein_coding	1
MIMAT0000556|miR-324-3p|microRNA	ENSMUST00000106223|1810043H04Rik-001|protein_coding	1
MIMAT0000661|miR-214-3p|microRNA	ENSMUST00000036541|Arl5a-001|protein_coding	1
MIMAT0000661|miR-214-3p|microRNA	ENSMUST00000182790|Ano4-010|protein_coding	2
MIMAT0000661|miR-214-3p|microRNA	ENSMUST00000110090|Rab3a-003|protein_coding	1
MIMAT0000661|miR-214-3p|microRNA	ENSMUST00000038863|Lars2-201|protein_coding	1
MIMAT0000661|miR-214-3p|microRNA	ENSMUST00000036541|Arl5a-001|protein_coding	1
MIMAT0000661|miR-214-3p|microRNA	ENSMUST00000176572|Vmn1r25-001|protein_coding	1
MIMAT0000661|miR-214-3p|microRNA	ENSMUST00000060896|Col6a6-201|protein_coding	2
MIMAT0000661|miR-214-3p|microRNA	ENSMUST00000023123|Col2a1-001|protein_coding	1
MIMAT0000661|miR-214-3p|microRNA	ENSMUST00000098110|AA474408-201|protein_coding	1
MIMAT0000661|miR-214-3p|microRNA	ENSMUST00000060896|Col6a6-201|protein_coding	1
MIMAT0000661|miR-214-3p|microRNA	ENSMUST00000118317|Hipk1-001|protein_coding	1
MIMAT0000661|miR-214-3p|microRNA	ENSMUST00000039271|2610008E11Rik-001|protein_coding	1
MIMAT0000661|miR-214-3p|microRNA	ENSMUST00000036541|Arl5a-001|protein_coding	1
MIMAT0000661|miR-214-3p|microRNA	ENSMUST00000098441|Col6a6-202|protein_coding	1
MIMAT0000663|miR-218-5p|microRNA	ENSMUST00000033088|Rnf40-201|protein_coding	1
MIMAT0000663|miR-218-5p|microRNA	ENSMUST00000050544|Has2-001|protein_coding	1
MIMAT0000670|miR-222-3p|microRNA	ENSMUST00000172281|Gpaa1-002|protein_coding	2
MIMAT0000670|miR-222-3p|microRNA	ENSMUST00000057977|A730049H05Rik-001|protein_coding	1
MIMAT0000670|miR-222-3p|microRNA	ENSMUST00000113824|Clpx-201|protein_coding	1
MIMAT0000672|miR-199b-5p|microRNA	ENSMUST00000027373|Ppm1f-001|protein_coding	1
MIMAT0000740|miR-376a-3p|microRNA	ENSMUST00000027373|Ppm1f-001|protein_coding	2
MIMAT0003182|miR-494-3p|microRNA	ENSMUST00000044165|Itga9-001|protein_coding	1
MIMAT0003454|miR-423-3p|microRNA	ENSMUST00000006181|Napa-001|protein_coding	5
MIMAT0003485|miR-455-5p|microRNA	ENSMUST00000107815|Aldh16a1-002|protein_coding	1
MIMAT0003508|miR-501-5p|microRNA	ENSMUST00000043204|Fbxo33-001|protein_coding	5
MIMAT0004667|miR-199b-3p|microRNA	ENSMUST00000045652|Btbd7-201|protein_coding	1
MIMAT0004825|miR-423-5p|microRNA	ENSMUST00000098586|Sdhaf1-001|protein_coding	6
MIMAT0004894|miR-574-3p|microRNA	ENSMUST00000107479|Rapgefl1-001|protein_coding	1
MIMAT0004894|miR-574-3p|microRNA	ENSMUST00000014263|Ugt1a6a-001|protein_coding	1
MIMAT0017243|miR-669a-3p|microRNA	ENSMUST00000105687|Tmem201-001|protein_coding	1
MIMAT0017347|miR-669o-3p|microRNA	ENSMUST00000115816|Celf4-202|protein_coding	1
MIMAT0017347|miR-669o-3p|microRNA	ENSMUST00000107479|Rapgefl1-001|protein_coding	1
MIMAT0017347|miR-669o-3p|microRNA	ENSMUST00000045557|Slc7a5-001|protein_coding	1

MIMAT0017347|miR-669o-3p|microRNA	ENSMUST00000107479|Rapgefl1-001|protein_coding	1
MIMAT0019340|miR-3962|microRNA	ENSMUST00000038863|Lars2-201|protein_coding	1
MIMAT0020607|miR-5100|microRNA	ENSMUST00000021689|Evl-201|protein_coding	2

Chimeric reads identified in cells infected with MCMV Δm169 (NIH 3T3-PTH-mAGO2 cells)

miRNA	Gene	Unique read
MIMAT0000527|miR-16-5p|microRNA	ENSMUST00000034325|Lpar2-201|protein_coding	1
MIMAT0000531|miR-22-3p|microRNA	ENSMUST00000058286|Rps6kb1-002|protein_coding	1
MIMAT0000538|miR-31-5p|microRNA	ENSMUST00000003438|Mob3a-201|protein_coding	1
MIMAT0000670|miR-222-3p|microRNA	ENSMUST00000058039|Vmn1r54-001|protein_coding	1
MIMAT0004187|miR-744-5p|microRNA	ENSMUST00000093196|Hmgb1-002|protein_coding	1
MIMAT0004536|miR-151-5p|microRNA	ENSMUST00000069718|Fto-001|protein_coding	1
MIMAT0020607|miR-5100|microRNA	ENSMUST00000077735|Evl-202|protein_coding	1

References

Ahluwalia, J.K., Khan, S.Z., Soni, K., Rawat, P., Gupta, A., Hariharan, M., Scaria, V., Lalwani, M., Pillai, B., Mitra, D., and Brahmachari, S.K. (2008). Human cellular microRNA hsa-miR-29a interferes with viral nef protein expression and HIV-1 replication. Retrovirology *5*, 117.

Akiyama, S.K., Olden, K., and Yamada, K.M. (1995). Fibronectin and integrins in invasion and metastasis. Cancer Metastasis Rev *14*, 173-189.

Alexopoulou, A.N., Couchman, J.R., and Whiteford, J.R. (2008). The CMV early enhancer/chicken beta actin (CAG) promoter can be used to drive transgene expression during the differentiation of murine embryonic stem cells into vascular progenitors. BMC Cell Biol *9*, 2.

Amen, M.A., and Griffiths, A. (2011). Packaging of Non-Coding RNAs into Herpesvirus Virions: Comparisons to Coding RNAs. Front Genet *2*, 81.

Ameres, S.L., Martinez, J., and Schroeder, R. (2007). Molecular basis for target RNA recognition and cleavage by human RISC. Cell *130*, 101-112.

Ameres, S.L., and Zamore, P.D. (2013). Diversifying microRNA sequence and function. Nat Rev Mol Cell Biol *14*, 475-488.

Angulo, A., Chandraratna, R.A., LeBlanc, J.F., and Ghazal, P. (1998). Ligand induction of retinoic acid receptors alters an acute infection by murine cytomegalovirus. J Virol *72*, 4589-4600.

Angulo, A., Ghazal, P., and Messerle, M. (2000). The major immediate-early gene ie3 of mouse cytomegalovirus is essential for viral growth. J Virol *74*, 11129-11136.

Arvin, A., Campadelli-Fiume, G., Mocarski, E., Moore, P.S., Roizman, B., Whitley, R., and K, Y. (2007). Human Herpesviruses (Cambridge University Press).

Arvin, A.M., Fast, P., Myers, M., Plotkin, S., and Rabinovich, R. (2004). Vaccine development to prevent cytomegalovirus disease: report from the National Vaccine Advisory Committee. Clin Infect Dis *39*, 233-239.

Babiarz, J.E., Hsu, R., Melton, C., Thomas, M., Ullian, E.M., and Blelloch, R. (2011). A role for noncanonical microRNAs in the mammalian brain revealed by phenotypic differences in Dgcr8 versus Dicer1 knockouts and small RNA sequencing. Rna *17*, 1489-1501.

Bankier, A.T., Beck, S., Bohni, R., Brown, C.M., Cerny, R., Chee, M.S., Hutchison, C.A., 3rd, Kouzarides, T., Martignetti, J.A., Preddie, E., and et al. (1991). The DNA sequence of the human cytomegalovirus genome. DNA Seq *2*, 1-12.

Bartel, D.P. (2004). MicroRNAs: genomics, biogenesis, mechanism, and function. Cell *116*, 281-297.

Bartel, D.P. (2009). MicroRNAs: target recognition and regulatory functions. Cell *136*, 215-233.

Bazzini, A.A., Lee, M.T., and Giraldez, A.J. (2012). Ribosome Profiling Shows That miR-430 Reduces Translation Before Causing mRNA Decay in Zebrafish. Science *336*, 233-237.

Behm-Ansmant, I., Rehwinkel, J., Doerks, T., Stark, A., Bork, P., and Izaurralde, E. (2006). mRNA degradation by miRNAs and GW182 requires both CCR4:NOT deadenylase and DCP1:DCP2 decapping complexes. Genes & development *20*, 1885-1898.

Ben-Ami, O., Pencovich, N., Lotem, J., Levanon, D., and Groner, Y. (2009). A regulatory interplay between miR-27a and Runx1 during megakaryopoiesis. Proc Natl Acad Sci U S A *106*, 238-243.

Berezikov, E., Chung, W.J., Willis, J., Cuppen, E., and Lai, E.C. (2007). Mammalian mirtron genes. Mol Cell *28*, 328-336.

Bethune, J., Artus-Revel, C.G., and Filipowicz, W. (2012). Kinetic analysis reveals successive steps leading to miRNA-mediated silencing in mammalian cells. EMBO Rep *13*, 716-723.

Biswas, N., Sanchez, V., and Spector, D.H. (2003). Human cytomegalovirus infection leads to accumulation of geminin and inhibition of the licensing of cellular DNA replication. J Virol *77*, 2369-2376.

Blanc, M., Hsieh, W.Y., Robertson, K.A., Watterson, S., Shui, G., Lacaze, P., Khondoker, M., Dickinson, P., Sing, G., Rodriguez-Martin, S.*, et al.* (2011). Host defense against viral infection involves interferon mediated down-regulation of sterol biosynthesis. PLoS Biol *9*, e1000598.

Bodaghi, B., Slobbe-van Drunen, M.E., Topilko, A., Perret, E., Vossen, R.C., van Dam-Mieras, M.C., Zipeto, D., Virelizier, J.L., LeHoang, P., Bruggeman, C.A., and Michelson, S. (1999). Entry of human cytomegalovirus into retinal pigment epithelial and endothelial cells by endocytosis. Invest Ophthalmol Vis Sci *40*, 2598-2607.

Boeckh, M., and Geballe, A.P. (2011). Cytomegalovirus: pathogen, paradigm, and puzzle. J Clin Invest *121*, 1673-1680.

Bonin, L.R., and McDougall, J.K. (1997). Human cytomegalovirus IE2 86-kilodalton protein binds p53 but does not abrogate G1 checkpoint function. J Virol *71*, 5861-5870.

Borchert, G.M., Lanier, W., and Davidson, B.L. (2006). RNA polymerase III transcribes human microRNAs. Nat Struct Mol Biol *13*, 1097-1101.

Bracken, C.P., Szubert, J.M., Mercer, T.R., Dinger, M.E., Thomson, D.W., Mattick, J.S., Michael, M.Z., and Goodall, G.J. (2011). Global analysis of the mammalian RNA degradome reveals widespread miRNA-dependent and miRNA-independent endonucleolytic cleavage. Nucleic Acids Res *39*, 5658-5668.

Braun, J.E., Huntzinger, E., Fauser, M., and Izaurralde, E. (2011). GW182 proteins directly recruit cytoplasmic deadenylase complexes to miRNA targets. Mol Cell *44*, 120-133.

Bresnahan, W.A., Boldogh, I., Chi, P., Thompson, E.A., and Albrecht, T. (1997). Inhibition of cellular Cdk2 activity blocks human cytomegalovirus replication. Virology *231*, 239-247.

Bresnahan, W.A., Boldogh, I., Thompson, E.A., and Albrecht, T. (1996). Human cytomegalovirus inhibits cellular DNA synthesis and arrests productively infected cells in late G1. Virology *224*, 150-160.

Brocchieri, L., Kledal, T.N., Karlin, S., and Mocarski, E.S. (2005). Predicting coding potential from genome sequence: application to betaherpesviruses infecting rats and mice. J Virol *79*, 7570-7596.

Buck, A.H., Perot, J., Chisholm, M.A., Kumar, D.S., Tuddenham, L., Cognat, V., Marcinowski, L., Dolken, L., and Pfeffer, S. (2010). Post-transcriptional regulation of miR-27 in murine cytomegalovirus infection. Rna *16*, 307-315.

Buggele, W.A., and Horvath, C.M. (2013). MicroRNA profiling of Sendai virus-infected A549 cells identifies miR-203 as an interferon-inducible regulator of IFIT1/ISG56. J Virol *87*, 9260-9270.

Burroughs, A.M., Ando, Y., de Hoon, M.J., Tomaru, Y., Suzuki, H., Hayashizaki, Y., and Daub, C.O. (2011). Deep-sequencing of human Argonaute-associated small RNAs provides insight into miRNA sorting and reveals Argonaute association with RNA fragments of diverse origin. RNA Biol *8*, 158-177.

Cai, X., Hagedorn, C.H., and Cullen, B.R. (2004). Human microRNAs are processed from capped, polyadenylated transcripts that can also function as mRNAs. Rna *10*, 1957-1966.

Cargnello, M., and Roux, P.P. (2011). Activation and function of the MAPKs and their substrates, the MAPK-activated protein kinases. Microbiol Mol Biol Rev *75*, 50-83.

Castilla-Llorente, V., Nicastro, G., and Ramos, A. (2013). Terminal loop-mediated regulation of miRNA biogenesis: selectivity and mechanisms. Biochem Soc Trans *41*, 861-865.

Castillo, J.P., and Kowalik, T.F. (2004). HCMV infection: modulating the cell cycle and cell death. Int Rev Immunol *23*, 113-139.

Cazalla, D., Yario, T., and Steitz, J.A. (2010). Down-regulation of a host microRNA by a Herpesvirus saimiri noncoding RNA. Science *328*, 1563-1566.

Cha, T.A.T., E.; Kemble, G.W.; Duke, G.M.; Mocarski, E.S.; Spaete, R.R. (1996). Human cytomegalovirus clinical isolates carry at least 19 genes not found in laboratory strains. J. Virol. *70*, 78–83.

Chaisson, R.E., Gallant, J.E., Keruly, J.C., and Moore, R.D. (1998). Impact of opportunistic disease on survival in patients with HIV infection. AIDS *12*, 29-33.

Chan, G., Nogalski, M.T., and Yurochko, A.D. (2012). Human cytomegalovirus stimulates monocyte-to-macrophage differentiation via the temporal regulation of caspase 3. J Virol *86*, 10714-10723.

Chang, W.L., Barry, P.A., Szubin, R., Wang, D., and Baumgarth, N. (2009). Human cytomegalovirus suppresses type I interferon secretion by plasmacytoid dendritic cells through its interleukin 10 homolog. Virology *390*, 330-337.

Chee, M.S., Bankier, A.T., Beck, S., Bohni, R., Brown, C.M., Cerny, R., Horsnell, T., Hutchison, C.A., 3rd, Kouzarides, T., Martignetti, J.A., and et al. (1990). Analysis of the protein-coding content of the sequence of human cytomegalovirus strain AD169. Curr Top Microbiol Immunol *154*, 125-169.

Chekulaeva, M., Mathys, H., Zipprich, J.T., Attig, J., Colic, M., Parker, R., and Filipowicz, W. (2011). miRNA repression involves GW182-mediated recruitment of CCR4-NOT through conserved W-containing motifs. Nat Struct Mol Biol *18*, 1218-1226.

Chen, F., Li, Y., Wang, L., and Hu, L. (2011). Knockdown of BMI-1 causes cell-cycle arrest and derepresses p16INK4a, HOXA9 and HOXC13 mRNA expression in HeLa cells. Med Oncol *28*, 1201-1209.

Chen, W.J., Yin, K., Zhao, G.J., Fu, Y.C., and Tang, C.K. (2012). The magic and mystery of microRNA-27 in atherosclerosis. Atherosclerosis *222*, 314-323.

Chendrimada, T.P., Finn, K.J., Ji, X.J., Baillat, D., Gregory, R.I., Liebhaber, S.A., Pasquinelli, A.E., and Shiekhattar, R. (2007). MicroRNA silencing through RISC recruitment of eIF6. Nature *447*, 823-U821.

Cheung, T.W., and Teich, S.A. (1999). Cytomegalovirus infection in patients with HIV infection. Mt Sinai J Med *66*, 113-124.

Chhabra, R., Adlakha, Y.K., Hariharan, M., Scaria, V., and Saini, N. (2009). Upregulation of miR-23a-27a-24-2 cluster induces caspase-dependent and -independent apoptosis in human embryonic kidney cells. PLoS One *4*, e5848.

Chhabra, R., Dubey, R., and Saini, N. (2010). Cooperative and individualistic functions of the microRNAs in the miR-23a~27a~24-2 cluster and its implication in human diseases. Mol Cancer *9*, 232.

Chin, D., and Means, A.R. (2000). Calmodulin: a prototypical calcium sensor. Trends Cell Biol *10*, 322-328.

Choi, J., and Husain, M. (2006). Calmodulin-mediated cell cycle regulation - New mechanisms for old observations. Cell Cycle *5*, 2183-2186.

Cobbs, C.S., Harkins, L., Samanta, M., Gillespie, G.Y., Bharara, S., King, P.H., Nabors, L.B., Cobbs, C.G., and Britt, W.J. (2002). Human cytomegalovirus infection and expression in human malignant glioma. Cancer Res *62*, 3347-3350.

Compton, T., Nowlin, D.M., and Cooper, N.R. (1993). Initiation of human cytomegalovirus infection requires initial interaction with cell surface heparan sulfate. Virology *193*, 834-841.

Conti, C., Cirone, M., Sgro, R., Altieri, F., Zompetta, C., and Faggioni, A. (2000). Early interactions of human herpesvirus 6 with lymphoid cells: role of membrane protein components and glycosaminoglycans in virus binding. J Med Virol *62*, 487-497.

Cooper, P.D. (1961). The plaque assay of animal viruses. Adv Virus Res *8*, 319-378.

Couper, K.N., Blount, D.G., and Riley, E.M. (2008). IL-10: the master regulator of immunity to infection. J Immunol *180*, 5771-5777.

Cuenda, A., and Rousseau, S. (2007). p38 MAP-kinases pathway regulation, function and role in human diseases. Biochim Biophys Acta *1773*, 1358-1375.

Czech, B., and Hannon, G.J. (2011). Small RNA sorting: matchmaking for Argonautes. Nat Rev Genet *12*, 19-31.

Da Sacco, L., and Masotti, A. (2012). Recent insights and novel bioinformatics tools to understand the role of microRNAs binding to 5' untranslated region. Int J Mol Sci *14*, 480-495.

Das, A.T., Brummelkamp, T.R., Westerhout, E.M., Vink, M., Madiredjo, M., Bernards, R., and Berkhout, B. (2004). Human immunodeficiency virus type 1 escapes from RNA interference-mediated inhibition. J Virol *78*, 2601-2605.

Davison, A.J., Dolan, A., Akter, P., Addison, C., Dargan, D.J., Alcendor, D.J., McGeoch, D.J., and Hayward, G.S. (2003). The human cytomegalovirus genome

revisited: comparison with the chimpanzee cytomegalovirus genome. J Gen Virol *84*, 17-28.

De, A.K., Kodys, K.M., Yeh, B.S., and Miller-Graziano, C. (2000). Exaggerated human monocyte IL-10 concomitant to minimal TNF-alpha induction by heat-shock protein 27 (Hsp27) suggests Hsp27 is primarily an antiinflammatory stimulus. J Immunol *165*, 3951-3958.

Demmler, G.J. (1996). Congenital cytomegalovirus infection and disease. Adv Pediatr Infect Dis *11*, 135-162.

Dhar, D., Mapa, K., Pudi, R., Srinivasan, P., Bodhinathan, K., and Das, S. (2006). Human ribosomal protein L18a interacts with hepatitis C virus internal ribosome entry site. Arch Virol *151*, 509-524.

Dhillon, A.S., Hagan, S., Rath, O., and Kolch, W. (2007). MAP kinase signalling pathways in cancer. Oncogene *26*, 3279-3290.

Ding, X.C., and Grosshans, H. (2009). Repression of C. elegans microRNA targets at the initiation level of translation requires GW182 proteins. Embo J *28*, 213-222.

Dittmer, D., and Mocarski, E.S. (1997). Human cytomegalovirus infection inhibits G1/S transition. J Virol *71*, 1629-1634.

Djuranovic, S., Nahvi, A., and Green, R. (2012). miRNA-Mediated Gene Silencing by Translational Repression Followed by mRNA Deadenylation and Decay. Science *336*, 237-240.

Domanski, M., Molloy, K., Jiang, H., Chait, B.T., Rout, M.P., Jensen, T.H., and LaCava, J. (2012). Improved methodology for the affinity isolation of human protein complexes expressed at near endogenous levels. Biotechniques *0*, 1-6.

Dudzinski, D.M., Igarashi, J., Greif, D., and Michel, T. (2006). The regulation and pharmacology of endothelial nitric oxide synthase. Annu Rev Pharmacol Toxicol *46*, 235-276.

Dudzinski, D.M., and Michel, T. (2007). Life history of eNOS: partners and pathways. Cardiovasc Res *75*, 247-260.

Ensser, A., and Fleckenstein, B. (2005). T-cell transformation and oncogenesis by gamma2-herpesviruses. Adv Cancer Res *93*, 91-128.

Fabian, M.R., Sonenberg, N., and Filipowicz, W. (2010). Regulation of mRNA translation and stability by microRNAs. Annu Rev Biochem *79*, 351-379.

Fang, K., Fu, W., Beardsley, A.R., Sun, X., Lisanti, M.P., and Liu, J. (2007). Overexpression of caveolin-1 inhibits endothelial cell proliferation by arresting the cell cycle at G0/G1 phase. Cell Cycle *6*, 199-204.

Faust, D., Schmitt, C., Oesch, F., Oesch-Bartlomowicz, B., Schreck, I., Weiss, C., and Dietrich, C. (2012). Differential p38-dependent signalling in response to cellular stress and mitogenic stimulation in fibroblasts. Cell Commun Signal *10*, 6.

Feng, J., Iwama, A., Satake, M., and Kohu, K. (2009). MicroRNA-27 enhances differentiation of myeloblasts into granulocytes by post-transcriptionally downregulating Runx1. Br J Haematol *145*, 412-423.

Filen, S., Ylikoski, E., Tripathi, S., West, A., Bjorkman, M., Nystrom, J., Ahlfors, H., Coffey, E., Rao, K.V.S., Rasool, O., and Lahesmaa, R. (2010). Activating Transcription Factor 3 Is a Positive Regulator of Human IFNG Gene Expression. J Immunol *184*, 4990-4999.

Flemington, E.K. (2001). Herpesvirus lytic replication and the cell cycle: arresting new developments. J Virol *75*, 4475-4481.

Friedman, R.C., Farh, K.K.H., Burge, C.B., and Bartel, D.P. (2009). Most mammalian mRNAs are conserved targets of microRNAs. Genome Res *19*, 92-105.

Galbiati, F., Volonte, D., Liu, J., Capozza, F., Frank, P.G., Zhu, L., Pestell, R.G., and Lisanti, M.P. (2001). Caveolin-1 expression negatively regulates cell cycle

progression by inducing G(0)/G(1) arrest via a p53/p21(WAF1/Cip1)-dependent mechanism. Mol Biol Cell *12*, 2229-2244.

Ghosh, Z., Mallick, B., and Chakrabarti, J. (2009). Cellular versus viral microRNAs in host-virus interaction. Nucleic Acids Res *37*, 1035-1048.

Giono, L.E., and Manfredi, J.J. (2006). The p53 tumor suppressor participates in multiple cell cycle checkpoints. J Cell Physiol *209*, 13-20.

Giraldez, A.J., Mishima, Y., Rihel, J., Grocock, R.J., Van Dongen, S., Inoue, K., Enright, A.J., and Schier, A.F. (2006). Zebrafish MiR-430 promotes deadenylation and clearance of maternal mRNAs. Science *312*, 75-79.

Golias, C.H., Charalabopoulos, A., and Charalabopoulos, K. (2004). Cell proliferation and cell cycle control: a mini review. Int J Clin Pract *58*, 1134-1141.

Gonzalez-Gonzalez, E., Lopez-Casas, P.P., and del Mazo, J. (2008). The expression patterns of genes involved in the RNAi pathways are tissue-dependent and differ in the germ and somatic cells of mouse testis. Biochim Biophys Acta *1779*, 306-311.

Gorry, P.R., McPhee, D.A., Verity, E., Dyer, W.B., Wesselingh, S.L., Learmont, J., Sullivan, J.S., Roche, M., Zaunders, J.J., Gabuzda, D.*, et al.* (2007). Pathogenicity and immunogenicity of attenuated, nef-deleted HIV-1 strains in vivo. Retrovirology *4*, 66.

Gottardo, F., Liu, C.G., Ferracin, M., Calin, G.A., Fassan, M., Bassi, P., Sevignani, C., Byrne, D., Negrini, M., Pagano, F.*, et al.* (2007). Micro-RNA profiling in kidney and bladder cancers. Urol Oncol *25*, 387-392.

Grassmann, R., and Jeang, K.T. (2008). The roles of microRNAs in mammalian virus infection. Biochim Biophys Acta *1779*, 706-711.

Gray, M.C., and Hewlett, E.L. (2011). Cell cycle arrest induced by the bacterial adenylate cyclase toxins from Bacillus anthracis and Bordetella pertussis. Cell Microbiol *13*, 123-134.

Greaves, R.F., and Mocarski, E.S. (1998). Defective growth correlates with reduced accumulation of a viral DNA replication protein after low-multiplicity infection by a human cytomegalovirus ie1 mutant. J Virol *72*, 366-379.

Griffiths-Jones, S., Saini, H.K., van Dongen, S., and Enright, A.J. (2008). miRBase: tools for microRNA genomics. Nucleic Acids Res *36*, D154-158.

Guo, H., Ingolia, N.T., Weissman, J.S., and Bartel, D.P. (2010). Mammalian microRNAs predominantly act to decrease target mRNA levels. Nature *466*, 835-840.

Guo, Y.E., Riley, K.J., Iwasaki, A., and Steitz, J.A. (2014). Alternative capture of noncoding RNAs or protein-coding genes by herpesviruses to alter host T cell function. Mol Cell *54*, 67-79.

Guttilla, I.K., and White, B.A. (2009). Coordinate regulation of FOXO1 by miR-27a, miR-96, and miR-182 in breast cancer cells. J Biol Chem *284*, 23204-23216.

Ha, M., and Kim, V.N. (2014). Regulation of microRNA biogenesis. Nat Rev Mol Cell Biol *15*, 509-524.

Haase, A.D., Jaskiewicz, L., Zhang, H., Laine, S., Sack, R., Gatignol, A., and Filipowicz, W. (2005). TRBP, a regulator of cellular PKR and HIV-1 virus expression, interacts with Dicer and functions in RNA silencing. EMBO Rep *6*, 961-967.

Hagemeier, C., Caswell, R., Hayhurst, G., Sinclair, J., and Kouzarides, T. (1994). Functional Interaction between the Hcmv Ie2 Transactivator and the Retinoblastoma Protein. Embo Journal *13*, 2897-2903.

Han, J., Lee, Y., Yeom, K.H., Kim, Y.K., Jin, H., and Kim, V.N. (2004). The Drosha-DGCR8 complex in primary microRNA processing. Genes & development *18*, 3016-3027.

Han, J., Lee, Y., Yeom, K.H., Nam, J.W., Heo, I., Rhee, J.K., Sohn, S.Y., Cho, Y., Zhang, B.T., and Kim, V.N. (2006). Molecular basis for the recognition of primary microRNAs by the Drosha-DGCR8 complex. Cell *125*, 887-901.

Hannus, M., Beitzinger, M., Engelmann, J.C., Weickert, M.T., Spang, R., Hannus, S., and Meister, G. (2014). siPools: highly complex but accurately defined siRNA pools eliminate off-target effects. Nucleic Acids Res *42*, 8049-8061.

Hausser, J., Syed, A.P., Selevsek, N., van Nimwegen, E., Jaskiewicz, L., Aebersold, R., and Zavolan, M. (2013). Timescales and bottlenecks in miRNA-dependent gene regulation. Mol Syst Biol *9*, 711.

Hausser, J., and Zavolan, M. (2014). Identification and consequences of miRNA-target interactions--beyond repression of gene expression. Nat Rev Genet *15*, 599-612.

Hayashi, M.L., Blankenship, C., and Shenk, T. (2000). Human cytomegalovirus UL69 protein is required for efficient accumulation of infected cells in the G1 phase of the cell cycle. Proc Natl Acad Sci U S A *97*, 2692-2696.

Hayer, A., Stoeber, M., Ritz, D., Engel, S., Meyer, H.H., and Helenius, A. (2010). Caveolin-1 is ubiquitinated and targeted to intralumenal vesicles in endolysosomes for degradation. J Cell Biol *191*, 615-629.

Hayhurst, G.P., Bryant, L.A., Caswell, R.C., Walker, S.M., and Sinclair, J.H. (1995). CCAAT box-dependent activation of the TATA-less human DNA polymerase alpha promoter by the human cytomegalovirus 72-kilodalton major immediate-early protein. J Virol *69*, 182-188.

He, L., and Hannon, G.J. (2004). MicroRNAs: small RNAs with a big role in gene regulation. Nat Rev Genet *5*, 522-531.

Helwak, A., Kudla, G., Dudnakova, T., and Tollervey, D. (2013). Mapping the human miRNA interactome by CLASH reveals frequent noncanonical binding. Cell *153*, 654-665.

Helwak, A., and Tollervey, D. (2014). Mapping the miRNA interactome by cross-linking ligation and sequencing of hybrids (CLASH). Nat Protoc *9*, 711-728.

Henley, S.A., and Dick, F.A. (2012). The retinoblastoma family of proteins and their regulatory functions in the mammalian cell division cycle. Cell Div *7*, 10.

Herbein, G., and Kumar, A. (2014). The oncogenic potential of human cytomegalovirus and breast cancer. Front Oncol *4*, 230.

Hertel, L., and Mocarski, E.S. (2004). Global analysis of host cell gene expression late during cytomegalovirus infection reveals extensive dysregulation of cell cycle gene expression and induction of Pseudomitosis independent of US28 function. J Virol *78*, 11988-12011.

Hodinka, R.L. (2007). Human Cytomegalovirus. In Manual of clinical microbiology, P.R. Murray, ed. (Washington, D.C.: ASM Press), pp. 1549-1563.

Huang, J., Wang, F., Argyris, E., Chen, K., Liang, Z., Tian, H., Huang, W., Squires, K., Verlinghieri, G., and Zhang, H. (2007). Cellular microRNAs contribute to HIV-1 latency in resting primary CD4+ T lymphocytes. Nat Med *13*, 1241-1247.

Humphreys, D.T., Westman, B.J., Martin, D.I., and Preiss, T. (2005). MicroRNAs control translation initiation by inhibiting eukaryotic initiation factor 4E/cap and poly(A) tail function. Proc Natl Acad Sci U S A *102*, 16961-16966.

Humphreys, I.R., de Trez, C., Kinkade, A., Benedict, C.A., Croft, M., and Ware, C.F. (2007). Cytomegalovirus exploits IL-10-mediated immune regulation in the salivary glands. J Exp Med *204*, 1217-1225.

Huntzinger, E., and Izaurralde, E. (2011a). Gene silencing by microRNAs: contributions of translational repression and mRNA decay. Nat Rev Genet *12*, 99-110.

Huntzinger, E., and Izaurralde, E. (2011b). Gene silencing by microRNAs: contributions of translational repression and mRNA decay. Nature Reviews Genetics *12*, 99-110.

Hynes, R.O. (2002). Integrins: bidirectional, allosteric signaling machines. Cell *110*, 673-687.

Jacobs, J.J., Kieboom, K., Marino, S., DePinho, R.A., and van Lohuizen, M. (1999). The oncogene and Polycomb-group gene bmi-1 regulates cell proliferation and senescence through the ink4a locus. Nature *397*, 164-168.

Janssen, H.L., Reesink, H.W., Lawitz, E.J., Zeuzem, S., Rodriguez-Torres, M., Patel, K., van der Meer, A.J., Patick, A.K., Chen, A., Zhou, Y.*, et al.* (2013). Treatment of HCV infection by targeting microRNA. N Engl J Med *368*, 1685-1694.

Jault, F.M., Jault, J.M., Ruchti, F., Fortunato, E.A., Clark, C., Corbeil, J., Richman, D.D., and Spector, D.H. (1995). Cytomegalovirus infection induces high levels of cyclins, phosphorylated Rb, and p53, leading to cell cycle arrest. J Virol *69*, 6697-6704.

Ji, J., Zhang, J., Huang, G., Qian, J., Wang, X., and Mei, S. (2009). Over-expressed microRNA-27a and 27b influence fat accumulation and cell proliferation during rat hepatic stellate cell activation. FEBS Lett *583*, 759-766.

Jin, Y., Chen, Z., Liu, X., and Zhou, X. (2013). Evaluating the microRNA targeting sites by luciferase reporter gene assay. Methods Mol Biol *936*, 117-127.

Johnson, R.A., Huong, S.M., and Huang, E.S. (1999). Inhibitory effect of 4-(4-fluorophenyl)-2-(4-hydroxyphenyl)-5-(4-pyridyl)1H - imidazole on HCMV DNA replication and permissive infection. Antiviral Res *41*, 101-111.

Johnson, R.A., Huong, S.M., and Huang, E.S. (2000). Activation of the mitogen-activated protein kinase p38 by human cytomegalovirus infection through two distinct pathways: a novel mechanism for activation of p38. J Virol *74*, 1158-1167.

Johnson, R.A., Wang, X., Ma, X.L., Huong, S.M., and Huang, E.S. (2001). Human cytomegalovirus up-regulates the phosphatidylinositol 3-kinase (PI3-K) pathway: inhibition of PI3-K activity inhibits viral replication and virus-induced signaling. J Virol *75*, 6022-6032.

Jones, B.C., Logsdon, N.J., Josephson, K., Cook, J., Barry, P.A., and Walter, M.R. (2002). Crystal structure of human cytomegalovirus IL-10 bound to soluble human IL-10R1. Proc Natl Acad Sci U S A *99*, 9404-9409.

Juckem, L.K., Boehme, K.W., Feire, A.L., and Compton, T. (2008). Differential initiation of innate immune responses induced by human cytomegalovirus entry into fibroblast cells. J Immunol *180*, 4965-4977.

Juranic Lisnic, V., Babic Cac, M., Lisnic, B., Trsan, T., Mefferd, A., Das Mukhopadhyay, C., Cook, C.H., Jonjic, S., and Trgovcich, J. (2013). Dual analysis of the murine cytomegalovirus and host cell transcriptomes reveal new aspects of the virus-host cell interface. PLoS Pathog *9*, e1003611.

Kahl, C.R., and Means, A.R. (2003). Regulation of cell cycle progression by calcium/calmodulin-dependent pathways. Endocr Rev *24*, 719-736.

Kang, T., Lu, W., Xu, W., Anderson, L., Bacanamwo, M., Thompson, W., Chen, Y.E., and Liu, D. (2013). MicroRNA-27 (miR-27) targets prohibitin and impairs adipocyte differentiation and mitochondrial function in human adipose-derived stem cells. J Biol Chem *288*, 34394-34402.

Kapp, L.D., and Lorsch, J.R. (2004). The molecular mechanics of eukaryotic translation. Annu Rev Biochem *73*, 657-704.

Karginov, F.V., Cheloufi, S., Chong, M.M., Stark, A., Smith, A.D., and Hannon, G.J. (2010). Diverse endonucleolytic cleavage sites in the mammalian transcriptome depend upon microRNAs, Drosha, and additional nucleases. Mol Cell *38*, 781-788.

Katso, R., Okkenhaug, K., Ahmadi, K., White, S., Timms, J., and Waterfield, M.D. (2001). Cellular function of phosphoinositide 3-kinases: implications for development, homeostasis, and cancer. Annu Rev Cell Dev Biol *17*, 615-675.

Kauffmann, A., and Huber, W. (2010). Microarray data quality control improves the detection of differentially expressed genes. Genomics *95*, 138-142.

Kedde, M., and Agami, R. (2008). Interplay between microRNAs and RNA-binding proteins determines developmental processes. Cell Cycle *7*, 899-903.

Kew, V.G., Yuan, J., Meier, J., and Reeves, M.B. (2014). Mitogen and stress activated kinases act co-operatively with CREB during the induction of human cytomegalovirus immediate-early gene expression from latency. PLoS Pathog *10*, e1004195.

Khan, A.A., Betel, D., Miller, M.L., Sander, C., Leslie, C.S., and Marks, D.S. (2009). Transfection of small RNAs globally perturbs gene regulation by endogenous microRNAs. Nat Biotechnol *27*, 549-555.

Kim, S.Y., Kim, A.Y., Lee, H.W., Son, Y.H., Lee, G.Y., Lee, J.W., Lee, Y.S., and Kim, J.B. (2010). miR-27a is a negative regulator of adipocyte differentiation via suppressing PPAR gamma expression. Biochem Biophys Res Commun *392*, 323-328.

Kimura, S.H., Ikawa, M., Ito, A., Okabe, M., and Nojima, H. (2001). Cyclin G1 is involved in G2/M arrest in response to DNA damage and in growth control after damage recovery. Oncogene *20*, 3290-3300.

Kincaid, R.P., and Sullivan, C.S. (2012). Virus-encoded microRNAs: an overview and a look to the future. PLoS Pathog *8*, e1003018.

Kotenko, S.V., Saccani, S., Izotova, L.S., Mirochnitchenko, O.V., and Pestka, S. (2000). Human cytomegalovirus harbors its own unique IL-10 homolog (cmvIL-10). Proc Natl Acad Sci U S A *97*, 1695-1700.

Kovacs, D., Rakacs, M., Agoston, B., Lenkey, K., Semrad, K., Schroeder, R., and Tompa, P. (2009). Janus chaperones: assistance of both RNA- and protein-folding by ribosomal proteins. FEBS Lett *583*, 88-92.

Kozomara, A., and Griffiths-Jones, S. (2011). miRBase: integrating microRNA annotation and deep-sequencing data. Nucleic Acids Res *39*, D152-157.

Lanzieri, T.M., Dollard, S.C., Bialek, S.R., and Grosse, S.D. (2014). Systematic review of the birth prevalence of congenital cytomegalovirus infection in developing countries. Int J Infect Dis *22*, 44-48.

Lecellier, C.H., Dunoyer, P., Arar, K., Lehmann-Che, J., Eyquem, S., Himber, C., Saib, A., and Voinnet, O. (2005). A cellular microRNA mediates antiviral defense in human cells. Science *308*, 557-560.

Lee, R.C., Feinbaum, R.L., and Ambros, V. (1993). The C. elegans heterochronic gene lin-4 encodes small RNAs with antisense complementarity to lin-14. Cell *75*, 843-854.

Lee, Y., Hur, I., Park, S.Y., Kim, Y.K., Suh, M.R., and Kim, V.N. (2006). The role of PACT in the RNA silencing pathway. Embo J *25*, 522-532.

Lee, Y., Kim, M., Han, J., Yeom, K.H., Lee, S., Baek, S.H., and Kim, V.N. (2004). MicroRNA genes are transcribed by RNA polymerase II. Embo J *23*, 4051-4060.

Leh, V., Yot, P., and Keller, M. (2000). The cauliflower mosaic virus translational transactivator interacts with the 60S ribosomal subunit protein L18 of Arabidopsis thaliana. Virology *266*, 1-7.

Lerner, M., Lundgren, J., Akhoondi, S., Jahn, A., Ng, H.F., Akbari Moqadam, F., Oude Vrielink, J.A., Agami, R., Den Boer, M.L., Grander, D., and Sangfelt, O. (2011). MiRNA-27a controls FBW7/hCDC4-dependent cyclin E degradation and cell cycle progression. Cell Cycle *10*, 2172-2183.

Li, H., Wang, B.B., Yang, A., Lu, R., Wang, W.C., Zhou, Y., Shi, G.L., Kwon, S.W., Zhao, Y.M., and Jin, Y. (2009). Ly-1 Antibody Reactive Clone Is an Important Nucleolar Protein for Control of Self-Renewal and Differentiation in Embryonic Stem Cells. Stem Cells *27*, 1244-1254.

Li, J., Kim, T., Nutiu, R., Ray, D., Hughes, T.R., and Zhang, Z. (2014). Identifying mRNA sequence elements for target recognition by human Argonaute proteins. Genome Res *24*, 775-785.

Li, R., and Hayward, S.D. (2013). Potential of protein kinase inhibitors for treating herpesvirus-associated disease. Trends Microbiol *21*, 286-295.

Liang, T., Yu, J., Liu, C., and Guo, L. (2014). An exploration of evolution, maturation, expression and function relationships in mir-23 approximately 27 approximately 24 cluster. PLoS One *9*, e106223.

Libri, V., Helwak, A., Miesen, P., Santhakumar, D., Borger, J.G., Kudla, G., Grey, F., Tollervey, D., and Buck, A.H. (2012). Murine cytomegalovirus encodes a miR-27 inhibitor disguised as a target. Proc Natl Acad Sci U S A *109*, 279-284.

Lim, S., and Kaldis, P. (2013). Cdks, cyclins and CKIs: roles beyond cell cycle regulation. Development *140*, 3079-3093.

Lin, Q., Gao, Z., Alarcon, R.M., Ye, J., and Yun, Z. (2009). A role of miR-27 in the regulation of adipogenesis. FEBS J *276*, 2348-2358.

Lindstrom, M.S. (2009). Emerging functions of ribosomal proteins in gene-specific transcription and translation. Biochem Biophys Res Commun *379*, 167-170.

Liu, J., Carmell, M.A., Rivas, F.V., Marsden, C.G., Thomson, J.M., Song, J.J., Hammond, S.M., Joshua-Tor, L., and Hannon, G.J. (2004). Argonaute2 is the catalytic engine of mammalian RNAi. Science *305*, 1437-1441.

Liu, T., Tang, H., Lang, Y., Liu, M., and Li, X. (2009). MicroRNA-27a functions as an oncogene in gastric adenocarcinoma by targeting prohibitin. Cancer Lett *273*, 233-242.

Ljungman, P., Hakki, M., and Boeckh, M. (2010). Cytomegalovirus in hematopoietic stem cell transplant recipients. Infect Dis Clin North Am *24*, 319-337.

Llave, C., Xie, Z., Kasschau, K.D., and Carrington, J.C. (2002). Cleavage of Scarecrow-like mRNA targets directed by a class of Arabidopsis miRNA. Science *297*, 2053-2056.

Lu, M., and Shenk, T. (1999). Human cytomegalovirus UL69 protein induces cells to accumulate in G1 phase of the cell cycle. J Virol *73*, 676-683.

Lukac, D.M., Harel, N.Y., Tanese, N., and Alwine, J.C. (1997). TAF-like functions of human cytomegalovirus immediate-early proteins. J Virol *71*, 7227-7239.

Lund, E., Guttinger, S., Calado, A., Dahlberg, J.E., and Kutay, U. (2004). Nuclear export of microRNA precursors. Science *303*, 95-98.

Ma, Y., Yu, S., Zhao, W., Lu, Z., and Chen, J. (2010). miR-27a regulates the growth, colony formation and migration of pancreatic cancer cells by targeting Sprouty2. Cancer Lett *298*, 150-158.

Mahajan, V.S., Drake, A., and Chen, J. (2009). Virus-specific host miRNAs: antiviral defenses or promoters of persistent infection? Trends Immunol *30*, 1-7.

Malinda, K.M. (2009). In vivo matrigel migration and angiogenesis assay. Methods Mol Biol *467*, 287-294.

Malumbres, M., and Barbacid, M. (2009). Cell cycle, CDKs and cancer: a changing paradigm. Nat Rev Cancer *9*, 153-166.

Mandaric, S., Walton, S.M., Rulicke, T., Richter, K., Girard-Madoux, M.J., Clausen, B.E., Zurunic, A., Kamanaka, M., Flavell, R.A., Jonjic, S., and Oxenius, A. (2012).

IL-10 suppression of NK/DC crosstalk leads to poor priming of MCMV-specific CD4 T cells and prolonged MCMV persistence. PLoS Pathog *8*, e1002846.

Manning, W.C., and Mocarski, E.S. (1988). Insertional mutagenesis of the murine cytomegalovirus genome: one prominent alpha gene (ie2) is dispensable for growth. Virology *167*, 477-484.

Marcinowski, L., Tanguy, M., Krmpotic, A., Radle, B., Lisnic, V.J., Tuddenham, L., Chane-Woon-Ming, B., Ruzsics, Z., Erhard, F., Benkartek, C.*, et al.* (2012). Degradation of cellular mir-27 by a novel, highly abundant viral transcript is important for efficient virus replication in vivo. PLoS Pathog *8*, e1002510.

Margolis, M.J., Pajovic, S., Wong, E.L., Wade, M., Jupp, R., Nelson, J.A., and Azizkhan, J.C. (1995). Interaction of the 72-kilodalton human cytomegalovirus IE1 gene product with E2F1 coincides with E2F-dependent activation of dihydrofolate reductase transcription. J Virol *69*, 7759-7767.

Maroney, P.A., Yu, Y., Fisher, J., and Nilsen, T.W. (2006). Evidence that microRNAs are associated with translating messenger RNAs in human cells. Nat Struct Mol Biol *13*, 1102-1107.

Martinez, F.P., Cosme, R.S., and Tang, Q. (2010). Murine cytomegalovirus major immediate-early protein 3 interacts with cellular and viral proteins in viral DNA replication compartments and is important for early gene activation. J Gen Virol *91*, 2664-2676.

Masamha, C.P., and Benbrook, D.M. (2009). Cyclin D1 Degradation Is Sufficient to Induce G(1) Cell Cycle Arrest despite Constitutive Expression of Cyclin E2 in Ovarian Cancer Cells. Cancer Res *69*, 6565-6572.

Mathonnet, G., Fabian, M.R., Svitkin, Y.V., Parsyan, A., Huck, L., Murata, T., Biffo, S., Merrick, W.C., Darzynkiewicz, E., Pillai, R.S.*, et al.* (2007). MicroRNA inhibition of translation initiation in vitro by targeting the cap-binding complex eIF4F. Science *317*, 1764-1767.

McLaughlin, M.M., Kumar, S., McDonnell, P.C., Van Horn, S., Lee, J.C., Livi, G.P., and Young, P.R. (1996). Identification of mitogen-activated protein (MAP) kinase-activated protein kinase-3, a novel substrate of CSBP p38 MAP kinase. J Biol Chem *271*, 8488-8492.

Meister, G., Landthaler, M., Patkaniowska, A., Dorsett, Y., Teng, G., and Tuschl, T. (2004). Human Argonaute2 mediates RNA cleavage targeted by miRNAs and siRNAs. Mol Cell *15*, 185-197.

Mertens-Talcott, S.U., Chintharlapalli, S., Li, X., and Safe, S. (2007). The oncogenic microRNA-27a targets genes that regulate specificity protein transcription factors and the G2-M checkpoint in MDA-MB-231 breast cancer cells. Cancer Res *67*, 11001-11011.

Michaelis, M., Doerr, H.W., and Cinatl, J. (2009). The story of human cytomegalovirus and cancer: increasing evidence and open questions. Neoplasia *11*, 1-9.

Min, H., and Yoon, S. (2010). Got target? Computational methods for microRNA target prediction and their extension. Exp Mol Med *42*, 233-244.

Min, W., Wen-li, M., Zhao-hui, S., Ling, L., Bao, Z., and Wen-ling, Z. (2009). Microarray analysis identifies differentially expressed genes induced by human papillomavirus type 18 E6 silencing RNA. Int J Gynecol Cancer *19*, 547-563.

Mocarski, E.S., Kemble, G.W., Lyle, J.M., and Greaves, R.F. (1996). A deletion mutant in the human cytomegalovirus gene encoding IE1(491aa) is replication defective due to a failure in autoregulation. Proc Natl Acad Sci U S A *93*, 11321-11326.

Mocarski, E.S., Shenk, T., & Pass, R. F. (2007). Fields of virology. In Cytomegalovirus (Philadelphia Lipincott Williams & Wilkins), pp. 2701-2772.

Mocarski ES, S.T., Pass RF (2007). Cytomegaloviruses, Vol 2 (Philadelphia: Lippincott Williams & Wilkins).

Modzelewski, A.J., Holmes, R.J., Hilz, S., Grimson, A., and Cohen, P.E. (2012). AGO4 regulates entry into meiosis and influences silencing of sex chromosomes in the male mouse germline. Dev Cell *23*, 251-264.

Moore, J.D. (2013). In the wrong place at the wrong time: does cyclin mislocalization drive oncogenic transformation? Nature Reviews Cancer *13*, 201-208.

Moore, M.J., Zhang, C., Gantman, E.C., Mele, A., Darnell, J.C., and Darnell, R.B. (2014). Mapping Argonaute and conventional RNA-binding protein interactions with RNA at single-nucleotide resolution using HITS-CLIP and CIMS analysis. Nat Protoc *9*, 263-293.

Morgan, D.O. (1999). Regulation of the APC and the exit from mitosis. Nat Cell Biol *1*, E47-53.

Morrison, D.K. (2012). MAP kinase pathways. Cold Spring Harb Perspect Biol *4*.

Mosser, D.M., and Zhang, X. (2008). Interleukin-10: new perspectives on an old cytokine. Immunol Rev *226*, 205-218.

Muganda, P., Mendoza, O., Hernandez, J., and Qian, Q. (1994). Human cytomegalovirus elevates levels of the cellular protein p53 in infected fibroblasts. J Virol *68*, 8028-8034.

Murakami, Y., Aly, H.H., Tajima, A., Inoue, I., and Shimotohno, K. (2009). Regulation of the hepatitis C virus genome replication by miR-199a. Journal of hepatology *50*, 453-460.

Murphy, E., Rigoutsos, I., Shibuya, T., and Shenk, T.E. (2003). Reevaluation of human cytomegalovirus coding potential. Proc Natl Acad Sci U S A *100*, 13585-13590.

Murphy, E.A., Streblow, D.N., Nelson, J.A., and Stinski, M.F. (2000). The human cytomegalovirus IE86 protein can block cell cycle progression after inducing transition into the S phase of permissive cells. J Virol *74*, 7108-7118.

Murphy, K., Travers, P., and Walport, M. (2008). Janeway's Immunobiology, 7 edn (New York: Garland Science).

Myatt, S.S., Wang, J., Monteiro, L.J., Christian, M., Ho, K.K., Fusi, L., Dina, R.E., Brosens, J.J., Ghaem-Maghami, S., and Lam, E.W. (2010). Definition of microRNAs that repress expression of the tumor suppressor gene FOXO1 in endometrial cancer. Cancer Res *70*, 367-377.

Nassetta, L., Kimberlin, D., and Whitley, R. (2009). Treatment of congenital cytomegalovirus infection: implications for future therapeutic strategies. J Antimicrob Chemother *63*, 862-867.

Nathans, R., Chu, C.Y., Serquina, A.K., Lu, C.C., Cao, H., and Rana, T.M. (2009). Cellular microRNA and P bodies modulate host-HIV-1 interactions. Mol Cell *34*, 696-709.

Neff, B.J., Weibel, R.E., Buynak, E.B., McLean, A.A., and Hilleman, M.R. (1979). Clinical and laboratory studies of live cytomegalovirus vaccine Ad-169. Proc Soc Exp Biol Med *160*, 32-37.

Nielsen, C.B., Shomron, N., Sandberg, R., Hornstein, E., Kitzman, J., and Burge, C.B. (2007). Determinants of targeting by endogenous and exogenous microRNAs and siRNAs. Rna *13*, 1894-1910.

Nithianandarajah-Jones, G.N., Wilm, B., Goldring, C.E., Muller, J., and Cross, M.J. (2012). ERK5: structure, regulation and function. Cell Signal *24*, 2187-2196.

Noris, E., Zannetti, C., Demurtas, A., Sinclair, J., De Andrea, M., Gariglio, M., and Landolfo, S. (2002). Cell cycle arrest by human cytomegalovirus 86-kDa IE2 protein resembles premature senescence. J Virol *76*, 12135-12148.

O'Carroll, D., and Schaefer, A. (2013). General principals of miRNA biogenesis and regulation in the brain. Neuropsychopharmacology *38*, 39-54.

Okamoto, K., and Beach, D. (1994). Cyclin-G Is a Transcriptional Target of the P53 Tumor-Suppressor Protein. Embo Journal *13*, 4816-4822.

Okamoto, T., Schlegel, A., Scherer, P.E., and Lisanti, M.P. (1998). Caveolins, a family of scaffolding proteins for organizing "preassembled signaling complexes" at the plasma membrane. J Biol Chem *273*, 5419-5422.

Okamura, K., Hagen, J.W., Duan, H., Tyler, D.M., and Lai, E.C. (2007). The mirtron pathway generates microRNA-class regulatory RNAs in Drosophila. Cell *130*, 89-100.

Olsen, P.H., and Ambros, V. (1999). The lin-4 regulatory RNA controls developmental timing in Caenorhabditis elegans by blocking LIN-14 protein synthesis after the initiation of translation. Dev Biol *216*, 671-680.

Othumpangat, S., Walton, C., and Piedimonte, G. (2012). MicroRNA-221 modulates RSV replication in human bronchial epithelium by targeting NGF expression. PLoS One *7*, e30030.

Otsuka, M., Jing, Q., Georgel, P., New, L., Chen, J., Mols, J., Kang, Y.J., Jiang, Z., Du, X., Cook, R.*, et al.* (2007). Hypersusceptibility to vesicular stomatitis virus infection in Dicer1-deficient mice is due to impaired miR24 and miR93 expression. Immunity *27*, 123-134.

Pajovic, S., Wong, E.L., Black, A.R., and Azizkhan, J.C. (1997). Identification of a viral kinase that phosphorylates specific E2Fs and pocket proteins. Mol Cell Biol *17*, 6459-6464.

Parker, J.S. (2010). How to slice: snapshots of Argonaute in action. Silence *1*, 3.

Pasdeloup, D., McElwee, M., Beilstein, F., Labetoulle, M., and Rixon, F.J. (2013). Herpesvirus tegument protein pUL37 interacts with dystonin/BPAG1 to promote capsid transport on microtubules during egress. J Virol *87*, 2857-2867.

Pasquinelli, A.E., Reinhart, B.J., Slack, F., Martindale, M.Q., Kuroda, M.I., Maller, B., Hayward, D.C., Ball, E.E., Degnan, B., Muller, P.*, et al.* (2000). Conservation of the sequence and temporal expression of let-7 heterochronic regulatory RNA. Nature *408*, 86-89.

Pedersen, I.M., Cheng, G., Wieland, S., Volinia, S., Croce, C.M., Chisari, F.V., and David, M. (2007). Interferon modulation of cellular microRNAs as an antiviral mechanism. Nature *449*, 919-922.

Penkert, R.R., and Kalejta, R.F. (2011). Tegument protein control of latent herpesvirus establishment and animation. Herpesviridae *2*, 3.

Petersen, C.P., Bordeleau, M.E., Pelletier, J., and Sharp, P.A. (2006). Short RNAs repress translation after initiation in mammalian cells. Mol Cell *21*, 533-542.

Pillai, R.S., Bhattacharyya, S.N., Artus, C.G., Zoller, T., Cougot, N., Basyuk, E., Bertrand, E., and Filipowicz, W. (2005). Inhibition of translational initiation by Let-7 MicroRNA in human cells. Science *309*, 1573-1576.

Poma, E.E., Kowalik, T.F., Zhu, L., Sinclair, J.H., and Huang, E.S. (1996). The human cytomegalovirus IE1-72 protein interacts with the cellular p107 protein and relieves p107-mediated transcriptional repression of an E2F-responsive promoter. J Virol *70*, 7867-7877.

Potenza, N., Papa, U., Mosca, N., Zerbini, F., Nobile, V., and Russo, A. (2011). Human microRNA hsa-miR-125a-5p interferes with expression of hepatitis B virus surface antigen. Nucleic Acids Res *39*, 5157-5163.

Prichard, M.N.P., M.E.; Duke, G.M.; Spaete, R.R.; Kemble, G.W. (2001). A review of genetic differences between limited and extensively passaged human cytomegalovirus strains. Rev. Med. Virol. *11*, 191–200.

Prueitt, R.L., Yi, M., Hudson, R.S., Wallace, T.A., Howe, T.M., Yfantis, H.G., Lee, D.H., Stephens, R.M., Liu, C.G., Calin, G.A., *et al.* (2008). Expression of microRNAs and protein-coding genes associated with perineural invasion in prostate cancer. Prostate *68*, 1152-1164.

Randall, R.E., and Goodbourn, S. (2008). Interferons and viruses: an interplay between induction, signalling, antiviral responses and virus countermeasures. J Gen Virol *89*, 1-47.

Rasmussen, C.D., and Means, A.R. (1989). Calmodulin Is Required for Cell-Cycle Progression during G1 and Mitosis. Embo Journal *8*, 73-82.

Rawlinson, W.D., Farrell, H.E., and Barrell, B.G. (1996). Analysis of the complete DNA sequence of murine cytomegalovirus. J Virol *70*, 8833-8849.

Reimer, C.L., Borras, A.M., Kurdistani, S.K., Garreau, J.R., Chung, M., Aaronson, S.A., and Lee, S.W. (1999). Altered regulation of cyclin G in human breast cancer and its specific localization at replication foci in response to DNA damage in p53+/+ cells. J Biol Chem *274*, 11022-11029.

Reinhart, B.J., Slack, F.J., Basson, M., Pasquinelli, A.E., Bettinger, J.C., Rougvie, A.E., Horvitz, H.R., and Ruvkun, G. (2000). The 21-nucleotide let-7 RNA regulates developmental timing in Caenorhabditis elegans. Nature *403*, 901-906.

Rhoades, M.W., Reinhart, B.J., Lim, L.P., Burge, C.B., Bartel, B., and Bartel, D.P. (2002). Prediction of plant microRNA targets. Cell *110*, 513-520.

Rincon, M., Flavell, R.A., and Davis, R.A. (2000). The JNK and P38 MAP kinase signaling pathways in T cell-mediated immune responses. Free Radic Biol Med *28*, 1328-1337.

Rincon, M., and Pedraza-Alva, G. (2003). JNK and p38 MAP kinases in CD4+ and CD8+ T cells. Immunol Rev *192*, 131-142.

Ronkina, N., Kotlyarov, A., Dittrich-Breiholz, O., Kracht, M., Hitti, E., Milarski, K., Askew, R., Marusic, S., Lin, L.L., Gaestel, M., and Telliez, J.B. (2007). The mitogen-activated protein kinase (MAPK)-activated protein kinases MK2 and MK3 cooperate in stimulation of tumor necrosis factor biosynthesis and stabilization of p38 MAPK. Mol Cell Biol *27*, 170-181.

Ronkina, N., Kotlyarov, A., and Gaestel, M. (2008). MK2 and MK3--a pair of isoenzymes? Front Biosci *13*, 5511-5521.

Ruby, J.G., Jan, C.H., and Bartel, D.P. (2007). Intronic microRNA precursors that bypass Drosha processing. Nature *448*, 83-86.

Salvant, B.S., Fortunato, E.A., and Spector, D.H. (1998). Cell cycle dysregulation by human cytomegalovirus: influence of the cell cycle phase at the time of infection and effects on cyclin transcription. J Virol *72*, 3729-3741.

Santhakumar, D., Forster, T., Laqtom, N.N., Fragkoudis, R., Dickinson, P., Abreu-Goodger, C., Manakov, S.A., Choudhury, N.R., Griffiths, S.J., Vermeulen, A.*, et al.* (2010). Combined agonist-antagonist genome-wide functional screening identifies broadly active antiviral microRNAs. Proc Natl Acad Sci U S A *107*, 13830-13835.

Sauvageau, M., and Sauvageau, G. (2010). Polycomb group proteins: multi-faceted regulators of somatic stem cells and cancer. Cell Stem Cell *7*, 299-313.

Scherer, P.E., Lewis, R.Y., Volonte, D., Engelman, J.A., Galbiati, F., Couet, J., Kohtz, D.S., van Donselaar, E., Peters, P., and Lisanti, M.P. (1997). Cell-type and tissue-specific expression of caveolin-2. Caveolins 1 and 2 co-localize and form a stable hetero-oligomeric complex in vivo. J Biol Chem *272*, 29337-29346.

Schneider, W.M., Chevillotte, M.D., and Rice, C.M. (2014). Interferon-stimulated genes: a complex web of host defenses. Annu Rev Immunol *32*, 513-545.

Scott, G.K., Mattie, M.D., Berger, C.E., Benz, S.C., and Benz, C.C. (2006). Rapid alteration of microRNA levels by histone deacetylase inhibition. Cancer Res *66*, 1277-1281.

Shellam, G.R., Redwood, A.J., Smith, L.M., and Gorman, S. (2007). Murine cytomegalovirus and other herpesviruses. In The mouse in biomedical research J.G. Fox, S.W. Barthold, M.T. Davission, C.E. Newcomer, F.W. Quimby, and A.L. Smith, eds. (Elsevier, Inc), pp. 1-26.

Shenk T.E, S.M.F. (2008). Human Cytomegalovirus, Vol 325 (springer).

Shin, C., Nam, J.W., Farh, K.K., Chiang, H.R., Shkumatava, A., and Bartel, D.P. (2010). Expanding the microRNA targeting code: functional sites with centered pairing. Mol Cell *38*, 789-802.

Shirasaki, T., Honda, M., Shimakami, T., Horii, R., Yamashita, T., Sakai, Y., Sakai, A., Okada, H., Watanabe, R., Murakami, S.*, et al.* (2013). MicroRNA-27a regulates lipid metabolism and inhibits hepatitis C virus replication in human hepatoma cells. J Virol *87*, 5270-5286.

Sinclair, J., Baillie, J., Bryant, L., and Caswell, R. (2000). Human cytomegalovirus mediates cell cycle progression through G(1) into early S phase in terminally differentiated cells. J Gen Virol *81*, 1553-1565.

Skalsky, R.L., and Cullen, B.R. (2010). Viruses, microRNAs, and host interactions. Annu Rev Microbiol *64*, 123-141.

Skelding, K.A., Rostas, J.A., and Verrills, N.M. (2011). Controlling the cell cycle: the role of calcium/calmodulin-stimulated protein kinases I and II. Cell Cycle *10*, 631-639.

Skotzko, M., Wu, L., Anderson, W.F., Gordon, E.M., and Hall, F.L. (1995). Retroviral vector-mediated gene transfer of antisense cyclin G1 (CYCG1) inhibits proliferation of human osteogenic sarcoma cells. Cancer Res *55*, 5493-5498.

Slobedman, B., Barry, P.A., Spencer, J.V., Avdic, S., and Abendroth, A. (2009). Virus-encoded homologs of cellular interleukin-10 and their control of host immune function. J Virol *83*, 9618-9629.

Smee, D.F., Colletti, A., Alaghamandan, H.A., and Allen, L.B. (1989). Evaluation of continuous cell lines in antiviral studies with murine cytomegalovirus. Arch Virol *107*, 253-260.

Smith, C. (2006). Sharpening the tools of RNA interference. Nat Methods *3*, 475-484.

Smith, M.L., Kontny, H.U., Bortnick, R., and Fornace, A.J., Jr. (1997). The p53-regulated cyclin G gene promotes cell growth: p53 downstream effectors cyclin G and Gadd45 exert different effects on cisplatin chemosensitivity. Exp Cell Res *230*, 61-68.

Smith, M.S., Bentz, G.L., Smith, P.M., Bivins, E.R., and Yurochko, A.D. (2004). HCMV activates PI(3)K in monocytes and promotes monocyte motility and transendothelial migration in a PI(3)K-dependent manner. J Leukoc Biol *76*, 65-76.

Song, K.S., Scherer, P.E., Tang, Z., Okamoto, T., Li, S., Chafel, M., Chu, C., Kohtz, D.S., and Lisanti, M.P. (1996). Expression of caveolin-3 in skeletal, cardiac, and smooth muscle cells. Caveolin-3 is a component of the sarcolemma and co-fractionates with dystrophin and dystrophin-associated glycoproteins. J Biol Chem *271*, 15160-15165.

Song, L.P., Liu, H., Gao, S.J., Jiang, W., and Huang, W.L. (2010). Cellular MicroRNAs Inhibit Replication of the H1N1 Influenza A Virus in Infected Cells. J Virol *84*, 8849-8860.

Spector, D.H. (2015). Human cytomegalovirus riding the cell cycle. Med Microbiol Immunol *204*, 409-419.

Speir, E., Modali, R., Huang, E.S., Leon, M.B., Shawl, F., Finkel, T., and Epstein, S.E. (1994). Potential role of human cytomegalovirus and p53 interaction in coronary restenosis. Science *265*, 391-394.

Spencer, J.V., Lockridge, K.M., Barry, P.A., Lin, G., Tsang, M., Penfold, M.E., and Schall, T.J. (2002). Potent immunosuppressive activities of cytomegalovirus-encoded interleukin-10. J Virol *76*, 1285-1292.

Spurgers, K.B., Alefantis, T., Peyser, B.D., Ruthel, G.T., Bergeron, A.A., Costantino, J.A., Enterlein, S., Kota, K.P., Boltz, R.C., Aman, M.J.*, et al.* (2010). Identification of essential filovirion-associated host factors by serial proteomic analysis and RNAi screen. Mol Cell Proteomics *9*, 2690-2703.

Stamminger, T., Puchtler, E., and Fleckenstein, B. (1991). Discordant expression of the immediate-early 1 and 2 gene regions of human cytomegalovirus at early times after infection involves posttranscriptional processing events. J Virol *65*, 2273-2282.

Steed, A.L., Barton, E.S., Tibbetts, S.A., Popkin, D.L., Lutzke, M.L., Rochford, R., and Virgin, H.W.t. (2006). Gamma interferon blocks gammaherpesvirus reactivation from latency. J Virol *80*, 192-200.

Stevenson, J., Krycer, J.R., Phan, L., and Brown, A.J. (2013). A practical comparison of ligation-independent cloning techniques. PLoS One *8*, e83888.

Stewart, P.L., and Nemerow, G.R. (2007). Cell integrins: commonly used receptors for diverse viral pathogens. Trends Microbiol *15*, 500-507.

Strauch, E.M., Fleishman, S.J., and Baker, D. (2014). Computational design of a pH-sensitive IgG binding protein. Proc Natl Acad Sci U S A *111*, 675-680.

Su, C., Hou, Z., Zhang, C., Tian, Z., and Zhang, J. (2011). Ectopic expression of microRNA-155 enhances innate antiviral immunity against HBV infection in human hepatoma cells. Virol J *8*, 354.

Su, H., Trombly, M.I., Chen, J., and Wang, X. (2009). Essential and overlapping functions for mammalian Argonautes in microRNA silencing. Genes & development *23*, 304-317.

Sung, H., and Schleiss, M.R. (2010). Update on the current status of cytomegalovirus vaccines. Expert Rev Vaccines *9*, 1303-1314.

Tan, Y., Rouse, J., Zhang, A., Cariati, S., Cohen, P., and Comb, M.J. (1996). FGF and stress regulate CREB and ATF-1 via a pathway involving p38 MAP kinase and MAPKAP kinase-2. Embo J *15*, 4629-4642.

Tang, Q., Murphy, E.A., and Maul, G.G. (2006). Experimental confirmation of global murine cytomegalovirus open reading frames by transcriptional detection and partial characterization of newly described gene products. J Virol *80*, 6873-6882.

Tang-Feldman, Y.J., Lochhead, S.R., Lochhead, G.R., Yu, C., George, M., Villablanca, A.C., and Pomeroy, C. (2013). Murine cytomegalovirus (MCMV) infection upregulates P38 MAP kinase in aortas of Apo E KO mice: a molecular mechanism for MCMV-induced acceleration of atherosclerosis. J Cardiovasc Transl Res *6*, 54-64.

Thomson, D.W., Bracken, C.P., and Goodall, G.J. (2011). Experimental strategies for microRNA target identification. Nucleic Acids Res *39*, 6845-6853.

Thurlow, J.K., Rixon, F.J., Murphy, M., Targett-Adams, P., Hughes, M., and Preston, V.G. (2005). The herpes simplex virus type 1 DNA packaging protein UL17 is a virion protein that is present in both the capsid and the tegument compartments. J Virol *79*, 150-158.

Tokuyama, M., Lorin, C., Delebecque, F., Jung, H., Raulet, D.H., and Coscoy, L. (2011). Expression of the RAE-1 family of stimulatory NK-cell ligands requires activation of the PI3K pathway during viral infection and transformation. PLoS Pathog *7*, e1002265.

Travis, A.J., Moody, J., Helwak, A., Tollervey, D., and Kudla, G. (2014). Hyb: a bioinformatics pipeline for the analysis of CLASH (crosslinking, ligation and sequencing of hybrids) data. Methods *65*, 263-273.

Triboulet, R., Mari, B., Lin, Y.L., Chable-Bessia, C., Bennasser, Y., Lebrigand, K., Cardinaud, B., Maurin, T., Barbry, P., Baillat, V.*, et al.* (2007). Suppression of microRNA-silencing pathway by HIV-1 during virus replication. Science *315*, 1579-1582.

Trobaugh, D.W., Gardner, C.L., Sun, C.Q., Haddow, A.D., Wang, E.Y., Chapnik, E., Mildner, A., Weaver, S.C., Ryman, K.D., and Klimstra, W.B. (2014). RNA viruses can hijack vertebrate microRNAs to suppress innate immunity. Nature *506*, 245-+.

Ule, J., Jensen, K.B., Ruggiu, M., Mele, A., Ule, A., and Darnell, R.B. (2003). CLIP identifies Nova-regulated RNA networks in the brain. Science *302*, 1212-1215.

Umbach, J.L., and Cullen, B.R. (2009). The role of RNAi and microRNAs in animal virus replication and antiviral immunity. Genes & development *23*, 1151-1164.

Urbich, C., Kaluza, D., Fromel, T., Knau, A., Bennewitz, K., Boon, R.A., Bonauer, A., Doebele, C., Boeckel, J.N., Hergenreider, E.*, et al.* (2012). MicroRNA-27a/b controls endothelial cell repulsion and angiogenesis by targeting semaphorin 6A. Blood *119*, 1607-1616.

Vidyasagar, A., Wilson, N.A., and Djamali, A. (2012). Heat shock protein 27 (HSP27): biomarker of disease and therapeutic target. Fibrogenesis Tissue Repair *5*, 7.

Wagner, M., Jonjic, S., Koszinowski, U.H., and Messerle, M. (1999). Systematic excision of vector sequences from the BAC-cloned herpesvirus genome during virus reconstitution. J Virol *73*, 7056-7060.

Wang, D., and Shenk, T. (2005). Human cytomegalovirus UL131 open reading frame is required for epithelial cell tropism. J Virol *79*, 10330-10338.

Wang, F.Z., Weber, F., Croce, C., Liu, C.G., Liao, X., and Pellett, P.E. (2008). Human cytomegalovirus infection alters the expression of cellular microRNA species that affect its replication. J Virol *82*, 9065-9074.

Wang, G., Fulkerson, C.M., Malek, R., Ghassemifar, S., Snyder, P.W., and Mendrysa, S.M. (2012). Mutations in Lyar and p53 are synergistically lethal in female mice. Birth Defects Res A Clin Mol Teratol *94*, 729-737.

Wang, X., Wang, H.K., McCoy, J.P., Banerjee, N.S., Rader, J.S., Broker, T.R., Meyers, C., Chow, L.T., and Zheng, Z.M. (2009). Oncogenic HPV infection interrupts the expression of tumor-suppressive miR-34a through viral oncoprotein E6. Rna *15*, 637-647.

Westerhout, E.M., Ooms, M., Vink, M., Das, A.T., and Berkhout, B. (2005). HIV-1 can escape from RNA interference by evolving an alternative structure in its RNA genome. Nucleic Acids Res *33*, 796-804.

Wiebusch, L., Asmar, J., Uecker, R., and Hagemeier, C. (2003a). Human cytomegalovirus immediate-early protein 2 (IE2)-mediated activation of cyclin E is cell-cycle-independent and forces S-phase entry in IE2-arrested cells. J Gen Virol *84*, 51-60.

Wiebusch, L., and Hagemeier, C. (1999). Human cytomegalovirus 86-kilodalton IE2 protein blocks cell cycle progression in G(1). J Virol *73*, 9274-9283.

Wiebusch, L., Neuwirth, A., Grabenhenrich, L., Voigt, S., and Hagemeier, C. (2008). Cell cycle-independent expression of immediate-early gene 3 results in G1 and G2 arrest in murine cytomegalovirus-infected cells. J Virol *82*, 10188-10198.

Wiebusch, L., Uecker, R., and Hagemeier, C. (2003b). Human cytomegalovirus prevents replication licensing by inhibiting MCM loading onto chromatin. EMBO Rep *4*, 42-46.

Wightman, B., Ha, I., and Ruvkun, G. (1993). Posttranscriptional regulation of the heterochronic gene lin-14 by lin-4 mediates temporal pattern formation in C. elegans. Cell *75*, 855-862.

Wilczynska, A., and Bushell, M. (2015). The complexity of miRNA-mediated repression. Cell Death Differ *22*, 22-33.

Winter, J., and Diederichs, S. (2011). Argonaute proteins regulate microRNA stability: Increased microRNA abundance by Argonaute proteins is due to microRNA stabilization. RNA Biol *8*, 1149-1157.

Wolfstein, A., Nagel, C.H., Radtke, K., Dohner, K., Allan, V.J., and Sodeik, B. (2006). The inner tegument promotes herpes simplex virus capsid motility along microtubules in vitro. Traffic *7*, 227-237.

Wu, J., Hu, D., Yang, G., Zhou, J., Yang, C., Gao, Y., and Zhu, Z. (2011). Down-regulation of BMI-1 cooperates with artemisinin on growth inhibition of nasopharyngeal carcinoma cells. J Cell Biochem *112*, 1938-1948.

Wu, L., Fan, J., and Belasco, J.G. (2006). MicroRNAs direct rapid deadenylation of mRNA. Proc Natl Acad Sci U S A *103*, 4034-4039.

Xie, N., Cui, H., Banerjee, S., Tan, Z., Salomao, R., Fu, M., Abraham, E., Thannickal, V.J., and Liu, G. (2014). miR-27a regulates inflammatory response of macrophages by targeting IL-10. J Immunol *193*, 327-334.

Yi, R., Qin, Y., Macara, I.G., and Cullen, B.R. (2003). Exportin-5 mediates the nuclear export of pre-microRNAs and short hairpin RNAs. Genes Dev *17*, 3011-3016.

Zarubin, T., and Han, J. (2005). Activation and signaling of the p38 MAP kinase pathway. Cell Res *15*, 11-18.

Zauberman, A., Lupo, A., and Oren, M. (1995). Identification of p53 target genes through immune selection of genomic DNA: the cyclin G gene contains two distinct p53 binding sites. Oncogene *10*, 2361-2366.

Zdanowicz, A., Thermann, R., Kowalska, J., Jemielity, J., Duncan, K., Preiss, T., Darzynkiewicz, E., and Hentze, M.W. (2009). Drosophila miR2 primarily targets the m7GpppN cap structure for translational repression. Mol Cell *35*, 881-888.

Zhang, X., Graves, P., and Zeng, Y. (2013). Overexpression of human Argonaute2 inhibits cell and tumor growth. Biochim Biophys Acta *1830*, 2553-2561.

Zhang, Z., Liu, S., Shi, R., and Zhao, G. (2011). miR-27 promotes human gastric cancer cell metastasis by inducing epithelial-to-mesenchymal transition. Cancer Genet *204*, 486-491.

Zhou, Q., Gallagher, R., Ufret-Vincenty, R., Li, X., Olson, E.N., and Wang, S. (2011). Regulation of angiogenesis and choroidal neovascularization by members of microRNA-23~27~24 clusters. Proc Natl Acad Sci U S A *108*, 8287-8292.

Zhu, H., Shen, Y., and Shenk, T. (1995). Human cytomegalovirus IE1 and IE2 proteins block apoptosis. J Virol *69*, 7960-7970.